UNIVERSIDAD COMPLUTENSE DE MADRID

FACULTAD DE CIENCIAS FÍSICAS

Departamento de Física Aplicada III

TESIS DOCTORAL

Effects of pulmonary surfactant proteins SP-B and SP-C on the Physical properties of Biological membranes

Efectos de las proteínas SP-B y SP-C del surfactante pulmonar en las propiedades físicas de membranas biológicas

MEMORIA PARA OPTAR AL GRADO DE DOCTOR

PRESENTADA POR

Elisa Parra Ortiz

Directores

Jesús Pérez Gil
Antonio Cruz Rodríguez

Madrid, 2013

UNIVERSIDAD COMPLUTENSE DE MADRID

Facultad de Ciencias Físicas

Departamento de Física Aplicada III

EFFECTS OF PULMONARY SURFACTANT PROTEINS SP-B AND SP-C ON THE PHYSICAL PROPERTIES OF BIOLOGICAL MEMBRANES

Ph.D. Thesis
by

ELISA PARRA ORTIZ

Supervisors:

Jesús Pérez Gil, Ph.D.

Antonio Cruz Rodríguez, Ph.D.

Madrid, 2013

UNIVERSIDAD COMPLUTENSE DE MADRID

Facultad de Ciencias Físicas

Departamento de Física Aplicada III

EFECTOS DE LAS PROTEÍNAS SP-B Y SP-C DEL SURFACTANTE PULMONAR EN LAS PROPIEDADES FÍSICAS DE MEMBRANAS BIOLÓGICAS

Tesis Doctoral
por

ELISA PARRA ORTIZ

Directores:

Dr. Jesús Pérez Gil

Dr. Antonio Cruz Rodríguez

Madrid, 2013

The present Doctoral Thesis has been performed at the Department of Biochemistry and Molecular Biology I of Complutense University, Madrid, under the supervision of Professors Jesús Pérez Gil and Antonio Cruz Rodríguez.

Part of the experimental work was carried out at the Department of Physical Chemistry I of University Complutense, in collaboration with the group of Professor Francisco Monroy; at the Laboratory of Molecular Biophysics, in the Department of Physics at Jaume I University (Castellón, Spain), supervised by Professors Antonio Alcaraz González and Vicente Aguilella Fernández; at the facilities of the Electron Microscopy National Center in Complutense University and in collaboration with Professor Evan Evans and his research group at University of British Columbia (Vancouver, Canada) and Duke University (Dunham, NC, USA).

The financial support for the realization of the present Thesis was obtained from the Ministry of Science and Innovation (projects CSD2007-00010, BIO2009-09694, BFU2010-11538-E).

A mi familia y amigos.
A Javi.

TABLE OF CONTENTS

Page

ACKNOWLEDGEMENTS/AGRADECIMIENTOS

Gracias en primer lugar a mis Directores de Tesis, los Dres. Jesús Pérez Gil y Antonio Cruz Rodríguez, por darme la oportunidad de iniciarme en el mundo de la investigación como parte de un grupo dinámico y de tanta calidad. Jesús, muchas gracias por haber confiado en mí desde el primer momento, por haberme abierto esa puerta hacia la Biología que tanto me apetecía cruzar, por darme la oportunidad de viajar y conocer tantos lugares y tanta gente interesante. Espero que ese afán por descubrir, por intentar cosas nuevas, por no conformarte con lo que hay, esa curiosidad científica y esa gran capacidad de trabajo los mantengas siempre. Antonio, muchas gracias por esas conversaciones en el laboratorio, por tus consejos, tu amabilidad y por estar siempre dispuesto a ayudar. Tienes muy buenas ideas que espero que te lleven a hacer grandes cosas.

Gracias al Dr. Francisco Monroy y a su grupo de investigación por toda la ayuda recibida y por una colaboración tan fructífera, especialmente a Lara, por tu simpatía y por los buenos momentos juntas.

Gracias a los Dres. Antonio Alcaraz y Vicente Aguilella y a su grupo de investigación, en especial a María y Carmina, por la cálida acogida en vuestro laboratorio, vuestra hospitalidad y por ese buen ambiente que se respira en el grupo. Siempre recordaré con cariño esos meses con vosotros en Castellón y en algún que otro congreso.

I would like to express my warmest gratitude to Prof. Evan Evans for trusting me and my possibilities, for teaching me so many things, for considering me a member of your great scientific family and for sharing wonderful moments all around the world: Madrid, Vancouver, San Diego... I can barely express in words how grateful I feel. This collaboration would not have been possible without the kind support of his great team: grateful thanks to Andrew Leung, for your technical assistance, for being so helpful and for your joy and hospitality; also to Wieslawa Rawicz, Igor Kuznetsov and Koji Kinoshita for all your help and for the great times in Vancouver.

De vuelta a Madrid, me gustaría agradecer especialmente a la Dra. Pilar Estrada por acogerme en el L7, por el buen ambiente que allí se respira y por tu simpatía y dulzura. Gracias también a Ángeles por todo el tiempo que hemos compartido juntas en el laboratorio, por tantas risas y buenos momentos y por tu gran capacidad de volcarte en los demás y ayudarnos con cualquier cosa que necesitemos.

Muchas gracias a Mercedes, por toda tu ayuda en el día a día y por tu sentido del humor. Nuria, muchas gracias por tu simpatía, tu sonrisa y por hacernos la vida un poco más fácil con tu ayuda y tus gestiones. Gracias a todos mis compañeros del L4.2: Begoña, Elena, Virginia (¡ánimo!), Álex, Nuria, Alicia y Sonia, por los buenos momentos dentro y fuera del Departamento. Gracias también a todos los integrantes del L4.1, pasados y presentes, por compartir esta etapa conmigo. Muchas gracias en especial a todos los miembros del L3: Miguel, Jesús, Dani, Rodrigo, Alba e Iria, por tantos cafés, cañas, comidas y alguna que otra cena durante estos años, y por tantos buenos momentos. Gracias también a Laurita por

compartir nuestras penas y alegrías y por tu amistad; te deseo toda la suerte del mundo para tu nueva etapa.

Muchas gracias a mis grandes amigas además de compañeras, Bárbara y Elisa, por ser también mis maestras, porque admiro vuestra forma de ser y de ver la vida y por compartir tanto conmigo. Muchas gracias también a mis ciudadrealeños por España y por el mundo, por los ánimos y el interés, y porque el hecho de teneros ahí desde hace tantos años es siempre una referencia en mi vida y un gran apoyo. Gracias también a mis chicas: Clara, Leti, María, Paula y Zahira, por todo lo que hemos vivido juntas y porque los años en Madrid no habrían sido lo mismo sin vosotras.

Y por último, quiero agradecer especialmente a mi familia por todo el interés en mi trabajo y por el apoyo. Muchas gracias a Felisa por cuidarnos y querernos tanto. Gracias, abuelos, por vuestro cariño, por todo lo que siempre nos habéis dado y por estar orgullosos de vuestros nietos. Muchas gracias a mis padres y a mi hermana por quererme y apoyarme siempre y por creer en mí mucho más que yo misma. Papá, mamá, gracias por haberme inculcado el amor por los libros, el gusto por aprender cosas nuevas y por haberme transmitido una pequeña parte de vuestra capacidad de trabajo y dedicación. Y muy en especial, gracias a Javi por aparecer en mi vida, por ser mi compañero de aventuras y desventuras, por ayudarme a poner los pies en la tierra pero también por soñar conmigo, por compartir esta etapa juntos y porque esto es sólo el comienzo.

LIST OF ABBREVIATIONS

AFM	Atomic force microscopy
BAL	Bronchoalveolar lavage
Chol	Cholesterol
DAG	Diacylglycerol
DHPE	1,2-dihexadecanoyl-*sn*-glycero-3-phosphoethanolamine
DMSO	Dimethyl sulfoxide
DOPC	1,2-dioleoyl-*sn*-glycero-3-phosphocholine
DOPG	1,2-dioleoyl-*sn*-glycero-3-phospho-(1'-rac-glycerol)
DPhPC	1,2-diphytanoyl-*sn*-glycero-3-phosphocholine
DPhPS	1,2-diphytanoyl-*sn*-glycero-3- phosphoserine
DPPC	1,2-dipalmitoyl-*sn*-glycero-3-phosphocholine
DPPG	1,2-dipalmitoyl-*sn*-glycero-3-phospho-(1'-rac-glycerol)
ESR	Electron spin resonance
FDn	Fluorescein isothiocyanate dextran of n KDa
FITC	Fluorescein isothiocyanate
HPLC	High-performance liquid chromatography
IgG	Immunoglobulin G
ITO	Indium-tin oxide
GUV/GV	Giant unilamellar vesicle/Giant vesicle
H_I	Direct hexagonal lipid phase
H_{II}	Inverse hexagonal lipid phase
LB	Lamellar bodies
L_d	Liquid disordered phase (in the presence of cholesterol)
L_e	Liquid expanded phase in monolayers
LF	Lipid fraction of surfactant

L_o	Liquid ordered phase (in the presence of cholesterol)
LUV	Large unilamellar vesicle
L_α	Fluid phase in bilayers
L_β	Gel phase in bilayers
MLV	Multilamellar vesicle
n-PCSL	n-phosphatidylcholine spin label
NMR	Nuclear magnetic resonance
NS	Native surfactant
OE	Organic extract of surfactant
PAGE-SDS	Polyacrylamide gel electrophoresis in the presence of SDS
PC	Phosphatidylcholine
PE	Phosphatidylethanolamine
PF	Hydrophobic protein fraction of surfactant
PG	Phosphatidylglycerol
PI	Phosphatidylinositol
PL	Phospholipids
PLM	Planar lipid membrane
POPC	1-palmitoyl-2-oleoyl-*sn*-glycero-3-phosphocholine
PS	Phosphatidylserine
SDS	Sodium dodecyl sulfate
S_o	Solid ordered phase in monolayers
SUV	Small unilamellar vesicle
TEM	Transmission electron microscopy
T_m	Lipid melting temperature
TM	Tubular myelin

LIST OF FIGURES AND TABLES

Page

FIGURES

TABLES

THESIS ABSTRACT

INTRODUCTION

The respiratory system is responsible for obtaining the energy required to maintain cell functions; in this context, lungs have been evolutionarily designed and optimized to facilitate gas exchange between the atmosphere and the circulatory system. Through the blood-gas barrier, both the oxygen entrance into the blood capillaries and the carbon dioxide release from the bloodstream into the atmosphere take place. It is widely accepted that both processes are produced by spontaneous diffusion, being the amount of gas that diffuses through the tissue directly proportional to tissue surface and inversely proportional to its thickness. Thus, the blood-gas barrier is perfectly adapted to this function: it is extremely thin and has an overall surface of 70 m^2, approximately. This enormous surface is achieved by really high levels of airway ramification, which finally reaches the respiratory units, small and thin-walled air sacs called alveoli. In human lungs, the total number of alveoli could be around 300 millions. Thus, lung structure must be optimized to perform such a physical and mechanical work of continuously renewing the air in contact with that surface. An essential part of lung structure and function is the pulmonary surfactant system, whose main function is stabilizing the air-liquid alveolar interfase during the breathing cycles against the physical forces that tend to collapse it. Deficiencies or alterations in this system are directly related to diverse respiratory pathologies, such as the neonatal respiratory distress syndrome or the acute respiratory distress syndrome, associated with lung damage.

The pulmonary surfactant is a membrane-based material produced and secreted by type II pneumocytes, a specialized cell type from the alveolar epithelium, and consists of a complex mixture of phospholipids, neutral lipids and proteins, which can be obtained from bronchoalveolar lavages of animal lungs. Around 90% of the total surfactant mass corresponds to lipids, including the presence of a large fraction (around 41% of the total mass) of dipalmitoylphosphatidylcholine (DPPC), a phospholipid that is rather unusual in any other tissue, presenting two saturated acyl chains that allow it reaching extremely high levels of lateral packing. A significant fraction of surfactant, around 25%, corresponds to different unsaturated phospholipid species, including another unusual lipid in animal membranes: phosphatidylglycerol, an anionic phospholipid, whose polar head is negatively charged at physiological pH. Besides, there are two families of surfactant-specific proteins: hydrophilic proteins SP-A and SP-D, which play crucial roles in innate defense, and hydrophobic proteins SP-B and SP-C, both essential to regulate the biophysical properties of surfactant membranes, on which the present Doctoral Thesis is focused.

Pulmonary surfactant activity inside the alveoli includes three main processes that have been evolutionarily optimized in order to achieve a proper interfacial behavior: (*i*) transfer of the surface active material from the aqueous hypophase to positions close to the interface, followed by fast adsorption into the interface when alveolar area increases upon inspiration; (*ii*) surface tension reduction to values below 2 mN/m upon lateral

compression during expiration; and (*iii*) efficient re-spreading capacities along the cyclical area changes of the alveolar interface. The components of pulmonary surfactant directly involved in surface tension reduction are phospholipids, specifically DPPC, but in order to achieve efficient adsorption and re-spreading, the presence of hydrophobic proteins SP-B and SP-C has been widely demonstrated to be indispensable.

SP-B is the only surfactant protein strictly required for air breathing, being its lack or deficiency incompatible with life. This small protein exhibits a high lipid affinity and has been proven to promote aggregation, fusion and lysis of phospholipid vesicles *in vitro*, which suggest that it could be involved in lipid remodeling processes required for converting bilayers into interfacial films. Besides, it enhances interfacial adsorption and has been proposed to act as a bridge between bilayers and monolayers, promoting the formation of multilayer surfactant reservoirs during alveolar compression and lipid return to the interfacial films during expansion. SP-B is also responsible for reaching the lowest surface tensions at the air-water interface by an optimal lipid packing and for stabilizing these highly-compressed structures. On the other hand, SP-C is a transmembrane protein whose N-terminal segment is doubly palmitoylated. N-terminal interaction with lipid membranes induces perturbations in lipid packing, so it has been proposed that SP-C could be in charge of disrupting bilayer organization in order to promote interfacial adsorption. Furthermore, SP-C appears to be crucial for maintaining a tight association between the multilayer reservoirs and the interfacial film even at the most compressed states that occur at the end of exhalation.

Together, hydrophobic proteins SP-B and SP-C are essential for the biophysical function of pulmonary surfactant in respiratory dynamics. They appear to have very different, even antagonist effects on their interaction with surfactant membranes, but their concerted action seems to be extremely efficient in terms of surface tension reduction and stabilization of the alveolar air-water interface, and would also impart a rather dynamic character to surfactant membranes.

OBJECTIVES

Pulmonary surfactant proteins SP-B and SP-C are usually considered as lipoproteins due to their extremely hydrophobic character and their profound interaction with the lipid fraction of pulmonary surfactant membranes, and are responsible for the proper biophysical activity of surfactant complexes to stabilize the respiratory surface along breathing dynamics. Nevertheless, the specific molecular mechanisms by which both proteins modulate the behavior of surfactant lipid bilayers and monolayers are not perfectly described, including a large variety of effects on surfactant complexes and model membranes that are closely related to their biophysical function.

The main objective of the present Thesis is to contribute to the understanding of the different effects that hydrophobic proteins SP-B and SP-C originate in lipid membranes and that could be related to their biological function. In particular, the specific objectives addressed in the present work include:

1. Characterization of the native and quasi-native environments of hydrophobic proteins SP-B and SP-C in different surfactant membrane models, in terms of structural complexity and fluidity, and evaluation of the possible impact of both proteins on those membrane properties.

2. Detailed study of the effect of SP-B and SP-C on lipid membrane permeability towards different polar molecules. Electrophysiological characterization of their effects on lipid bilayers subjected to electric potential differences and ion concentration gradients. Proposal of a possible mechanism for the action of both proteins that could be responsible to modulate the permeability of lipid bilayers.

3. Biophysical characterization of the impact of hydrophobic proteins SP-B and SP-C on the mechanical properties of lipid membranes, particularly with respect to bilayer elasticity and how both proteins affect the rupture process of phospholipid membranes subjected to persistent mechanical tensions.

MAIN RESULTS AND CONCLUSIONS

The present work reveals further details on the investigation of pulmonary surfactant proteins SP-B and SP-C and provides new evidences that could help to unravel the possible mechanisms of action and functions of both proteins in their physiological context. Here, the ability of both proteins to impact on membrane structure and connectivity, to modify membrane permeability towards ions and water-soluble molecules and to affect mechanical properties and strength of phospholipid membranes have been investigated by employing different biochemical and biophysical experimental approaches and techniques. A brief summary of the main results and conclusions is presented below.

First of all, different membrane materials obtained from bronchoalveolar lavages of porcine lungs have been characterized, in particular native surfactant complexes, their organic extract, including both the hydrophobic proteins and surfactant lipids, and their different lipid and protein fractions reconstituted as membranes. A characterization of these materials in terms of membrane accessibility and fluidity was performed by employing spectroscopic techniques, in particular, fluorescence spectroscopy and electron spin resonance (ESR), in order to highlight the complexity of the natural system. The presence of SP-B and SP-C in native surfactant complexes and membranes reconstituted from its native lipid species clearly enhances membrane accessibility, apparently with different kinetics and concentration dependence: SP-B was found to be extremely efficient in facilitating the permeability of the fluorescent probe FM1-43, even for subphysiological protein densities (0.1-0.5% w/w), while SP-C showed a more gradual effect both in time and concentration dependence. By employing ESR, subtle differences were observed between native surfactant complexes and membranes reconstituted from its organic extract or the whole lipid fraction in terms of fluidity/lipid mobility. Native surfactant complexes (NS) exhibited lower mobilities than that observed in membranes reconstituted from its organic extract (OE) or lipid fraction (LF) for the whole temperature range analyzed, from 22 to 60ºC, probably due to the native structure and complexity. Besides, a potential effect

of hydrophobic proteins SP-B and SP-C on lipid mobility was detected, since their presence increased lipid packing but only at temperatures lower than 37ºC, the physiological temperature and also the ordered-to-disordered melting temperature of surfactant membranes. Nevertheless, no evidences for clear thermotropic transitions were found when studying the thermal evolution of the spectra obtained from the different materials.

Furthermore, a direct visualization of the different surfactant membrane materials was achieved by transmission electron microscopy, which provided interesting information about their degree of complexity. The most complex structures were those observed in native surfactant complexes, followed by membranes reconstituted from its organic extract and the lipid fraction, in this order. These differences in complexity and multilamerallity among materials can be related to fluidity/lipid mobility observations but do not correspond with different degrees of membrane accessibility, since even the most complex samples have been demonstrated to be highly permeable. Furthermore, SP-B showed a dramatic effect on membrane ultrastructure, creating large inter-bilayer contacts on POPC vesicles that had been subjected to extrusion, apparently reproducing part of the native complexity of surfactant.

A detailed study of model membrane permeability towards different polar molecules in the presence of physiological amounts of SP-B and/or SP-C has been performed by monitoring the entrance of different fluorescently-labeled dyes to giant vesicles by fluorescence microscopy. POPC giant vesicles containing either SP-B or SP-C or their physiological mixture were highly permeable to FM1-43, whose polar character prevents its translocation across pure lipid bilayers, showing a complete labeling of every outer and inner membrane. Those giant vesicles were also permeable to the water-soluble dye calcein, which pointed out to the creation of aqueous pores on phospholipid membranes promoted by the presence of SP-B and SP-C, whose sizes appeared to be rather heterogeneous as assessed by incubating the lipid-protein giant vesicles in the presence of fluorescent dextrans of different molecular sizes. A threshold in dextran permeability was found for membranes containing the whole hydrophobic protein fraction or isolated SP-B: only dextrans with hydrodynamic radii shorter than 1.5 and 4 nm, respectively, were able to permeate. In contrast, SP-C induced membrane permeability towards all tested dextrans, in a higher or lower proportion depending on their molecular size. Also by employing fluorescence microscopy, the localization of hydrophobic proteins SP-B and SP-C on the surface of POPC membranes was achieved by immunolabeling of giant lipid-protein vesicles with fluorescent specific antibodies, which were able to detect intensely fluorescent protein clusters spread across the vesicle surface, especially at regions such as intermembrane contacts, vesicle protuberances or tethers, which could suggest a certain degree of protein aggregation or oligomerization.

Besides, electrophysiology measurements on planar lipid membranes have proven that SP-B and SP-C, both together and separately, are able to induce membrane electroporation even at very low, subphysiological concentrations, upon application of an electric potential difference. Pores created by the whole hydrophobic protein fraction of surfactant or by isolated SP-B or SP-C showed a wide variety of conductance states, from

pS to nS, being difficult to identify characteristic single-channel conductances, although the most frequent conductance values were significantly higher for isolated SP-B and SP-C proteins than for their physiological mixture. Furthermore, pore conductances presented some voltage sensitivity, especially those created in the presence of SP-C. In the presence of different ion concentration gradients and no applied voltage, it has been demonstrated that lipid composition strongly influenced the pore selectivity for anions or cations. A total inversion of the selectivity was found between pores created in electrically neutral zwitterionic bilayers, selective for anions, and in negatively charged membranes, selective for cations, an observation that is consistent with the formation of toroidal or proteolipid pores, in which the hydrophilic parts of both the proteins and the phospholipids structure the pore walls.

Finally, micromechanical studies on SP-B- and SP-C-containing bilayers by micropipette aspiration of giant unilamellar vesicles have been performed by using a high-resolution and computer-controlled setup. They showed that subphysiological amounts of either SP-B or SP-C have very little effect on POPC bilayer elasticity, although a slight rigidification was observed. Besides, the kinetic and thermodynamical analysis of the process of vesicle rupture under increasing mechanical stress suggested the possible existence of a precursor state for bilayer breakdown that has been proposed to be the necessary symmetry break of the molecular organization prior to the creation of a hydrophilic pore and subsequent bilayer breakdown. Furthermore, SP-B was demonstrated to impact dramatically on the failure frequencies of aspirated vesicles by probably enhancing the creation of these pre-pore states or by reducing the line tension at the hole edges, while SP-C showed no significant effects in this process.

A more profound investigation about SP-B and SP-C pore-forming abilities and their effects on mechanical properties of surfactant membranes will allow a better comprehension of the biological system and the interaction between their components, essential for the development of new therapies and the improvement of the current formulations of clinical surfactants designed for the treatment of different respiratory pathologies.

RESUMEN DE LA TESIS

INTRODUCCIÓN

El sistema respiratorio es el encargado de la obtención de la energía necesaria para el mantenimiento de las funciones celulares; los pulmones, en este contexto, son órganos evolutivamente diseñados para optimizar el intercambio gaseoso entre el aire y el sistema circulatorio. A través de la barrera hematogaseosa se produce, por un lado, el paso del oxígeno a los capilares sanguíneos y, por otro lado, la eliminación del dióxido de carbono que se produce como desecho metabólico en el organismo. Es ampliamente aceptado que ambos procesos se llevan a cabo por difusión simple, siendo la cantidad de gas que difunde a través de un tejido directamente proporcional a la superficie del mismo e inversamente proporcional a su espesor. La interfase hematogaseosa está bien adaptada a la función de intercambio gaseoso, puesto que es extremadamente delgada y cubre una superficie total de aproximadamente 70 m^2. Esta gran superficie se logra gracias a un altísimo grado de ramificación de las vías respiratorias, que terminan en unos pequeños sacos denominados alveolos, llegando a existir cerca de 300 millones de alveolos en el pulmón humano. Esta estructura de los pulmones debe estar optimizada para llevar a cabo un trabajo físico y mecánico de tales características, forzando la renovación del aire en contacto con dicha superficie. Una parte esencial de su estructura la constituye una sustancia secretada por el pulmón: el surfactante pulmonar. Su función principal consiste en estabilizar la interfase aire-liquido respiratoria frente a las fuerzas físicas que tienden a su colapso durante los ciclos de inspiración-espiración. Deficiencias o alteraciones en este complejo están en el origen de diversas patologías respiratorias como el síndrome de distrés respiratorio en neonatos prematuros, o el síndrome de distrés respiratorio agudo asociado a daño pulmonar.

El surfactante pulmonar es un material fabricado y secretado por los neumocitos tipo II, un tipo celular especializado del epitelio alveolar, y consiste en una mezcla compleja de fosfolípidos, lípidos neutros y proteínas. Puede ser obtenido a partir de lavados bronco-alveolares de pulmones animales con soluciones fisiológicas. Dentro de los componentes lipídicos, hay que destacar la presencia de una especie fosfolipídica inusual en cualquier otro tejido: la dipalmitoilfosfatidilcolina o DPPC (41%, aproximadamente), que posee dos cadenas de ácido graso saturadas, lo que le permite alcanzar un grado más alto de empaquetamiento lateral que el que aparece en la mayor parte de las membranas de células animales. Por otro lado, la presencia de fosfolípidos insaturados supone alrededor de un 25% de la masa total de surfactante, y también aparece otra especie lipídica poco frecuente en membranas animales, aunque sí aparece en células vegetales: el fosfatidilglicerol (PG), un fosfolípido aniónico, es decir, con una cabeza polar cargada negativamente a pH fisiológico. Además, el surfactante pulmonar posee cuatro proteínas específicas: SP-A, SP-B, SP-C y SP-D, que se dividen en dos familias: las proteínas hidrofílicas, SP-A y SP-D, que tienen un papel fundamental en la defensa innata del pulmón, y las hidrofóbicas, SP-B y SP-C, que son esenciales para regular las propiedades biofísicas de los lípidos del surfactante, y en las cuales se centra la presente Tesis Doctoral.

La actividad del surfactante pulmonar en los espacios alveolares comprende tres procesos principales que han sido evolutivamente optimizados para lograr un adecuado comportamiento biofísico: (*i*) transferencia de material tensioactivo desde la hipofase acuosa hasta las proximidades de la interfase, seguido por la adsorción interfacial de las moléculas activas durante la inspiración; (*ii*) reducción de la tensión superficial hasta valores por debajo de 2 mN/m durante la compresión de la superficie respiratoria que se produce en la espiración; y (*iii*) re-expansión de la película interfacial durante los cambios cíclicos de área que experimenta la superficie alveolar. Los componentes del surfactante directamente implicados en la reducción de la tensión superficial son los fosfolípidos, en concreto la DPPC, pero para que los procesos de adsorción y re-expansión sean eficaces es imprescindible la presencia de las proteínas hidrofóbicas SP-B y SP-C.

La proteína SP-B es, entre todas las proteínas del surfactante, la única indispensable para iniciar la respiración aérea. Posee una alta afinidad por los lípidos y tiene la capacidad de provocar agregación, fusión y lisis de vesículas fosfolipídicas *in vitro*, lo que sugiere que está implicada en la reordenación lipídica necesaria para la conversión de los complejos lipoproteicos en películas interfaciales. Además, acelera la adsorción interfacial y podría actuar como un puente entre bicapas y monocapas, permitiendo la formación de un reservorio de surfactante durante la compresión, así como la vuelta de este material a la interfase durante la expansión del alveolo. Además, esta proteína es imprescindible para alcanzar valores muy bajos de tensión superficial en películas altamente comprimidas, como las que deben formarse al final de la espiración. Por otro lado, la proteína SP-C es una proteína transmembrana cuyo segmento N-terminal se encuentra doblemente palmitoilado. La interacción de dicho extremo con las membranas fosfolipídicas produce perturbaciones en el empaquetamiento de los lípidos, por lo que se ha propuesto que dicho extremo sea el responsable de la actividad de la proteína para promover la adsorción de los lípidos a la interfase. Además, la SP-C sería fundamental para mantener la asociación de los complejos de reservorio de surfactante con la película interfacial en los estados de mayor compresión, alcanzados justo al final de la espiración.

En conjunto, las proteínas hidrofóbicas SP-B y SP-C son esenciales para la función biofísica del surfactante pulmonar a lo largo de la dinámica respiratoria. Parecen tener efectos muy diferentes e incluso antagónicos en su interacción con las membranas de surfactante, pero su acción combinada resulta ser extremadamente eficiente en términos de reducción de la tensión superficial y estabilización de la interfase aire-líquido junto con una gran dinamización de todo el sistema de membranas lipídicas dentro del alveolo.

OBJETIVOS

El principal objetivo de la presente Tesis es contribuir al entendimiento de los diferentes efectos que las proteínas SP-B y SP-C originan en membranas lipídicas y que podrían estar profundamente relacionados con su función biológica. En particular, los objetivos específicos del presente trabajo incluyen:

1. Caracterización de los entornos nativos y cuasi-nativos de las proteínas SP-B y SP-C en distintos modelos de membranas de surfactante pulmonar, en términos de su complejidad estructural y fluidez, y evaluación del posible impacto de ambas proteínas en dichas propiedades de la membrana.

2. Estudio detallado del efecto de las proteínas SP-B y SP-C en la permeabilidad de membranas lipídicas frente a diferentes moléculas polares. Caracterización electrofisiológica de sus efectos en bicapas lipídicas sometidas a diferencias de voltaje y gradientes de concentración iónica. Propuesta del posible mecanismo de acción de ambas proteínas responsable de la modulación de la permeabilidad de membranas lipídicas.

3. Caracterización biofísica del impacto de las proteínas SP-B y SP-C en las propiedades mecánicas de membranas lipídicas, en particular con respecto a la elasticidad de la bicapa y a su posible efecto sobre el proceso de ruptura de membranas fosfolipídicas sometidas a tensiones mecánicas persistentes.

PRINCIPALES RESULTADOS Y CONCLUSIONES

Los resultados que conforman el presente trabajo proporcionan nuevas evidencias acerca de los efectos físicos de las proteínas SP-B y SP-C del surfactante pulmonar que podrían contribuir a un mejor entendimiento de los mecanismos de acción y funciones de ambas proteínas en su contexto fisiológico. En el presente trabajo se ha estudiado mediante distintas técnicas bioquímicas y biofísicas la capacidad de dichas proteínas para influir en la estructura y conectividad de materiales membranosos, para alterar la permeabilidad de membranas fosfolipídicas frente a iones y ciertas moléculas solubles en agua, y para modificar las propiedades mecánicas de dichas membranas. A continuación se detallan los principales resultados y conclusiones que pueden extraerse de los mismos.

En primer lugar, se ha llevado a cabo un estudio de diferentes materiales membranosos procedentes de lavados broncoalveolares de pulmones de cerdo: complejos de surfactante nativo, su extracto orgánico (que incluye los lípidos y las proteínas hidrofóbicas) y sus diferentes fracciones lipídicas y proteicas reconstituidas en forma de membranas. Se realizó una caracterización de dichos materiales en términos de accesibilidad de las membranas desde el medio acuoso, complejidad estructural y fluidez empleando técnicas espectroscópicas, en particular, espectroscopía de fluorescencia y resonancia de espín electrónico (ESR), para analizar la complejidad del sistema natural. La presencia de las proteínas SP-B y SP-C en los complejos de surfactante nativo y en membranas reconstituidas a partir de las fracciones lipídicas del surfactante aumenta notablemente la accesibilidad de todas las membranas presentes en las muestras estudiadas, aparentemente con cinéticas muy diferentes y dependiendo en distinto grado de la concentración de proteína. La proteína SP-B parece ser extremadamente eficiente en aumentar la permeabilidad de membranas de POPC hacia la sonda FM1-43, permitiendo un total acceso casi instantáneo incluso para proporciones de proteína muy por debajo de la fisiológica (0.1-0.5% en peso), mientras que la proteína SP-C muestra un efecto más gradual tanto en función del tiempo transcurrido desde la adición de la sonda como en

función de su concentración en las membranas. Mediante ESR se observaron diferencias sutiles en términos de fluidez/movilidad lipídica entre los diferentes materiales estudiados. Los complejos de surfactante nativo presentan una menor movilidad lipídica/fluidez que la observada en membranas reconstituidas a partir del extracto orgánico o la fracción lipídica del surfactante para todo el rango de temperaturas estudiado, entre 22 y 60ºC, probablemente debido a una mayor complejidad estructural y composicional. Por otro lado, es posible detectar el efecto de las proteínas SP-B y SP-C, que supone un ligero descenso de la movilidad lipídica a temperaturas inferiores a 37ºC, la temperatura fisiológica, que también es la temperatura de transición de los lípidos de surfactante a un estado más fluido. Sin embargo, no se encuentran evidencias de claras transiciones de fase al estudiar la evolución térmica de los espectros obtenidos a partir de los tres materiales estudiados.

Por otro lado, se ha llevado a cabo una visualización directa de los distintos materiales membranosos estudiados mediante microscopía electrónica de transmisión, lo cual ha permitido obtener información acerca de su grado de complejidad. Las estructuras más complejas se encuentran en los complejos de surfactante nativo, seguido por las membranas reconstituidas a partir de su extracto orgánico y su fracción lipídica, en orden descendiente. Estas diferencias pueden estar relacionadas con los distintos grados de fluidez obtenidos, pero no se corresponden con diferencias en la accesibilidad de las membranas ya que los materiales más complejos se ha demostrado que son altamente permeables. Además, la proteína SP-B por sí sola, reconstituida en sencillas vesículas de POPC sometidas a extrusión, es capaz de originar grandes contactos entre membranas y recrear en cierta forma las complejas estructuras existentes en el surfactante nativo.

Así mismo, se realizó un estudio de la permeabilidad de membranas fosfolipídicas muy sencillas frente a distintas moléculas fluorescentes solubles en medios acuosos, y de cómo dicha permeabilidad se ve alterada por la presencia de cantidades fisiológicas de las proteínas SP-B y SP-C, empleando para ello microscopía de fluorescencia. Vesículas gigantes de POPC en presencia de SP-B, SP-C o de la mezcla fisiológica de ambas son altamente permeables frente a la sonda anfipática FM1-43, cuyo carácter polar le impide translocarse entre las hemicapas de una bicapa puramente lipídica, la sonda se inserta casi instantáneamente en todas las membranas que forman parte de las vesículas, tanto internas como externas. Dichas vesículas gigantes son también permeables a sondas polares como la calceína, lo que indica que las proteínas SP-B y SP-C podrían promover la formación de poros en membranas lipídicas. Los tamaños de dichos poros son aparentemente muy heterogéneos, como se ha comprobado mediante ensayos de permeabilidad de las vesículas gigantes frente a dextranos de diferentes tamaños moleculares. La proteína SP-C parece generar un aumento en la permeabilidad frente a todos los dextranos empleados, mientras que la SP-B y la mezcla fisiológica de ambas proteínas sólo permiten el paso de dextranos con radios hidrodinámicos menores a un cierto umbral: 4 y 1.5 nm, respectivamente. También se utilizó la microscopía de fluorescencia para llevar a cabo la localización de ambas proteínas en membranas de vesículas gigantes y la visualización de su distribución en ellas mediante un marcado con anticuerpos fluorescentes, cuyos resultados sugieren la posible existencia de agregados o *clusters* de las proteínas en membranas fosfolipídicas y su

localización en regiones asociadas a cambios estructurales y contactos directos entre membranas.

Por otro lado, se ha demostrado mediante estudios electrofisiológicos en membranas planas que las proteínas SP-B y SP-C, tanto incorporadas conjunta como individualmente en bicapas lipídicas sencillas, son capaces de electroporarlas en presencia de una diferencia de potencial incluso siendo reconstituidas en cantidades muy por debajo de las fisiológicas. Los poros creados por las proteínas mostraron una gran diversidad de niveles de conductancia iónica, desde pS hasta nS, haciendo imposible la identificación de conductancias características de un único canal, aunque los valores encontrados con mayor frecuencia eran significativamente mayores para las proteínas SP-B y SP-C por separado que para su mezcla fisiológica. Las conductancias iónicas de dichos poros mostraban cierta sensibilidad frente al voltaje, especialmente las de aquellos creados por la presencia de SP-C. En presencia de un gradiente de concentración iónica a ambos lados de la membrana y sin voltaje aplicado, se ha demostrado que la composición lipídica y en particular la carga eléctrica presente en las cabezas polares de los fosfolípidos determinan la preferencia de los poros por aniones o cationes: los poros formados en bicapas de lípidos zwiteriónicos son selectivos a aniones, mientras que en presencia de lípidos cargados negativamente, la selectividad se invierte, lo cual es consistente con la formación de los llamados poros toroidales o proteolipídicos, en los que tanto las superficies polares de las proteínas como las cabezas polares de los fosfolípidos estructuran las paredes del poro.

Finalmente, se ha llevado a cabo una caracterización de las propiedades mecánicas de membranas lipídicas mediante la aspiración de vesículas gigantes por micropipeta, técnica mediante la cual se ha observado una ligera disminución en la elasticidad de la bicapa en presencia de cantidades subfisiológicas de las proteínas SP-B y SP-C. Así mismo, gracias al equipo completamente automatizado y de alta resolución espacial y temporal montado y puesto a punto para realizar el presente trabajo, se ha llevado a cabo un estudio cinético y termodinámico del proceso de ruptura de las vesículas sometidas a tensiones mecánicas crecientes. Dicho análisis ha sugerido la posible existencia de un precursor previo a la ruptura de la membrana, interpretado como la necesaria ruptura de simetría en la organización molecular para dar lugar a la formación de un poro hidrofílico y el consecuente fallo en la integridad de la membrana. La proteína SP-B parece afectar significativamente a las frecuencias de ruptura, incrementándolas con respecto a las del lípido puro, posiblemente mediante la generación de un mayor número de sitios de ruptura de simetría en la bicapa o mediante la disminución de la tensión de línea del poro, mientras que la proteína SP-C no parece mostrar efectos significativos en el proceso.

Una investigación más profunda sobre las capacidades de las proteínas SP-B y SP-C para modular la formación de poros y sus efectos sobre las propiedades mecánicas de las membranas de surfactante permitirá seguir avanzando en el conocimiento del papel de estas proteínas en el comportamiento funcional de membranas y películas interfaciales, y muy especialmente en la comprensión de la interacción entre los distintos componentes del surfactante pulmonar, fundamental para el desarrollo de nuevas terapias y la mejora de las formulaciones de surfactantes clínicos actuales para el tratamiento de diversas patologías respiratorias.

1. INTRODUCTION

1.1 THE LUNG: ORIGIN, EVOLUTION AND PULMONARY PHYSIOLOGY

Throughout the evolution and diversification of the vertebrates, over the last 300 million years, lungs have evolved as the specific organs for air breathing with defined characteristics: they are internal structures lined by fluid and filled by gas, which cyclically inflate and deflate. All vertebrate groups have members with lungs, including some fishes and all reptiles, amphibians, birds and mammals, although these lungs can differ in their embryological origin, structure and function among the different animal groups (Daniels and Orgeig 2003). In mammals, the **bronchoalveolar lung** is a branching organ composed by tubes that progressively subdivide, starting from the trachea, bronchi, bronchioles to finally reach the respiratory units, called alveoli, where the respiratory gas exchange takes place. Humans have approximately 480 million alveoli whose mean diameters are around 200 μm (Ochs et al. 2004), which yield an enormous respiratory surface area of around 60 m^2. The respiratory system is responsible for ventilation, consisting of the cyclic process of inspiration-exhalation, and for **gas exchange** between the atmosphere and the bloodstream at the alveoli, where oxygen and carbon dioxide are subjected to passive diffusion by following their concentration gradient, making blood to become oxygenated and carbon dioxide to be removed and exhaled. This respiratory gas exchange takes place through a relatively complex physical barrier which consists of the thin aqueous film lining the alveolus, alveolar epithelial cells, the interstitial layer, endothelial cells forming the blood capillaries, the blood plasma and finally the erythrocyte membrane.

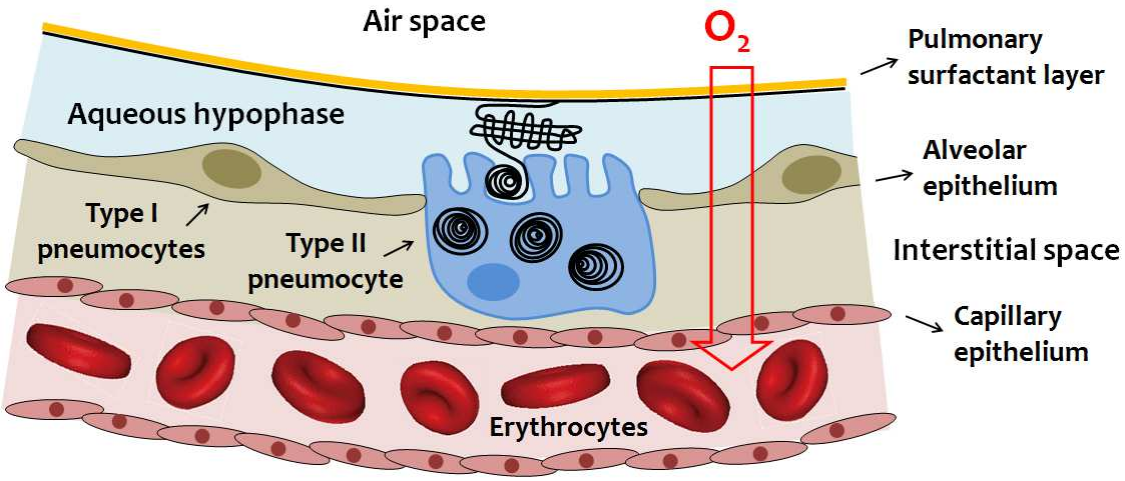

Fig. 1.1: Schematic representation of the respiratory blood-gas barrier.

Focusing on the alveolar epithelial cells, two differentiated types are distinguished: type I and type II pneumocytes. **Type I cells** cover approximately 90% of the total alveolar epithelium and have a squashed shape in order to facilitate gas diffusion. On the other hand, **type II pneumocytes** are the most abundant but, because of their cuboidal shape, only account for around 10% of the alveolar surface area. They are polarized cells, presenting microvilli on their apical surface, and are responsible for the production and

secretion of all the components of the pulmonary surfactant system, among other functions like the production of molecules involved in growth, inflammation, lesion and repair processes of lung tissue, such as cytokines and growth factors. Besides, alveolar macrophages are the third cellular type present inside alveoli, whose main function is maintaining a clean, pathogen-free respiratory surface (West 2008).

Due to the fluid lining inside the alveoli, consequence of cell metabolism, lungs must deal with the appearance of a surface tension at the interface between the fluid hypophase and the air. To cope with this, the so-called **pulmonary surfactant system** is a special material produced by pneumocytes type II that is in charge of eliminating the mechanical forces that tend to collapse the lungs, especially at the end of expiration, when the number of water molecules exposed to the air is minimal. This material was demonstrated to have a single evolutionary origin that preceded the evolution of vertebrates, since specific proteins and organelles belonging to mammalian surfactant have been found in reptiles, birds, amphibians, lungfishes and even in fish swimbladders (Daniels and Orgeig 2001). Lungs were developed as out-pouchings of the gut, being probably the main selection pressure for their evolution the aquatic hypoxia (Perry 1989). Surfactant-producing cells should have migrated with these air-filled gut pouches before surfactant got specialized in their current functions inside lungs during the evolution of air breathing (Daniels and Orgeig 2003).

1.2 PULMONARY SURFACTANT COMPOSITION AND FUNCTIONS

As explained above, the respiratory surface is stabilized by pulmonary surfactant, a complex mixture of lipids and proteins whose main function is minimizing the surface tension at the alveolar air-water interface in order to optimize the mechanics of breathing and avoid alveolar collapse, especially at the end of expiration. Its lack or deficiency is related to different pulmonary disorders and pathologies in newborn, children and adults.

The major components of pulmonary surfactant system are lipids (around 90% by weight, as shown in figure 1.2), including different lipid species: **phospholipids**, specially phosphatidylcholine (PC, approximately 60-70% by weight) and phosphatidylglicerol (PG, around 9%), predominate, but other lipids such as **cholesterol** (up to 8%) and neutral lipids (triglycerides, free fatty acids, around 5%) are also present in this mixture (Goerke 1998). On the other hand, an important surfactant fraction, approximately 10% by weight, is constituted by proteins, including **specific surfactant proteins**, which can be divided in two families: SP-A and SP-D (hydrophilic) and SP-B and SP-C (hydrophobic). SP-A is the most abundant, and is involved, together with SP-D, in innate defense mechanisms at the alveoli, while SP-B and SP-C are involved in the biophysical function of surfactant (Orgeig et al. 2010, Perez-Gil and Weaver 2010).

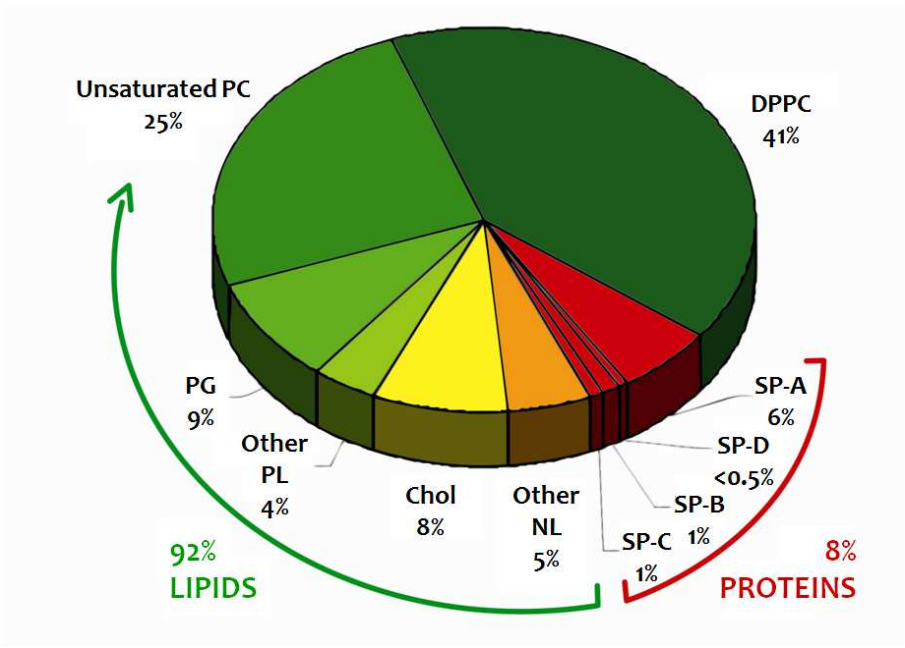

Fig. 1.2: Typical pulmonary surfactant composition, as obtained from bronchoalveolar lavages of mammalian lungs. PL: phospholipids; PC: phosphatidylcholine; DPPC: dipalmitoyl phosphatidylcholine; PG: phosphatidylglycerol; Chol: cholesterol; NL: neutral lipids; SP-A/B/C/D: surfactant protein A/B/C/D.

1.2.1 LIPID FRACTION

Phospholipids constitute the basic building blocks of most biological membranes and, particularly, of pulmonary surfactant. They are amphipathic molecules formed by a polar head and two highly hydrophobic acyl chains. The species that are mainly found in pulmonary surfactant membranes are glycerol-based phospholipids, whose polar region consists of a negatively charged phosphate group bonded to a variable polar group and a glycerol molecule. The polar group characterizes each type of phospholipid and includes zwitterionic groups (with zero overall net charge at physiological pH), such as phosphatidylcholine (PC) and phosphatidylethanolamine (PE), and anionic groups (with negative net charge) like phosphatidylglycerol (PG), phosphatidylserine (PS) and phosphatidylinositol (PI). The glycerol molecule is esterified by two fatty acids, which are hydrocarbon chains of different lengths and saturations and form the hydrophobic region of the phospholipid, as is illustrated in figure 1.3.

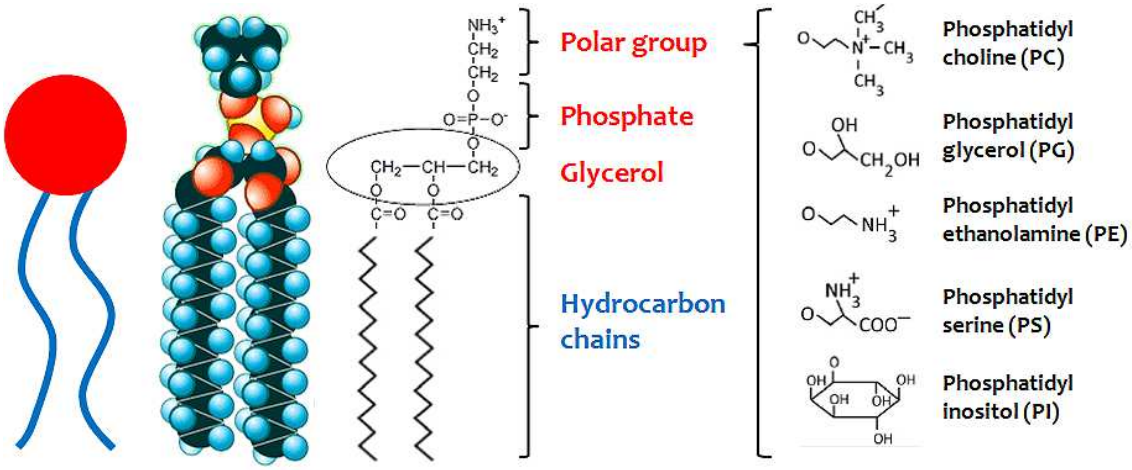

Fig. 1.3: Molecular structure of glycerophospholipids, including both the hydrophobic region (in blue) and the polar region (in red), showing the most common polar groups that can be bonded to the phosphate group in the polar head, which results in the different phospholipid species that can be found in pulmonary surfactant membranes.

1.2.1.1 Membrane self-assembly and lateral pressure profile

The biological importance of phospholipids lies in their special amphipathic character, which satisfy the principle of opposing forces that is needed for stable membrane equilibrium: on the one hand, their aliphatic chains contribute to membrane self-assembly in aqueous media, whose driving force is the hydrophobic effect between them; on the other hand, their polar headgroups interact with water molecules via hydrogen bonds and stabilize the membrane assembly (Marsh 2012). These macromolecular structures may be composed by hundreds of different lipids and proteins and, once self-assembled, the individual molecules interact with each other by different physical interactions, such as van der Waals, electrostatic and hydrophobic forces (Bagatolli et al. 2010). An extremely high interfacial tension between the hydrophobic regions and water creates a trans-bilayer stress profile across the lipid bilayer (Cantor 1997). As can be noticed in figure 1.4, at the polar-apolar interface plane, the lateral pressure turns negative, which is compensated by positive pressures in the headgroup region and among the acyl chains that are due to electrostatic repulsions. Due to the small thickness, approximately 4-5 nm, local variations in lateral pressure can reach even hundreds or thousands atmospheres (Lindahl and Edholm 2000), whereas the net internal pressure has a magnitude in the region of 30-35 mN/m (Marsh 1996).

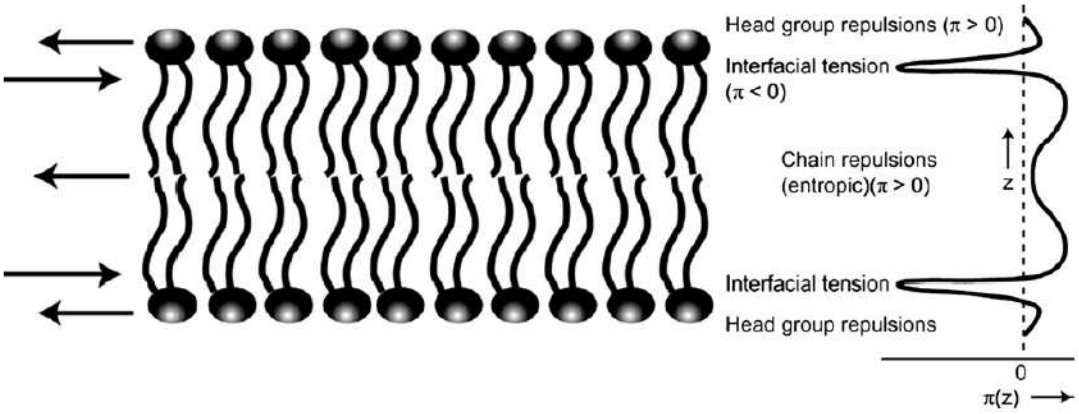

Fig. 1.4: Schematic representation of the lateral pressure (π) profile inside a lipid bilayer as a function of the depth in the membrane (z). Taken from (Bagatolli et al. 2010).

1.2.1.2 Surface activity

Following Laplace's theories, the pressure (*P*) inside a bubble is directly proportional to surface tension (γ) and inversely proportional to bubble radius (*R*): $\Delta P = 2\gamma/R$. This expression is known as Law of Laplace and implies that the smaller the radius is, the higher is the pressure over the bubble walls. Pulmonary alveoli can be considered as very small and interconnected bubbles, surrounded by thin water layers, which following Laplace's Law would be subjected to collapse pressures. Since their size is relatively heterogeneous, the smaller ones would be subjected to higher pressures and would tend to collapse earlier, especially at the end of expiration. The stabilization of the air-water interface would then include the progressive compensation of surface tension reduction coupled with the reduction of alveolar volume, which would be crucial in the context of ventilation. This is the main role played by the protective layer of surfactant that has been optimized along evolution.

Phospholipids, and specially the most predominant phosphatidylcholine, dipalmitoylphosphatidylcholine (DPPC), are responsible for the surface active function of pulmonary surfactant, i.e., for reducing the surface tension at the alveolar air-water interface. As shown in figure 1.5, water molecules establish special dipole-dipole interactions between them, the so-called hydrogen bonding, which are completely equilibrated in all space directions in the bulk of an aqueous phase. However, water molecules that are in direct contact with the gas phase are not able to establish these attractive interactions with the much less abundant gas molecules, so a net cohesive force appears perpendicularly to the air-water interface. Therefore, opening and maintaining this interface requires a certain energy supply to compensate water-water interactions that cannot be established at the interface. This energy, termed **surface tension**, has an approximate value of 70 mN/m in pure water at 37ºC. Since the respiratory surface is subjected to cyclic changes, continuous energy expenditure would be required in order to overcome the surface tension that tends to minimize the interface. The presence of an oriented layer of phospholipids, as is illustrated in figure 1.5, at the alveolar air-water

interface is responsible for a substantial surface tension reduction, since their polar heads are able to establish polar interactions with interfacial water molecules, thus reducing net cohesive forces between water molecules (Wustneck et al. 2005). The higher the concentration of amphipathic molecules at the interface, the fewer the number of water molecules exposed to the air and the lower the surface tension.

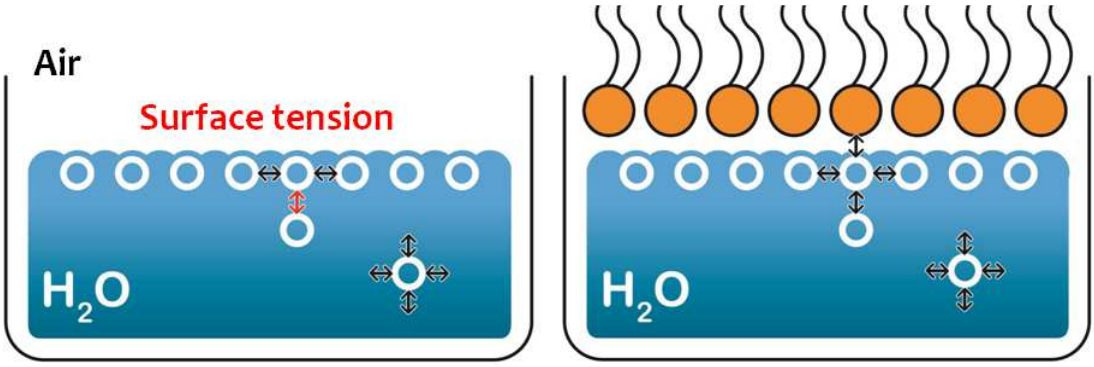

Fig. 1.5: Left, schematic representation of the molecular forces that give rise to surface tension: water molecules establish polar interactions between them, which are spatially equilibrated in the bulk of the aqueous medium but not at the air-water interface, where a net cohesive force appears. Surface tension is ~70 mN/m for pure water. Right, phospholipid monomolecular layer oriented at the air-water interface establishes transient interactions with the interfacial water molecules and thus reduces surface tension.

Fatty acid saturation is fairly important for surface tension reduction: for instance, unsaturated phospholipids such as dioleylphosphatidylcholine (DOPC), palmitoyloleyl phosphatidylcholine (POPC) or dioleylphosphatidylglycerol (DOPG) are esterified by oleic acid (18:1 *cis*-9), which presents a *cis* double bond between carbons 9 and 10, in the middle of the acyl chain. These double bonds cause the chains to bend and also restrict their conformational freedom, so unsaturated phospholipids present "kinks" at those particular chain positions. Unlike saturated phospholipids such as dipalmitoyl phosphatidylcholine (DPPC), which lack double bonds and therefore occupies smaller areas per molecule, unsaturated phospholipids cannot reach sufficiently high packing densities. Upon compression, DPPC can be packed to extremely dense, ordered and stable interfacial monolayers, yielding surface tension values near 1 mN/m (Hawco et al. 1981).

1.2.1.3 Lipid polymorphism

One direct result of the lateral pressure profile is the spontaneous membrane curvature, which appears as a consequence of the imbalance between these opposite forces that creates a net bending moment (Helfrich 1973, Marsh 1996). Thus, different structures result from an optimization of the hydrophobic effect with a variety of intra- and intermolecular interactions combined with several geometric constraints. A simplified way to rationalize the preference for a particular organization is the so-called shape-structure

concept of lipid polymorphism, illustrated in figure 1.6. According to this, most of the phospholipid species, such as phosphatidylcholines (PC), are considered to have a cylindrical shape since the cross-sectional area of the headgroup and the acyl chains are similar. Once self-assembled in the presence of water, they form preferentially flat bilayer structures, also called lamellar phases, where the spontaneous curvature is practically zero (see figure 1.6-B). However, when the cross-sectional areas of the lipid headgroup and acyl chains are rather different, other structures are spontaneously preferred: lipid molecules with headgroup cross-sectional areas larger than that of the hydrophobic region, such as detergent molecules and lysophospholipids, tend to aggregate as micelles, non-lamellar structures that present positive curvature, termed as direct hexagonal phase H_I (see figure 1.6-A). Lipids like diacylglycerol (DAG) and phosphatidylethanolamine (PE), which present a headgroup cross-sectional area smaller than the cross-sectional areas of acyl chains, preferentially form negatively-curved structures such as the inverted hexagonal phase H_{II} (see figure 1.6-C). Thus, the local shape of a membrane depends on the lipids present and their spatial distribution. Other external factors like temperature, pH or pressure can also influence the spontaneous curvature of membranes and determine the overall structure (Tilcock 1986). Furthermore, the insertion of amphiphilic peptides or proteins like gramicidin A, alamethicin, membrane-lytic peptides or viral fusion peptides can promote either positive of negative curvature (Epand 1998, Stachowiak et al. 2012).

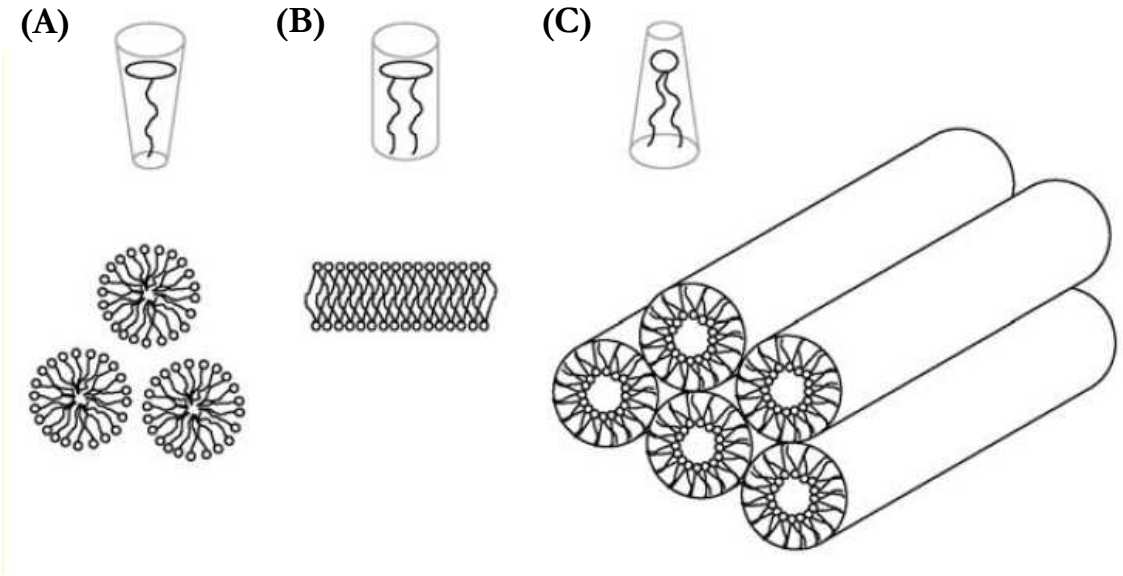

Fig. 1.6: Illustration of lipid polymorphism based on molecular shape. (A) Inverted conical lipids, such as detergents or lysophospholipids, aggregate as positively-curved structures (hexagonal phase H_I) like micelles. (B) Cylindrical-shaped lipids, like phosphatidylcholines (PC), tend to form lamellar bilayer structures. (C) Conical lipids like phosphatidylethanolamine (PE) or diacylglycerol (DAG) preferentially form negatively-curved structures (hexagonal phase H_{II}). Taken from (van den Brink-van der Laan et al. 2004).

1.2.1.4 Lateral organization and lipid domains

Molecular interactions between membrane components originate cooperative phenomena that are the reason not only for the structural self-assembly, but also for the creation of thermodynamic phases and the transitions between phases. The range over which the lipids "feel" each other, in terms of molecular orientation, lipid chain mobility, etc., is given by the coherence length, which measures the range of the local fluctuations in the bilayer plane and becomes specially large near phase transitions (Bagatolli et al. 2010).

Phospholipids present different levels of molecular ordering and mobility as a function of temperature, which are the basis for the so-called main transition: an increase in thermal energy takes the membrane from a more ordered state (gel phase or L_β) to a disordered, more fluid state (liquid phase or L_α), or vice versa in the case of a decrease in thermal energy. The main transition is a first-order phase transition, in which a discontinuity of entropy occurs and hence a latent heat is produced while the temperature of the system stays constant, and the emitted heat can be measured by employing calorimetric techniques. This transition involves a non-infinite coherence length, so the system is in a "mixed-phase" regime in which some parts may have completed the transition while some other parts have not, thus appearing lipid clusters in different phases (Mouritsen and Zuckermann 1985). The precise temperature at which the main transition occurs and both phases L_α and L_β exist in equilibrium is usually termed as melting temperature (T_m), which is higher for saturated species like DPPC (T_m = 41ºC) than for unsaturated phospholipids like POPC (T_m = -2ºC) or DOPC (T_m = -20ºC). If phospholipids are organized in monolayers at the air-water interface, the correspondence to the bilayer phases in terms of order and packing can be achieved also by compression and expansion: at low compressions, areas per lipid molecule are large, configurational freedom of acyl chains is also high and monolayers are in the so-called liquid expanded phase (L_e), similar to L_α in bilayers, while for high compression levels phospholipids can reach a highly packed state, the liquid condensed phase (L_c), whose low mobility is comparable to that of L_β state in bilayers (Nag et al. 1991). By compressing even further, interfacial films can reach extremely ordered states and produce solid-ordered phases (S_o), where molecules have no translational mobility; compression beyond a certain threshold induces film collapse and subsequently the expulsion of material into the air or water bulk phases (Discher et al. 1996).

The presence of cholesterol also modulates lipid packing in biological membranes: its incorporation into phospholipid bilayers or monolayers has a profound impact on membrane lateral structure and dynamics, originating two distinct liquid phases: liquid ordered (L_o) and liquid disordered (L_d) (Mouritsen and Jorgensen 1994, Bernardino de la Serna et al. 2004, Fidorra et al. 2009). Cholesterol partitions preferentially into the L_d phases, decreasing its fluidity in terms of orientational freedom and diffusion coefficient with respect to L_α phases, but also disrupts highly ordered gel phases leading to a more fluid state, the L_o phase (Mitchell and Litman 1998, Veatch et al. 2004). Within a complex mixture of phospholipids with different T_m and cholesterol, density and compositional fluctuations may arise, from the nm- to the μm- scale, in the range of temperatures

between their respective phase transitions, which leads to the coexistence of L_o/L_d phases and the formation of lipid membrane domains. This lateral heterogeneity, that can be found both in bilayers and monolayers, may imply changes in macroscopic properties such as compressibility, bending rigidity, permeability and alter the distribution and organization of membrane proteins and peptides. A large number of experimental evidences has proven this coexistence in, at least, ternary lipid bilayers and monolayers (Veatch and Keller 2003, Bernardino de la Serna et al. 2004, Bagatolli 2006), for example, in giant vesicles prepared from native surfactant, as shown in figure 1.7.

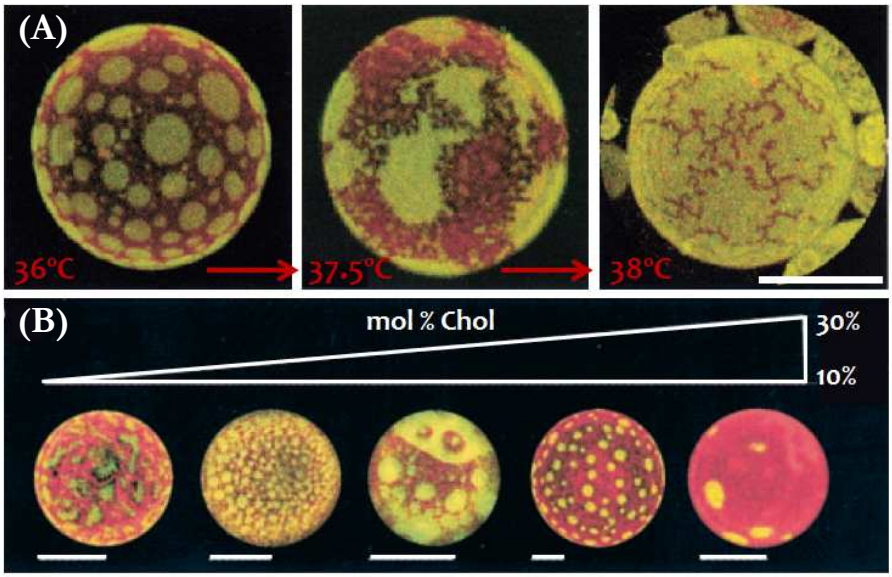

Fig. 1.7: (A) Confocal fluorescence images of giant unilamellar vesicles prepared from porcine pulmonary surfactant native material at the indicated temperatures, where melting and partial merging of two liquid phases, due to a thermotropic phase transition, can be observed. Scale bar = 20 μm. (B) Giant vesicles prepared from natural lung surfactant phospholipid mixtures containing different proportions of cholesterol (10, 15, 18, 21 and 30 % cholesterol in molar ratio with respect to phospholipids). Scale bars = 10 μm. In both sets of images, red fluorescence emission corresponds to the membrane probe $DiIC_{18}$, partinioning preferentially in L_o regions, while green emission comes from BODIPY-PC, which segregates in L_d domains. Taken from (Bernardino de la Serna et al. 2004).

Although the main phospholipid species in surfactant is DPPC, the presence of significant proportions of unsaturated phospholipids (around 25%) and cholesterol (8-10%) in surfactant native membranes reduces the melting temperature to values lower than 41ºC (the T_m of DPPC). Native surfactant therefore exhibits a fluid ordered-to-disordered transition at around 37ºC, the physiological temperature (Bernardino de la Serna et al. 2009), which is clearly observed in figure 1.7-A. Thus, the compositional complexity of surfactant imparts a highly dynamic character to native membranes, which, in the context of lungs, would be naturally maintained at the critical point between two fluid states, permitting large-scale fluctuations and long-range interactions to occur.

1.2.2 PROTEIN FRACTION

Pulmonary surfactant activity inside the alveoli involves different interfacial processes that require three essential properties, represented in figure 1.8: (i) fast adsorption into the interface when alveolar area increases upon inspiration; (ii) surface tension reduction to values below to 2 mN/m upon lateral compression during expiration, which means high compressibility; and (iii) efficient re-spreading capacities along the cyclical area changes of the alveolar interface (Perez-Gil and Keough 1998, Perez-Gil 2002). Pure phospholipid systems have been widely proven to be not good surfactants. Although DPPC is in principle able to reach extremely low surface tensions, its adsorption rate from bilayers in the aqueous hypophase into the air-water interface is extremely slow (Cruz et al. 2000). On the other hand, phospholipids with faster adsorption rates and better spreading abilities, such as unsaturated species, are unable to produce sufficiently low surface tensions when their films are compressed at the interface (Hawco et al. 1981). Conversely, lipid mixtures incorporating the hydrophobic surfactant proteins SP-B and SP-C have been extensively demonstrated to exhibit proper interfacial adsorption, film stability and re-spreading abilities (Serrano and Perez-Gil 2006, Perez-Gil 2008). Consistently with such a crucial role, the lack or deficiency of these proteins is associated with different respiratory pathologies (Wert et al. 2009). The hydrophilic but membrane-associated protein SP-A is not essential for respiratory mechanics, but it has been proven to promote interfacial adsorption as well (Casals et al. 1993).

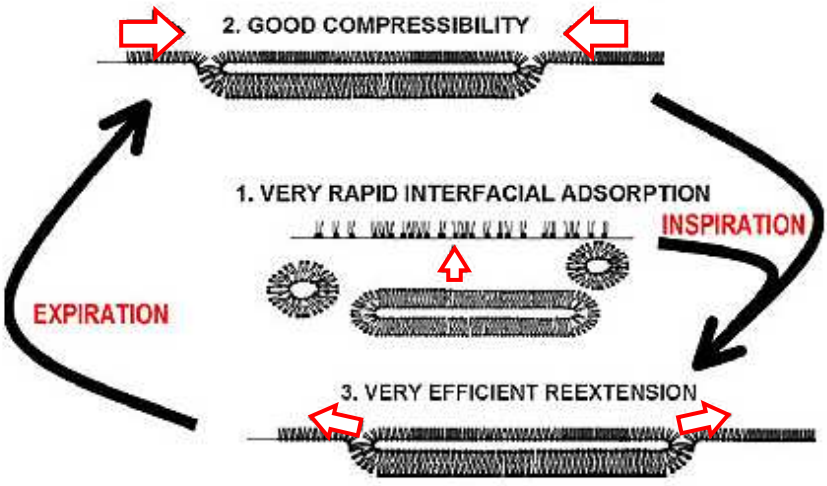

Fig. 1.8: Main processes included in pulmonary surfactant action during the compression-expansion breathing cycles at the respiratory interface. Taken from (Serrano and Perez-Gil 2006).

1.2.2.1 Hydrophilic proteins SP-A and SP-D

Aside from its biophysical function in stabilizing the respiratory surface, pulmonary surfactant has also a crucial role in innate immunity, primarily due to the presence of hydrophilic proteins **SP-A** and **SP-D**, which are responsible for pathogen recognition, binding and clearance of the alveolar spaces (Wright 2003, Ariki et al. 2012). They belong

to the collectin family of proteins and present a common structural pattern, including a N-terminal collagen-like region and a C-terminal lectin domain (see figure 1.9), which is able to bind to carbohydrates, specially oligosaccharides from viral and bacterial outer surfaces. Thus, these proteins have the ability to bind to and agglutinate a wide variety of microorganisms, such as virus, bacteria and fungi, and also allergens and environmental inorganic substrates (Lawson and Reid 2000). Pulmonary collectins also facilitate phagocytosis of these pathogenic entities by macrophages and monocytes in the alveolar spaces and are able to regulate inflammatory cellular responses by binding different stimulators and cell surface receptors (Ariki et al. 2012). In addition, a direct antimicrobial activity has been described for both proteins via membrane permeabilization (Wu et al. 2003). Interestingly, both proteins have been detected in a significant number of non-pulmonary tissues, like uterus, ovary and lacrimal gland in the case of SP-D (Akiyama et al. 2002) or sinus and middle ear mucosa in the case of SP-A (Dutton et al. 1999).

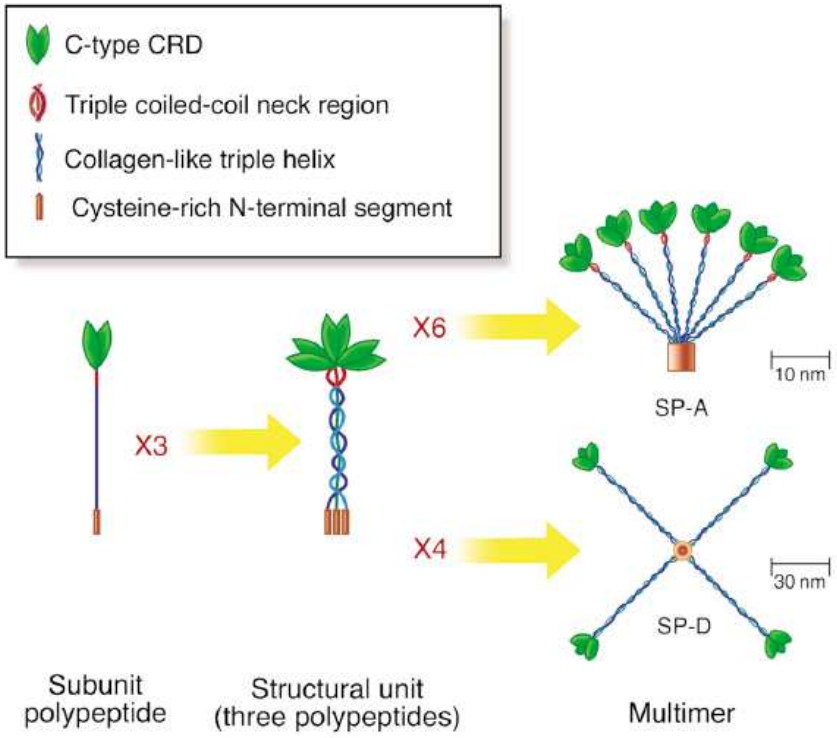

Fig. 1.9: Schematic representation of SP-A and SP-D molecular structures, where common structural features and the carbohydrate recognition domains (CRD) are highlighted. SP-A quaternary structure consists of a hexamer of trimers, while SP-D multimers are formed by tetramers of trimers. Taken from (Wright 2003).

Regarding their membrane-interacting abilities, SP-D is not usually associated with membranes, but it is known to have a crucial role in surfactant homeostasis by regulating the amount of pulmonary surfactant complexes in the alveolar spaces by still unknown mechanisms (Ikegami et al. 2009). On the other hand, SP-A associates with surfactant membranes via its globular carbohydrate recognition domains (CRD) and can promote vesicle aggregation in the presence of calcium (Casals 2001), which can be related to the

activity of the protein to enhance the adsorption of surfactant into the interface (Poulain et al. 1992, Saenz et al. 2007) and to the formation of tubular myelin, a membrane network whose function is still unclear but appears as an intermediate between secreted and interfacially adsorbed surfactant (see section 1.3 for further details). *In vitro* reconstitution of tubular myelin requires the presence of SP-A, SP-B, DPPC and PG (Suzuki et al. 1989).

1.2.2.2 Hydrophobic proteins SP-B and SP-C

SP-B is a 79-residue polypeptide that consists of four or five amphipathic α-helices connected by highly apolar loops, whose sequence contains a high proportion of hydrophobic amino acids (around 40%) and has a molecular weight of 8.7 KDa (Johansson and Curstedt 1997, Wustneck et al. 2005). The complete amino acid sequence of SP-B is shown in figure 1.10-A. SP-B presents 6 cysteines in highly conserved positions that lead to the formation of three intrachain disulphide bonds at positions Cys8-Cys77, Cys11-Cys71 and Cys31-Cys46, while a seventh cysteine (Cys48) creates an intermolecular disulphide bond that leads to the creation of a SP-B covalent homodimer of 19 kDa, the main protein configuration found in surfactant membranes (Hawgood et al. 1998), as sketched in figure 1.10-B. Besides, SP-B exhibits a positive net charge of +7*e*, which yields a preferential interaction with anionic phospholipids (Perez-Gil et al. 1995, Cabre et al. 2012).

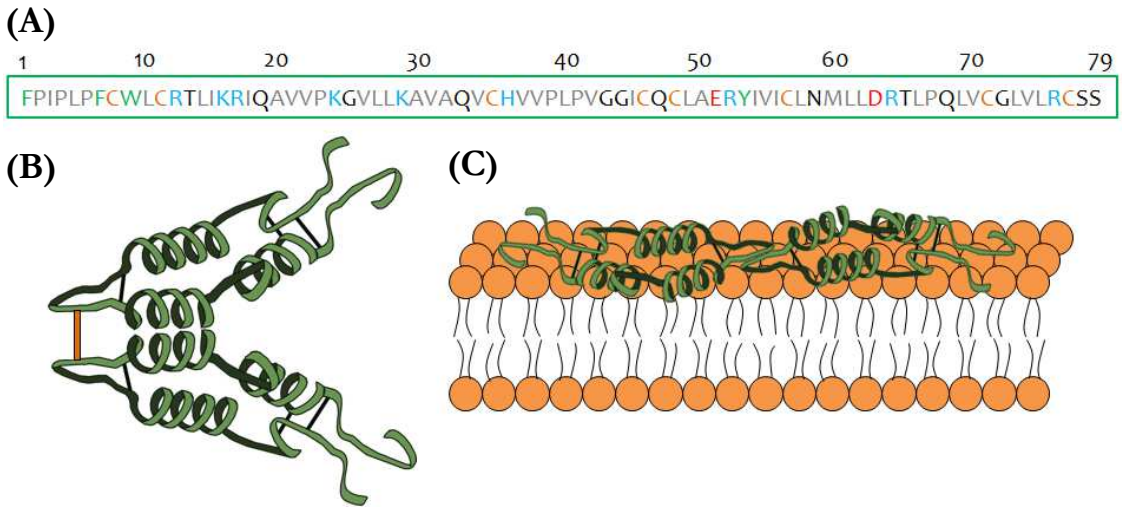

Fig. 1.10: (A) Amino acid sequence of porcine SP-B, where the colors correspond to different types of residues: hydrophobic (grey), positively (blue) and negatively (red) charged, aromatic (green) and cysteines (orange). (B) Structural model of the covalent dimer of SP-B based on its secondary structure estimation, showing the sequence of four α-helices separated by unstructured regions, and the intra- (black) and intermolecular disulphide bonds (orange bar). (C) Superficial orientation of SP-B dimer upon interaction with phospholipid membranes, parallel to the surface near the interface, although a more profound interaction has been also proposed.

Its amphipathic character and the presence of charged residues suggest an interfacial interaction of SP-B with both bilayers and monolayers, mediated by electrostatic

interactions with the phospholipid polar heads, leading a superficial orientation as supported by fluorescence anisotropy studies (Baatz et al. 1990, Baatz et al. 1991), NMR (Morrow et al. 1993) and, more recently, by time-resolved Förster resonance energy transfer, which discarded a deep penetration of the protein in the bilayer core both in POPC and membranes made of the whole surfactant protein fraction (Cabre et al. 2012), as is represented in figure 1.10-C. Nevertheless, a more profound interaction is suggested by other experimental evidences, like the reported acyl chain perturbation in the presence of SP-B that affects the thermodynamic properties of phospholipid membranes, as revealed by differential scanning calorimetry (Shiffer et al. 1993), or a restriction in acyl chain mobility in fluid phase, detected by electron spin resonance in DPPC/DPPG bilayers (Perez-Gil et al. 1995). Different depths of penetration have been proposed to result as a consequence of the occurrence of different modes of SP-B interaction with membranes, since several experimental evidences showed that different degrees of protein insertion depend on the method used to reconstitute SP-B/lipid samples: reconstitution from lipid/protein mixtures in organic solvents yields to a deeper insertion of SP-B than its addition to pre-hydrated phospholipid vesicles (Cruz et al. 1997, Cruz et al. 1998). The preferential distribution of SP-B within the liquid-disordered regions of both bilayers and monolayers has been widely demonstrated, partitioning 8-fold more preferentially than in liquid ordered regions (Nag et al. 1997, Bernardino de la Serna et al. 2004, Jimenez Cabre 2009).

Due to its structural features, SP-B belongs to the saposin-like protein family (SAPLIP), a family of membrane-associated proteins sharing small folds of around 80 amino acids that contain between three and five amphipathic α-helices and have highly conserved disulphide bonds. This family includes several recognized cytolysins and membrane-pore forming structures (Olmeda et al. 2013), but SP-B is the only one which is permanently membrane-associated due to its high hydrophobicity. Due to the fact that SP-B tertiary structure has not been resolved yet, several theoretical models have been proposed by comparing its secondary structure with other proteins belonging to the SAPLIP family. Sequence alignment between SP-B and NK-lysin, a tumor-lysing and antimicrobial polypeptide from the saposin-like family, predicted the existence of four amphipathic α-helices in segments 8-22, 27-38, 42-50 and 67-74 of the sequence separated by unstructured regions, which means that SP-B would be folded in two halves with the α-helices associated by pairs 1-4 and 2-3 (the so-called saposin fold, see figure 1.11-A) and the residue Cys48, which forms the intermolecular disulphide bond, would be located at the hydrophilic surface of helix 3 (Andersson et al. 1995). On the other hand, a model for the three-dimensional structure of the SP-B dimer was generated from the 3D structure of NK-lysin obtained by NMR, resulting in a globular closed saposin fold of five packed helices, including a central non-polar region around strictly conserved and charged residues Glu51 and Arg52 and located between two clusters of positively charged residues (Zaltash et al. 2000). Both residues would be lying at the monomer interface, as is shown in figure 1.11-B, and could create saline bridges between SP-B monomers, besides the disulphide bond at Cys48.

The existence of these reciprocal ion pairs could be related to the non-crucial role of Cys48 for SP-B activity (Ikegami et al. 2002), while proper function of the monomeric protein (a mutated form of Cys48Ser) seems to depend dramatically on monomer concentration (Zaltash et al. 2001), suggesting a potential formation of non-covalent bonds between Glu51 and Arg52 that would stabilize the dimer even in the absence of the disulphide bond. This proposed globular structure could be unfolded upon surface tension increase at the interfacial film, becoming the hydrophobic region totally exposed to the air, and folded again upon monolayer compression (Fullagar et al. 2003).

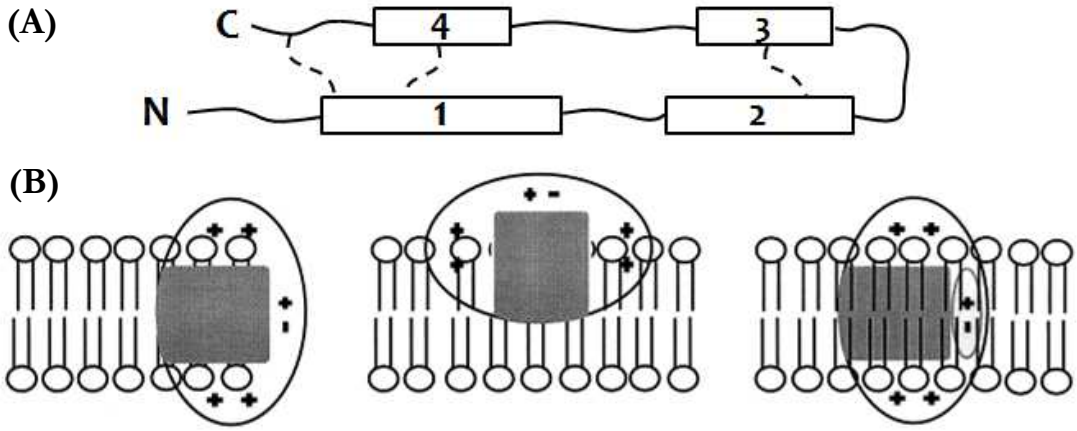

Fig. 1.11: (A) Schematic representation of a SP-B monomer according to the saposin-like topology, where the amphipathic α-helices are shown as rectangles 1-4 with their hydrophobic faces oriented towards the paper and intramolecular disulphide bonds are represented as dashed lines. Based on the model proposed in (Andersson et al. 1995). (B) Possible interactions between SP-B folded globular structure and lipid membranes, where the dimer is represented by the oval symbol, the hydrophobic region by the central grey area and the basic residue clusters are indicated by + signs. The pair + − represents the charged segments Glu51-Arg52 that could be involved in non-covalent bridges between monomers. Taken from (Zaltash et al. 2000).

Interestingly, a high tendency of SP-B to form larger oligomers has been observed (Wustneck et al. 2003), together with the formation of SP-B clusters in highly packed monolayers, associated to the L_c/L_e domain boundaries (Cruz et al. 2004). This observation could be related to the existence of SP-B/SP-B interactions, probably required for the creation and stabilization of multilamellar structures, supported by experimental evidences such as the required presence of SP-B at both sides of membranes in order to promote the formation of multilayer deposits (Cabre et al. 2009).

Regarding SP-B functions, it has been shown that SP-B induces aggregation, fusion and lysis of phospholipid vesicles *in vitro* (Ryan et al. 2005), which has been associated with *in vivo* activities such as lipid transfer between bilayers and monolayers and all the membrane restructuration processes that are required during the metabolic cycle of pulmonary surfactant (Cruz et al. 2000). SP-B, for instance, is known to be essential for the

formation of lamellar bodies (LB), the organelles through which type II pneumocytes assemble, store and secrete pulmonary surfactant membranes (Stahlman et al. 2000) (see section 1.3 for further details). It is also required, together with SP-A, for membrane rearrangement processes converting the onion-like LB particles into net-like structures called tubular myelin (TM) that spread along the alveolar aqueous subphase (Suzuki et al. 1989).

The other hydrophobic surfactant protein, **SP-C**, is the only component of pulmonary surfactant that has been found exclusively in the lung tissue (Weaver and Whitsett 1991). It has been described to be a monomer of 4.5 kDa and 35 residues that forms a single α-helix, 37 Å long, whose central 23 Å segment is highly hydrophobic, formed by aliphatic residues, predominantly valine, as was found by NMR in organic solvents (Johansson et al. 1994). Its amino acid sequence, shown in figure 1.12-B, includes two adjacent cysteines (Cys5 and Cys6) in a palindromic region close to the N-terminal (Ile-Pro-Cys-Cys-Pro-Val), which are both covalently palmitoylated by thioester bonds. Upon reconstitution in phospholipid membranes, as it is pictured in figure 1.12-C, the α-helix shows a parallel orientation with respect to lipid acyl chains, i.e., a transmembrane orientation, as was determined by infrared spectroscopy (Vandenbussche et al. 1992, Vandenbussche et al. 1992). The SP-C N-terminal tail exhibits a higher hydrophilicity although it also interacts with the membrane surface, providing to the protein a net charge of +2 that yields a preferential interaction with anionic phospholipids (Perez-Gil et al. 1995).

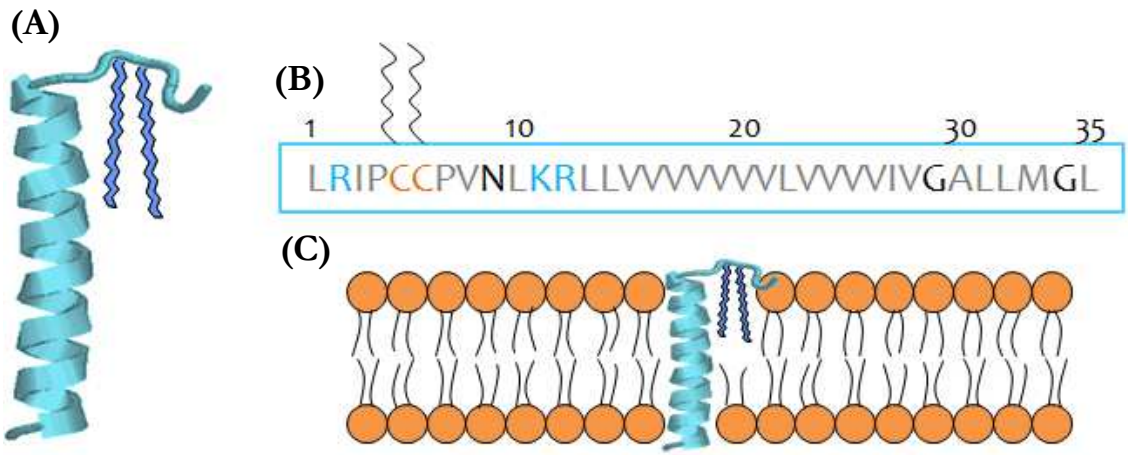

Fig. 1.12: (A) Molecular model of the SP-C monomer, based on the structure obtained by NMR of the protein in organic solvent (Johansson et al. 1994), showing the hydrophobic α-helix, the unstructured N-terminal segment and the two palmitic acids. (B) Amino acid sequence of porcine SP-C, where the colors correspond to different types of residues: hydrophobic (grey), positively charged (blue) and the two palmitoylated cysteines (orange). (C) Transmembrane orientation of SP-C monomer when incorporated into phospholipid membranes.

The double palmitoylation contributes to maintain a tight association of the protein N-terminal with bilayers and interfacial films, in such a way that recombinant SP-C, that lack of palmitic acids, is excluded from the interfacial film during compression more easily than palmitoylated SP-C (Plasencia et al. 2001, Lukovic et al. 2012). Although palmitoylation is not required to promote rapid interfacial adsorption of phospholipids, it was found to be essential to reach very low surface tensions of monolayers at high compression rates, always in the presence of SP-B and cholesterol (Baumgart et al. 2010), probably due to a specific SP-C-cholesterol interaction via its N-terminal, as has been suggested by different experimental approaches (Wang et al. 2005, Gomez-Gil et al. 2009). Palmitoylation is also crucial for the helical conformation of the protein: 70% of native SP-C is structured in α-helices, in contrast to the 60% of recombinant SP-C (Vandenbussche et al. 1992). Related to this, deacylated forms of the protein are easily transformed from α-helices into β-strands by increasing the pH, a mechanism that could be closely related to the amyloid fibril formation involved in alveolar proteinosis (Dluhy et al. 2003).

Regarding its interaction with lipids, SP-C has been determined to partition preferentially into liquid-disordered regions in both bilayers and interfacial films (Nag et al. 1996, Bernardino de la Serna et al. 2004). Besides, SP-C is believed to promote and stabilize membrane-membrane and membrane-interface contacts (Creuwels et al. 1995, Ross et al. 2002), facilitating lipid exchange between bilayers or between bilayers and monolayers, with a likely participation of the N-terminal segment, which has been reported to induce perturbations in lipid packing (Perez-Gil et al. 1992). Recent investigations suggest a possible ability of SP-C to counteract the deleterious effect of cholesterol in surfactant membranes, since excessive amounts of cholesterol impair surface activity, probably via a specific SP-C/cholesterol interaction (Gomez-Gil et al. 2009, Gomez-Gil et al. 2009). Some evidences have been found about the possible dimerization of SP-C in both organic solvents and lipid membranes through certain residues located in its C-terminal, specifically residues 28-34, highly conserved, which could precede formation of larger oligomers (Kairys et al. 2004, Luy et al. 2004).

Together, hydrophobic surfactant proteins SP-B and SP-C are essential for the biophysical activity of pulmonary surfactant. Indeed, the presence of these two proteins is absolutely necessary for an efficient interfacial adsorption, film stability and re-spreading processes of surfactant along the continuous compression-expansion breathing cycles (Serrano and Perez-Gil 2006). It is currently thought that the surface active function of surfactant is critically dependent on the existence of a multilayered film at the air-water interface, whose creation and stabilization would be promoted by the concerted action of SP-B and SP-C on membrane remodeling (Perez-Gil and Weaver 2010), as it is schematized in figure 1.13 and will be explained in further detail in section 1.3.

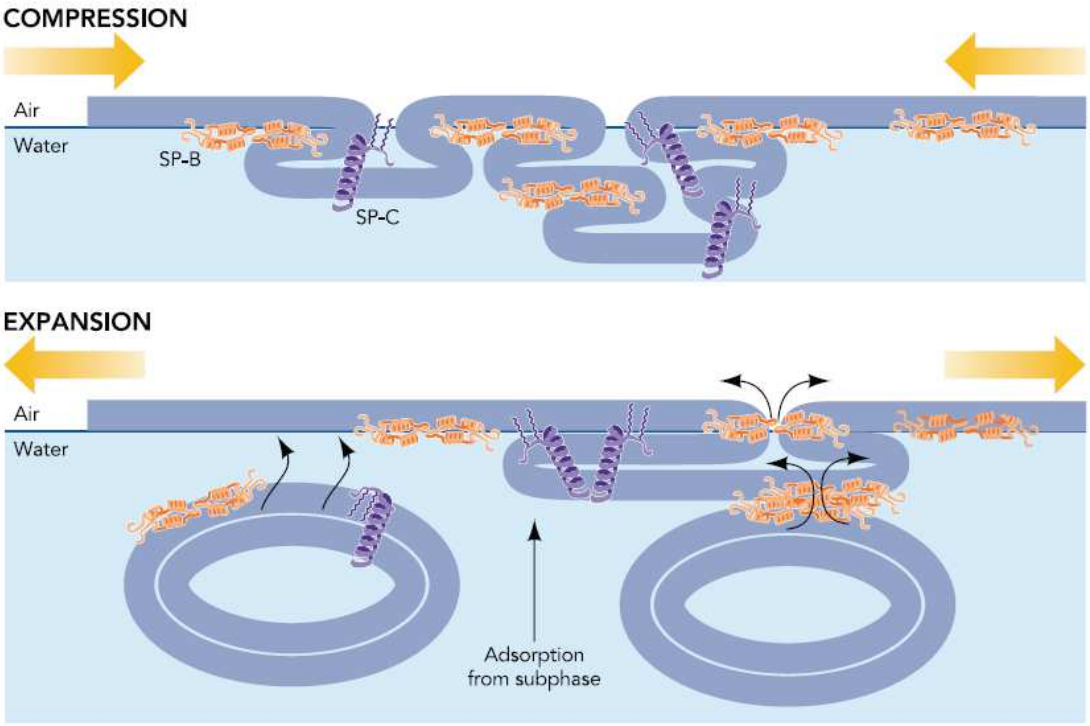

Fig. 1.13: Possible SP-B and SP-C actions during breathing cycles, including promotion of membrane contacts and fusion in order to facilitate adsorption from the alveolar hypophase during inhalation, and stabilization of the interfacial film during exhalation, besides the formation of associated multilayer folds with the material expelled from the interface. Taken from (Perez-Gil and Weaver 2010).

1.3 PULMONARY SURFACTANT METABOLISM

In order to accomplish its crucial role in respiratory physiology, pulmonary surfactant is subjected to different processes, including the production and synthesis of all its components, the assembly of membrane complexes, their secretion into the alveolar hypophase and the morphological transformations that lead to its adsorption, re-adsorption and final recycling, which all constitute the so-called lung surfactant "metabolism".

First, pulmonary surfactant complexes are assembled in type II pneumocytes, including the whole lipid fraction and hydrophobic proteins, and is stored as tightly packed membranes forming spherical structures known as **lamellar bodies** (LB) (Goerke 1998). Surfactant lipids are synthesized in the endoplasmic reticulum of type II cells and transported to the LB via different pathways, where they are assembled (Perez-Gil and Weaver 2010). Proteins SP-B and SP-C are synthesized as large precursors also in the endoplasmic reticulum and subjected to further processing through the Golgi, multivesicular bodies and lamellar bodies, until both proteins reach their mature forms and are correctly inserted in membranes, after several proteolytic steps coupled with a progressive acidification of exocytotic compartments (Beers 1996, Weaver 1998, Serrano et al. 2007). An antimicrobial activity has been described for the N-terminal propeptide of the precursor form of SP-B (proSP-B) thanks to the presence of another saposin-like protein

domain (Yang et al. 2010), which is secreted to the alveolar spaces after proSP-B processing, so it could be involved in innate host defense of the lung. Interestingly, SP-C processing to its mature form strictly requires the correct expression of SP-B in type II cells, probably related to SP-B lytic and fusogenic activites, which would make possible the access of proteases to the lumen of multivesicular bodies during the last steps in SP-C maturation (Weaver and Conkright 2001). Regarding SP-A, the third membrane-associated surfactant protein, it is mainly secreted into the alveolar hypophase by a different pathway, since only around 8% of total SP-A was found associated to LB (Ravasio et al. 2010).

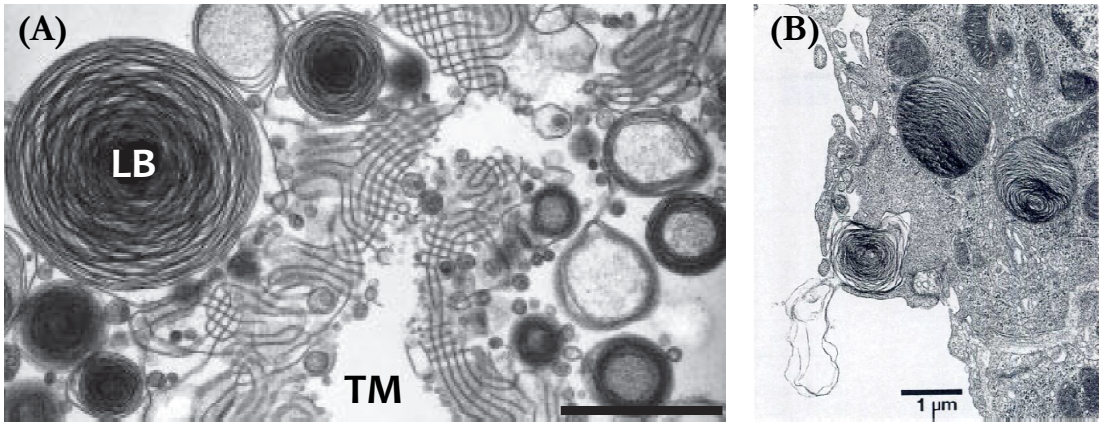

Fig. 1.14: (A) Electron micrograph section of secreted surfactant in lavages from rat lung, where lamellar bodies (LB) and tubular myelin (TM) are observed; the scale bar represents 1 μm. Taken from (Goerke 1998). (B) Lamellar body exocytosis by a type II pneumocyte in an adult rat lung, taken from (Rooney et al. 1994).

Lipid and protein assembly into the tightly-packed structure of lamellar bodies could be possible thanks to SP-B-promoted membrane-membrane interactions, widely described *in vitro* (Poulain et al. 1996, Cruz et al. 1997, Cruz et al. 2000). However, a different membrane protein has been found to be absolutely essential in LB biogenesis, called the ATP-binding cassette transporter A3 (ABCA3), which belongs to the family of membrane transporters that use ATP energy in order to pump molecules across membranes. ABCA3 is probably a lipid translocase responsible for pumping phospholipids across the limiting membrane of LB in order to promote a progressive accumulation of lipids into the inner leaflet, which is relaxed upon creation of membrane invaginations into the LB lumen (Ban et al. 2007, Cheong et al. 2007). Genetic deficiencies in ABCA3 lead to the absence of LB and fatal respiratory distress in newborns (Shulenin et al. 2004). Nevertheless, mature SP-B seems to be also crucial for LB formation, specially for reaching the extremely high levels of membrane packing found in native LB, since in the presence of ABCA3 but absence of SP-B membranes result loosely packed. Thus, a concerted action of ABCA3 and SP-B has been proposed in order to explain the tight packing of parallel or concentric membranes inside LB, which could be the driving force for an extremely fast membrane unravelling and adsorption to the interface (Perez-Gil 2008). As a matter of fact, surfactant complexes purified from bronchoalveolar lavages present slower kinetic rates of adsorption than LB directly obtained from type II cell cultures (Ravasio et al. 2010).

Via membrane fusion between the limiting membrane of LB and the plasma membrane of type II pneumocytes, LB are secreted to the alveolar hypophase (see figure 1.14-B), preceding the unpacking of these dense membrane structures that could be due to several effectors, such as changes in surface tension, hydration, pH or calcium concentration (Perez-Gil and Weaver 2010). Some experimental evidences have revealed that these highly packed membranes can be adsorbed spontaneously to the interface without passing through any intermediate state of loose packing (Haller et al. 2004). Nevertheless, some other extracellular structures have been found in the aqueous hypophase; a significant fraction of secreted surfactant rearrange in a lattice-like structure called **tubular myelin** (TM), shown in figure 1.14-A, consisting of square membrane networks of proteolipid tubes, showing a periodic lattice constant of around 40 nm (Nag et al. 1999). These dimensions are related to the molecular size of SP-A macromolecule, in such a way that, by genetic modifications in order to manipulate its size, the TM network dimensions change accordingly (Palaniyar et al. 2001). It was demonstrated that *in vitro* reconstitution of TM requires the strict presence of five components: phospholipids DPPC and PG, proteins SP-A and SP-B and calcium (Suzuki et al. 1989). In the current model for TM architecture, represented in figure 1.15, SP-A macromolecule would be creating the lattice squares by SP-A/SP-A interactions, while SP-B would be supporting or facilitating membrane-membrane interactions, probably followed by membrane fusion (Perez-Gil 2008). A direct conversion between LB and TM is suggested by several electron micrographs, where a continuity between spherical and lattice structures have been observed (Williams 1977). Despite its unusual structural features, no specific role in surfactant activities has been described for TM up to now.

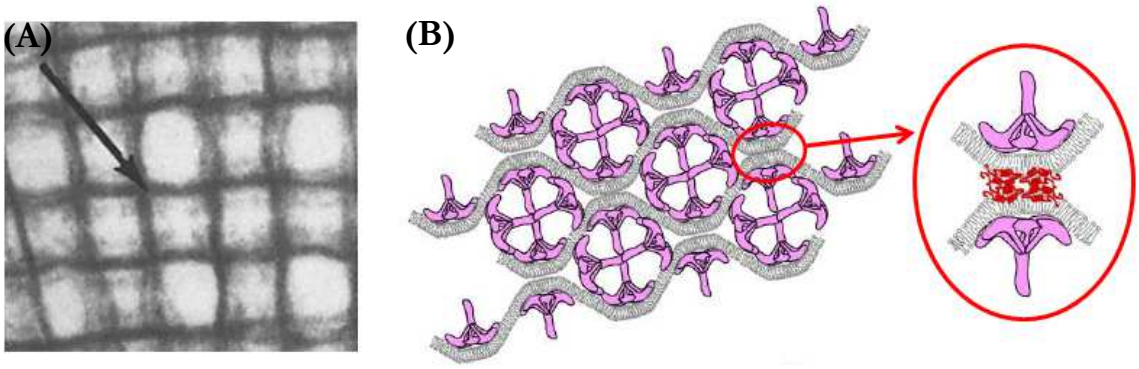

Fig. 1.15: (A) Electron micrograph at high magnification (×121000), showing a detail of small densities protruding from the corners of the TM network, taken from (Williams 1977). (B) Model for possible TM molecular assembly, based on SP-A/SP-A interactions mediating membrane coupling and SP-B/SP-B interactions promoting membrane contacts and maybe fusion. Modified from (Perez-Gil 2008).

Once the surfactant material is secreted and unpacked in the aqueous hypophase, the adsorption of these lipoprotein complexes to the air-water interface occurs very rapidly in order to stabilize it against the mechanical forces that tend to collapse the alveolus. As it was previously explained, the most crucial moment is the end of expiration, when pressure

reaches its maximum value and surface tension must be reduced near to 0 mN/m (Goerke 1998). The absence of double bonds in DPPC allows achieving extremely high packing levels in films subjected to compression, and therefore to reduce surface tension to extremely low values, in contrast to the other phospholipid species present in surfactant. According to this, the classical model for surfactant compression is based on a selective exclusion of low compressible compounds from the alveolar interface, through the so-called squeeze-out model, in order to get a DPPC-enriched film in solid-ordered phase during expiration (Watkins 1968, Clements 1977). As a matter of fact, the multilayer formation from monolayers of bovine lung surfactant extract subjected to high surface pressures has been recently studied, revealing that multilayers protrude from L_d phases and L_o/L_d edges and that they are enriched in unsaturated phospholipids, while saturated species mainly stay in the air-liquid interface (Keating et al. 2012). Nevertheless, the mechanisms by which these hypothetical lipid sorting could be possible are unclear, and some experimental data suggest that sufficiently fast compressions of fluid monolayers are able to reach surface tension lower than 5 mN/m (Smith et al. 2003). These supercompressed fluid films become metastable and show slow rates of relaxation, meaning that at low surface tensions, their viscosities increase dramatically, similarly to supercompressed liquids, and thus they could acquire the rheological properties of a solid. Therefore, unlike pure DPPC monolayers in the classical model, a metastable supercompressed fluid film would require no compositional change (Rugonyi et al. 2008).

With a selective lipid exclusion from the interfacial monolayer or not, the existence of multilayer stacks associated to the interface has been widely demonstrated by electron microscopy of alveolar secreted material (Schurch et al. 1995, Bachofen et al. 2005). These surface-associated structures could act as reservoirs of surface active molecules involved in the respiratory dynamics, including the participation of SP-B and SP-C in its formation, stability and recycling (Perez-Gil and Keough 1998, Veldhuizen and Haagsman 2000). Langmuir balance experiments together with AFM imaging have shown that both SP-B and SP-C facilitate reversible compression-driven transitions from bilayers to interfacial films, promoting the creation of these multilayered films at the interface: overcompressed lipid/SP-C films are able to create multilayers that remain associated to the interfacial monolayer, probably acting as lipid reservoirs for the compression-expansion cycles (Kramer et al. 2000), while SP-B apparently promotes the formation of bilayer patches associated to the interface (Krol et al. 2000) and the establishment of large membrane-membrane contacts in multilayered structures that, in the presence of phase segregation, show a high cohesivity (Bernardino de la Serna et al. 2013). In recent investigations, the differential role of both proteins have been analyzed in terms of surface activity and mechanical stability, and it was clearly demonstrated that SP-B is responsible for reaching the lowest surface tensions at the air-water interface by an optimal lipid packing and for stabilizing these highly-compressed structures; on the other hand, SP-C appears to negatively influence film stability, pointing out to a significant destabilizating effect that is interestingly reversed in the presence of SP-B (Schurch et al. 2010). Therefore, the concerted effect of both proteins may achieve the required surface tension reduction and film stability but would also impart a rather dynamic character to the lipid multilayers reservoirs, which are illustrated in figure 1.16.

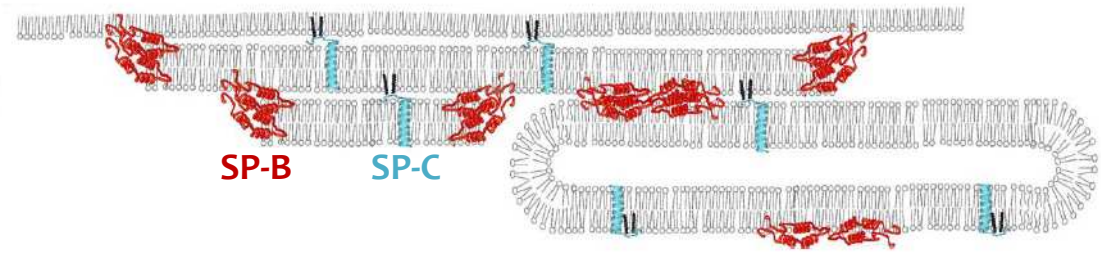

Fig. 1.16: Model of associated multilayers structures in pulmonary surfactant, promoted and stabilized by SP-B and SP-C. Taken from (Perez-Gil 2008).

In order to avoid surfactant accumulation in the alveolar spaces, secretion must be balanced by removal and recycling. Around 90% of lung surfactant is internalized via endocytosis by type II pneumocytes (Wright and Clements 1987), and the molecular compounds, both lipids and proteins, are recycled and stored again in LB. The remaining material is constituted by less active lipoprotein complexes, maybe inactivated by changes in lipid/protein organization, lipid and protein oxidation or incorporation of inhaled molecules, and are captured and degraded by alveolar macrophages (Perez-Gil and Weaver 2010). It has been proposed that proteins SP-A, SP-B and SP-C promote lipid recycling, since their presence is related to an enhancement of lipid uptake by type II cells (Weaver and Whitsett 1991). Regarding SP-D, its role in regulating alveolar pool size have been clearly demonstrated: the interaction between this collectin and phospholipid PI present in surfactant complexes alters surfactant structure and enhances their uptake by type II cells, but not macrophages (Ikegami et al. 2005, Ikegami et al. 2009).

1.4 SURFACTANT-RELATED PATHOLOGIES

Pulmonary surfactant alteration or deficiency can be associated to inflammation processes and respiratory dysfunction, usually leading to diverse syndromes and pathologies where the loss of surface-active, anti-inmflammatory and anti-pathogenic properties of surfactant could all contribute. One of the most important pathologies related to pulmonary surfactant is the so-called neonatal respiratory distress syndrome (NRDS). Lungs are the last organs to be developed during gestation; for instance, around 10% of premature newborns born before 29 weeks of gestation are affected by NRDS, which is caused by structural immaturity in the lungs and surfactant deficiency (Meyer and Zimmerman 2002). This syndrome is characterized by reduced amounts of phospholipids, SP-A, SP-B and SP-C in the alveolar spaces, causing an increase in the minimum surface tension and therefore respiratory distress. The usual treatments to prevent or revert NRDS are the promotion of lung maturation by the preventive administration of glucocorticoids or the supplementation of an exogenous surfactant, and mortality has been drastically reduced in the last years (Rushing and Ment 2004). Interestingly, therapeutic surfactant currently in use are usually purified from animal sources and sometimes modified with specific components to improve their surface activity (Blanco and Perez-Gil 2007). Besides

NRDS, exogenous surfactant application has been demonstrated to be also useful for the treatment of chronic bronchitis (Anzueto et al. 1997).

Also related to surfactant alterations, acute respiratory distress syndrome (ARDS) can appear in both adult and infant lungs as a consequence of acute lung injury, and it is characterized by inflammation that leads to alveolar and vascular damage, surfactant inactivation, atelectasis (alveolar collapse) and alterations in the gas exchange, yielding to hipoxemia and organ failure (Dushianthan et al. 2011). Surface active proteins from blood serum compete with lung surfactant for the alveolar interfaces and surfactant function is inhibited, increasing surface tension values since serum proteins are not as efficient as surfactant for surface tension reduction. Similar to ARDS, the meconium aspiration syndrome (MAS) occurs when a newborn inhales his first stool before or during delivery due to prenatal stress. Meconium is mainly composed by cholesterol and bile acids, which alters the surface properties of lung surfactant and compete with it to occupy the interface, yielding surfactant inhibition (Lopez-Rodriguez et al. 2011). Supplementation therapies with exogenous surfactants have not been successful in the treatment of these syndromes, but new strategies are being designed for surfactant reactivation after inhibition, such as exposure of therapeutic surfactants to different polymers such as hyaluronic acid (Lopez-Rodriguez et al. 2012).

On the other hand, several pathologies are not related to external agents but to congenital deficiencies in surfactant protein expression, which could lead to surfactant dysfunction (Weaver and Beck 1999, Nogee et al. 2000, Nesslein et al. 2005). For instance, idiopathic pulmonary fibrosis (IPF) consists of an intrinsic modification of surfactant composition, being unable to reach the minimum surface tension values required during respiration. It is a rare lung disease but dramatically induce chronic damage to pulmonary epithelium, ultimately causing the growth of fibrotic tissue inside alveoli. It has been related to mutations in genes encoding SP-A and SP-C (Kropski et al. 2013) and to the presence of very low concentrations of SP-B, SP-C and PG, together with an increase of PI and sphingomyelin (Gunther et al. 1999, Gunther et al. 1999). In this case, therapies with exogenous surfactants have been proposed to avoid cellular damage due to high surface tensions.

In general terms, severe SP-B deficiency, i.e., over 75% reduction of its total content in alveolar airspaces, results in fatal respiratory distress syndrome like in the case of alveolar proteinosis, indicating that SP-B is strictly required for postnatal lung function (Nogee et al. 1993, Nogee et al. 1994, Melton et al. 2003). Surprisingly, SP-C lack or dysfunction is not as critical as SP-B, and animals can breath and survive (Glasser et al. 2001), although it has been related to chronic and severe respiratory pathologies associated with emphysema and intracellular lipid accumulation in type II cells (Glasser et al. 2003) and pulmonary fibrosis, suggesting that SP-C could inhibit collagen accumulation and lung inflammation (Lawson et al. 2005). Apparently, SP-B is sufficient for surfactant function in vivo, but the conservation of SP-C among species and several experimental evidences suggest an important function of SP-C for an efficient stabilization of the respiratory epithelium at long term.

2. OBJECTIVES

Pulmonary surfactant proteins SP-B and SP-C are usually considered as lipoproteins due to their extremely hydrophobic character and their profound interaction with the lipid fraction of pulmonary surfactant membranes, and are responsible for the proper biophysical activity of surfactant complexes to stabilize the respiratory surface along breathing dynamics. Nevertheless, the specific molecular mechanisms by which both proteins modulate the behavior of surfactant lipid bilayers and monolayers are not perfectly described, including a large variety of effects on surfactant complexes and model membranes that are closely related to their biophysical function.

The main objective of the present Thesis is to contribute to the understanding of the different effects that hydrophobic proteins SP-B and SP-C originate in lipid membranes and that could be related to their biological function. In particular, the specific objectives addressed in the present work include:

1. Characterization of the native and quasi-native environments of hydrophobic proteins SP-B and SP-C in different surfactant membrane models, in terms of structural complexity and fluidity, and evaluation of the possible impact of both proteins on those membrane properties.

2. Detailed study of the effect of SP-B and SP-C on lipid membrane permeability towards different polar molecules. Electrophysiological characterization of their effects on lipid bilayers subjected to electric potential differences and ion concentration gradients. Proposal of a possible mechanism for the action of both proteins that could be responsible to modulate the permeability of lipid bilayers.

3. Biophysical characterization of the impact of hydrophobic proteins SP-B and SP-C on the mechanical properties of lipid membranes, particularly with respect to bilayer elasticity and how both proteins affect the rupture process of phospholipid membranes subjected to persistent mechanical tensions.

3. MATERIALS AND METHODS

3.1 PURIFICATION OF MATERIALS FROM ANIMAL SOURCE

3.1.1 ISOLATION OF PULMONARY SURFACTANT FROM PORCINE LUNGS

Native complexes of pulmonary surfactant and its protein and lipid fractions were obtained from bronchoalveolar lavages of porcine lungs, following a methodology optimized at the laboratory (Curstedt et al. 1987, Casals et al. 1989, Taeusch et al. 2005). Porcine lungs were obtained from recently slaughtered pigs in the slaughterhouses of Guadalix de la Sierra and Mercamadrid (Madrid), and were transported in ice to the laboratory, where they were immediately processed.

In order to extract the bronchoalveolar lavage of each pair of lungs, 2.5 liters of cold 5mM Tris buffer, pH 7, 150 mM NaCl, were introduced by the trachea, and after massaging the lungs, the saline solution was poured into a flask, filtering it with a gauze to separate the tissue debris. These lavages were subjected to several centrifugations, the first of them at 1000 g, 4ºC for 5 minutes (Sorvall 2T centrifuge, GSA rotor, 2000 rpm) in order to remove cells and tissue remains. The supernatant, the **bronchoalveolar lavage (BAL)** free of cells, was stored at -20ºC.

Subsequently, the pulmonary surfactant was purified from the BAL by centrifuging it at 100000 g for 1h at 4ºC (Beckman ultracentrifuge, 70 Ti angular rotor, 31000 rpm, K-factor 208.9), discarding the supernatant that mainly contains the small surfactant aggregates. The pellets were subjected to a new centrifugation, this time in a density gradient of NaBr/NaCl, in order to separate surfactant from potential blood contaminants; to this end, the pellets were first homogenized and resuspended in NaBr 16% NaCl 0.9%. A volume of 4 ml of this suspension was placed at the bottom of a centrifuge tube (SW40 Beckman); carefully, 6 ml of NaBr 13% NaCl 0.9% were placed just above, and finally, 2.5 ml of NaCl 0.9% at the top of the tube. This way, a discontinuous density gradient was created, which allowed to separate the surfactant complexes from the rest of material, with a higher density, mainly rests of erythrocytes. The tubes were centrifuged in a swinging bucket rotor (SW40 Ti, 120231 g, K-factor 325) at 26000 rpm for 2h at 4ºC, with no brake in order to avoid disruptions in the gradient. Thus, a more or less compact band of material was obtained between the first two layers of the gradient, which was extracted and homogenized in NaCl 0.9% to obtain what has been considered along this Thesis as the **native surfactant (NS)**. After volume aliquoting, it was stored at -80ºC.

3.1.2 ORGANIC EXTRACTION OF NATIVE SURFACTANT

The hydrophobic fraction of surfactant, containing all surfactant lipids and proteins SP-B and SP-C was obtained by extraction of purified NS with organic solvents. The organic extraction was based in the methodology described by Bligh and Dyer (Bligh and Dyer 1959). First, native surfactant samples were mixed with an equal volume of chloroform and two volumes of methanol (HPLC grade, Scharlau), vortexed for 30 seconds and heated up to 40ºC for 30 minutes in order to induce the flocculation of

hydrophilic proteins. Afterwards, one volume of water and one volume of chloroform were added, and the samples were centrifuged at 3000 g, 4ºC, for 5 minutes. After each centrifugation, a biphasic system was obtained, keeping aside the organic phases (bottom) and mixing the aqueous phases (top of the tube) with two volumes of chloroform, which was centrifuged again. This centrifugation step was repeated three times, and the aqueous phase resulting of the last centrifugation step was discarded, while the mixture of the organic phases were kept and washed with a small volume of 0.15M KCl (around 25% of total volume) in order to eliminate possible water traces. Finally, the **organic extract (OE)** obtained this way, dissolved in chloroform/methanol 2:1 (v/v), was stored at -20ºC.

3.1.3. PURIFICATION OF HYDROPHOBIC PROTEINS SP-B AND SP-C

3.1.3.1 From porcine bronchoalveolar lavages

After the organic extraction of surfactant, the following step was to separate their different components. First, a certain volume of organic extract was concentrated to the desired final volume, around 0.5 ml, and it was subjected to a size-exclusion chromatography in a Sephadex LH-20 gel (GE Healthcare, column dimensions 73 × 2.9 cm), eluted in chloroform/methanol 2:1 (v/v) solution. This technique leads to the separation of molecular species with different sizes or, more specifically, hydrodynamic radii, thanks to the fact that the gel, consistent of polymer beads, creates a three-dimensional porous network through which the mobile phase flows: the pore size is selected in order to achieve that the large molecules could not flow through them, while the small ones diffuse inside the matrix. The smaller a particle is, the longer their way through the column is, so a final elution of molecules in decreasing order of hydrodynamic radii is achieved. In the case of Sephadex LH-20, its hydrophobic character lead to simultaneous phenomena, such as the molecular adsorption to the matrix, that also influences the diffusion process.

The eluent was collected in 1 ml fractions using an automatic fraction collector, and the chromatographic profile was obtained by measuring the absorption of each one of the fractions at two different wavelengths, λ = 240 y 280 nm, with a UV/visible spectrometer Beckman DU840. A series of peaks was obtained, corresponding to the elution of the different molecules in the organic solution, as can be seen in panel A of figure 3.1. The first peak, as it was checked by electrophoresis and aminoacid analysis, contained the hydrophobic proteins of surfactant in its physiological ratio (around 1:1 by weight), whereas the second and third peaks contain the phospholipids and the neutral lipids (cholesterol, mainly) present in surfactant, respectively, as can be checked by phospholipid and cholesterol quantification assays (see section 3.2). Thus, it is possible to separate the different surfactant fractions (lipids and hydrophobic proteins) in order to study them, or even to combine them in different ways in order to study their interactions. In the present work, the different surfactant lipid fractions were obtained, including the whole **lipid fraction** (LF, peaks II + III), **lipid fraction without cholesterol** (LFΔChol, peak II), or the whole **hydrophobic protein fraction** (PF, peak I) of native surfactant.

Further on, a subsequent chromatographic step was carried out in order to separate the two hydrophobic proteins, SP-B and SP-C. After concentrating a certain volume of the previously obtained PF down to 0.5 ml of final volume, a second size-exclusion chromatography in Sephadex LH-60 (GE Healthcare, column dimensions 73 × 2.9 cm). The mobile phase was chloroform/methanol 1:1 (v/v) HPLC containing 0.5% HCl 0.1N in this case. The elution profile was obtained from the absorption of each fraction at 240 and 280 nm (see graph B in figure 3.1), and consisted of two main peaks: the first one corresponded to **SP-B**, which absorbs both at 240 and 280 nm, and the second to **SP-C**, which only absorbs at 240 nm due to the fact that this protein lacks aromatic residues.

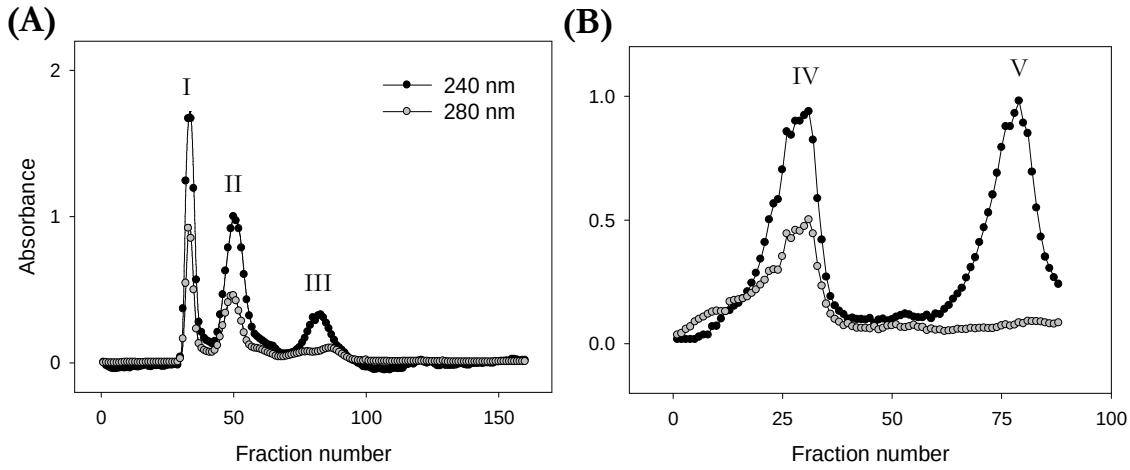

Fig. 3.1: (A) Elution profile from LH-20 chromatography to separate the hydrophobic components of pulmonary surfactant. From left to right, the molecules elute in decreasing size order, corresponding the different peaks to the hydrophobic protein fraction PF (I), the phospholipids (II) and the neutral lipids (III). (B) Elution profile from LH-60 chromatography to separate the PF, the peaks corresponding to SP-B (IV) and SP-C (V).

3.1.3.2 From porcine pulmonary tissue

In order to get a better yield in the purification of hydrophobic surfactant proteins, it is possible to use an alternative procedure that allowed processing a large amount of lung tissue (Perez-Gil et al. 1993). Instead of using BAL as the protein source, the purification was in this case carried out from whole porcine lung tissue. This method is not useful to purify surfactant lipids, since they get mixed with lipids from blood and cell membranes, but permits the extraction of larger amounts of hydrophobic proteins, in the range of mg. The pulmonary tissue was first minced and then exhaustively washed with ice cold saline; afterwards, it was filtered with a gauze and subjected to a first centrifugation step at 1000 g, 4ºC, for 5 minutes. Supernatants were collected and centrifuged again at 3300 g, 4ºC, for 2 hours, to obtain pellets enriched in the largest pulmonary surfactant complexes, which were subsequently subjected to organic extraction and size-exclusion chromatographies in order to purify the hydrophobic protein fraction.

3.2 ANALYTICAL METHODS

3.2.1 PHOSPHOLIPID QUANTIFICATION ASSAY

The quantification of phospholipid content in the different samples studied in this Thesis was carried out using the method developed by Rouser and colleagues (Rouser et al. 1966), which quantifies the phosphorus in phospholipids after conversion to inorganic phosphate. To this point, the samples were placed at the bottom of test tubes (either in organic solvent or in aqueous solution) and they were dried completely. Afterwards, in order to achieve phosphorus mineralization, they were incubated for 30 minutes in a sand bath at 260ºC with 450 µl of perchloric acid, covered with glass bubbles to avoid evaporation. Then, a colorimetric reaction was performed by adding 3.5 ml of milliQ water, 0.5 ml of ammonium molibdate 2.5% (p/v) and 0.5 ml of ascorbic acid 10% (p/v) to each of the tubes, and incubating them for 7 minutes at 100ºC. After stopping the reaction by introducing the tubes in ice, the absorbance at 820 nm of each tube was determined in an UV/visible spectrometer Beckman DU840. Simultaneously to the sample tubes, the same processes were applied to different inorganic phosphate solutions of known phosphorus concentration, which were used as calibration standards.

3.2.2 CHOLESTEROL QUANTIFICATION ASSAY

In order to determine the cholesterol concentration of different lipid fractions of surfactant, a commercial kit was employed (IVD, Spinreact), which is based on the enzymatic activity of cholesterol oxidase. In the presence of this enzyme, cholesterol creates a coloured compound whose concentration and, therefore, its colour intensity, is directly proportional to cholesterol concentration. By measuring the absorbance at 505 nm with respect to a blank, both for the sample and for a standard solution with known concentration, cholesterol concentrations of the different samples were estimated.

3.2.3 PROTEIN QUANTIFICATION BY AMINO ACID ANALYSIS

The concentration of the hydrophobic surfactant proteins in the native fractions isolated either from BAL or from pulmonary tissue was determined by amino acid analysis. Owing to their high hydrophobicity and their low content in aromatic residues, the most usual quantification methods, such as Lowry or Bradford methods (Lowry et al. 1951, Bradford 1976) are not reliable for these two proteins.

The amino acid analysis was performed as it follows: first, the samples were placed at the bottom of test tubes, then dried under nitrogen in order to evaporate the solvent, and resuspended in 100 µl of 6N HCl solution with phenol 0.1% (p/v), containing a known amount of *nor*leucine that was used as internal standard. Then, the test tubes were closed under vacuum and incubated for 24 hours at 110ºC in order to lead to the complete acid hydrolysis of proteins under non-oxidative conditions. After that, the tubes were opened and their contents were dried, first under a nitrogen flow and then in a vacuum centrifuge

for 2 hours, and 3 successive lavages with 100 µl of milliQ water were done, drying the tubes again in a vacuum centrifuge for 2 hours after each one, in order to remove all the HCl traces. Finally, the samples were resuspended in 100 µl of analysis buffer and processed in a Beckman System 6300 High Performance automatic analyzer.

3.2.4 PROTEIN CHARACTERIZATION IN POLYACRYLAMIDE GEL ELECTROPHORESIS

The purity of the hydrophobic proteins SP-B and SP-C purified either from BAL or from pulmonary tissue was routinely checked by polyacrylamide gel electrophoresis in the presence of sodium dodecyl sulfate or SDS (PAGE-SDS). This technique leads to the separation of different molecules that exhibit different mobilities inside an electric field. As the matrix for this process, gels made from different amounts of polyacrylamide are employed: a concentrating gel, containing a 4% of acrylamide, through which all the protein molecules migrate at the same velocity; followed by a separating gel, here prepared with a 16% of acrylamide. Depending on their size, each protein moves differently through the gel matrix: the smaller a protein is, the easier it moves through the gel and the faster it migrates. The acrylamide percentage chosen here, 16%, allows an optimal separation between the proteins studied in the present work. On the other hand, the anionic detergent SDS denaturises secondary and non-disulfide-linked tertiary structures and provides a negative charge to each protein in proportion to its mass. Both gels are polymerized between two glasses in a gel caster, with a comb inserted at the top of the concentrating gel in order to create wells for sample application.

As for the sample preparation, they were previously dried and resuspended in loading buffer (which contains 10% glycerol, 62.5 mM Tris, 2.3% SDS and the tracking dye bromophenol blue, pH 6.8), containing the reducing agent β-mercaptoethanol at 5% in the cases where the reduction of protein disulfide bonds was desired. The samples were incubated at 100ºC for 5 minutes in order to promote protein denaturation and SDS binding. Once 15-20 µl of each of the samples and a mixture of molecular weight standards (between 7 and 40 KDa, purchased from Bio-Rad) were applied in the adjacent wells, the electrophoresis was performed with a Mini-PROTEAN Tetra Cell system (Bio-Rad) using a constant electric current of 25 mA per gel. Samples run parallel in individual lanes and proteins migrate at different rates based on their size. After the electrophoresis was completed, which can be monitored by following the tracking colored dye, the separation of components from the original mixture as one or more distinct bands, one band per component, is obtained, and the molecular weight of each band could be estimated thanks to the standards.

In order to visualize the separated proteins and the standards, gels were subjected to **silver staining**, following the methodology described by Heukeshoven y Dernick (Heukeshoven and Dernick 1988). The gel was first immersed in the fixing solution, an aqueous solution of 40% v/v ethanol and 10% acetic acid, for 30 minutes, and afterwards in the incubation solution, consisting of 30% (v/v) ethanol, 7% (w/v) sodium acetate,

0.2% (w/v) sodium thiosulfate and 0.25% (v/v) glutaraldehyde 50% solution for, at least, 30 minutes. Then, the gel was immersed for 40 minutes into the staining solution, containing 0.1% (w/v) silver nitrate and 0.02% (v/v) formaldehyde 37% solution, which originated the "latent" image by reduced silver precipitation. During the development phase, the gel was immersed into an aqueous solution of 2.5% (w/v) sodium carbonate and 0.01% (v/v) formaldehyde 37% solution, and the reaction was stopped in 1.5% (w/v) EDTA solution.

3.3 LIPID AND LIPID-PROTEIN SAMPLE PREPARATION

In the different experiments that are part of the present work, several types of membrane materials were employed: native pulmonary surfactant membranes obtained from BAL; multilamellar vesicle suspensions (MLV), consisting of vesicles formed by a large number of concentric lipid bilayers and with a high polydispersion in size, from nm to μm; small unilamellar vesicles (SUV), whose diameters are in the range between 15-50 nm; large unilamellar vesicles (LUV), in the range of 100 nm; and giant unilamellar vesicles (GUV), which have a micrometric size. These preparations were obtained either from native materials, such as organic extract, lipid fractions or hydrophobic proteins of pulmonary surfactant, or from commercial phospholipids such as the molecular species dioleylphosphatidylcholine (DOPC) or palmitoyloleylphosphatidylcholine (POPC), both purchased from Avanti Polar Lipids Inc., in order to create model membranes in which the hydrophobic proteins SP-B and/or SP-C are integrated.

All the lipid and lipid-protein stock solutions in organic solvent were stored inside glass vials, and kept under argon atmosphere at -20ºC in order to avoid solvent evaporation and lipid oxidation.

3.3.1 PREPARATION OF MULTILAMELLAR VESICLES (MLV)

Multilamellar vesicles were obtained by the **evaporation-rehydration method**: first, proper volumes of the lipid or lipid-protein stock solutions in organic solvents were mixed in order to get the desired final concentrations. The mixtures were placed inside test tubes and dried under a nitrogen flow and in a vacuum centrifuge for 2 hours in order to remove solvent traces, obtaining a dry lipid film at the bottom of the tubes. Right after, the membranes were reconstituted by hydration of the dry film in the desired medium; in the present work, a buffer solution 5 mM Tris pH 7 containing 150 mM NaCl was added to the tubes, incubating them at 45ºC for 1 hour with orbital shaking at 1400 rpm. The incubation temperature was chosen to be higher than the transition temperatures of all the phospholipids: the highest transition temperature corresponds to DPPC (T_m = 41 ºC), the main component of pulmonary surfactant; thus, at 45ºC, all the phospholipid species were in a fluid state during hydration. MLV preparations were stored at 4ºC before using them.

3.3.2 PREPARATION OF SMALL UNILAMELLAR VESICLES (SUV)

Multilamellar suspensions were used as starting material to obtain suspensions of single bilayer vesicles. An easy and fast procedure to get unilamellar vesicles is **sonication**, which consists of the application of ultrasounds to the sample in such a way that the more complex, multilamellar structures are destroyed and small, unilamellar vesicles are obtained, with diameters around 15-50 nm. The sonicator transforms an electric current into high energy vibrations that are transmitted to the lipid suspension through a thin titanium probe immersed into it, generating ultrasonic waves that create microscopic bubbles by cavitation inside the suspension. The bubbles expand and originate membrane rupture that, when membranes reseal, produce spherical vesicles with a high curvature. The resulting vesicles, SUV, are highly unstable and they tend to fuse in order to form larger vesicles, so the experiments must be carried out immediately after sonication.

In the present work, a sonicator Hierlscher UP200 implemented with a titanium microprobe was employed, fixing the sonication parameters in 0.6 cycles and 65% of amplitude. The desired materials were sonicated for several cycles of 2 minutes (4 cycles in the case of native surfactant and 2 cycles for the MLV of different materials), until a complete decrease of turbidity was observed. SUV suspensions were used immediately.

3.3.3 PREPARATION OF LARGE UNILAMELLAR VESICLES (LUV)

Also from the multilamellar suspensions, it is possible to obtain unilamellar vesicles by a different technique, the **extrusion** through a polycarbonate filter with pores of a certain size in order to get unilamellar vesicles of a similar diameter (usually, around 100 nm). The advantage here is that this method allows a better control of vesicle sizes, and these preparations present a higher stability and homogeneity than SUV.

In order to get these LUV preparations, native surfactant complexes isolated from BAL and the MLV suspensions obtained from different lipid and lipoprotein mixtures were subjected to 5 freeze-thaw cycles (alternating between liquid nitrogen and hot water at 50ºC), in order to partially break the membranes. Then, the extrusion process was performed with a Mini-Extruder (Avanti Polar Lipids Inc.) equipped with 10 mm diameter drain discs and polycarbonate membranes Nuclepore Track-Etch with 100 nm diameter pores, both from Whatman. Once assembled together, the whole extrusion system (extruder, syringes filled with the suspensions and holder/heating block) were thermostated over the transition temperatures of the phospholipids (45ºC for native materials, 37ºC for POPC). The MLV suspensions were forced to pass 11 times through the filters until the turbidity was decreased, so finally, LUV suspensions of lipid or lipoprotein vesicles with diameters around 100 nm were obtained, which were either immediately used or stored at 4ºC and used the same day.

3.3.4 PREPARATION OF GIANT UNILAMELLAR VESICLES (GUV)

The vesicle preparations explained in the previous sections are useful for a large number and type of techniques, but their small sizes make impossible their direct visualization under optical microscopes. Sometimes, it is interesting to have a micrometric size lipid model that can be directly observed or manipulated in order to study different properties of the lipid bilayers. During the last century, a number of methods to prepare the so-called giant vesicles have been developed and optimized in order to get mostly unilamellar vesicles with diameters between 5 and 100 μm (Walde 2010). In the present work, two different methods were employed:

3.3.4.1 Electroformation method

Giant vesicle suspensions from very simple lipid or lipoprotein mixtures (POPC or POPC plus SP-B/SP-C) were prepared by membrane hydration in the presence of an electric field (Angelova and Dimitrov 1986, Mathivet et al. 1996). The efficiency of this technique is based on the direct application of the lipid film on the electrodes that generate the field, which were, in our case, **indium-tin oxide (ITO) coated glass slides**, 70-100 Ω/sq surface resistivity, purchased from Sigma-Aldrich.

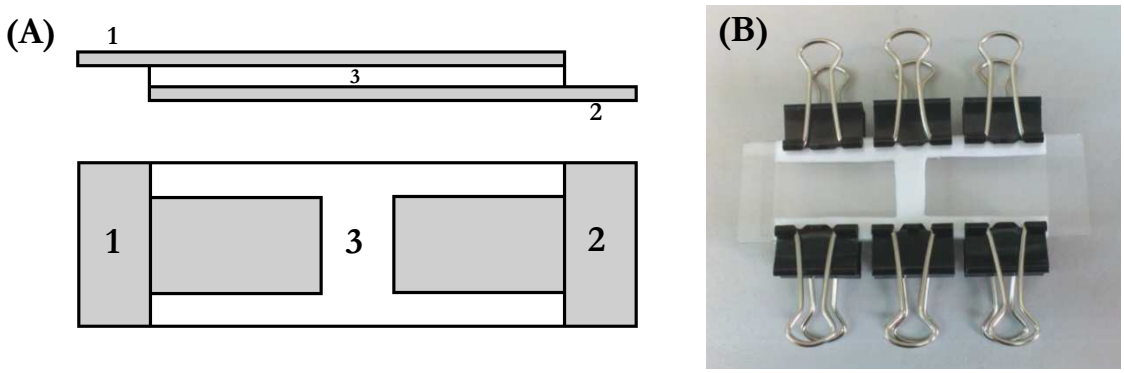

Fig. 3.2: (A) Side and top view of a double electroformation chamber made with two ITO-coated glass slides (1 and 2) and a Teflon spacer (3). (B) Picture of the chamber adjusted with paper clips.

First, small drops of lipid or lipoprotein stocks 1 mg/ml in chloroform HPLC (around 10-15 μl) were placed and spread over the conductive side of ITO glasses, which were quickly introduced in a vacuum chamber to avoid lipid oxidation and let them dry for 2 hours until the complete evaporation of the organic solvent. After that, the two lipid-covered slides were mounted to build the electroformation chamber, with the conducting sides face to face, separated by a 2 mm thick Teflon spacer pre-coated with vacuum grease (see figure 3.2). The chamber was then adjusted by paper clips and filled with a warm sucrose solution to hydrate the lipid or lipoprotein dry films. Finally, the chamber was completely sealed at both sides with a very moldable vinyl paste (CritoSeal, from Leica BioSystems), and connected to a function generator (FG 100, Telonic Instruments Ltd.). This experimental set-up has been adapted from (Veatch 2007).

The **electroformation** process was performed at 38ºC in two different stages: a first stage of 3 hours in which a 1.5 V amplitude and 8 Hz sinusoidal signal was applied, during which the membranes start hydrating and it is thought that the vesicles increase in size; in a second and shorter stage, of only 30 minutes, the amplitude was kept constant at 1.5 V and the frequency was decreased to 4 Hz, which is believed to help closing the spherical structures and facilitating their release from the electrode. After the electroformation, the preparations were carefully extracted from the chamber aspirating with a Pasteur pipette to avoid the rupture of unilamellar vesicles, and they were immediately used or stored at 4ºC.

3.3.4.2 Slow hydration method

There is some controversy about the electroformation method and whether the application of an electric field during vesicle formation leads to a certain arrangement of electric charges on the surface of phospholipid membranes and, thus, to a certain polarization. On the other hand, it was demonstrated that the presence of electric charges on the membranes affects their mechanical properties (Zhou and Raphael 2007). Therefore, in order to carry out the characterization of certain mechanical properties of giant vesicles as it is included in the present work, a different method for GUV preparation was chosen: the so-called **natural or slow hydration of membranes**, with no external field applied, as it has been optimized over the years in order to get a high efficiency method in terms of number of unilamellar vesicles present in the preparations (Needham et al. 1988, Olbrich et al. 2000), especially in the case of simple lipid compositions such as pure POPC.

In the present study and employing this methodology, GUV were prepared from pure POPC and POPC supplemented with small amounts of SP-B or SP-C. To this end, small volumes of lipid or lipoprotein stocks 5 mg/ml in chloroform HPLC (around 20-25 μl) were spread onto roughened Teflon discs, which were previously pre-coated with a saturated sucrose solution. The disc was placed at the bottom of a glass beaker and the lipid film was dried for 4-5 hours inside a vacuum chamber. After that, the dry film was prehydrated for 15 minutes by a humidified argon flow, and the Teflon disc was covered by a warm sucrose solution and let hydrated overnight at 37ºC. Finally, the preparation was taken from the incubator and, after several minutes at room temperature, a faint, white "cloud" formed by the membranous hydrated material appeared floating in the solution, that was carefully collected aspirating with a Pasteur pipette, and stored at 4ºC or used immediately.

3.4 FLUORESCENCE SPECTROSCOPY

In order to characterize the structure and accessibility of different membrane materials, either from native or from commercial sources, fluorescent membrane probes were incorporated into the samples and their emission was studied by fluorescence spectroscopy. Two fluorescent amphipathic dyes were selected: **Nile Red** and **FM®1-43** (both from Molecular Probes Inc.), whose molecular structures are shown in figure 3.3.

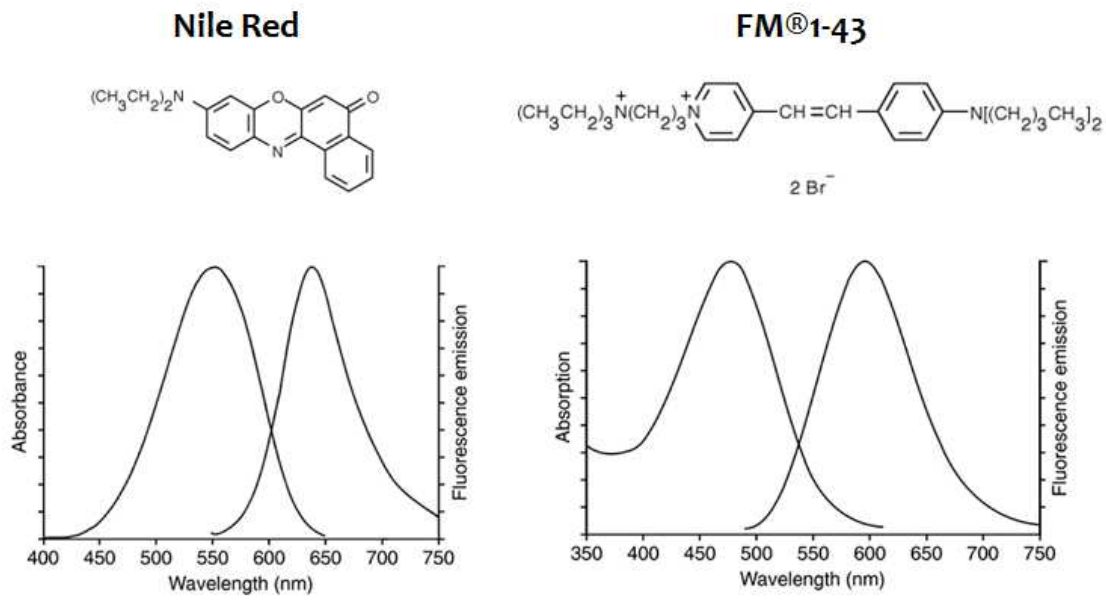

Fig. 3.3: Chemical structures and fluorescence excitation/emission spectra of amphipathic dyes Nile Red and FM1-43, taken from Molecular Probes web site: http://www.invitrogen.com.

Optimal concentrations for their incorporation into phospholipid membranes were determined, chosen as the minimal concentration required to get the maximal fluorescence emission intensity in a given amount of lipids, specifically, 1 ml of POPC MLV suspension concentrated at 100 μg/ml. In that way, the concentration did not get to crowding or self-quenching of the fluorescence emission of the probe molecules. The optimal concentrations were found to be 3 μM for Nile Red and 2 μM for FM1-43. Dye stocks were prepared in DMSO and stored in glass vials at -20ºC.

In order to perform the accessibility assays, native surfactant complexes and MLV, LUV and SUV suspensions prepared from the different materials were aliquoted and diluted to the desired final phospholipid concentrations, quantified by phosphorus analysis, in a final volume of 1 ml of saline buffer 5 mM Tris 150 mM NaCl, pH 7. Small aliquots of the amphipathic probes in DMSO were added to the sample tubes to get the desired final concentrations, either 3 μM for Nile Red or 2 μM for FM®1-43, while the tubes were vortexed to favor the homogeneous distribution of the probes. The tubes were incubated at room temperature and protected from light for 30 minutes, which was estimated to be a good incubation time for the incorporation of the probes in the membranes, before the fluorescence emission was measured. To follow incorporation kinetics of the dye FM1-43, the fluorescence emission was measured immediately after the addition of the dye to the suspensions, and emission spectra were obtained every 5-10 minutes.

All fluorescence emission spectra were registered in a spectrofluorimeter JASCO FP 6200 thermostated at 37ºC, using 5 nm excitation and 10 nm emission slitwidths. Nile Red fluorescent emission was monitored upon excitation at 548 nm, and its emission was

registered between 550 and 700 nm, while samples labeled by FM1-43 were excited at 479 nm and their emission was recorded from 500 to 650 nm.

3.5 ELECTRON SPIN RESONANCE WITH MEMBRANE SPIN LABELS

In the present work, differences between native pulmonary membranes were studied in terms of their fluidity as a function of temperature by using electron spin resonance spectroscopy (ESR), also known as electron paramagnetic resonance. This spectroscopic technique allows to characterize materials that contains unpaired electrons; since biological membranes usually lack unpaired electrons, non-reactive radical molecules have been specially designed as extrinsic probes to provide information about their environment, the so-called **spin labels**. Specifically, in the present work, phosphatidylcholines (PC) labeled with a nitroxide radical located in the n-th position of their acyl chain *sn*-2, known as **n-PCSL** (n-phosphatidylcholine spin label), were employed. The spin labels 1-palmitoyl-2-stearoyl-(n-doxyl)-*sn*-glycero-3-phosphocholine, with the doxyl radical situated in positions 5 or 14 (being carbon 1 the closest to the polar head), termed 5- and 14-PCSL, were purchased from Avanti Polar Lipids dissolved in chloroform HPLC. Their molecular structures are shown in figure 3.4.

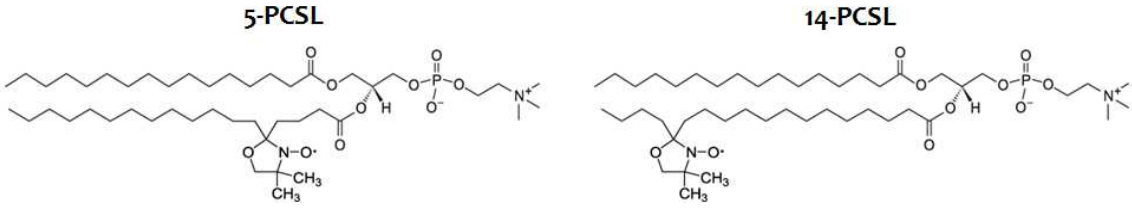

Fig. 3.4: Chemical structures of spin-labeled phospholipids 5- and 14-PCSL, taken from Avanti Polar Lipids web site: http://avantilipids.com.

Spin-labeled samples were prepared from different materials: in the case of organic extract of surfactant (EO) and lipid fraction (LF), n-PCSL lipids were mixed in the proper amounts with stocks of EO or LF in chloroform-methanol 2:1 in order to get a final probe concentration of 1% (mol/mol) with respect to phospholipids. Using these mixtures, MLV were prepared in saline buffer 5 mM Tris 150 mM NaCl as described in section 3.3.1. In the case of native surfactant membranes, which were already in aqueous medium, the spin-labeled lipids were dried in order to evaporate the chloroform and resuspended in DMSO, a water-miscible organic solvent. Proper amounts of the spin probes in DMSO were added to NS suspensions in order to get a final concentration of 1% (mol/mol) of the probes. The dilution of DMSO in water produces the exposure of probe molecules to the aqueous medium and their immediate incorporation into NS membranes.

The spin-labeled samples were introduced in 100 μl glass capillaries and centrifuged at 3000 rpm for 5 minutes. The supernatants were discarded in order to remove possible contributions of free probe, and the pellets, with a thickness of a few millimeters, were

place in the cavity of a Bruker EMX ESR spectrometer, equipped with a temperature control system by nitrogen flow, located at the Nuclear Magnetic Resonance and Electron Spin Resonance Services of Complutense University. ESR spectra from the studied materials were obtained at several temperatures in the range between 22 and 65ºC.

3.6 TRANSMISSION ELECTRON MICROSCOPY

In the present study, transmission electron microscopy was employed in order to achieve a direct observation of native surfactant complexes and the structures formed from the reconstitution of organic extract and lipid fraction of surfactant as MLV. Also, microscopy images of LUV made from POPC or POPC supplemented with 1% by weight of SP-B, SP-C or their physiological mixture (the hydrophobic protein fraction obtained from LH-20 chromatography, see section 3.1.3) were obtained.

Transmission electron microscopy is based in the use of a fine electron beam accelerated to an extremely high speed as the "illumination" source, interacting with the specimen as it passes through, so the observation is not diffraction-limited as it is in optical microscopes and a nanometer resolution is achieved. By placing a physical barrier with a small aperture angle below the sample plane, the electrons that are scattered further than a certain distance from the optical axis are excluded, resulting in an image that is darker in the regions where a higher sample density was present.

The samples were prepared at a phospholipid concentration of 3 mg/ml for surfactant membranes and MLV of native materials, and 1 mg/ml for POPC-based LUV, all of them in saline buffer 5 mM Tris 150 mM NaCl. In order to obtain well contrasted images of these biological materials, samples were subjected to **negative staining**: first, and in order to fix the vesicles to the microscopy supports, small drops (~100μl) of the suspension were placed on Parafilm (Bemis Company Inc.) and, over each one of the drops, carbon-coated cupper grids (Electron Microscopy Sciences) were laid and incubated at room temperature for 4 minutes. Then, each grid was washed by placing it on the top of small drops of distilled water, repeating the process 3 times, and finally placing the grid over a small drop of 2% uranyl acetate (Electron Microscopy Sciences) for 40 seconds, which was the negative staining agent.

After fixing and staining the samples, they were observed under a JEOL JEM 1010 Transmission Electron Microscope of 100 KV located at the Electron Microscopy National Center in Complutense University. Images were processed with Soft Imaging Viewer software (Olympus Soft Imaging Solutions GmbH).

3.7 FLUORESCENCE MICROSCOPY FOR THE STUDY OF MEMBRANE PERMEABILITY

In order to study the possible effect of hydrophobic surfactant proteins SP-B and/or SP-C on membrane permeability, changes on the permeability of giant POPC vesicles caused by the presence of these proteins were directly visualized by fluorescence microscopy. Giant vesicles of POPC or POPC plus 1% by weight of SP-B, SP-C or their physiological mixture (the hydrophobic protein fraction of surfactant, PF) were prepared by using the electroformation method described in section 3.3.4.1. In order to facilitate their observation, in some preparations, small aliquots of the fluorescently-labeled lipid Texas Red DHPE (purchased from Molecular Probes Inc.) were added to the lipid or lipid-protein stocks at 1% molar concentration. A certain number of unilamellar vesicles were obtained, but the preparations were mainly composed of oligolamellar vesicles, with several bilayers encapsulated by the outermost bilayer. Further on, giant vesicles prepared in a 200 mOsm sucrose solution were transferred to equiosmolar glucose solutions containing different fluorescent probes depending on the specific assay: the amphipathic dye **FM®1-43** (final concentration of 0.05 mM, purchased from Molecular Probes Inc.); the fluorescent and water-soluble probe **calcein** (final concentration of 1 mM, purchased from Sigma-Aldrich); or water-soluble dextrans of different average sizes and labeled with fluorescein (fluorescein isothiocyanate- or **FITC-dextrans** of 4, 10, 20, 40, 250 and 500 KDa, final concentration of 1 mM, purchased from Sigma-Aldrich). The estimated hydrodynamic radii of the different dextrans are listed in table 3.1.

	MW (KDa)	Radius (nm)
FD4	3-5	1.4
FD10	10	2.3
FD20	20	3.3
FD40	40	4.5
FD250/500	250/500	> 9

Table 3.1: Approximate Stokes' radii for FITC-dextrans, taken from Sigma-Aldrich product information.

Vesicles were incubated in those glucose-fluorescent probe solutions at room temperature, protected from light, for 3 hours, and after that they were diluted again in glucose 200 mOsm in order to dilute the preparation and facilitate the visualization of individual vesicles, as well as to reduce the fluorescent background. The preparations incubated with FM1-43 and calcein were observed under a fluorescence microscope Nikon Eclipse TE2000 with a 100W mercury lamp, equipped with Texas Red and FITC filter sets, and recorded with a cooled CCD camera (Nikon DS-1QM, 14 fps, 1 Mpixel). These specific experiments, including vesicle preparation and FM1-43 and calcein permeability assays, were carried out in the Laboratory of Membrane Mechanics and Biorheology of the Department of Physical Chemistry (Complutense University) in collaboration with Francisco Monroy's group. In the permeability assays with FITC-dextrans, the fluorescence was monitored with a fluorescence microscope Leica DM-4000B illuminated by a mercury

lamp (Leica EL6000) and equipped with L5 and TX2 fluorescence filter sets and a cooled digital camera (Model C10600-10B ORCA-R2, Hamamatsu). All giant vesicle suspensions were observed freshly made and 24 and 48 hours later, and in general terms no significant changes were observed through the days. The observations were made at room temperature (25 ± 1ºC) and images were processed with ImageJ free software (Schneider et al. 2012).

3.8 DIRECT VISUALIZATION OF SP-B AND SP-C LOCATION RECONSTITUTED IN MODEL MEMBRANES BY GUV IMMUNOFLUORESCENCE

POPC giant vesicles (GV) supplemented with 1% by weight of isolated proteins SP-B or SP-C were prepared by electroformation, following the methodology described in section 3.3.4.1. Vesicles were labeled with a fluorescent phospholipid, Texas Red DHPE (Molecular Probes Inc.) at a final concentration of 1% molar with respect to POPC, previously added to the lipoprotein stock. Once electroformed in a 200 mOsm sucrose solution, 25 µl of each giant vesicle preparation of POPC plus SP-B or SP-C were first diluted in 375 µl of an equiosmolar glucose solution and incubated at room temperature (25 ± 1ºC) with the **primary, non-fluorescent antibody**, a polyclonal rabbit antibody against either SP-B or SP-C (Anti-Mature SP-B or SP-C, both purchased from Seven Hills Bioreagents), depending on the protein present in each GV preparation. Several dilutions were tested for both primary antibodies, between 1/5000 and 1/50000 (v/v).

After one hour incubation, the excess antibody was washed from the GV suspension with a short-spin centrifugation: since the sucrose-glucose density gradient enhances GV precipitation, vesicles tend to pellet. 25 µl were collected from the bottom of the tube and diluted in 375 µl of the 200 mM glucose solution, and the secondary antibody was added at a final dilution of 1/10000 (v/v); for **immunofluorescence detection**, Alexa Fluor® 488 Goat Anti-Rabbit IgG (H+L) was used (Molecular Probes Inc.). GV were incubated with the secondary antibody at room temperature for 30 minutes and then centrifuged again for vesicle precipitation and excess antibody removal, collecting the bottom 25 µl of the preparation that were finally diluted in 100 µl glucose.

Preparations were imaged using a fluorescence upright microscope Leica DM-4000B illuminated by a mercury lamp (Leica EL6000) and equipped with L5 and TX2 fluorescence filter sets. Images were recorded with a cooled digital camera (Model C10600-10B ORCA-R2, Hamamatsu) and analyzed with Leica Microsystems LAS AF Lite and ImageJ software (Schneider et al. 2012).

3.9 ELECTROPHYSIOLOGY STUDIES OF IONIC CONDUCTANCE AND SELECTIVITY OF SP-B AND SP-C IN PLANAR LIPID MEMBRANES

In order to determine the extent of membrane perturbation induced by hydrophobic proteins SP-B and SP-C and to quantify the effect of both proteins on the ionic conductance and selectivity of model membranes, an electrophysiological characterization was performed by using the technique of protein reconstitution in **planar lipid membranes (PLM)**, in collaboration with the Group of Molecular Biophysics at Jaume I University (Castellón, Spain), supervised by Profs. Antonio Alcaraz and Vicente M. Aguilella.

Different commercial phospholipids were used, specifically: 1,2-dioleyl-sn-glycero-3-phosphocholine (DOPC); 1,2-dioleyl-sn-glycero-3- phosphoserine (DOPG); 1,2-diphytanoyl-sn-glycero-3-phosphocholine (DPhPC); and 1,2-diphytanoyl-sn-glycero-3-phosphoserine (DPhPS), all purchased from Avanti Polar Lipids. Stocks of these lipids or mixtures of them were prepared in pentane at a final concentration of 5 mg/ml, first evaporating their original solvent, chloroform, under an argon flow. Lipid-protein stocks were prepared as well, mixing very low amounts of either or both of the two surfactant proteins SP-B and SP-C in chloroform-methanol with the lipids, in order to get a final concentration of 0.01% by weight (around $1/10^5$ protein to lipid by molar ratio) of the hydrophobic protein fraction (PF) obtained by LH-20 chromatography, or 0.005% by weight of each protein, SP-B or SP-C (around $2/10^5$ and $1/10^5$ protein to lipid by molar ratio, respectively), isolated by LH-60 chromatography. Purification of all proteins used in these experiments was carried out starting from pulmonary tissue (see section 3.1.3).

3.9.1 EXPERIMENTAL SET-UP

The experimental procedure is based on the methodology developed by Dr. Bezrukov's group (Bezrukov and Vodyanoy 1993), using a **Teflon chamber** consisting of two compartments with a capacity of around 2 ml each. Both compartments are separated by a very thin Teflon film, between 12-15 μm thick, in which a **70-100 μm diameter orifice** was previously made; a picture of the experimental chamber is shown in figure 3.5. All the joints between the film and the compartments are sealed with vacuum grease. The orifice was created by approximating an incandescent platinum tip of around 15 μm of diameter to the film; the creation of the hole is directly visualized with a microscope connected to a CCD camera.

Once the chamber was mounted, **stable bilayers** were casted by monolayer apposition on the orifice by using the so-called Montal-Mueller technique (Mueller et al. 1962, Montal and Mueller 1972). First, lipid or lipoprotein monolayers were prepared by spreading small drops (around 10 μl) of the corresponding 5 mg/ml pentane stock on top of the subphases that filled each compartment of the chamber. In the present study, the subphases were saline solutions of different KCl concentrations buffered with 5 mM HEPES at pH 5.5. After 10 minutes, a reasonable length of time for pentane evaporation, a

monolayer was covering the air-water interface of each compartment, and subphase levels were then slowly raised by two syringes in such a way that the two monolayers came into contact through their acyl chains when crossing the orifice (see figure 3.6). In order to increase Teflon affinity for phospholipid acyl chains, the orifice is previously treated with hexadecane 1% (v/v) in pentane, which imparts certain hydrophobicity to the film surface. The bilayer was finally formed at both sides of the central orifice, which was directly detected and its thickness could be estimated by capacitance measurements. All bilayers were casted and all measurements were done at room temperature, 25 ± 1ºC.

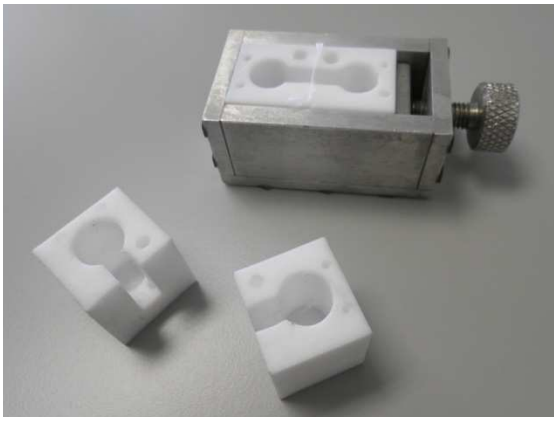

Fig. 3.5: Experimental chamber used for the electrophysiological studies, consisting of two Teflon compartments separated by a thin film with a small orifice in the middle.

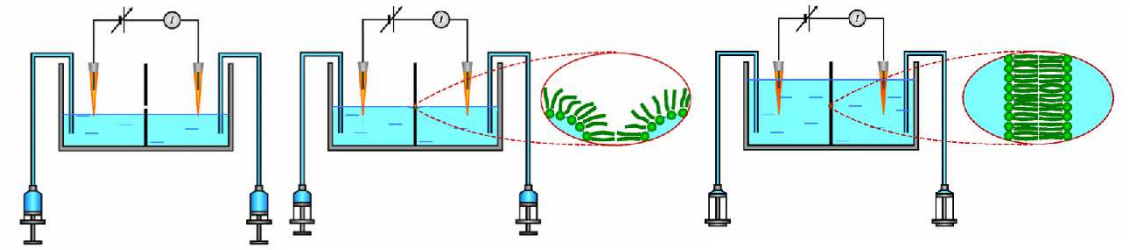

Fig. 3.6: Sketch representing bilayer formation by monolayer apposition over the orifice separating both compartments. Taken from UJI Biophysics Group web site: http://www.gm.uji.es.

The experimental chamber was connected to a signal amplifier with a pair of electrodes that were in contact with the solutions and must be able to measure electric currents in the order of picoamperes with a high precision, presenting therefore a very low electric capacity (Bockris and Reddy 1970). Commercial electrodes usually contain glass materials or porous membranes with a high capacity, being inappropriate for these types of fine measurements, so the electrodes employed here were fabricated in the laboratory. To this purpose, two high-purity silver filaments (99.5%) of 1 mm diameter, 2 cm length, were connected between them and subjected to a process of electrolysis: immersed in 0.1M HCl and connected to the positive pole of a current generator, an electric current of 5 mA/cm^2

was applied for 3 hours while gentle agitation, in order to favor the homogeneous deposit of the chloride ions on the electrode surface. The negative pole of the generator was connected to a platinum filament in contact with the solution. The chloride present in the surface of these Ag/AgCl electrodes is highly reactive and sensitive to the chloride concentration of solutions in which the electrodes have to be immersed during the experiments; for this reason, the electrodes were encapsulated in a gel 2M KCl solution, that acts as saline bridge. The gel phase was achieved by adding to the KCl solution 1.5% (p/v) of agarose while continuous stirring at 120ºC. The **Ag/AgCl electrodes** were then assembled within standard 250 ml pipette tips, filled with the agarose bridge; the electrodes fabricated by this way present a high resolution (typical asymmetry < 0.1 mV) and a very low electric capacity. The electric potential applied by these electrodes was defined as positive when it is higher at the chamber compartment that was closer to the experimenter, the side of protein addition (*cis* side), while the opposite side (*trans* side) is set to ground.

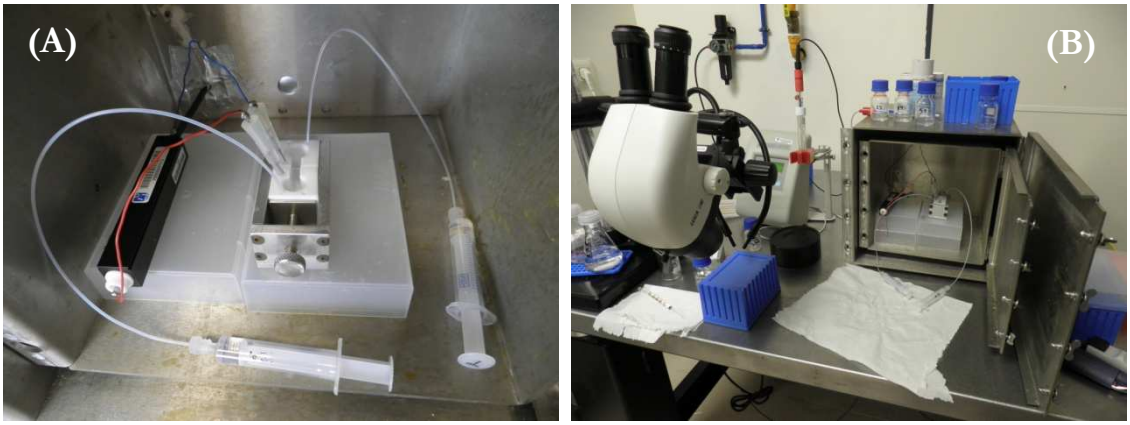

Fig. 3.7: (A) Experimental chamber together with the hand-made electrodes. (B) Double-screen Faraday cage in which the chamber was introduced for every experiment, placed on an anti-vibration table.

The electrodes were connected to a high resolution Axopatch 200B amplifier (Molecular Devices, Sunnyvale, CA). A low-pass filter of 15 KHz was implemented in order to attenuate the high-frequency signals from the system wiring, and the data were directly recorded into the computer hard disk with a sampling rate of 50 KHz. The analogical signal was digitized by a Digidata Axon 1322A digitizer (Axon Instruments, Molecular Devices Corp.) and the data was subsequently analyzed with the software Clampex 10 (Molecular Devices Corp.). The experimental chamber was isolated from external noise sources with a double Faraday cage (Amuneal Manufacturing Corp.) and the metal cage was placed on a vibration isolation table (see figure 3.7).

3.9.2 CHANNEL CONDUCTANCE MEASUREMENTS

In order to study the ionic conductance of PLM in the presence of surfactant proteins SP-B and/or SP-C, the amplifier in the voltage-clamp mode was used for applying

potential and measuring electric current. Lipoprotein bilayers of DOPC or DOPC/DOPG 85:15 were formed by apposition of two different monolayers: a lipoprotein monolayer in the *cis* side, containing a very small amount of either SP-B, SP-C or PF added to the lipid or lipid mixture; and the same pure lipid or lipid mixture monolayer in the *trans* side, with no protein molecules, in order to get a controlled orientation of the proteins in the PLM.

Bilayers were casted in a 100 mM KCl solution buffered with 5 mM HEPES, pH 5.5 and, by applying a certain electric potential between both sides of the chamber, an electric current could be detected and current traces were recorded. Using the Clampex 10 software, traces were subsequently filtered using a Bessel (8-pole) filter with a 50 Hz -3dB cut-off frequency, and the recorded values of electric current (I) were calculated by obtaining histograms of each trace, and performing a Gaussian peak fitting. Given the applied potential (in the range of ±100 mV in the present study), **ionic conductance (G)** was calculated for each single current level simply by dividing the calculated current I by the applied voltage. Although protein density in bilayers was very low in order to facilitate the detection of single-channel events, it was impossible to know how many individual channels were opened in each recorded trace, so a visual examination of all the records was used to find the stepwise changes of electric current in each trace (ΔI). **Stepwise conductances (ΔG)** were then calculated by dividing these current changes ΔI by the applied voltage.

3.9.3 REVERSAL POTENTIAL MEASUREMENTS

Lipoprotein bilayers of DOPC or DOPC/DOPG 85:15 were formed in the presence of different KCl concentrations at each side of the experimental chamber (50 mM KCl in *trans* side; 100, 150, 200, 300 and 2500 mM in *cis* side, pH 5.5). A net ionic current appeared due to the concentration gradient, which was manually set to zero by adjusting the potential applied by the amplifier. These potential contains two contributions: the **reversal potential ($\mathbf{E_{rev}}$)** or potential needed to compensate the ionic flow inside the channel created by the concentration gradient, and the **liquid junction potential (LJP)** generated at the interface between the solution and the saline bridge of the electrode. This last contribution is a consequence of the experimental method and gives no information about the ionic transport through the channel, so it must be subtracted. In our experimental set-up, the measured zero current potential consisted in the following three contributions:

$$V_{exp} = V_{P_{cis}} - V_{P_{trans}} = \left(V_{P_{cis}} - V_{cis}\right) + \left(V_{cis} - V_{trans}\right) + \left(V_{trans} - V_{P_{trans}}\right) \quad (3.1)$$

Where V_{Pcis}-V_{cis} and V_{trans}-V_{Ptrans} are the LJP generated at the interfaces of the two saline bridges with the solutions in *cis* and *trans* sides, respectively, and V_{cis}-V_{trans} is the potential generated at both sides of the channel, the reversal potential. In the conductance measurements, *cis* and *trans* solutions are the same, so the LJP are equal but opposite in sign, so they cancel each other and the contribution to the experimental measurement is zero. However, reversal potential measurements are done in asymmetrical conditions, so the LJP values should be considered. In this study, they were theoretically calculated from

the Henderson's equation, which gives the diffusion potential that appears in an interface in the presence of an ion concentration gradient (Alcaraz et al. 2009):

$$V_L - V_R = -\frac{RT}{F}\frac{\sum_i z_i D_i\left(c_{i,L} - c_{i,R}\right)}{\sum_i z_i^2 D_i\left(c_{i,L} - c_{i,R}\right)} ln\left(\frac{\sum_i z_i^2 D_i c_{i,L}}{\sum_i z_i^2 D_i c_{i,R}}\right) \quad (3.2)$$

Where subscript i refers to the different ionic species in the solution (in this case, only two, K^+ and Cl^-); L and R to left and right side of the interface; z_i is the valence of the ionic specie; and D_i is the diffusion coefficients for the different ions. The diffusion coefficients in free solution are 1.96 for K^+ and 2.03 for Cl^- (both in 10^{-5} cm^2/s) (Robinson and Stokes 1957). This equation is applied to calculate both LJP, V_{Pcis}-V_{cis} and V_{trans}-V_{Ptrans}. Since the difference between the mobility of anion and cation is negligible, the contribution of the LJP to the measured zero current potential is very small (~1 mV) for all the KCl concentrations, but it was subtracted to the experimental values in order to obtain accurate E_{rev} values.

3.10 MICROPIPETTE ASPIRATION OF LIPID AND LIPOPROTEIN GUV TO STUDY MECHANICAL PROPERTIES OF MEMBRANES

The impact of the presence of hydrophobic surfactant proteins SP-B or SP-C in a phospholipid bilayer in terms of mechanical properties and stability was studied with micromechanical experiments on giant unilamellar vesicles. GUV were prepared by slow hydration of lipid or lipoprotein films (see section 3.3.4.2), starting from pure lipid stocks of 1-palmitoyl-2-oleyl-*sn*-glycero-3-phosphocholine (POPC, purchased from Avanti Polar Lipids) or lipoprotein stocks of mixtures in chloroform of POPC and small amounts of SP-B or SP-C, specifically, 10^{-6} and 10^{-5} proteins in molar ratio with respect to lipids, obtained and isolated from pulmonary tissue (see section 3.1.3). GUV were prepared in a 200 mOsm/kg sucrose solution and diluted manifold in 205-208 mOsm/kg glucose solution right before experimentation; the difference of inner and outside solutions created a refractive index and a density gradient across the membrane, yielding to an excellent image contrast and a fast sedimentation of the vesicles inside the chamber.

GUV were mechanically tested by employing the micropipette aspiration technique, in which precise tension protocols were applied to membranes while continuously recording the membrane deformation using a high-speed videocamera. The set-up has been optimized in order to achieve an automated and high resolution technique (Heinrich and Rawicz 2005). This experimental set-up was assembled and implemented in the facilities of the Electron Microscopy Center at Complutense University assisted and supervised by Wieslawa Rawicz and Andrew Leung, from University of British Columbia (Vancouver, Canada), and Igor Kuznetsov and Prof. Evan Evans, from Duke University (Durham, NC, US).

In general terms, the set-up that have been used in the present work consists of three major subsystems, shown in figure 3.8: a first one, to apply and measure pressure in the

micropipette (I); a second one, to visualize and record the micromanipulation and membrane deformation (II); and a third one, to control and run the experiments with custom-written software (III). The different elements will be described in detail in the following sections.

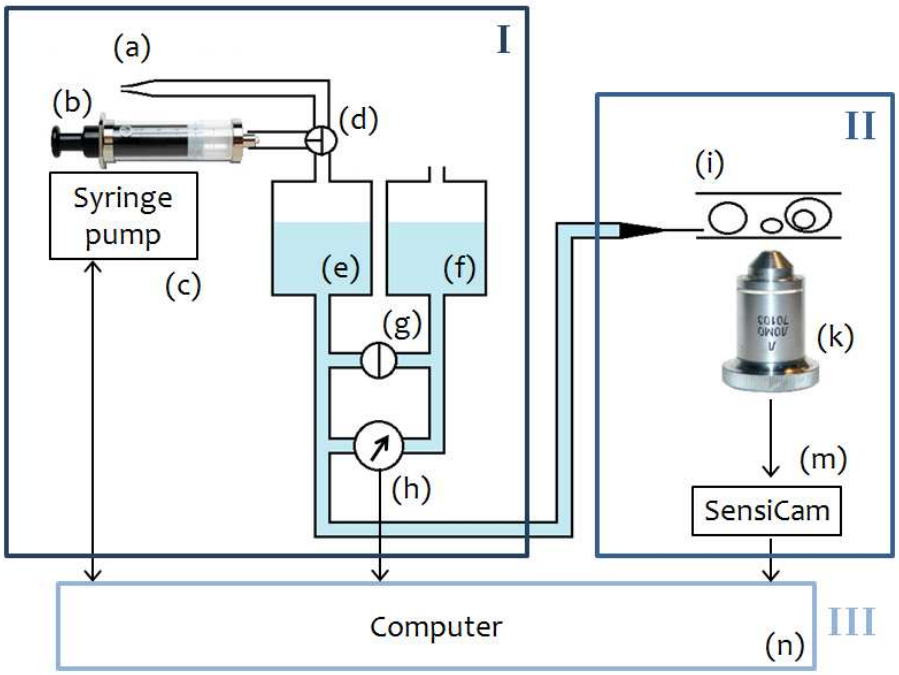

Fig. 3.8: Main elements of the micropipette aspiration experimental set-up: (a) mouthpiece for pressure application; (b) air-tight glass syringe; (c) computer-controlled syringe pump; (d) three-way valve; (e) main water reservoir; (f) reference water reservoir; (g) two-way stop valve; (h) differential pressure transducer; (i) experimental chamber; (k) microscope objective; (m) high-speed CCD camera; (n) computer with interfaces to syringe pump, pressure transducer and camera. Based on (Heinrich and Rawicz 2005).

3.10.1 MICROPIPETTE

The pressure was applied to the GUV through a micrometric glass pipette, fabricated from 0.75 mm o.d., 0.4 mm i.d. borosilicate glass capillaries (A-M Systems), that were pulled with a **vertical pipette puller** (Model 720, David Kopf Instruments). In order to cut the pipette to the desired diameter, around 10 μm i.d., and to get clear, even pipette edges, perpendicular to pipette walls, a home-made **microforge** was employed: a small amount of low-melting-point glass was placed on a platinum heating wire and heated over its melting point; then, the pulled pipette tip is dipped into the molten forge glass by micromanipulation, letting the glass to flow inwards the capillary. When the glass meniscus reached to the point where the pipette had the desired inner diameter, the heater was turned off, yielding to the solidification of the glass. A quick, sharp blow in the microforge usually resulted in an even, perpendicular break of the pipette. All the process was continuously monitored and controlled by 15× eyepieces.

Then, the pipette was backfilled with 200 mOsm/kg glucose solution using MicroFil syringe needles (model MF34G-5, World Precision Instruments, Inc.), carefully avoiding air bubbles inside the micropipette. The pipette was cut to the desired length (between 3-4 cm) and placed in a holding chuck (Research Instruments, Inc.). In order to monitor it properly and get accurate measurements, the pipette must be oriented perpendicular to the optical axis of the microscope, and also a fine control of its position in the 3 dimensions is required; for these reasons, the pipette holder was mounted on a **3 axis stage** (Model M-461-XYZ-M, Newport Corp.), rigidly attached to the microscope base, and equipped with motorized micrometers (Thermo Oriel at Spectra Physics) whose motion was controlled with a 3D game joystick and custom-written software.

3.10.2 PRESSURE APPLICATION AND MEASUREMENT

The holding chuck of the micropipette was connected to the main water reservoir (part e in figure 3.8) of the pressure system, and pressure can be applied inside the pipette by two main ways: by lowering the position of the main water reservoir with respect to the vertical position of the reference reservoir (part f in figure 3.8); or by evacuating the air volume above the water in the main reservoir. In the experimental set-up used in the present work, the latter was the chosen method, and the creation of a vacuum in the main reservoir was completely automated by using a bidirectional and computer-controlled **syringe pump** (part c in figure 3.8, Model PHD 2000 Infuse/Withdraw High Force, Harvard Apparatus, Inc.).

The pressure difference between the two partly filled water reservoirs was measured by a **pressure transducer** (part h in figure 3.8, Model DP15, Validyne Engineering) assembled with a no. 32 diaphragm, optimal for the desired pressure range (0-140 cm H_2O ~0-14 KPa). The transducer was connected to a demodulator (Model CD23, also purchased from Valydine) that was interfaced via a standard PCI board with the data acquisition software in the computer; the demodulator was calibrated adjusting the zero and applying a known pressure difference to adjust the gain settings.

The transducer and all the tubing of the pressure system were assembled and filled with distilled and degassed water in order to avoid air bubbles. A picture of the whole pressure system is shown in figure 3.9.

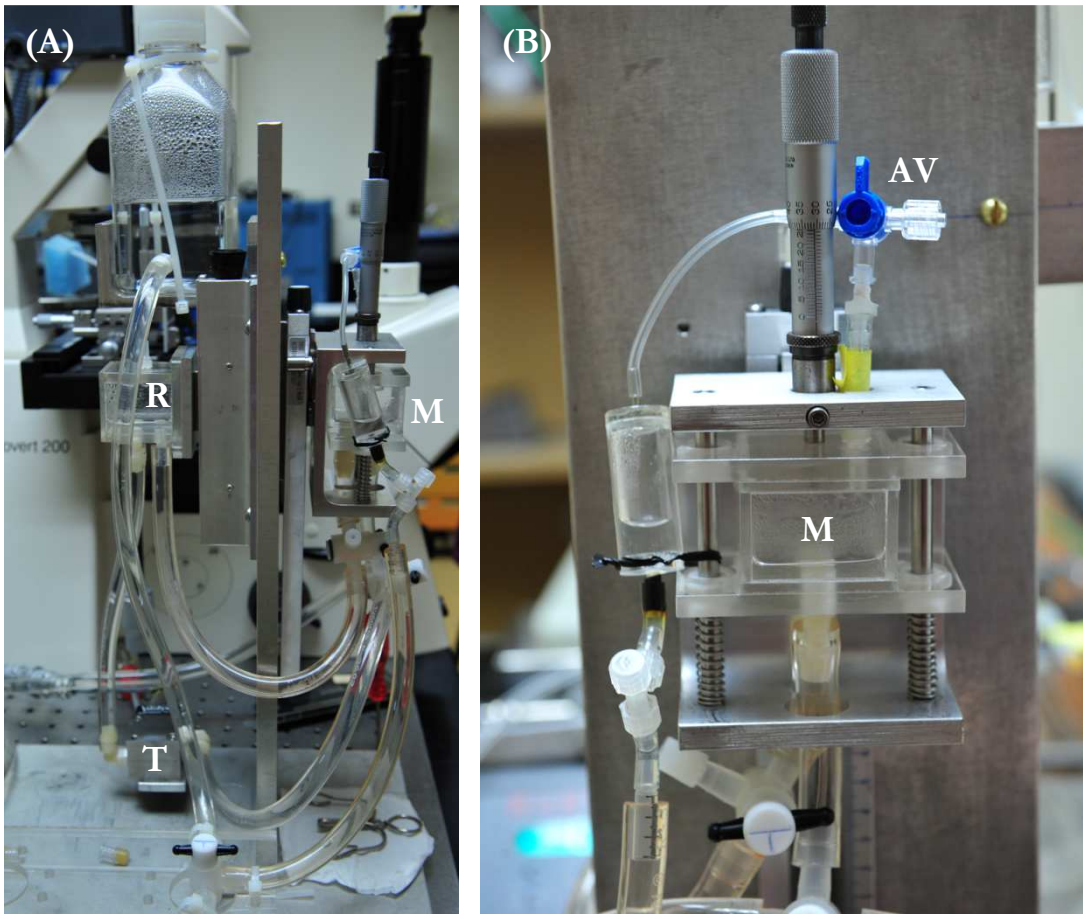

Fig. 3.9: (A) Side view of the system for pipette pressurization, including the two water reservoirs, reference reservoir (R) and main reservoir (M), tubing connections and valves and the pressure transducer (T). (B) Detail of the main water reservoir (M) with the air valve (AV) open.

3.10.3 VIDEO MICROSCOPY

In order to visualize, control and manipulate the GUV preparation and the micropipette, an **Axiovert 200 inverted microscope** (Carl Zeiss Microimaging, Inc.) was used, equipped with **Hoffman Modulation Contrast optics** (Modulation Optics, Inc.). This optical system produces a high-contrast and high-resolution image, converting optical gradients of the specimen, such as refraction indexes, into intensity variations thanks to three special components added to the microscope (figure 3.10): the HMC objective, containing a three-region filter called modulator; the HMC condenser, consisting of a lens system and slits that correspond to the HMC objective, whose image must be aligned to the modulator; and the HMC polarizer, which is rotated to control the image contrast by varying the background intensity and partial coherence of the illumination.

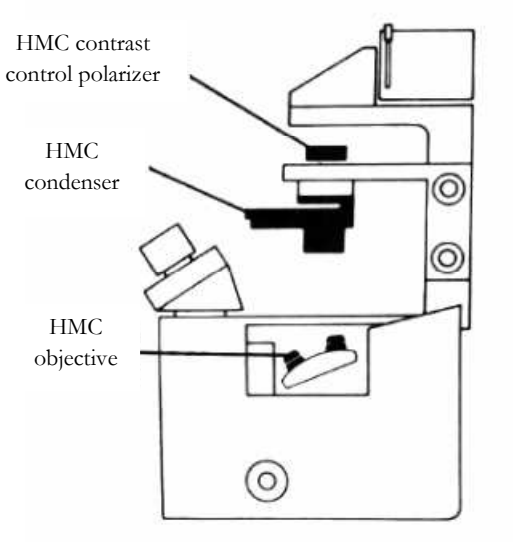

Fig. 3.10: Hoffman Modulation Contrast components on an inverted microscope. Modified from HMC user guide.

The main videocamera of the set-up is a **high-speed camera** SensiCam (The COOKE Corp.) equipped with an external cooling fan to minimize vibrations and whose fast frame rate mode allowed real-time image analysis up to 1500 fps, if using a small region of interest; in our case, a region of 32 full-length (640 pixels) video lines centered at the axis of symmetry of the experiment, the pipette middle axis. This region was subsequently binned into one single line, right before reading out from the camera in order to improve the signal-to-noise ratio and the transfer speed, thus resulting a one-dimension, axial intensity profile. Since the field of view had to be reduced at such extent, a supplementary video system was implemented for continuous visualization on a second monitor (not shown in figure 3.8), by using a **B/W analog camera** (Model CCD-72 from Dage-MTI).

Besides, a distance measure tool in this second video image was used to obtain the reference geometric parameters at the beginning of each experiment, once the chosen GUV was aspirated: the vesicle radius R_v; the projection length L_p of the aspirated membrane portion of the vesicle inside the pipette; and the pipette radius R_p (see figure 3.11). This last parameter was measured in a very careful and systematic way, since most measurements are very sensitive to it. One of the most reliable methods is using a second pulled capillary, which is introduced inside the micropipette, and measuring its diameter at the pipette entrance.

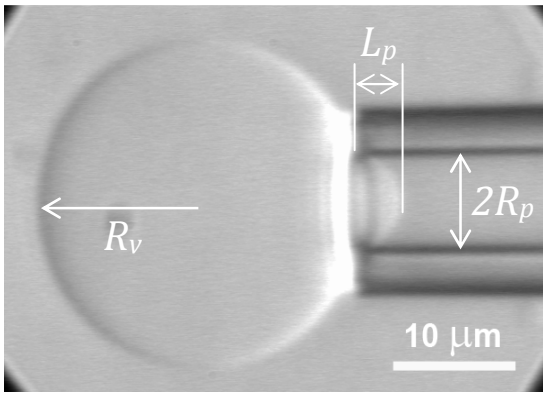

Fig. 3.11: Image of a pipette-aspirated giant vesicle obtained from the B/W analog camera, where the main geometrical parameters of the experiment are indicated with the notation used in the text.

3.10.4 DATA ACQUISITION AND IMAGE ANALYSIS

Custom-written **computer software** facilitates data acquisition and device control for micropipette aspiration experiments with giant vesicles; the program, written on LabVIEW (National Instruments), was developed by Igor Kuznetsov, Ph.D. (Duke University, US). The software main screen is shown in figure 3.12. In general terms, the program controls the main aspects of each experiment: sets the initial values that describe the geometry of the experiment (vesicle diameter D_v, projection length L_p and pipette diameter D_p); sets the pump at the desired suction pressure and speed; contains the screen and pump calibration controls; enables the vesicle visualization and alignment of the vesicle-pipette axis of symmetry in the middle of the SensiCam region of interest (the 32 horizontal lines mentioned before).

The experiments performed in the present study consisted of increasing pressure ramps at a given loading rate, starting from a low initial pressure of around -2 cm H_2O and finishing at the vesicle rupture. The resulting axial intensity profiles are recorded at a very high sampling rate as a function of applied pressure; the program contains two controls which set how the profiles are saved during and at the end of the experiment: the data is saved at the highest frame rate (1500 fps) for the last N points, being N the value set in "batch" (see figure 3.12), while all previous data is decimated at 1:M ratio, i.e., every M-th profile is saved, being M the value set in "quotient". The program monitors the real-time image during the experiment and detects the vesicle rupture when the outer vesicle edge is aspirated by the pipette, ending the intensity profile recording.

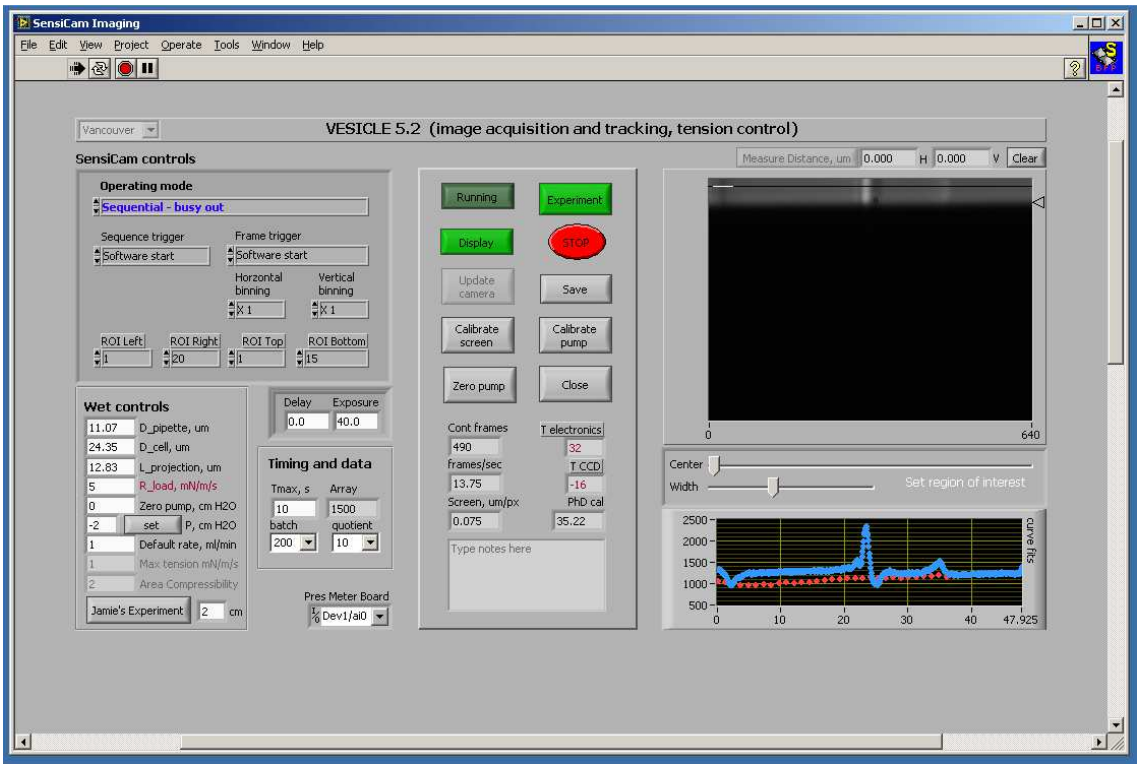

Fig. 3.12: Main panel of the LabVIEW program used to control the micropipette experiments. On the left side, controls for SensiCam setup and the program inputs, containing the wet controls and timing and data saving options; in the middle, program controls and indicators like screen and pump calibration factors; and on the right side, the Sensicam region of interest and the real-time intensity profile.

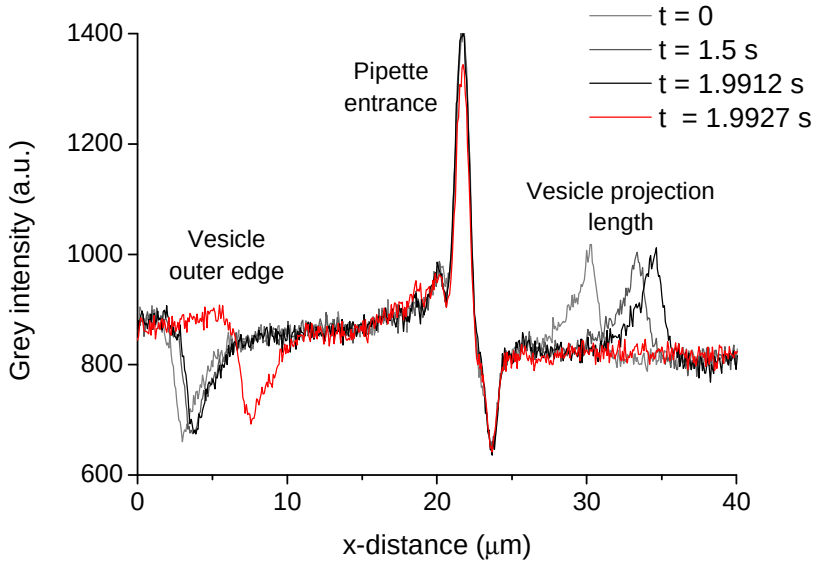

Fig. 3.13: Four selected intensity profiles corresponding to a vesicle aspiration experiment, including the first frame (lightest grey line, low initial pressure), two intermediate frames and the moment of rupture captured in the last frames (red line). The characteristic signatures of the diffraction patterns of the vesicle and pipette are identified.

Once the experiment is completed, the output data is saved in a .txt file, containing all the recorded intensity profiles, and also a .log file is created with the general information about the experiment, such as the geometrical parameters, the aspiration speed or the pump calibration factor. A separate Visual C++ **data analysis program** uses the intensity profiles to calculate the geometry changes of the vesicle as a function of the aspiration pressure and time: it loads and displays all the intensity profiles recorded in a single experiment, allowing the user to flip through them sequentially. This program was created by Prof. Volkmar Heinrich (currently at UC Davis College of Engineering, US). In the first intensity profile, the user selects three regions where certain patterns are located, each one identified with the position of a certain local intensity feature (maximum, minimum of inflection point, see figure 3.14): the outer edge of the vesicle (minimum), the pipette entrance (maximum and minimum) and the edge of the projection length of the vesicle inside the pipette (maximum). The motion of the second pattern, corresponding to pipette drifts in the axial direction, is subtracted to the other patterns motion, so that the positions of membrane edges are corrected for any drift.

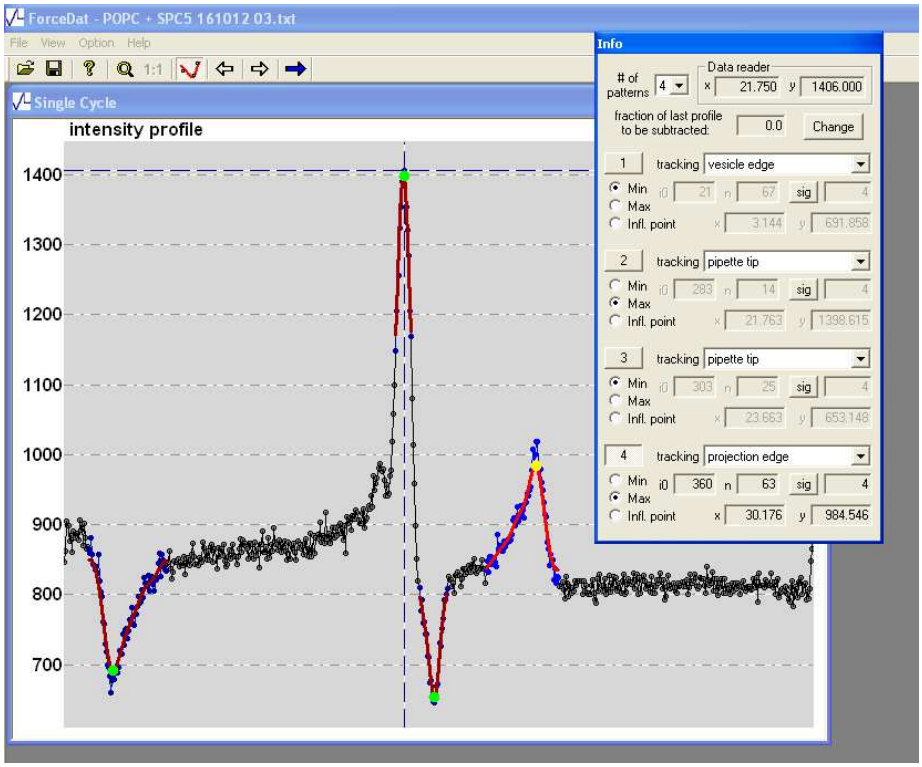

Fig. 3.14: Main screen of the Visual C++ data analysis program showing the first frame recorded in an aspiration test. From left to right, the three regions are selected to fit the intensity patterns: vesicle outer edge, pipette tip and projection length.

Then, the program is run and a suitable pattern-tracking algorithm readjusts the positions of the three intensity patterns in each recorded profile and finally generates an output file in which the three tracked positions (from now on, notated as X_v, X_t and X_p, see figure 3.15) are saved as a function of time and applied pressure. It is assumed that the tracked displacements of the intensity patterns do not reflect the absolute positions of

these edges, but are a very accurate way to trace the edge movement. (Heinrich and Rawicz 2005) can be consulted for further details.

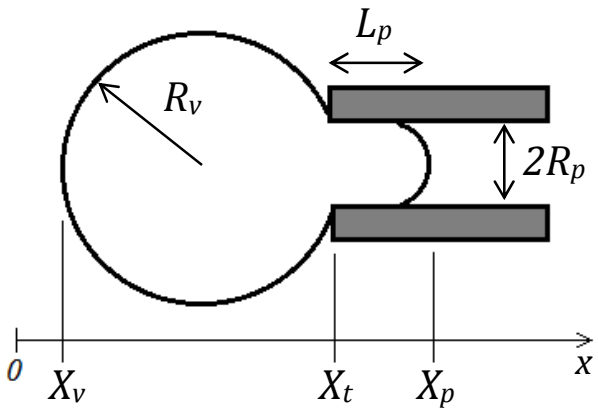

Fig. 3.15: Sketch to illustrate the three track positions: outer vesicle edge, pipette tip and projection length (X_v, X_t and X_p, respectively).

The C++ analysis program also calculates from these three values the geometrical changes of the vesicle (area, volume) as a function of time and pressure, assuming that the geometry of the vesicle is described accurately by spherical and cylindrical parts. In order to calculate the instantaneous values of R_v, L_p, vesicle area and volume, the program is based in the mathematical expressions that follow.

Starting from the change in the vesicle outer edge, reflected as the negative change in the distance between the true edge and the pipette entrance, R_v can be worked out:

$$\Delta X_v = X_v - X_{v_0} = -\Delta\left(R_v + \sqrt{R_v^2 - R_p^2}\right)$$

$$\Rightarrow\ R_v = \frac{1}{2}\left(C_v - X_v + \frac{R_p^2}{C_v - X_v}\right) \quad (3.3)$$

Where $C_v = X_{v_0} + R_{v_0} + \sqrt{R_{v_0}^2 - R_p^2}$ is a constant offset calculated from the initial vesicle radius R_{v_0} measured right before the experiment. The instantaneous value of the projection length is simply given by:

$$L_p = L_{p_0} + X_p - X_{p_0} \quad (3.4)$$

Instantaneous vesicle area and volume are given by the approximate expressions:

$$A(R_v, L_p) = 4\pi R_v^2 + 2\pi R_p L_p - \pi R_p^2 \quad (3.5)$$

$$V(R_v, L_p) = \frac{4}{3}\pi R_v^3 + \pi R_p^2 L_p - \frac{1}{3}\pi R_p^3 \quad (3.6)$$

The instantaneous values for R_v, L_p, A and V can all be corrected from pipette axial drifts simply by correcting the values of X_v and X_p:

$$X_{v_{corr}} = X_v - X_t + X_{t_0}$$

$$X_{p_{corr}} = X_p - X_t + X_{t_0}$$

And introducing them in expressions (3.3)-(3.6).

However, in the present work, we assume that the **vesicle volume remains constant** during the vesicle aspiration tests: the pipette suction needed to expand the surface of a 20 μm phospholipid vesicle (~1 KPa) is small compared to osmotic driving forces (~100 KPa) required to transport water molecules across the bilayer and small compared to the osmotic activity of trapped sucrose (~500 KPa) (Rawicz et al. 2000). Then, the instantaneous values of R_v and A are then obtained from the constant volume of the vesicle $V_0 = V\left(R_{v_0}, L_{p_0}\right)$ calculated with the expression (3.6):

$$R_{v_{calc}} = \sqrt[3]{\frac{3V_0}{4\pi} - \frac{3}{4}R_p^2 L_p + \frac{1}{4}R_p^3} = \sqrt[3]{R_{v_0}^3 - \frac{3}{4}R_p^2\left(L_p - L_{p_0}\right)} \quad (3.7)$$

$$A_{calc} = A\left(R_{v_{calc}}, L_{p_{corr}}\right) \quad (3.8)$$

Therefore, using this constant area assumption, changes in vesicle area are only due to the inward movement of the projection length inside the pipette.

For the vesicle **area expansion tests** carried out in the present work, in which the bilayer elasticity was measured, the deformation of the membrane was studied as a resultant of the applied force in order to obtain mechanical information. Thus, the C++ analysis program calculates the following magnitudes at each instant: the tension suction pressure Δp applied to the bilayer produces a uniform membrane tension σ that depends on the pipette radius R_p and the instantaneous vesicle radius R_v (Kwok and Evans 1981):

$$\sigma = \frac{\Delta p}{2} \cdot \frac{R_p}{1 - R_p/R_v} \quad (3.9)$$

Apparent area expansivity (or compressibility) is a derived from a superposition of smoothing of thermal bending undulations and reduction in lipid surface density (Rawicz et al. 2000). Therefore, the relative area expansion was corrected for thermal fluctuations, and it is given by:

$$\alpha_{k_c} = \alpha - \frac{k_B T}{8\pi k_c} ln \frac{\sigma A}{\sigma_0 A_0} \quad (3.10)$$

Where $\alpha = \frac{A - A_0}{A_0}$ is the fractional increase in apparent projected area A of the vesicle, k_B is the Boltzmann constant, T is the temperature and k_c is the bilayer bending modulus, whose experimental value for POPC bilayers has been determined to be $8.5 \cdot 10^{-20}$ J (Mathai

et al. 2008). Both tension and relative area dilation were obtained from the constant volume assumption.

On the other hand, the **membrane rupture analysis** was performed for each vesicle aspiration experiment starting from two main values: the lysis tension at the very moment of vesicle rupture, obtained from expression (3.9) and assuming constant volume; and the exact loading rate that the vesicle was subjected to during the experiment, calculated as the slope of calculated tension (assuming constant volume) and time. Although the loading rate was initially set before each experiment, the experimental one, obtained under the constant volume assumption, must be subsequently calculated. Figure 3.16 shows how these two values were obtained for each vesicle aspiration test. From these two values, R_σ and σ_{lysis}, vesicle lifetimes were then determined with this simple expression:

$$t_{lysis} = \frac{\sigma_{lysis}}{R_\sigma} \quad (3.11)$$

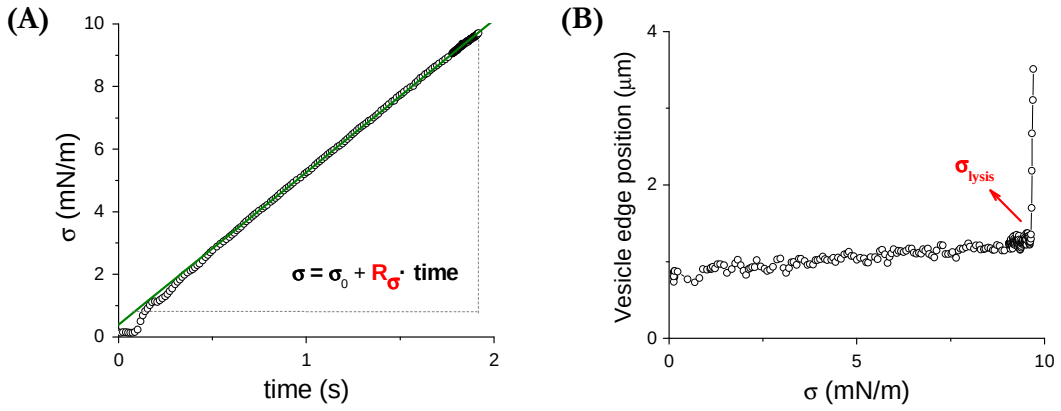

Fig. 3.16: (A) Time evolution of the applied tension, calculated from the assumption of constant volume, from which the experimental loading rate R_σ was obtained from a linear fit. (B) Trace of vesicle outer radius as a function of applied tension, in which the tension value at the moment of rupture σ_{lysis} can be identified with a high accuracy.

4. STRUCTURE, PERMEABILITY AND FLUIDITY OF SURFACTANT AND MODEL MEMBRANES

Part of the experiments included in the present chapter were carried out in collaboration with Lara H. Moleiro, Iván López-Montero and Francisco Monroy (Dep. Physical Chemistry, Fac. Chemistry, Universidad Complutense, Madrid) and published in the following article:

"A combined action of pulmonary surfactant proteins SP-B and SP-C modulates permeability and dynamics of phospholipid membranes" Biochemical Journal 438:555-64. 2011

4.1 INTRODUCTION

The pulmonary surfactant system is an excellent example of dynamic membrane polymorphism and how it controls some biological functions through specific lipid-lipid and lipid-protein interactions. Surfactant is assembled by alveolar type II pneumocytes in the form of tightly packed membranes stored in specialized organelles called lamellar bodies (LB) (Weaver et al. 2002). Once secreted, surfactant develops a membrane-based network that covers very rapid and efficiently the whole alveolar surface. From surfactant assembly until its adsorption into the interface, several restructuration processes take place: membrane packing and unpacking in LBs, rearrangement of LB membranes into tubular myelin (TM), reorganization of surfactant membranes to form layers close to the air-water interface, and transfer of surface active lipid species from these complexes into the interface -and vice versa- during expansion-compression respiratory cycles (see review (Perez-Gil 2008) for further details). Surfactant proteins, specifically SP-B and SP-C, have a major role in facilitating all of these processes, but the precise molecular mechanism is still under investigation.

In the present chapter, the effects of surfactant proteins on phospholipid membranes were first studied by analyzing the incorporation of two membrane-sensitive fluorescent probes, Nile Red and FM®1-43. **Nile Red** is a phenoxazone dye that fluoresces intensely in organic solvents and membrane environments, but is completely quenched in aqueous media (Greenspan et al. 1985). The emission properties of this probe depend strongly on the relative hydrophobicity of the surrounding environment. Phospholipid bilayers are highly permeable to Nile Red, so in principle it should label every single membrane in the samples. On the other hand, **FM1-43** is a water-soluble styryl dye that also exhibits high affinity for lipid environments, although it does not translocate through lipid bilayers due to its high polarity; thus, it only labels the hemilayer accessible from the addition medium. Besides, FM1-43 only emits fluorescence once incorporated into membranes, as water molecules strongly quench its fluorescent emission (Betz et al. 1996).

Particularly, the dependence of the accessibility of membranes and the environment sensed by the probes has been evaluated in terms of the lipid and protein composition. Secondly, the fluidity of membranes with different compositions has been studied as a function of temperature by electron spin resonance (ESR) spectroscopy. Thirdly, the structure of different membrane materials was imaged by transmission electron microscopy (TEM) and the observations were correlated to the different lipid and protein composition. Samples characterized in this study include complexes of native surfactant purified from porcine lungs and membranes reconstituted from whole surfactant organic extract or from partial fractions obtained by size-exclusion chromatography.

Finally, the effect of proteins SP-B and SP-C on the permeability of model membranes has been analyzed by fluorescence microscopy, through the reconstitution of POPC giant vesicles (GV) in the absence or presence of the hydrophobic protein fraction of surfactant or isolated SP-B or SP-C. Permeability towards different fluorescent probes has been observed, which allowed us to characterize the permeabilization effect of these proteins. The membrane-partitioning probe FM1-43, the water-soluble fluorophore calcein

-a typical leakage marker-, and fluorescently labeled dextrans of different sizes, FITC-dextrans from 4 to 500 KDa, which are water soluble and membrane impermeable as well, were employed to determine the size range of molecules that are able to permeate through model membranes supplemented by proteins SP-B and/or SP-C. Fluorescence microscopy was also employed to get a direct visualization of the protein distribution on POPC membranes by giant vesicle immunofluorescence.

4.2 RESULTS

4.2.1 ACCESSIBILITY OF NATIVE, QUASI-NATIVE AND MODEL MEMBRANES TO FLUORESCENT PROBES

To assess the effect of the presence of hydrophobic surfactant proteins SP-B and/or SP-C on the permeability of phospholipids membranes we have taken advantage of the fluorescent emission of two extrinsic probes, Nile Red and FM1-43, which are permeable and impermeable, respectively, to membranes.

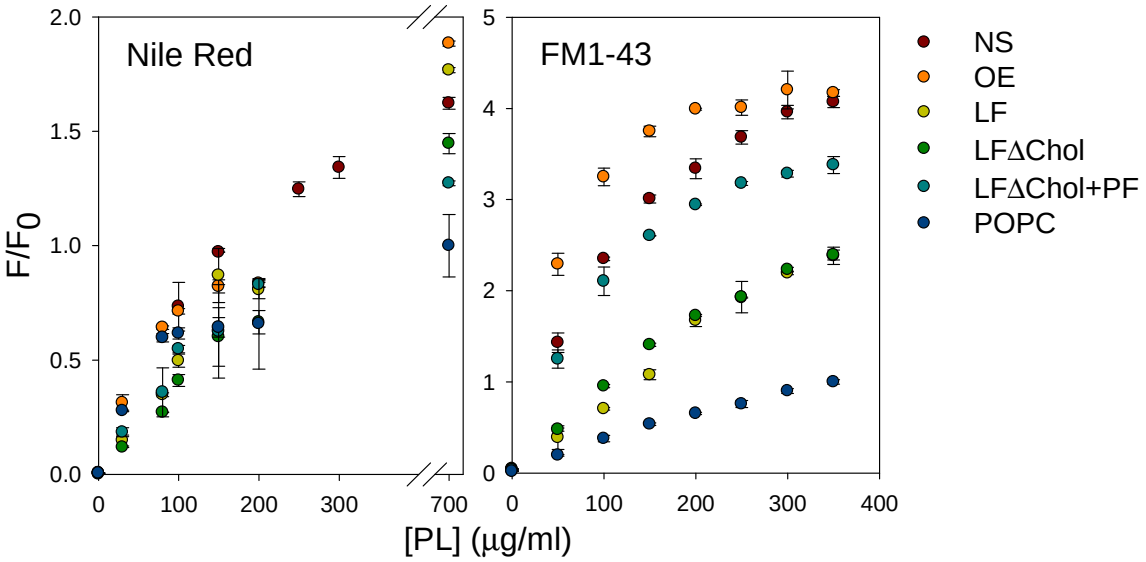

Fig. 4.1: Dependence of Nile Red and FM1-43 fluorescent emission on phospholipid concentration in membranes prepared form the different materials tested. All values have been referred to POPC model membranes, being F_0 the maximum emission of each probe incorporated into the most concentrated preparation of POPC MLV: 700 µg/ml in the case of Nile Red and 350 µg/ml for FM1-43.

Figure 4.1 compares the emission fluorescence intensity of Nile Red and FM1-43 (added at 3 and 2 µM, respectively) as a function of their incorporation into increasing concentrations of different lipid and lipid/protein suspensions, including native pulmonary surfactant complexes (NS) and multilamellar vesicles (MLV) reconstituted from the whole surfactant organic extract (OE), the protein-free lipid fraction of surfactant (LF), the

surfactant lipid fraction depleted of cholesterol (LFΔChol) or the lipid fraction depleted of cholesterol but supplemented with the hydrophobic protein fraction of surfactant (LFΔChol+PF). For comparison, Nile Red and FM1-43 fluorescence in equivalent concentrations of multilamellar vesicles of POPC has been also determined. All membrane preparations used in the present chapter were hydrated in 5 mM Tris 150 mM NaCl pH 7.

The effect of the presence of the different membrane components on the fluorescence of both probes was completely different. The fluorescence emission of Nile Red showed similar dependence on lipid concentration, within the experimental error, for the different materials tested, up to concentrations around 200 μg/ml (left panel in figure 4.1), indicating that all these materials exhibited similar accessibility to this membrane-permeable probe. For the highest lipid amounts, some differences in the emission intensity of Nile Red became relevant, probably as a consequence of local differences in the polarity of the environment sensed by the probe. For instance, this membrane probe showed higher emissions in materials containing cholesterol and other neutral lipids (NS, OE and LF) than in membranes prepared from fractions depleted of cholesterol and, specially, in pure POPC membranes. This is probably a consequence of the well-known effect of cholesterol to seal membranes and reduce their level of hydration. The environment sensed by Nile Red in cholesterol-containing surfactant membranes would then be more dehydrated, and therefore more hydrophobic, than that in cholesterol-free bilayers, leading to a higher intensity of fluorescence emission. There were no apparent effects of the protein content on the fluorescence of this probe.

In contrast to Nile Red, the fluorescence emission of FM1-43 is remarkably different between the diverse membrane compositions (right panel of figure 4.1). The probe showed around two-fold higher fluorescence in protein-containing membranes, i.e., those from native surfactant (NS), its organic extract (OE) or its lipid fraction depleted of cholesterol but supplemented with SP-B and SP-C (LFΔChol+PF), than in those made of protein-free surfactant lipids (LF, LFΔChol and POPC). FM1-43 fluorescence emission in surfactant lipid membranes was also substantially higher than that measured in POPC bilayers. Therefore, the presence of proteins SP-B and SP-C appeared to be important to provide lipid membranes with full accessibility to membrane-impermeable probes such as FM1-43.

The differences in accessibility to FM1-43 of the different membrane suspensions are probably manifested due to their multilamellar character. The outermost impermeable membranes would impede exposure of inner membranes to the probe. In figure 4.2 we have compared probe accessibility of native surfactant membranes, membranes reconstituted from the whole surfactant organic extract, and model POPC bilayers when preparing suspensions with different degree of lamellarity. As shown in the right panel of figure 4.2, FM1-43 produced higher fluorescence emissions in unilamellar vesicles (LUV, prepared by extrusion, or SUV, by sonication) than in multilamellar suspensions of POPC at any given phospholipid concentration as a consequence of the larger membrane surface exposed to the external medium, where the dye was added. In contrast, there were no apparent differences in the fluorescent emission of the probe partitioning in unilamellar or multilamellar suspensions of either native surfactant or its organic extract. Again, this result

points out to a potential effect of surfactant proteins to facilitate accessibility of the membrane-impermeable probe across different membranes.

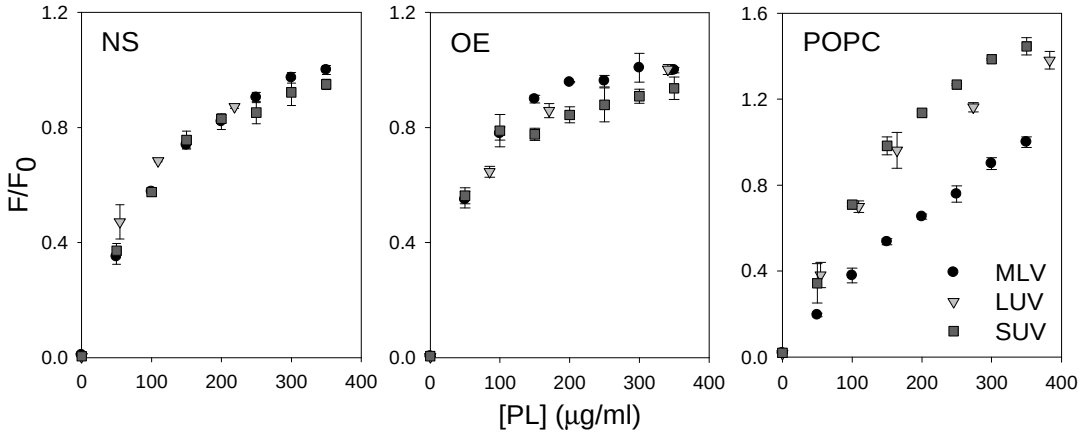

Fig. 4.2: Comparison of the level of FM1-43 accessibility to unilamellar and multilamellar membrane suspensions made from native pulmonary surfactant (NS), its organic extract (OE) or POPC. The reference value F_0 is specific for each material, corresponding to FM1-43 fluorescence emission incorporated into the most concentrated preparation of each sample in MLV form (350 μg/ml).

To test whether the mere presence of SP-B and/or SP-C would be enough to facilitate FM1-43 partition across membranes, the effect of introducing surfactant proteins on probe accessibility was studied by comparing unilamellar and multilamellar suspensions of simple POPC vesicles. Figure 4.3 compares FM1-43 fluorescence when added to increasing concentrations of MLV or LUV suspensions of POPC in the absence or presence of hydrophobic surfactant proteins. POPC membranes were supplemented with the whole protein fraction of surfactant (PF, the physiological SP-B/SP-C mixture, added to the phospholipids at an equivalent lipid-to-protein ratio to that obtained in the LH-20 chromatography) or supplemented with 1% (w/w) of isolated SP-B or SP-C. PF, SP-B and SP-C employed for these experiments were purified from BAL, as was described in section 3.1.3.1. Figure 4.3 (left panel) shows how FM1-43 emission was around 4-fold higher in all protein-containing MLVs than in pure POPC membranes, with small but consistent differences between the different protein-containing samples. The order of membrane accessibility to the probe appeared to be the following: SP-B > PF > SP-C. In contrast, the differences between protein-containing and protein-free membranes in terms of FM1-43 fluorescence were less remarkable in the case of POPC LUV suspensions (right panel of figure 4.3).

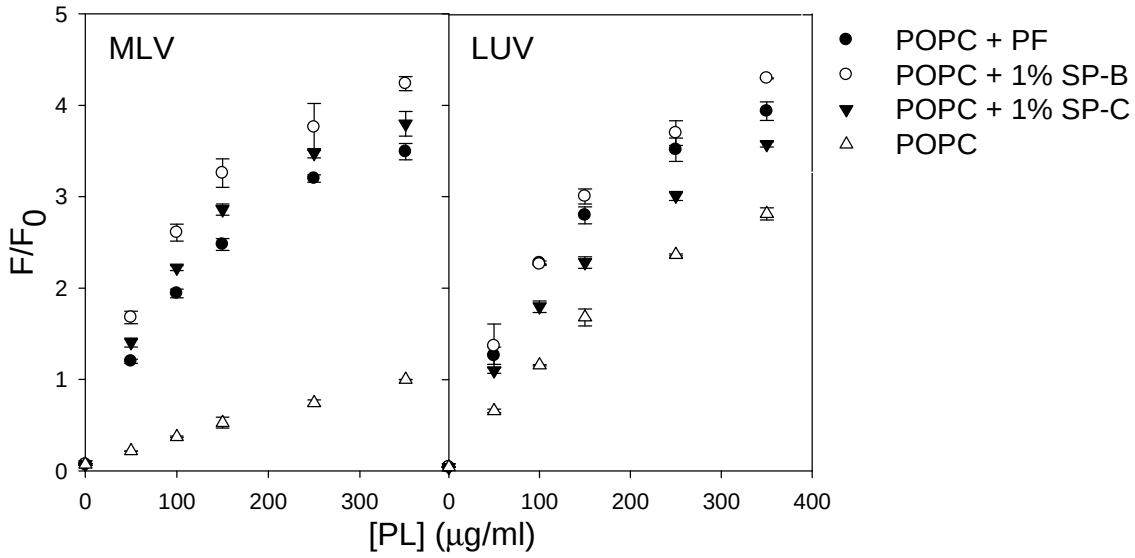

Fig. 4.3: Comparison of FM1-43 fluorescence emission in multilamellar (MLV) and unilamellar (LUV) preparations of model POPC membranes supplemented with the hydrophobic surfactant protein fraction (PF), 1% (w/w) SP-B or 1% (w/w) SP-C. The reference value F_0 corresponds to FM1-43 emission in the POPC MLV sample with the highest lipid concentration tested.

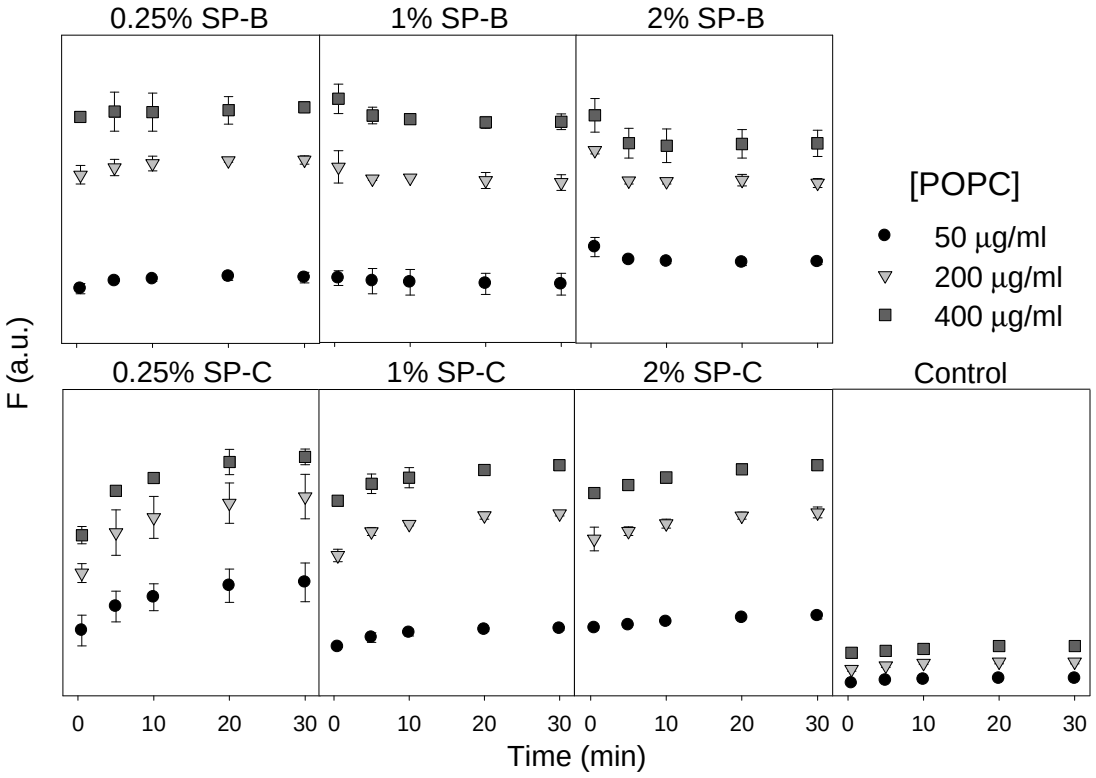

Fig. 4.4: Kinetic analysis of FM1-43 incorporation to increasing concentrations of POPC multilamellar vesicles containing different proportions of SP-B or SP-C (by weight with respect to phospholipids). Results are shown in comparison with the control sample, MLV of pure POPC.

In order to get further insight into the different effect of SP-B and SP-C on facilitating FM1-43 transfer across multilamellar membrane arrays, FM1-43 incorporation kinetics to POPC multilamellar suspensions was studied by adding the fluorescent dye to POPC MLV containing 0.25, 1 or 2% (protein to lipid by weight) of either purified SP-B or SP-C. Physiological proportions of these proteins are thought to be around 1% in native surfactant, but in this case much lower, subphysiological proportions were employed in order to maximize kinetic differences. As shown in figure 4.4, incorporation kinetics of FM1-43 into POPC membranes were significantly different between SP-B- and SP-C-containing membranes. In the case of SP-B, the fluorescence emission of the probe reached its maximum value during the first 30 seconds after dye addition, while in the case of SP-C-containing samples the emission increased gradually along the first 30 minutes, being the difference in kinetics maximal at the lowest proportion of the protein.

The dependence of FM1-43 emission on SP-B and SP-C content in POPC MLV membranes was also analyzed. Maximal emission intensities were obtained for different protein densities and compared in figure 4.5. Below 0.5% protein to lipid ratio (w/w), SP-B produced always higher fluorescence, hence better probe partition across membranes, than SP-C. The lowest proportion of SP-B tested, 0.1% (a molar ratio around $1/10^4$ protein to lipids) was already able to produce the maximum level of FM1-43 incorporation into POPC membranes, suggesting that SP-B is extremely efficient in facilitating permeability of this membrane-impermeable probe across bilayers. The effect of increasing amounts of the other protein, SP-C, appeared to be much more gradual, in such a way that FM1-43 partition in POPC membranes is clearly SP-C concentration-dependent.

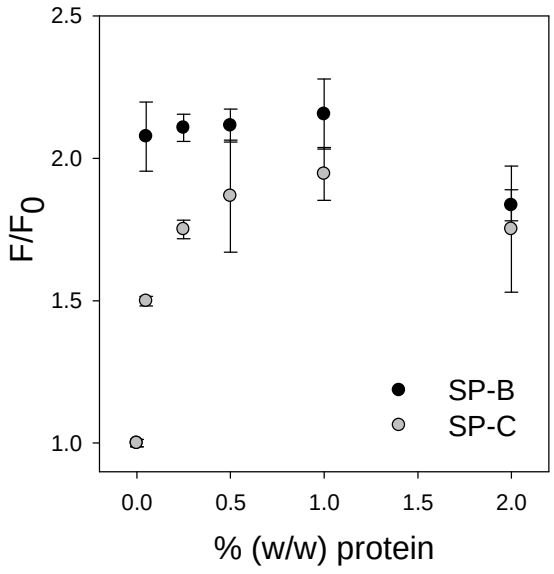

Fig. 4.5: FM1-43 fluorescence emission in POPC multilamellar vesicles (200 μg/ml) as a function of protein density, comparing SP-B and SP-C effect on membranes.

4.2.2 MEMBRANE FLUIDITY OF NATIVE AND QUASI-NATIVE MATERIALS BY ELECTRON SPIN RESONANCE

In order to get a deeper characterization of membranes from native surfactant or from quasi-native materials purified from surfactant, electron spin resonance (ESR) spectroscopy was employed in order to study the fluidity of the different membrane materials as a function of temperature, which can be related to lipid mobility inside the bilayer. This technique can provide information about the degree of mobility of phospholipid hydrocarbon chains thanks to the incorporation of spin probes consisting of different PC molecules labeled by a nitroxide radical (the spin label) at the n-th position of their *sn*-2 acyl chain, termed as n-PCSL, which report local differences of mobility inside the bilayer as a function of depth. In the present work, two different spin labels have been employed, as described in section 3.6: 5-PCSL, whose unpaired electron lies at the 5-th position of the acyl chain, relatively close to the phospholipid polar head; and 14-PCSL, with the free radical located close to the middle plane of the bilayer. Native surfactant (NS) and MLV prepared with its organic extract (OE), the whole lipid fraction of surfactant (LF) and POPC were thus spin-labeled with these two probes at 1% probe-to-lipid molar ratio, as explained in detail in Materials and Methods, section 3.5.

In the presence of a magnetic field, the energy levels of an unpaired electron are split as a consequence of the quantization of its spin angular momentum, what is known as the Zeeman effect; by applying an electromagnetic radiation, it is possible to induce a transition between the two levels, whenever the photon energy is equal to the energetic separation between levels (Wertz and Bolton 1986). ESR spectra are therefore radiation absorption spectra, generally in the range of microwaves, obtained by either varying the frequency of radiation and keeping the magnetic field constant, or vice versa. Here, and most commonly in practice, the frequency was fixed at 10 GHz while the magnetic field was linearly varied until it reached the transition energy value; at this point, the transition occurred between the lowest energy Zeeman level (where the electron population is larger) and the highest energy level due to the relaxation processes, yielding a net energy absorption which was registered. The ESR spectra are usually presented as the first derivative of these absorption registers. The central peak reflects this electron interaction with the magnetic field already mentioned, but when studying spin labels as nitroxide-labeled phospholipids incorporated in membranes, two extra peaks appear in the spectra (see figure 4.6): they are the result of the hyperfine coupling between the electron spin and the spin of a neighbor nucleus, causing the splitting of each one of the Zeeman levels and the appearance of 2I+1 lines in the spectrum, separated from the adjacent line a distance that is equivalent to the **hyperfine coupling constant (A_{max})**. In the ESR spectra included here, the nucleus that interacts with the unpaired electron is the nitrogen (I = 1) from the nitroxide radical, yielding powder ESR spectra consisting of three lines.

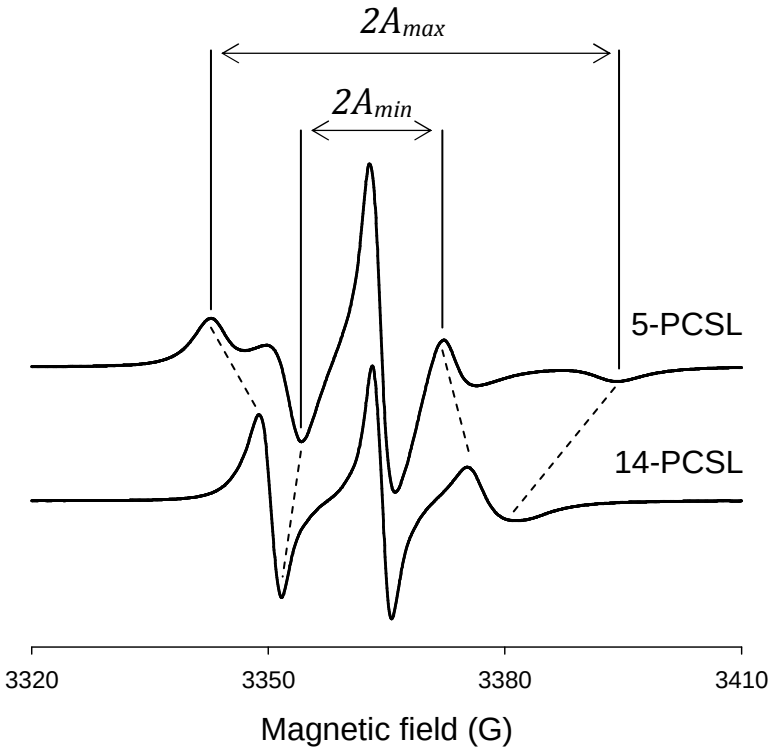

Fig. 4.6: Powder ESR spectra of the two spin-labels incorporated in POPC multilamellar vesicles, recorded at microwave frequency of 10 GHz. The total spectral width, twice the hyperfine coupling constant A_{max}, and Zeeman linewidth $2A_{min}$, are indicated for both spectra. Magnetic field units are Gauss (G), where 1G = 10^{-4} Tesla.

The spectral width is related to the degree of mobility and anisotropy of the spin label in its local environment: when the free radical is located in a low viscosity, isotropic medium, a narrow spectra with narrow peaks is obtained, but when the mobility and degrees of freedom are reduced, the resulting spectra is both wider and asymmetric (Griffith et al. 1965). The example shown in figure 4.6 illustrates these differences in probe mobility: the 5-PCSL spectrum is wider and more asymmetric than that of the 14-PCSL probe, meaning that the latter senses a freer movement than the former one due to the different position of the free radical inside the hydrocarbon chain. The most important expression of anisotropy was the appearance of the second "shoulder" in the hyperfine lines, which disappeared in the spectrum corresponding to the deepest spin probe, with higher mobility (Perez-Gil et al. 1995). Besides, another well-known effect in anisotropic ESR spectra can be observed here: the line corresponding to high field is wider than the low-field line, due to the fact that the linewidth is proportional to the mean value of the square displacement of the line with respect to the main peak (Wertz and Bolton 1986).

When studying native surfactant membranes and multilamellar preparations reconstituted from the organic extract or the lipid fraction of surfactant, similar differences were observed between the mobilities of the 5-th and the 14-th chain position probes. Besides, **powder ESR spectra** were obtained for native surfactant (NS), its organic extract (OE) and surfactant whole lipid fraction (LF) for several temperatures in the range

between 22 and 65ºC; these spectra are called "powder spectra" because they are the resultant of all emission contributions from a randomly oriented sample, formed by pelleted multilamellar vesicle suspensions and not oriented layers. Noticeable temperature dependence was observed in all the materials, reflected as a progressive narrowing of the whole spectra and of each one of the peaks for increasing temperatures, as can be observed in figure 4.7.

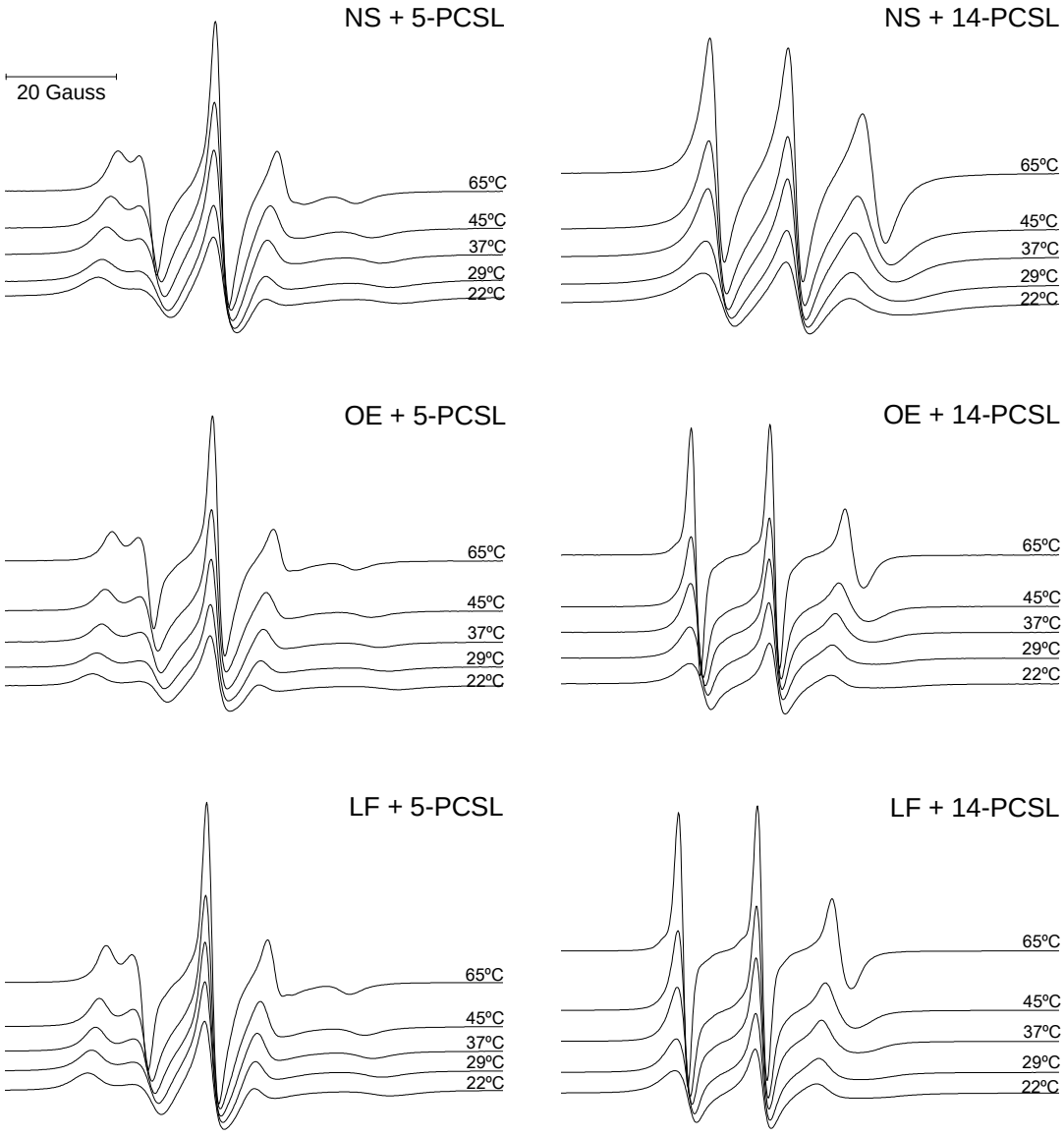

Fig. 4.7: Powder ESR spectra of the membrane spin labels 5- and 14-PCSL incorporated into native surfactant membranes (NS), organic extract (OE) MLV and surfactant lipid fraction (LF) MLV at five selected temperatures. Spectra were aligned in the x axis in order to align the centers of the Zeeman line.

Similarly to the spectra in POPC, the differences in spin probe spectra at different depths in the acyl chains are evident, with a wider and more anisotropic spectra from the probe 5-PCSL compared to that from 14-PCSL in the three tested materials. The spectra of

the probe 14-PCSL appeared to be wider in NS membranes than in OE or LF multilamellar preparations, indicating that the spin probe was somehow located in a less fluid environment, with a lower degree of freedom. Figure 4.8 compares the ESR spectra of both probes, 5- and 14-PCSL, incorporated into NS, OE and LF at two selected temperatures: 22ºC, below the phase transition of surfactant lipid membranes, and 37ºC, the physiological temperature, close to the melting point of surfactant. Again, configurational freedom as sensed by the most superficial probe, 5-PCSL, was very similar in the three membrane environments, while more important differences appeared at deeper positions inside the bilayer, especially at 37ºC.

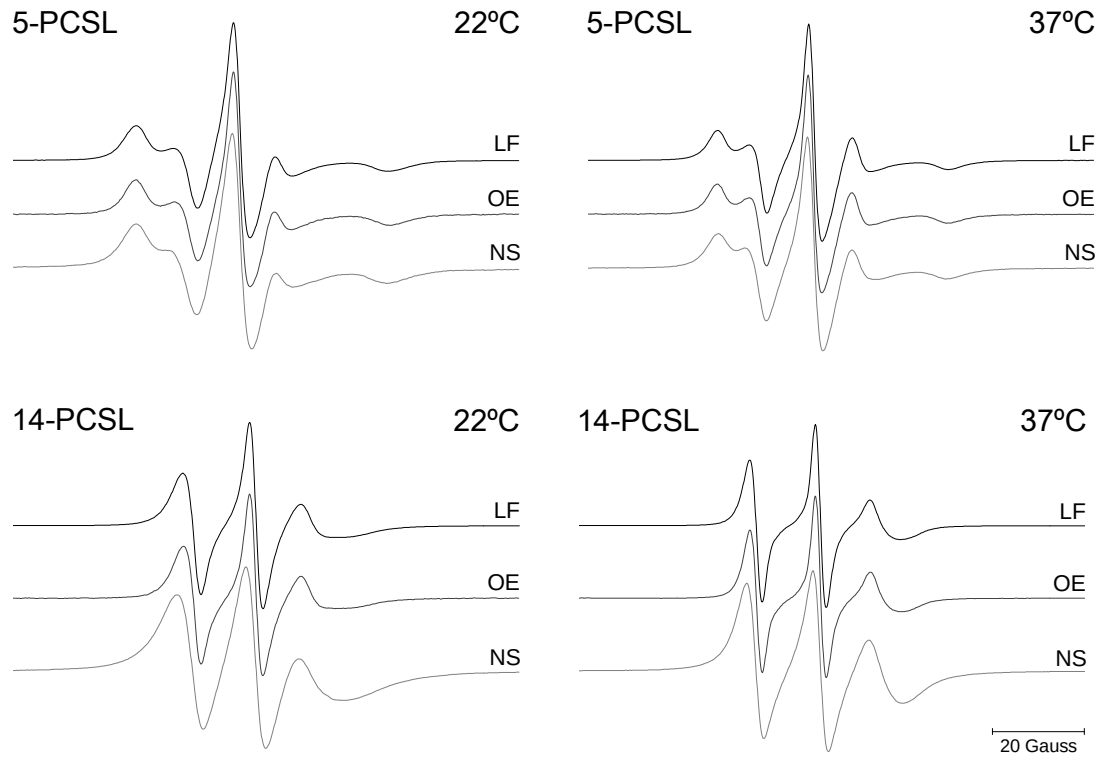

Fig. 4.8: Powder ESR spectra of the membrane spin labels 5-PCSL (top) and 14-PCSL (bottom panels) incorporated in native surfactant (NS), organic extract (OE) MLV and surfactant lipid fraction (LF) MLV at two different temperatures: 22 (left) and 37ºC (right panels). Spectra were aligned in the x axis in order to align the centers of the Zeeman line.

In order to extract more information from the ESR spectra and their temperature dependence, the **thermotropic profiles** of the two spin probes in the different membrane materials were obtained. The order parameter (S) is considered to measure the amplitude of the wobbling motion of the hydrocarbon chain at the segment sensed by the given spin probe. For instance, an increase in the order parameter indicates a decrease in the angle of the movement, which is translated into a decrease in spin probe mobility and, therefore, into a lower membrane fluidity. The order parameter can be calculated from the ESR spectra parameters by using the following equation (Marsh 1981):

$$S = 0.5407\frac{A_{max} - A_{min}}{a_0} \;;\; \text{where } a_0 = \frac{A_{max} + 2A_{min}}{3}$$

The experimental values of A_{max} and A_{min} were directly estimated from the ESR spectra, as was previously indicated in figure 4.6. The order parameter S was then plotted as a function of temperature for each spin probe incorporated in the different samples (see figure 4.9).

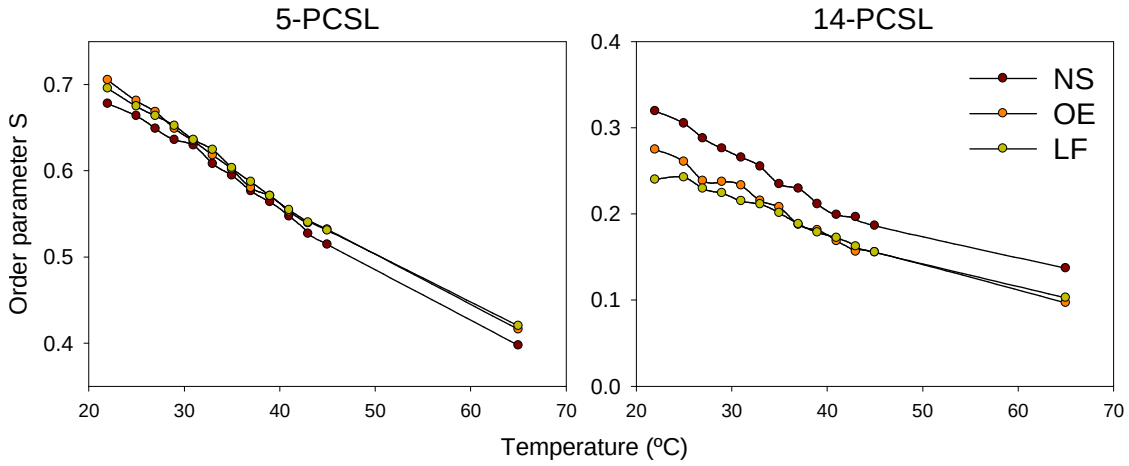

Fig. 4.9: Thermotropic profiles of the order parameter S at the acyl chain segments sensed by the two spin probes, 5- and 14-PCSL, incorporated in the three tested membrane materials, native surfactant (NS) and MLV reconstituted from its organic extract (OE) or its protein-free lipid fraction (LF).

The thermotropic profiles of the probe 5-PCSL were very similar in the three membrane materials, as shown in the left panel of figure 4.9, with an almost linear decrease of the order parameter of around 0.007/ºC for the three samples. There were no apparent evidences for sudden changes in order at certain temperatures, which would have revealed the existence of more or less cooperative phase transitions. This result indicates that the fluidity of the three types of membranes appears to be very similar at the regions of the acyl chains close to the polar heads.

On the other hand, the degree of mobility increased remarkably; for example, at 25ºC, 5-PCSL spectra allowed the estimation of an order parameter of 0.664 in NS, while that from 14-PCSL spectra decreased to 0.305. Furthermore, subtle differences appeared between the different samples: native surfactant showed for the whole temperature range a higher order parameter than the rest of materials, meaning that the spin probe had a reduced mobility and therefore sensed a less fluid environment than in membranes reconstituted from surfactant organic extract or its lipid fraction. This reduced fluidity/lipid mobility could be related either to the native structure of surfactant membranes as assembled *in vivo* or with the presence of the main surfactant protein, SP-A, which has been reported to potentiate membrane aggregation and packing. Interestingly, OE membranes presented a slightly lower mobility than membranes from LF for the lowest temperatures

tested, between 22 and 35ºC, but differences in probe mobility disappeared for 37ºC and higher temperatures. This result could be connected to the presence or absence of the hydrophobic proteins SP-B and SP-C, whose presence would affect the lipid mobility but only at temperatures below 35-37ºC. In summary, subtle differences between NS, OE and LF were found in membrane fluidity at significant, close to physiological, temperatures, which can be attributable to the presence of different protein fractions, specially hydrophobic proteins SP-B and SP-C, which could enhance lipid packing at temperatures lower than 37ºC, approximately the melting point of surfactant lipids.

4.2.3 VISUALIZATION OF NATIVE, QUASI-NATIVE AND MODEL MEMBRANES BY TRANSMISSION ELECTRON MICROSCOPY

As mentioned above, membrane accessibility and lipid packing, in terms of acyl chain mobility, can be closely related to the degree of complexity of membrane assemblies. In order to visualize the structure of the different native, quasi-native and model materials that have been studied in the two previous sections, negative staining of membrane samples was carried out by following the methodology described in section 3.6, and they were subsequently imaged by TEM.

First, native surfactant complexes (NS) purified from bronchoalveolar lavages as described in section 3.1.1, dissolved in saline buffer, 5 mM Tris 150 mM NaCl, and with no further processing except the negative stain, presented a huge complexity and a high level of aggregation as can be observed in figure 4.10. Relatively large membrane stacks, folded sometimes in small angles (image D) or even torsioned (image C), together with highly aggregated multilamellar vesicles (images A and B) were observed.

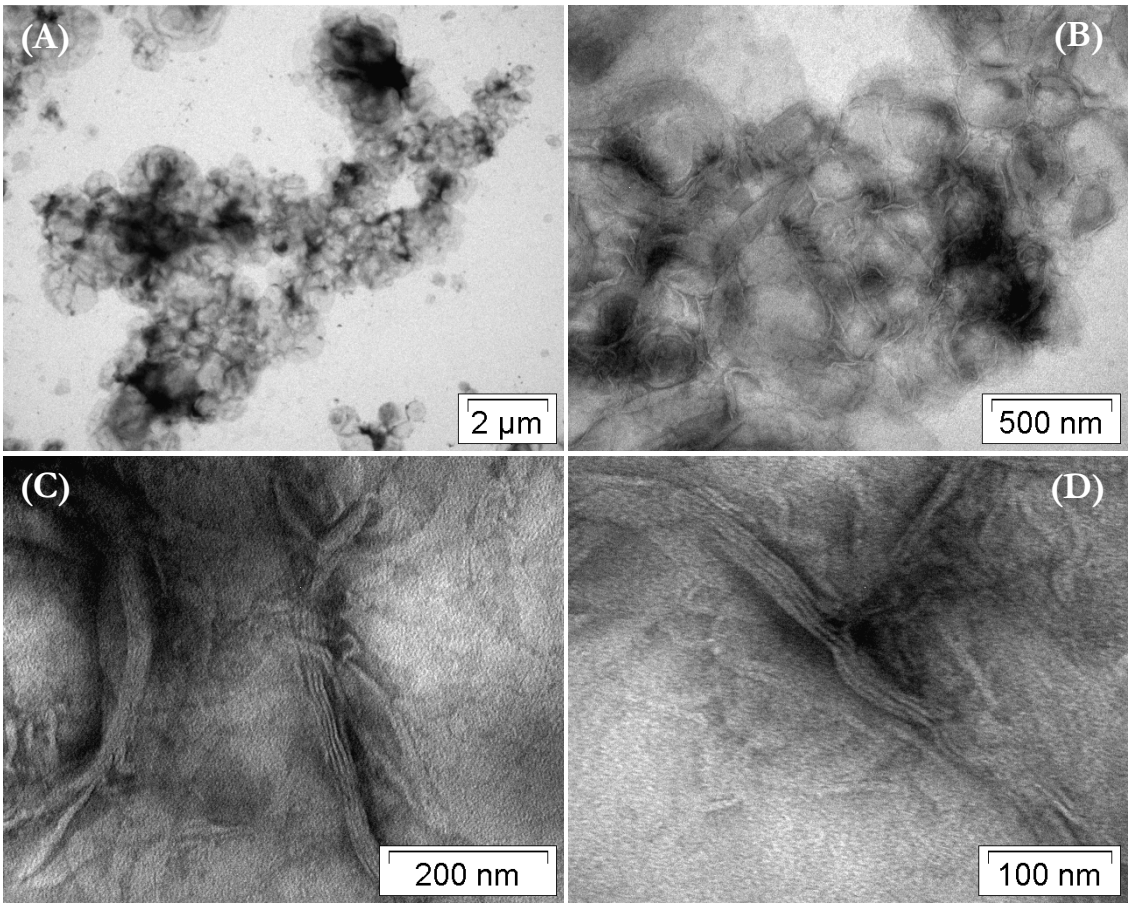

Fig. 4.10: Electron microscopy images of native surfactant complexes (NS), treated by negative staining, taken with different magnifications between 10k and 300k.

Membranes reconstituted from whole surfactant organic extract (OE), composed by the lipid fraction and the hydrophobic proteins SP-B and SP-C as explained in section 3.1.2, also presented a complex structure as shown in figure 4.11. Multilamellar arrays of vesicles (see images A and B), large membrane stacks with a high degree of lamellarity (images C and D) and complex structures were found in the sample, but, in general terms, the membrane structures seemed to be more spherical than those observed in native surfactant complexes.

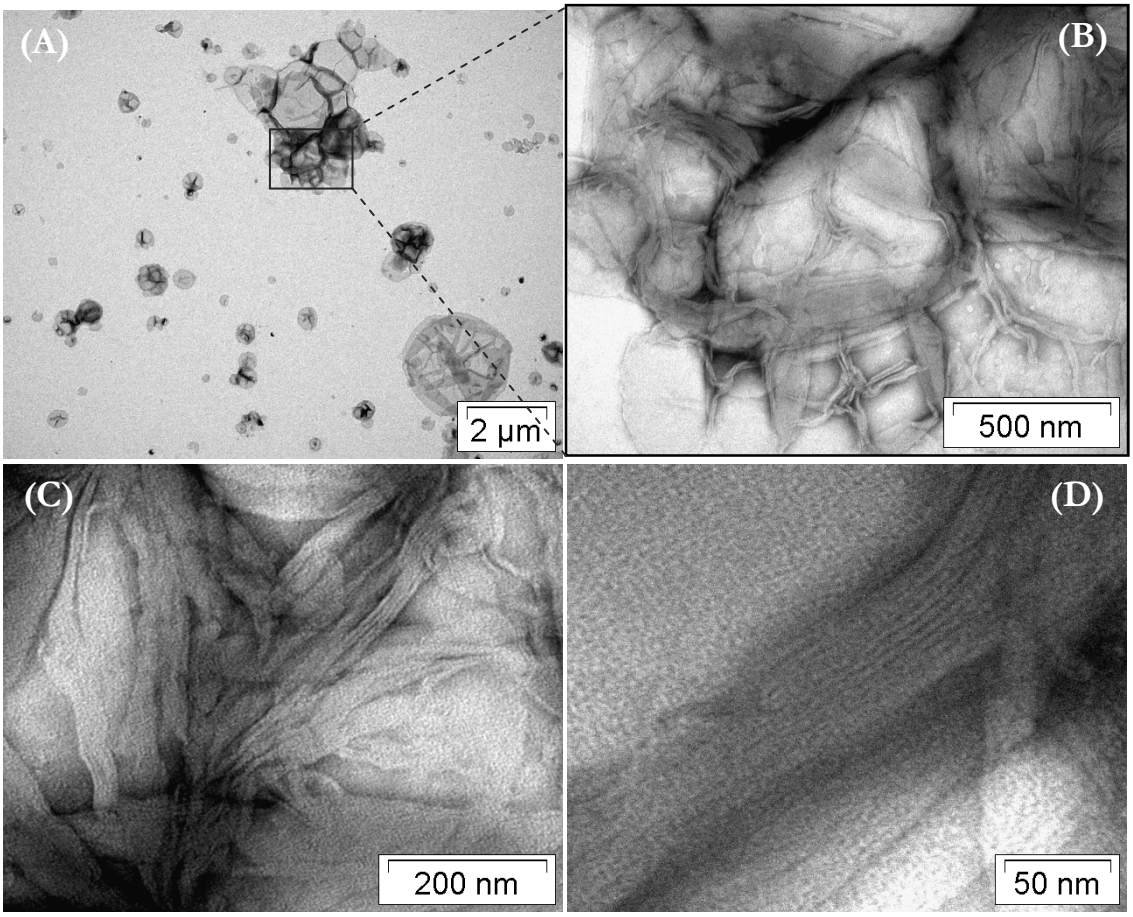

Fig. 4.11: Electron microscopy images of samples reconstituted from surfactant organic extract (OE), treated by negative staining and taken with different magnifications between 10k and 500k.

The third material visualized by TEM consisted of membranes reconstituted from protein-free lipid fraction of surfactant (LF), obtained by LH-20 chromatography of the organic extract, as described in section 3.1.3.1. As is illustrated in figure 4.12, in general terms, these samples contained more spherical and individual vesicles and showed a lower level of aggregation between them, although the heterogeneity was still high.

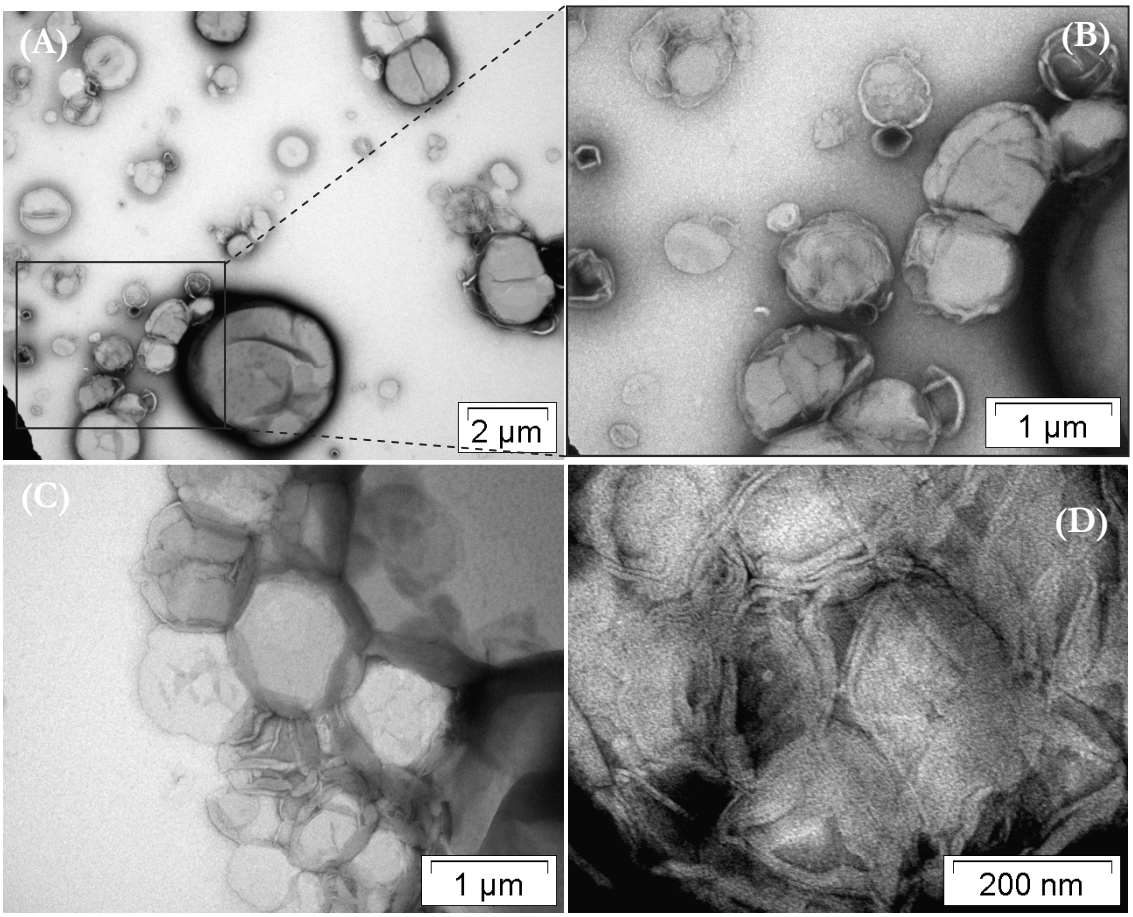

Fig. 4.12: Electron microscopy images of membranes reconstituted from surfactant lipid fraction (LF), treated by negative staining and taken with different magnifications between 10k and 200k.

The hydrophobic proteins SP-B and SP-C were also separated from surfactant lipids by LH-20 chromatography to obtain a mixture of both close to the physiological proportion, the hydrophobic protein fraction (PF), which could be subsequently separated from each other by LH-60 chromatography, as described in section 3.1.3. PF or isolated SP-B and SP-C were then mixed with a model phospholipid, POPC, and large unilamellar vesicles were prepared by extrusion, as explained in section 3.3.2, and subjected to negative staining and TEM visualization as well. Figure 4.13 shows representative images of these lipid and lipoprotein samples: pure POPC suspensions contained a relatively homogeneous vesicle population, with sizes around the expected ones (100 nm diameter), low degree of lamellarity, sometimes aggregated but generally isolated, and in general with no contacts between each other (see image A in figure 4.13). Similarly, suspensions of POPC supplemented with PF seemed relatively homogeneous and with low lamellarity (image B). In contrast, samples of POPC containing 1% of SP-B by weight with respect to phospholipids presented a high complexity, since they consisted of large and apparently multilamellar membrane complexes, some of them in the range of micrometer (see image C), in spite of the fact that they were originally extruded through 100 nm pore membranes. Vesicles prepared with POPC supplemented with 1% (w/w) SP-C showed a higher level of

aggregation than the first two samples (POPC and POPC+PF), but mostly consisted of unilamellar and oligolamellar vesicles with a rather spherical shape as well.

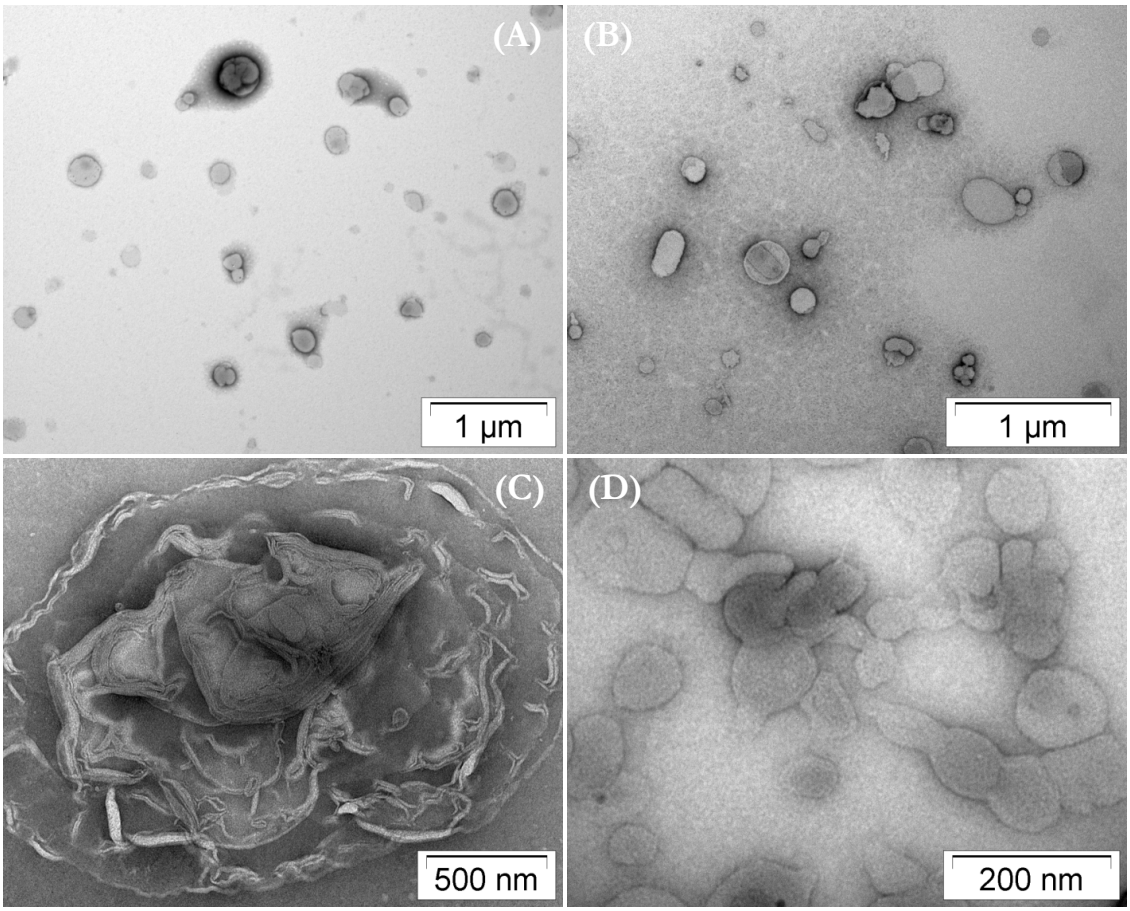

Fig. 4.13: Electron microscopy images of vesicle suspensions prepared by extrusion of membranes made from different lipid or lipid-protein mixtures: pure POPC (A); POPC supplemented with the hydrophobic surfactant protein fraction, POPC+PF, maintaining the native protein-to-lipid ratio (B); and POPC containing isolated SP-B (C) and SP-C (D) at 1% by weight with respect to phospholipids. Samples were prepared by negative staining.

The visualization of these diverse materials reveals several features: the complexity of membrane ultrastructure appears to be in descending order: NS > OE > LF, with the most complex structures being those adopted by the materials that were subjected to less processing, like NS and, to a lesser extent, OE. This could also be connected to the results on membrane fluidity as evaluated by ESR (section 4.2.2), suggesting that both higher complexity and protein content are likely connected to the observed differences in lipid mobility/fluidity between NS, OE and LF membranes. Finally, membrane ultrastructure is apparently directly related to the presence of surfactant proteins, especially SP-B, which seems to affect dramatically membrane organization, creating large bilayer-bilayer contacts and somehow recapitulating the native ultrastructure. Surprisingly, membrane materials showing such a degree of complexity and multilamellarity were demonstrated to be highly accessible to membrane-partitioning of water-soluble dyes.

4.2.4 MEMBRANE PERMEABILITY TOWARDS FLUORESCENT MOLECULES

4.2.4.1 Giant vesicle permeability to FM1-43

Following the experiments described in section 4.2.1, and in order to achieve a direct visualization of the effect of surfactant proteins on FM1-43 membrane labeling in a more homogeneous and controlled membrane structural context, model POPC giant vesicles (GV) were prepared by electroformation (see section 3.3.4.1) in the absence and presence of the hydrophobic surfactant proteins. Then, a series of fluorescence microscopy experiments were carried out in order to monitor the ability of the probe to label the external and internal membranes of these GV. Their large size allowed their direct visualization under an optical microscope and the simultaneous examination of fluorescent probe partition and membrane macroscopic morphology.

Figure 4.14 compares the morphology and FM1-43 labeling of two different samples: GV made of pure POPC and made of POPC containing the hydrophobic protein fraction (PF) obtained after the LH-20 chromatography (see section 3.1.3), at a proportion which mimics the lipid/protein ratio in surfactant organic extract. Two representative GV of each sample are shown here, exhibiting a clear oligolamellar structure under the optical microscope operated under phase contrast, but the observations were general for the whole vesicle preparation. Upon incubation with FM1-43, pure POPC GV were labeled only in the outermost layer (see images B and D in figure 4.14). In contrast, exposure to the probe produced almost instantaneous labeling of every membrane in POPC+PF vesicles (see images F and H in figure 4.14).

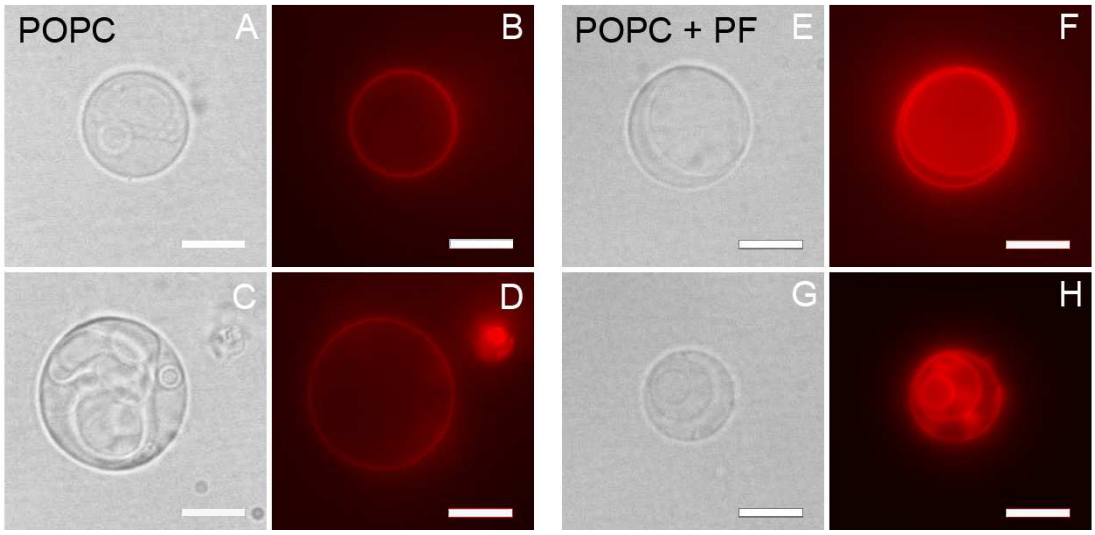

Fig. 4.14: Giant oligolamellar vesicles of POPC (A-D) and POPC supplemented with the hydrophobic protein fraction of pulmonary surfactant (E-H). Images A, C, E and G are bright field images; B, D, F and H, fluorescent images taken with the red filter set, corresponding to FM1-43 fluorescence. Scale bars: 10 μm.

Similar experiments were carried out with POPC giant vesicles supplemented with 1% by weight of either purified SP-B or SP-C, obtained after the LH-60 chromatography (section 3.1.3). Surprisingly, the morphology and characteristics of these GV containing only one of the surfactant proteins was substantially different to POPC or POPC+PF vesicles: on the one hand, no oligolamellar GV could be found in the POPC+SP-B preparation. As illustrated in figure 4.15, suspensions of POPC+SP-B vesicles were entirely composed of apparently giant unilamellar vesicles, with different sizes and a strong trend towards aggregation (see images A-D in figure 4.15), which were fully labeled by FM1-43. On the other hand, POPC+SP-C suspensions contained a large number of oligolamellar vesicles, but most of them became very unstable when observed under the microscope, showing a high tendency to distortion, rupture and reorganization.

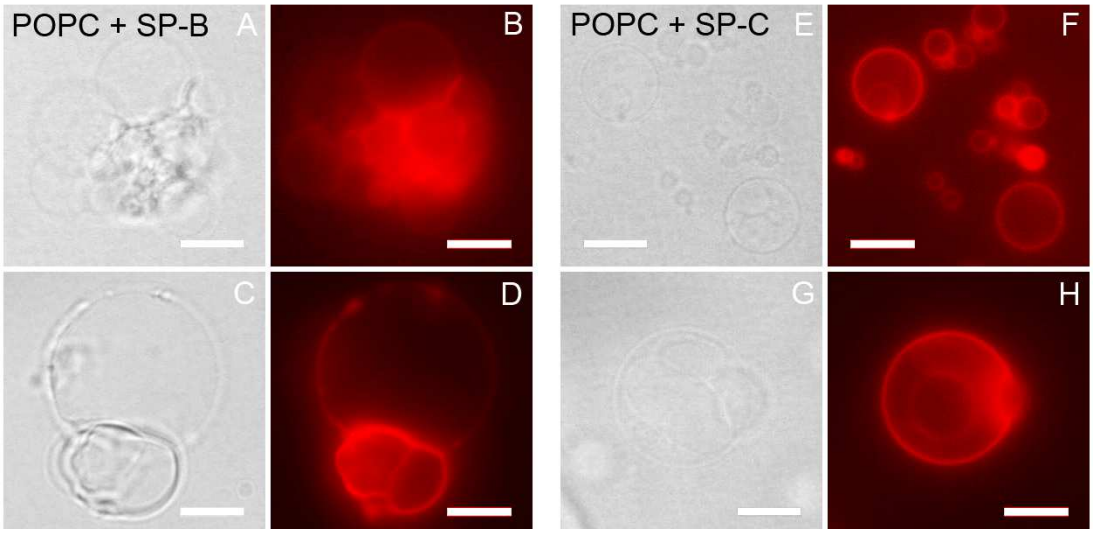

Fig 4.15: Giant oligolamellar vesicles of POPC supplemented with 1% (w/w) SP-B (images A-D) or 1% (w/w) SP-C (E-H). Images A, C, E and G are bright field images; B, D, F and H, fluorescent images taken with the red filter set, corresponding to FM1-43 fluorescence. Scale bars: 10 μm.

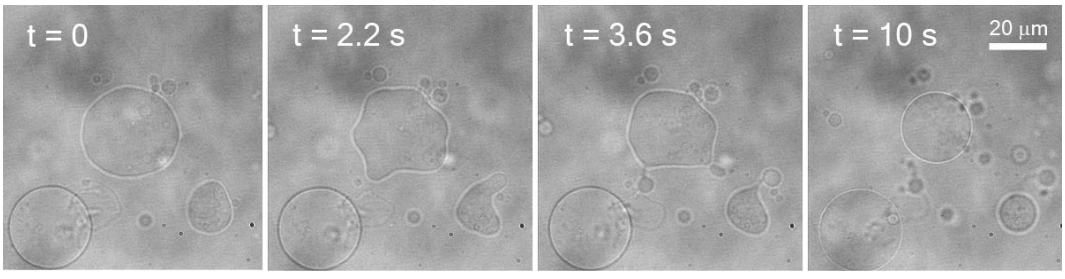

Fig. 4.16: Image sequence extracted from a video recorded in transmission mode. Giant vesicles of POPC + 1% (w/w) SP-C became very unstable and dynamic when observed under the microscope, showing frequent membrane fluctuations and protrusions that in many cases ended in the fragmentation of the vesicle.

To illustrate this last observation, figure 4.16 presents sequential frames taken from a video recording, showing the rupture of two giant vesicles containing SP-C: certain membrane regions protruded and formed evaginations that finally released smaller vesicles to the medium, before becoming again spherical and stable. Such dynamical behavior was never observed during these permeability assays for pure lipid or SP-B-containing vesicles.

4.2.4.2 Giant vesicle permeability to calcein

Permeability to FM1-43 of phospholipid membranes containing hydrophobic surfactant proteins SP-B and SP-C was demonstrated above, but there are different possible mechanisms that could cause inner membrane accessibility to this membrane-partitioning probe: i) the existence of membrane-membrane contacts promoted by the proteins, which would create a direct "lipid path" for probe internalization; ii) flip-flop processes between outer and inner hemilayers, followed by water partitioning of some probe molecules into the internal bilayers; or iii) the creation of water pores by surfactant proteins, since FM1-43 water solubility would allow it to cross the external bilayers through the pores. The amphipathic character of FM1-43 makes impossible to distinguish between these mechanisms, so a series of permeability assays was performed using a different fluorescent dye that is water soluble and impermeable to pure phospholipid membranes, such as the typical marker used to detect vesicle leakage, the probe calcein.

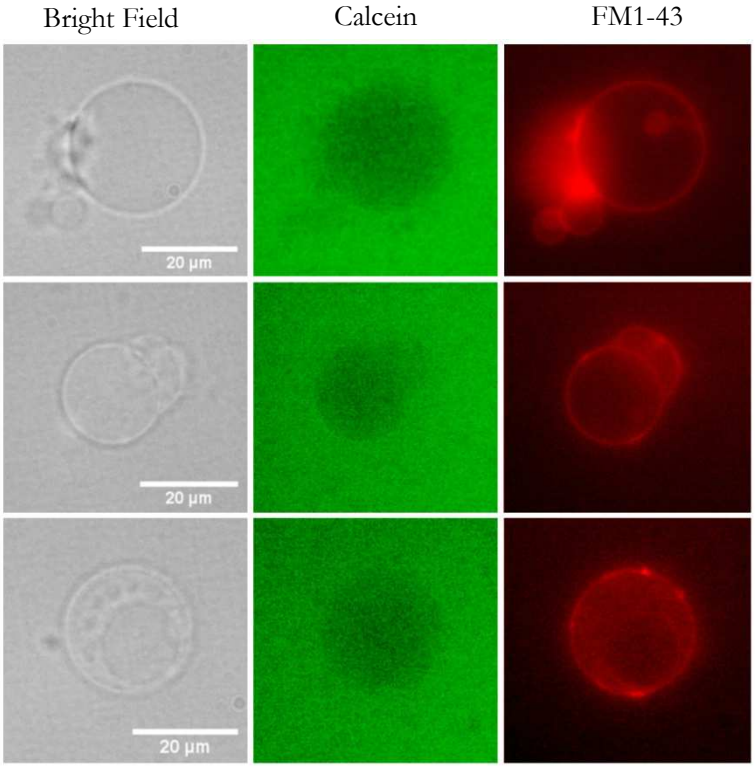

Fig. 4.17: Pure POPC giant vesicles incubated in a calcein solution for 4 hours, then diluted in a glucose solution and labeled with FM1-43 prior to the observation. The first column corresponds to transmission images; the second and the third columns, to fluorescent images obtained with FITC and Texas Red filter sets, respectively.

The ability of calcein to permeate through POPC giant vesicles in the absence or presence of the proteins was therefore tested, and some representative images were taken from each preparation and shown in the next figures. Figure 4.17 illustrates how pure POPC GV can be incubated for several hours in a calcein solution without internalization of the dye. Vesicles appeared as dark spheres when observed under the blue light used to excite calcein. In contrast, incubation with calcein of POPC vesicles containing the hydrophobic surfactant protein fraction (PF) led to the entrance of the dye. Figure 4.18 illustrates how calcein was able to enter into protein-containing POPC vesicles, showing even higher fluorescence that the external medium. Since the vesicles were diluted in a glucose solution after dye incubation, causing a decrease in calcein external concentration, this indicates that the equilibration of calcein across the membrane was not instantaneous and may be a slow process.

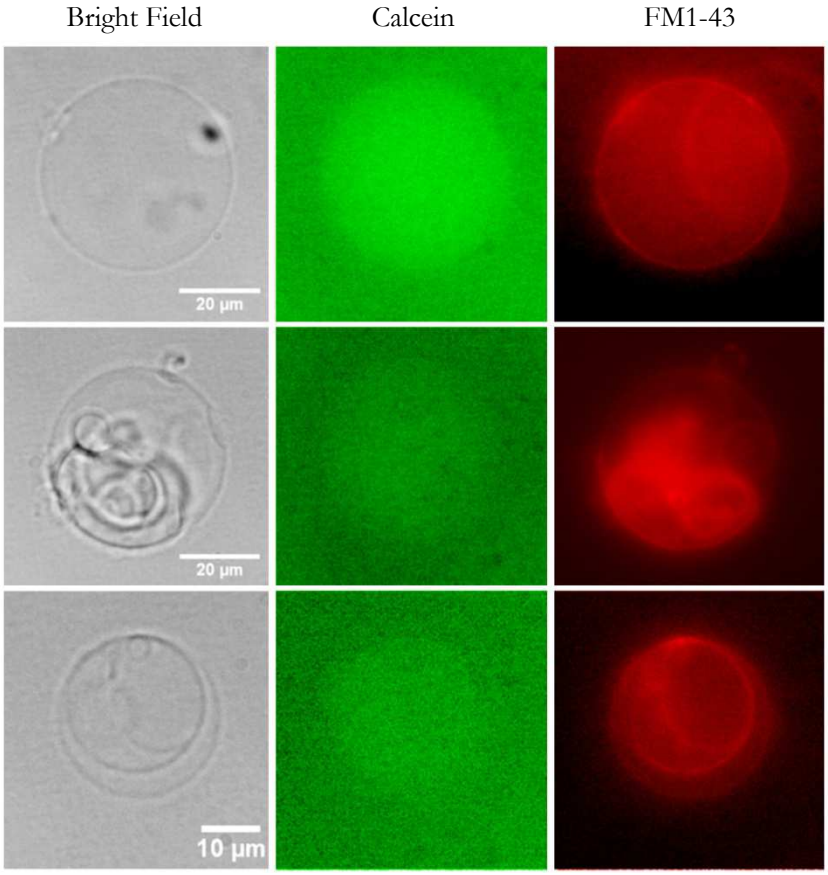

Fig. 4.18: POPC giant vesicles containing the hydrophobic protein fraction (PF), which were incubated in a calcein solution for 4 hours, then diluted in a glucose solution and labeled with FM1-43 prior to the observation. The first column corresponds to transmission images; the second and the third columns, to fluorescent images obtained with FITC and Texas Red filter sets, respectively.

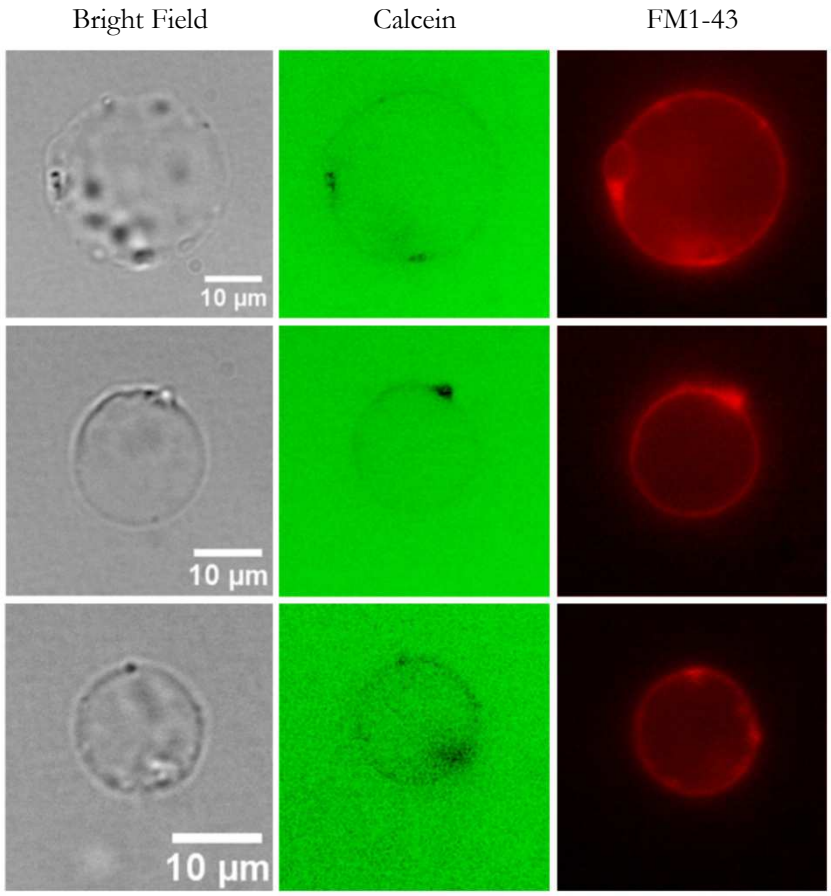

Fig. 4.19: POPC giant vesicles containing 1% (w/w) SP-B, incubated in calcein, diluted in a glucose solution and labeled with FM1-43 prior to the observation. The first column corresponds to transmission images; the second and the third columns, to fluorescent images obtained with FITC and Texas Red filter sets, respectively.

Calcein could also permeate through POPC vesicles containing isolated SP-B or SP-C, but with some differences compared to GV containing their physiological mixture PF. In the presence of either SP-B or SP-C, no differences in fluorescence intensity could be noticed between the external medium and inner vesicle compartments (see figure 4.19 and 4.20), indicating that calcein fluorescence was rapidly equilibrated between the internal and external media. Interestingly, images of calcein fluorescence in SP-B-containing GV showed large segments of the membrane that were much darker than the aqueous calcein solution, suggesting that calcein could be excluded from these regions.

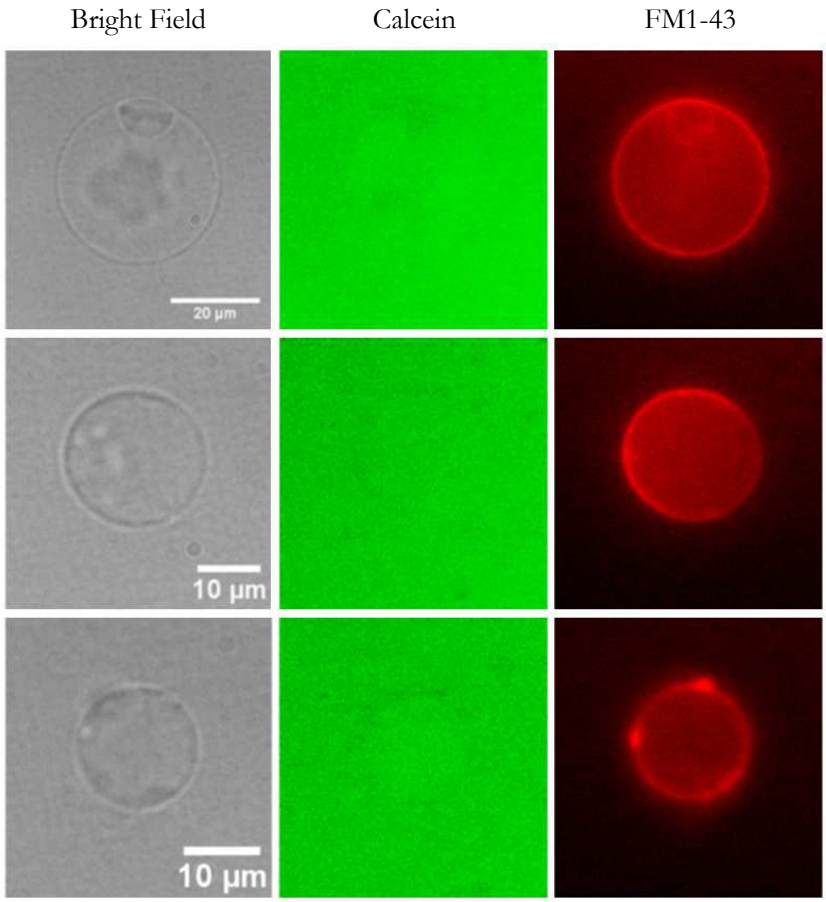

Fig. 4.20: POPC giant vesicles containing 1% (w/w) SP-C, incubated in calcein, diluted in a glucose solution and labeled with FM1-43 prior to the observation. The first column corresponds to transmission images; the second and the third columns, to fluorescent images obtained with FITC and Texas Red filter sets, respectively.

4.2.4.3 FITC-dextran permeability and estimation of pore size

Fluorescently labeled dextrans of different sizes, FITC-dextrans (FD) from 4 to 500 KDa, which are water soluble and membrane impermeable as well, were employed to determine the size range of molecules that are able to permeate through model membranes supplemented by proteins SP-B and/or SP-C. Lipoprotein giant vesicles, together with pure lipid vesicles that were used as non-permeable controls, were incubated for 3 hours in FITC-dextran aqueous solutions at room temperature as was described in Materials and Methods, section 3.7. Pure POPC vesicles were observed to be not permeable to any of the different dextrans tested, especially to the largest ones, with the exception of a small number of vesicles in which some permeability failures were noticed when incubated with the shortest dextran chains. See for instance the vesicle located at the bottom right of the first row of microscopy images in figure 4.21, which appears full of FITC dye, instead of dark like the impermeable ones.

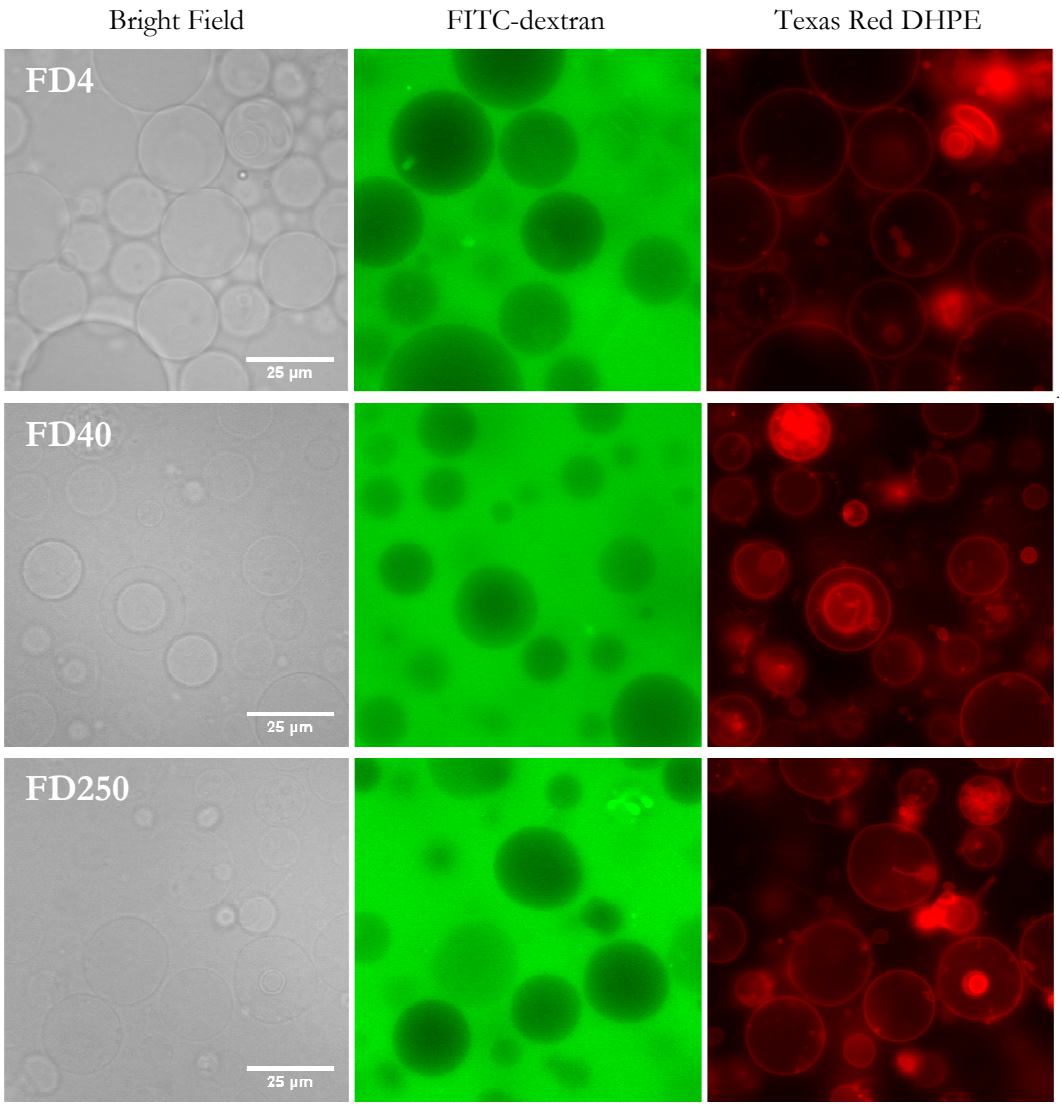

Fig. 4.21: POPC giant vesicles labeled with Texas Red DHPE and incubated in the presence of FITC-dextrans with three different average chain sizes (4, 40 and 250 KDa from up to down). The first column corresponds to transmission images; the second and the third columns, to fluorescent images obtained with FITC and Texas Red filter sets, respectively.

On the other hand, POPC giant vesicles containing physiological amounts of the SP-B and SP-C mixture obtained by LH-20 chromatography of the surfactant organic extract, turned out to be permeable to the smallest dextran tested, with an average molecular weight of 4 KDa, which corresponds to a hydrodynamic radius of approximately 1.4 nm, but not to the larger dextrans, as can be observed in figure 4.22, where some representative giant vesicles are shown.

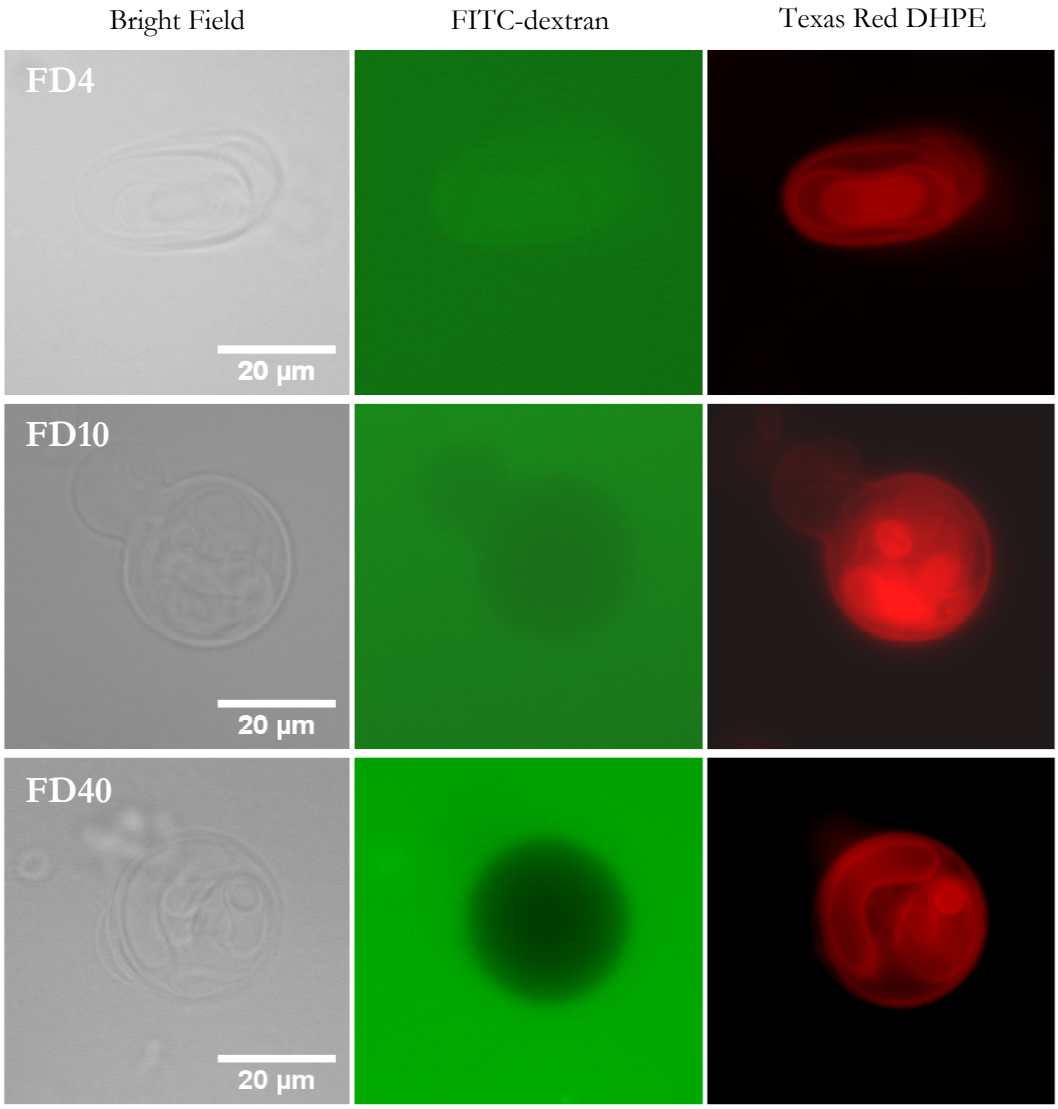

Fig. 4.22: POPC giant vesicles containing the hydrophobic protein fraction PF, labeled with Texas Red DHPE and incubated in the presence of FITC-dextrans with three different average chain sizes (4, 10 and 40 KDa from up to down). The first column corresponds to transmission images; the second and the third columns, to fluorescent images obtained with FITC and Texas Red filter sets, respectively.

However, when analyzing giant vesicle permeability in the presence of either SP-B or SP-C, the scenario appeared to be different. POPC giant vesicles supplemented by the physiological concentration of isolated SP-B (1% by weight with respect to phospholipids) appeared to be permeable to FD4, and also to FD10 and FD20 but not in a all-or-none fashion: permeability ratios to FD10 and FD20 were estimated as the percentage of permeated (filled) vesicles with respect to the total number of observed vesicles, and are shown in table 4.1, left columns. When testing permeability to larger FITC-dextrans (>4nm hydrodynamic radii), giant vesicles containing SP-B appeared to be impermeable. On the other hand and surprisingly, upon incorporation of isolated SP-C into POPC bilayers at a physiological concentration (1% by weight of phospholipids), giant vesicles appeared to be

permeable to all tested FITC-dextrans, from 4 to 500 KDa, although the ratio between permeated (filled vesicles) and the total number of observed vesicles varied accordingly to the distribution of dextran sizes, decreasing when the dextran size increased. Some fluorescent images of the permeability assays performed with different sized FITC-dextrans are shown in figures 4.23 and 4.24 for SP-B- and SP-C-containing vesicles, respectively.

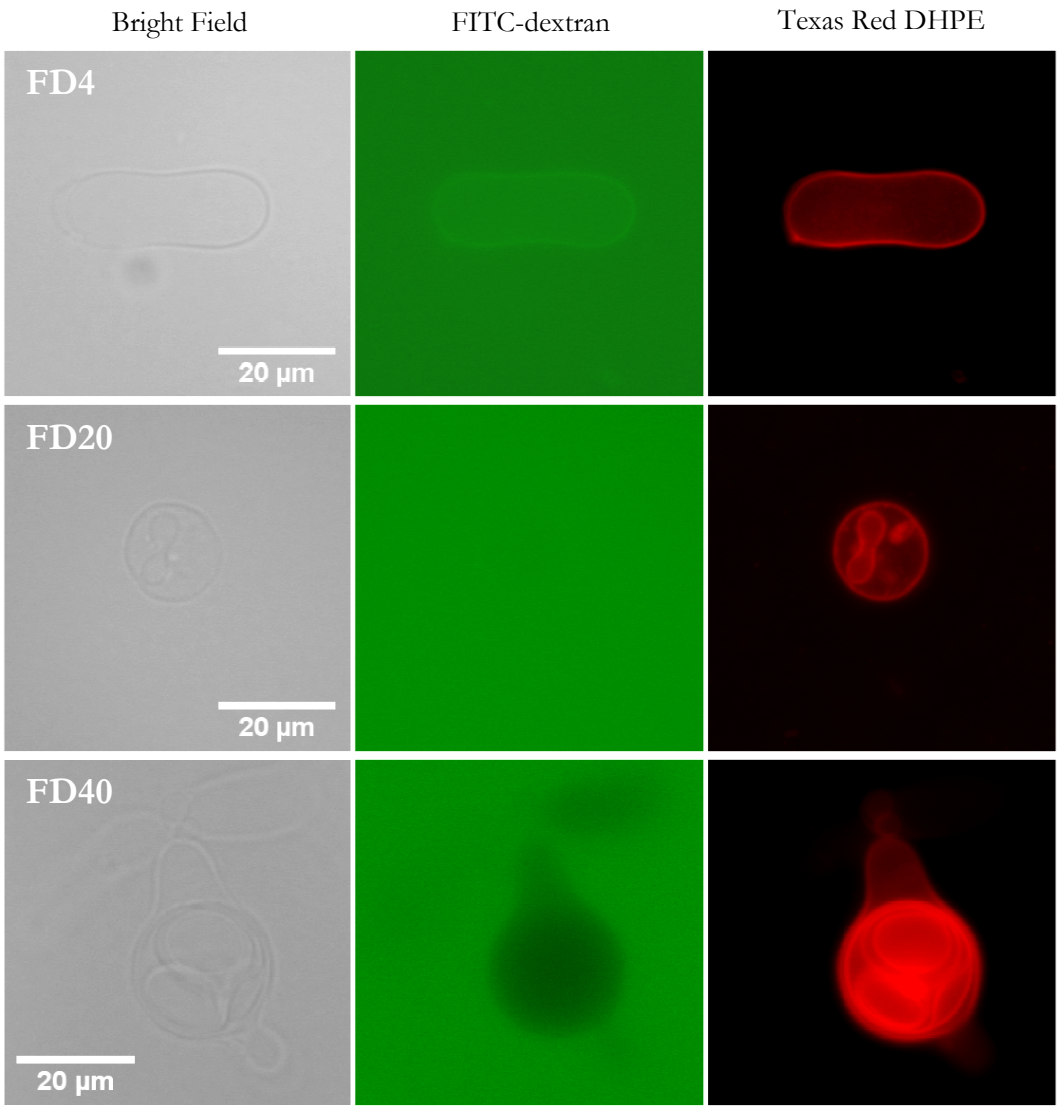

Fig. 4.23: POPC giant vesicles containing 1% (w/w) SP-B, labeled with Texas Red DHPE and incubated in FITC-dextrans with three different average chain sizes (4, 20 and 40 KDa from up to down). The first column corresponds to transmission images; the second and the third columns, to fluorescent images obtained with FITC and Texas Red filter sets, respectively.

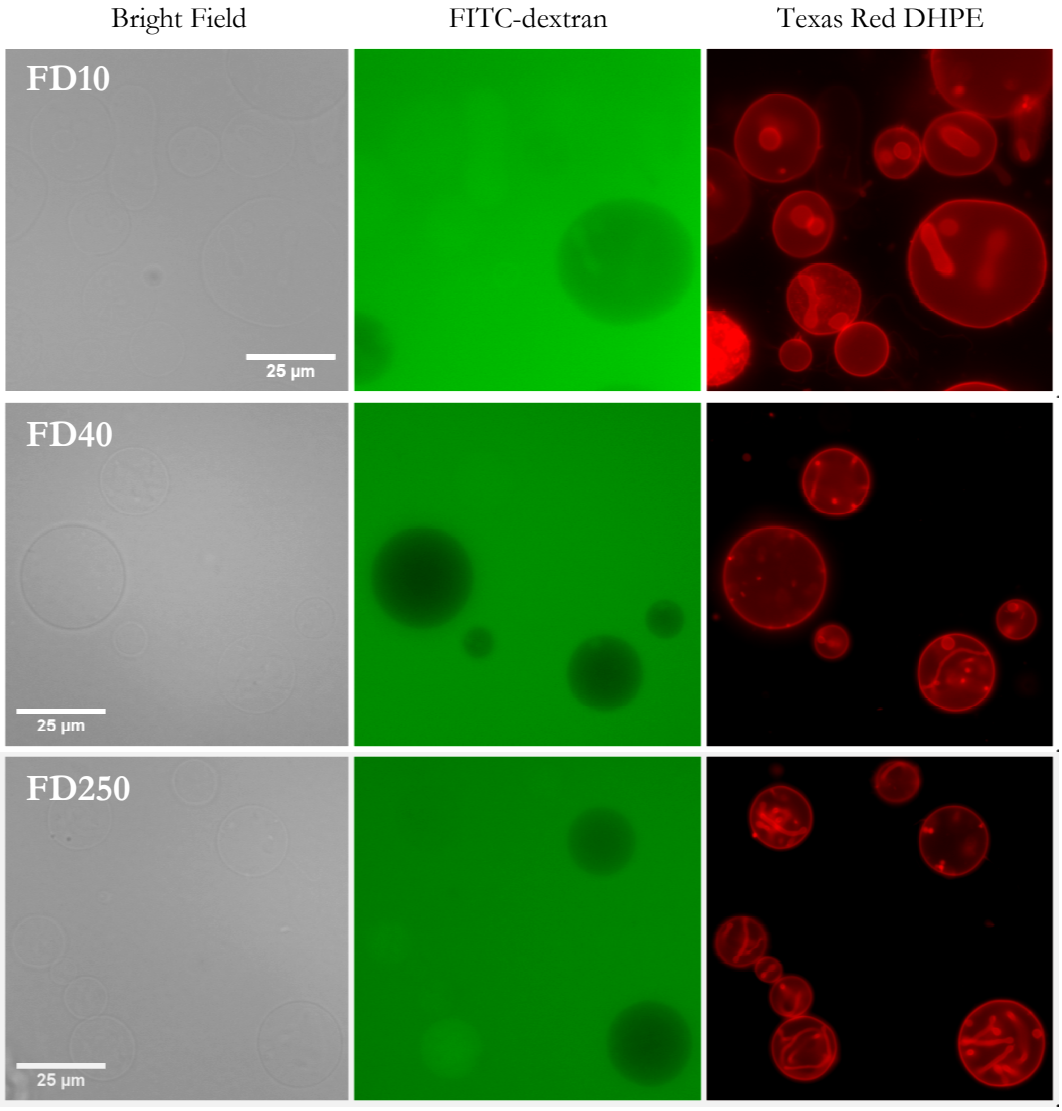

Fig. 4.24: POPC giant vesicles containing 1% (w/w) SP-C, labeled with Texas Red DHPE and incubated in FITC-dextrans with three different average chain sizes (10, 40 and 250 KDa from up to down). The first column corresponds to transmission images; the second and the third columns, to fluorescent images obtained with FITC and Texas Red filter sets, respectively.

Results for SP-B and SP-C-containing vesicles in terms of total number of permeable and non-permeable vesicles, together with the estimated values of permeability ratios for each dextran size, are presented in table 4.1. To summarize, these results indicate that the pore sizes created by the proteins are rather heterogeneous, and their average values can be estimated from the permeability ratios: POPC giant vesicles containing 1% of the hydrophobic protein fraction appeared to be permeable to both calcein (600 Da) and FD4 (4 KDa) but not to the larger dextrans, which yields a cutoff in hydrodynamic radius at around 1.5 nm. SP-B-containing vesicles yielded a higher threshold, approximately 4 nm (up to 20 KDa in molecular weight), of dextran hydrodynamic radii which were able to permeate through these lipoprotein membranes. Finally, SP-C supplemented at

physiological ratios made POPC membranes to be permeable, in a higher or lower proportion depending on dextran molecular size, to practically all tested FITC-dextrans, between 4 (R ~ 1.4 nm) and 500 KDa (R > 9 nm). These results are presented in figure 4.25, where permeability ratios are plotted as a function of dextran molecular weight in both linear and logarithmic scales.

	POPC + 1% SP-B			POPC + 1% SP-C		
FITC-dextran	Permeable	Non permeable	Ratio	Permeable	Non permeable	Ratio
4 KDa	20	-	100%	49	3	94%
10 KDa	11	22	33%	62	74	46%
20 KDa	5	20	20%	43	68	39%
40 KDa	-	24	0%	23	52	31%
250 KDa	-	13	0%	24	83	22%
500 KDa	-	12	0%	11	60	15%

Table 4.1: Estimation of permeability ratios for SP-B- and SP-C-containing vesicles as a function of dextran molecular size.

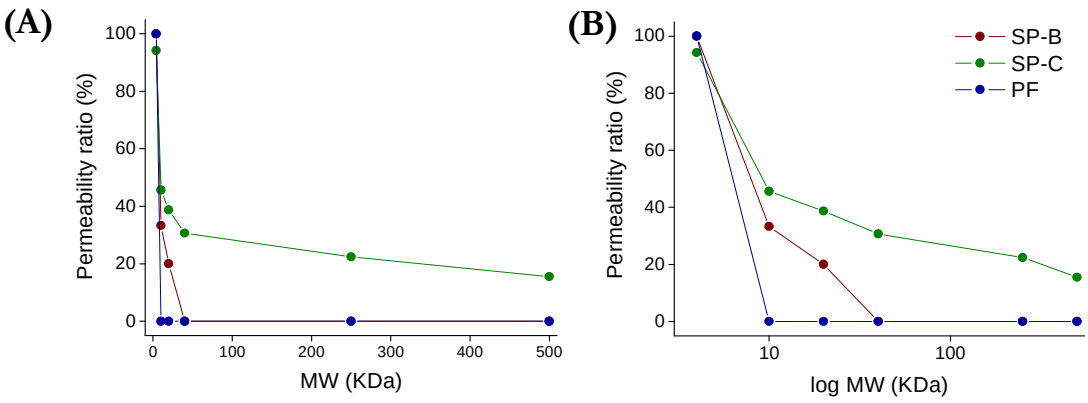

Fig. 4.25: Estimated permeability ratios of giant vesicles containing 1% SP-B, SP-C or PF as a function of dextran molecular size plotted in linear (A) and in logarithmic scales (B).

4.2.4.4 Giant vesicle immunofluorescence to visualize SP-B and SP-C

Fluorescence microscopy was also employed to get a direct visualization of protein layout on POPC membranes, following a technique widely used for cellular samples but barely employed for model systems: immunofluorescence of giant lipoprotein vesicles. It consists of incubating first SP-B- and SP-C-containing vesicles with their respective primary antibodies, anti-SP-B or anti-SP-C, and then adding the secondary antibody, fluorescent immunoglobulin G (see section 3.8 in Materials and Methods for further details), which recognizes a certain sequence in the primary antibodies and binds to them, being the fluorescence emission only localized in protein-containing regions, except in the case of non-specific binding. Therefore, several control experiments were performed in

order to evaluate a potential non-specific binding of the antibodies to giant vesicles: on the one hand, protein-free POPC giant vesicles were subjected to the same fluorescent immuno-labeling than lipid-protein vesicles, which showed the degree of labeling of both primary and secondary antibodies to pure phospholipid membranes; and, on the other hand, lipoprotein vesicles (containing SP-B and/or SP-C) were incubated in the presence of the secondary antibody IgG but in the absence of primary antibody, anti-SP-B or anti-SP-C, showing the extent of fluorescent labeling when SP-B or SP-C are present in the membrane but no specific linkage between them and IgG is present. Some representative images are shown in figure 4.26. In all cases, vesicles were labeled with a small amount of fluorescent phospholipids, specifically with Texas Red DHPE.

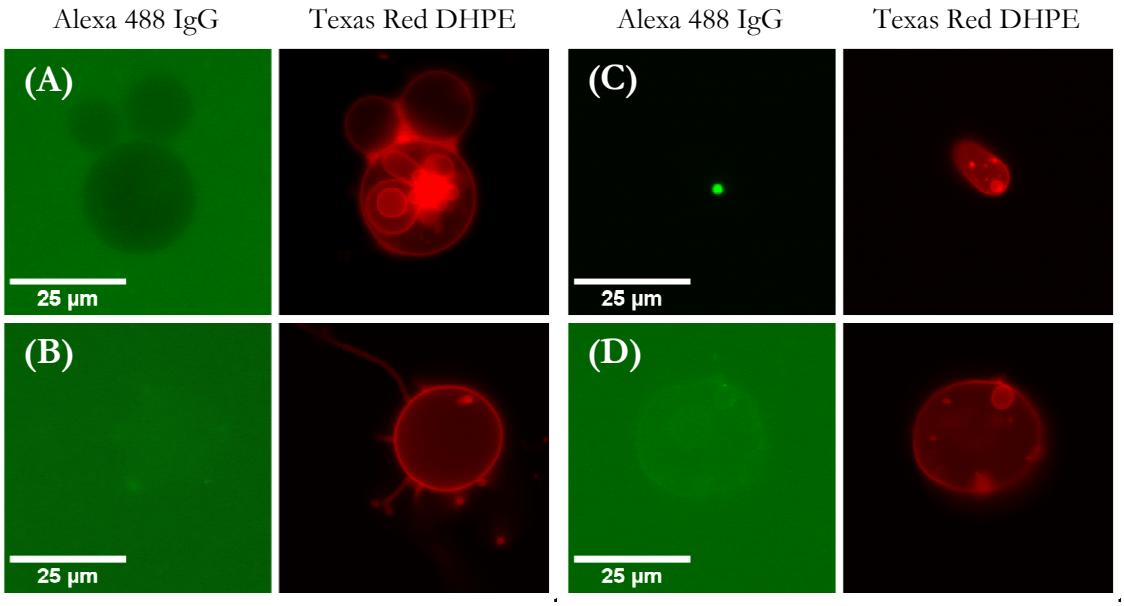

Fig. 4.26: Left, fluorescence microscopy images of protein-free POPC giant vesicles subjected to immuno-labeling, first incubated with anti-SP-B from rabbit at a 1/5000 dilution in images (A) and 1/25000 in (B), and then incubated with fluorescent anti-rabbit IgG at 1/2500. Right, two selected lipoprotein POPC vesicles containing 1% (w/w) SP-B (C) or 1% (w/w) SP-C (D) incubated only with the secondary antibody IgG at 1/10000 without pre-exposure to anti-SP-B nor anti-SP-C primary antibodies. The first and second columns in all cases correspond to fluorescent images obtained with FITC and Texas Red filter sets, respectively.

When pure POPC vesicles were subjected to immunofluorescence labeling, no specific green fluorescence (corresponding to Alexa 488 dye fluorescent emission) was found to be associated to the membrane, only a green background was observed even for high exposure times as can be seen in images A and B in figure 4.26. In the case of the highest primary antibody concentration tested (1/5000 of the final volume), membrane impermeability towards soluble molecules was highlighted again, as can be noticed in image B. The second type of immuno-labeling controls that was carried out revealed in some cases a subtle fluorescent green emission of lipoprotein vesicles (POPC plus SP-B or SP-C

at 1% by weight of phospholipids) in the absence of specific primary antibodies anti-SP-B or anti-SP-C, as can be observed in image D of figure 4.26. In very few cases, some small vesicles appeared to be full of green fluorescent dye were found, like the one in image C of figure 4.26, probably due to the already demonstrated enhanced POPC permeability in the presence of SP-B and SP-C.

On the other hand, when lipoprotein vesicles were incubated with both primary and secondary antibodies in order to achieve a fluorescent immuno-detection of hydrophobic proteins SP-B or SP-C, higher levels of fluorescent labeling were observed to be associated to the membrane and, interestingly, brighter fluorescent spots were found in certain parts of the giant vesicles. A small but representative selection of microscopic images taken from POPC plus SP-B or SP-C preparations, subjected to the immunofluorescence method described in section 3.8, is shown in figures 4.27 y 4.28. These fluorescence images suggest that SP-B and SP-C could be located and possibly highly aggregated in certain membrane regions, like those which are contact areas between different membranes (see for instance image B in figure 4.28) or those associated to shape transformations or vesicle deformations (see image A in figure 4.27).

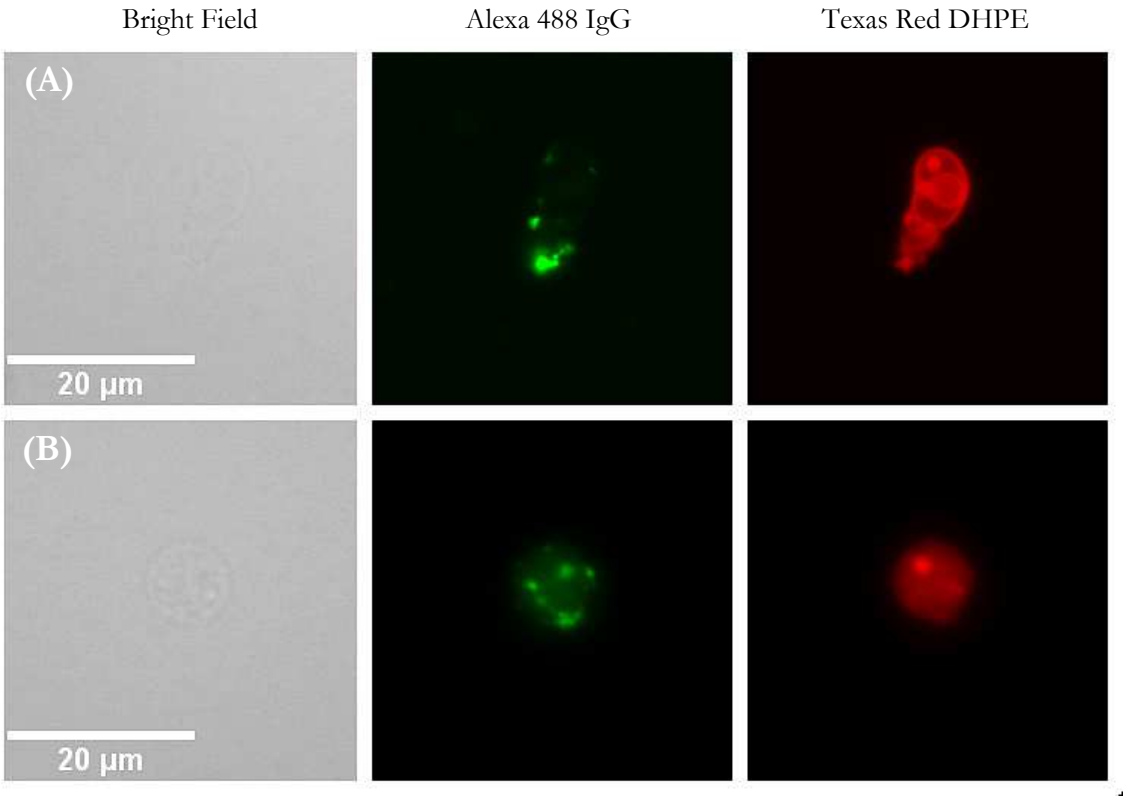

Fig. 4.27: Fluorescence microscopy images of POPC giant vesicles containing 1% (w/w) SP-B subjected to immuno-labeling, first incubated with the primary antibody anti-SP-B from rabbit at a 1/5000 dilution and then incubated with fluorescent anti-rabbit IgG at 1/10000. The first column corresponds to transmission images; the second and the third columns, to fluorescent images obtained with FITC and Texas Red filter sets, respectively.

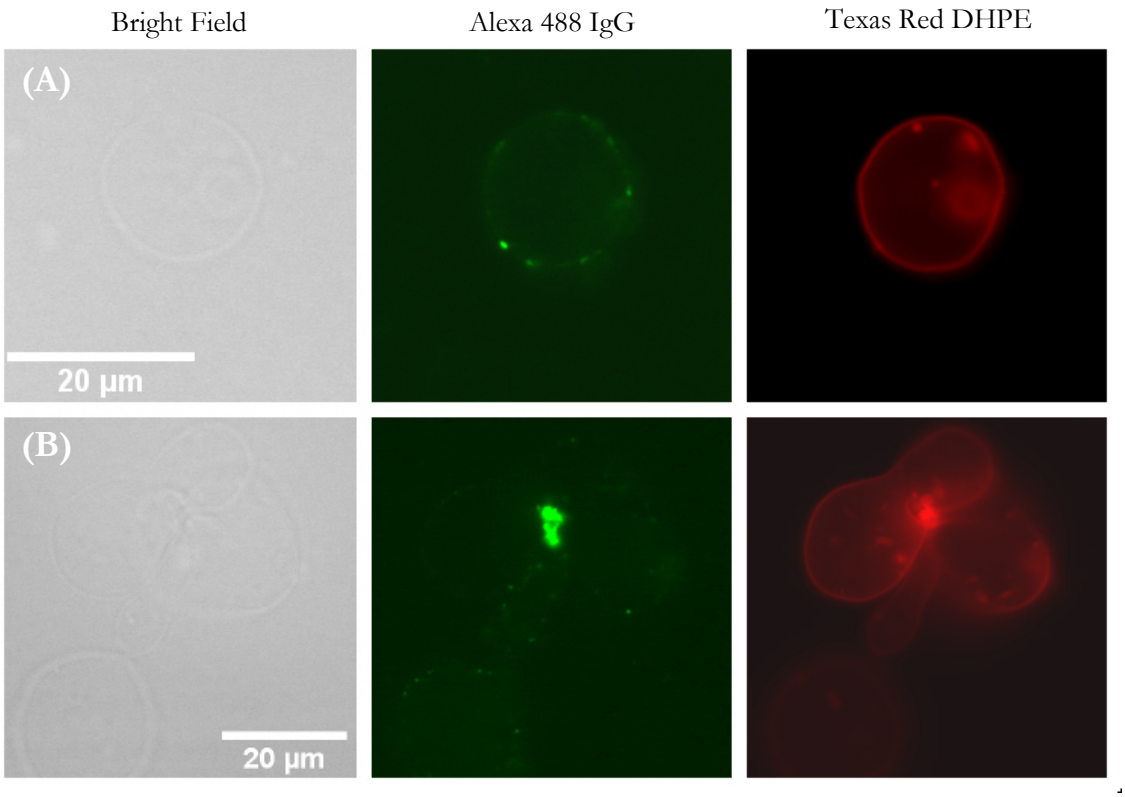

Fig. 4.28: Fluorescence microscopy images of POPC giant vesicles containing 1% (w/w) SP-C subjected to immuno-labeling, first incubated with the primary antibody anti-SP-C from rabbit at a 1/5000 dilution and then incubated with fluorescent anti-rabbit IgG at 1/10000. The first column corresponds to transmission images; the second and the third columns, to fluorescent images obtained with FITC and Texas Red filter sets, respectively.

A number of bright, independent spots with higher fluorescent emission than the rest of the membrane were always found in the different observed vesicles, like those shown in both figure 4.27 and 4.28, meaning a certain level of IgG aggregation at these lipoprotein membranes that can be interpreted as a primary antibody aggregation in the areas where most proteins are located.

Finally, POPC vesicles containing 1% (w/w) of the hydrophobic protein fraction PF were also subjected to immuno-labeling processes with either of the primary antibodies: anti-SP-B on the one hand or anti-SP-C on the other hand, and incubating afterwards in the presence of the fluorescent secondary antibody Alexa 488 IgG. Therefore, two independent immuno-detections were performed for the same vesicle preparation: one for detecting SP-B and the other for detecting SP-C. Some representative images are presented in figure 4.29, where POPC+PF giant vesicles incubated with anti-SP-B (images A and B) and anti-SP-C (C and D) and subsequently labeled with fluorescent IgG are shown.

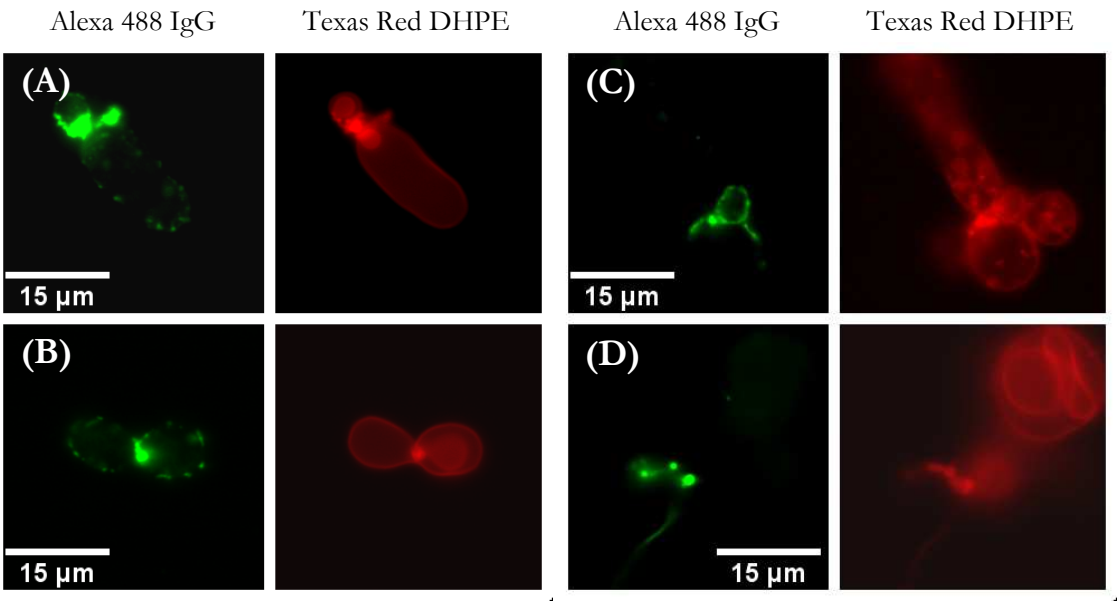

Fig. 4.29: Fluorescence microscopy images of POPC giant vesicles containing 1% (w/w) of the hydrophobic protein fraction PF subjected to immuno-labeling, first incubated with the primary antibody anti-SP-B (images A and B) or anti-SP-C (images C and D) at a 1/5000 dilution and then incubated with fluorescent IgG at 1/10000. First and second columns correspond to fluorescent images obtained with FITC and Texas Red filter sets, respectively.

Anti-SP-B and, therefore, surfactant protein SP-B, detected by the green fluorescence of IgG, appeared to be located all through the membrane in independent, bright spots that can be clearly noticed in images A and B of figure 4.29, following the vesicle contours. Besides, much brighter fluorescent spots were observed at certain vesicle areas, specially at vesicle-vesicle contacts like the ones shown in both images. On the other hand, IgG bound to anti-SP-C, and presumably SP-C, were also found to be aggregated at certain membrane regions such as intermembrane contacts (see image C), vesicle protuberances or membrane tethers, like the one shown in image D. Unfortunately, a co-localization of the two proteins was not possible with these immuno-labeling assays since the secondary antibody binds both to anti-SP-B and anti-SP-C, which would lead to the simultaneous labeling of both primary antibodies with the same fluorescent properties and making impossible the identification of either SP-B or SP-C.

4.3 DISCUSSION

In the present chapter, the potential ability of hydrophobic surfactant proteins SP-B and SP-C to induce structural changes in phospholipid membranes has been investigated by different techniques: fluorescence spectroscopy and microscopy, electron spin resonance and transmission electron microscopy. The crucial role of both SP-C and SP-B has been shown to modulate membrane fluidity, structure and accessibility in the context

of native and quasi-native membranes. The experiments also illustrate how the mere addition of the physiological amount of both proteins to model phospholipid membranes, such as POPC, induces dramatic changes in their structure and integrity. Some clues about the importance of surfactant proteins on membrane properties were obtained by ESR: whereas the fluidity of native surfactant (NS) and membranes reconstituted from its organic extract (OE) and its lipid fraction (LF) appeared to be very similar at the acyl chain segments closer to the polar heads, the degree of mobility differed remarkably at deeper positions. NS showed for the whole temperature range a less fluid/dynamic environment than membranes reconstituted from OE and LF, as sensed by the spin probe 14-PCSL. It is likely due to the native structure and complexity, including the presence of hydrophilic proteins, especially SP-A, which interacts with lipids and promotes membrane aggregation (Ruano et al. 1996, Worthman et al. 2000). However, SP-A has been reported to interact just in a superficial manner with phospholipid membranes (Morrow et al. 2003), so its impact on deep chain positions of the bilayer could be objected. Another possible explanation for this apparent change in mobility of the deeper acyl chain positions in NS complexes with respect to OE and LF membranes could be the existence of intrinsic structural differences, specifically lipid polymorphism: in general, surfactant possesses a lipid composition that tends to arrange in lamellar phases, i.e., as relatively planar bilayers. However, other different lipid phases could be present in surfactant, such as the so-called hexagonal phase type I (H_I, oil-in-water), which presents their polar heads facing out while the hydrocarbon chains, highly packed, are facing the interior, as in micellar arrangements. In this particular case, a spin probe would sense higher packing/reduced mobilities near to the middle plane of the membrane when inserted in this hexagonal phase (Swamy et al. 1995). In the context of pulmonary surfactant, tubular myelin consists of square-lattices formed by tubular arrangements (Perez-Gil 2008) that are partially arranged in a sort of H_I phase, so the present findings could be related to the presence of this structure in NS. Finally, it could be also important to consider the different ways of spin-labeled sample preparation: in the case of OE and LF samples, spin probes were added to the organic mixture and mixed prior to membrane hydration, while they were solubilized in DMSO and added to the aqueous suspensions of NS. This could lead to different modes of interaction and incorporation of the probe into membranes, yielding to different degrees of labeling and effective sensing of the different membrane environments. Nevertheless, considering the high levels of membrane accessibility in NS, as proven by FM1-43 fluorescence assays, an efficient spin-probe insertion could be expected. Regarding the differences observed between OE and LF membranes, only below the physiological temperature, the probe 14-PCSL presented a reduced mobility in OE with respect to LF, which could be closely related to the presence or absence of hydrophobic proteins SP-B and SP-C. Although the overall shape of the spin probe thermotropic profiles presents no evidences of phase transition, it has been reported that pulmonary surfactant membranes exhibit a conspicuous transformation at temperatures close to the physiological values, including melting of ordered into disordered phases (Bernardino de la Serna et al. 2004, Bernardino de la Serna et al. 2009). ESR spectra are sensitive to membrane phase transitions (Perez-Gil et al. 1995) but did not revealed changes in mobility associated to the macroscopic thermotropic transitions observed in native surfactant materials. Similarly, in a previous study (Bernardino de la Serna et al. 2009), ESR spectra were not either sensitive to

reveal membrane segregation in native surfactant membranes, which was attributed to an intrinsically dynamic character of both ordered and disordered regions segregated by the compositional complexity of surfactant membranes.

The ability of proteins SP-B and SP-C to introduce significant perturbations into the structure and dynamics of surfactant phospholipid membranes has been largely documented. These perturbations have been mainly interpreted in the context of the role of the proteins to promote the structural transformations associated with pulmonary surfactant biogenesis, secretion and adsorption into the air-liquid interface. However, the intrinsic properties imparted by the particular lipid and protein composition of native-like pulmonary surfactant membranes have not been completely described. Little is known, for instance, with respect to the symmetric or asymmetric character of these membranes as they are assembled, or their permeability to polar solutes.

The accessibility of membranes with different native-like or model lipid and protein composition to the membrane-fluorescent probe FM1-43 was studied in the present work by fluorescence spectroscopy and fluorescence microscopy of giant phospholipid vesicles. This probe has been extensively used as a marker for lamellar body exocytosis, in order to obtain a direct visualization of pulmonary surfactant secretion in alveolar type II cells (Haller et al. 1998). FM1-43 stains intensely the whole lamellar body content immediately after the opening of the exocytotic fusion pore. This suggests the existence of a direct topological connection between all the lamellar body membranes and/or the inter-lamellar compartments. The starting hypothesis of the present chapter was that the assemblies in which hydrophobic proteins SP-B and SP-C participate are involved in the free diffusion of probes like FM1-43 across surfactant membranes once surfactant is released from type II pneumocytes.

The present results confirm that the hydrophobic proteins SP-B and SP-C are responsible for making phospholipid membranes highly permeable to polar molecules, as had been largely suspected. The ability of these proteins to alter the permeability barrier of phospholipid membranes had been reported, but mainly as a consequence of their interaction with membranes upon injection as concentrated solutions in organic solvents (Shiffer et al. 1988, Cruz et al. 1997, Chang et al. 1998). In the present chapter, it has been shown that native surfactant membranes are intrinsically permeable, that proteins SP-B and SP-C are responsible for the permeability properties of surfactant membranes, and that hydrophobic surfactant proteins are by themselves able to make a simple phospholipid membrane highly permeable to both membrane-partitioning probes, like Nile Red and FM1-43, and water-soluble probes, such as calcein and dextrans. This could be consistent with the assembly of some sort of proteinaceous or proteolipid pores in membranes, because the mere introduction of the hydrophobic surfactant proteins into a single lipid model membrane is enough to permeabilize it. Permeabilization of membranes by surfactant proteins produces as a consequence a rapid equilibration of molecules through pure lipid membranes that are intrinsically impermeable in the conditions tested here. Nevertheless, the idea that membrane-permeabilizing protein assemblies could be also promoting membrane-membrane contacts cannot be discarded, which would facilitate even further the rapid movement of polar and non-polar molecules through the different

membranes and compartments; in fact, the observations obtained by SP-B and SP-C immuno-detection shown in the present chapter suggest a predominant location of both hydrophobic proteins in contact areas between giant vesicle membranes. The effect of the proteins to facilitate lipid dynamics in large multilamellar arrays has been widely reported (Perez-Gil et al. 1995, Bernardino de la Serna et al. 2009). The present results introduce the effects on membrane permeability as an additional factor in surfactant dynamics.

Several studies had already suggested a potential effect of surfactant proteins on membrane permeability. SP-B has been reported to promote association and fusion of phospholipid membranes (Poulain et al. 1996, Chang et al. 1998). This SP-B-promoted fusion of lipid vesicles was described as "leaky", meaning that the protein-promoted merging of membrane compartments was always associated with leakage of at least part of the vesicle contents into the outer spaces. The results shown here suggest that leakage could not only occur at the fusion sites, but that membrane fusion and the subsequent transfer of the protein into the different lipid structures could end in the complete permeabilization of all the membranes. Besides, previous experiments had found difficulties in order to encapsulate polar solutes into membrane vesicles made from pulmonary surfactant, which is part of a relevant technology in the context of drug-delivering strategies, but this task may be more difficult to achieve than anticipated in the light of the present results. This permeabilization could be also behind the reported ability of hydrophobic surfactant proteins to permeabilize membranes to ions (Oelberg and Xu 2000), a property that was not explained in that work but is also addressed in the chapter 5 of the present Thesis.

The difference in the kinetics of membrane probe equilibration, as shown by fluorescence spectroscopy, is consistent with SP-B and SP-C promoting membrane permeability by different mechanisms. The almost instantaneous permeation of probes through phospholipid membranes containing minimal amounts of SP-B could be indicative of the protein forming true pores. The sequence of SP-B is homologous to saposins, a family of membrane-associated proteins that includes several recognized cytolysins and membrane-pore forming structures (Patthy 1991, Miteva et al. 1999, Leippe et al. 2005). Consistently with these results, pore-like oligomeric SP-B assemblies could be at the same time responsible to establish membrane-membrane contacts and to facilitate rapid transfer of lipids and polar molecules between the contacted membrane compartments. In contrast, the kinetics of probe permeation by SP-C is much slower than that promoted by SP-B, and much more dependent on a sufficiently high proportion of protein into the membranes. It can be proposed that, in contrast to SP-B, membrane permeabilization by SP-C could be rather dependent on the deep perturbation of the membrane core by the protein. These two different mechanisms of permeabilization proposed here for each protein, membrane pores for SP-B and membrane core disruption for SP-C, are also consistent with the dextran permeability tests performed here. SP-B was shown to make POPC vesicles permeable to soluble molecules smaller than a certain threshold, estimated to be around 4 nm of hydrodynamic radius (although this value could vary between 2-4 nm, based on the observed differences on FD4, FD10 and FD20 permeability ratios), which could mean that SP-B creates aqueous pores of approximately this inner radius. On the other hand, SP-C

was found to permeabilize phospholipid membranes in a less ordered fashion, making them permeable to all tested dextrans, even larger than 9 nm of hydrodynamic radii. Profound SP-C promoted membrane perturbations could be also the cause of the extraordinarily dynamic behavior imparted by SP-C into the membrane morphology, as observed in the GV fluctuations under the microscope. The ability of SP-C to introduce a dynamic contribution into phospholipid membranes has been already outlined, with the relatively polar N-terminal segment of the protein having a significant role (Plasencia et al. 2001, Plasencia et al. 2004).

The present results strongly suggest that the combination of SP-B and SP-C impart special properties to membranes, which are clearly distinct to the effects of each individual protein by itself. Surfactant membranes are more stable in the simultaneous presence of both SP-B and SP-C, while the individual proteins seem to have apparently opposite destabilizing effects. SP-B alone promotes transformation of single vesicles into large, complex, presumably multilamellar, membrane structures, as was shown by transmission electron microscopy. Besides, the aggregation observed in SP-B-containing POPC giant vesicles could be related to the potential cohesive effect of this protein (Bernardino de la Serna et al. 2013), and what has been interpreted as single-walled could be also oligolamellar vesicles whose bilayers are highly and cohesively attached. It is noteworthy that SP-B, fluorescently labeled by immunofluorescence of giant vesicles, appeared to be highly aggregated in membrane areas located at vesicle-vesicle contacts. This ability of the protein to promote association and eventually fusion of membranes, with the important participation of protein-protein interactions, has been in fact widely documented (Poulain et al. 1992, Poulain et al. 1996, Chang et al. 1998, Cruz et al. 2000, Ryan et al. 2005). SP-C, on the other hand, seems to strongly destabilize bilayers, promoting their disintegration and dispersion. This activity could be behind the ability of the protein to promote insertion of phospholipids into the interface (Oosterlaken-Dijksterhuis et al. 1991, Perez-Gil et al. 1992). However, the incorporation of the SP-B/SP-C physiological mixture, PF, with the precise protein stoichiometry obtained from the natural surfactant mixtures, apparently maintains the morphology of the lipid-protein membranes, at least in the context of the models studied here, suggesting that SP-B and SP-C might modulate each other.

An obvious possibility is that both proteins may be participating in common macromolecular protein complexes in the context of surfactant membranes. The differences in permeability induced upon introduction of single or combined proteins into giant liposomes are very illustrative. In the presence of SP-B/SP-C physiological mixture, lipid membranes are permeable to calcein, which can permeate presumably through limited size pores, considering that dilution of external calcein does not produce a concomitant immediate dilution of calcein from the internal liposome compartments. Equilibration of inner and outer calcein concentrations is much faster in GV containing either SP-B or SP-C, suggesting that the permeation structures assembled by a single protein permit a much rapid flow of the probe. Besides, dextran permeability assays suggested that the whole protein fraction PF could create aqueous pores with inner radii smaller than 1.5 nm, while isolated SP-B and SP-C created larger pores or membrane defects. Recent results certainly suggest that a concerted action of the two proteins facilitates breathing dynamics in vivo

(Almlen et al. 2008). Initial studies did not provide evidences for specific SP-B/SP-C interactions (Plasencia et al. 2001); however, a detailed study that employed time-resolved Förster resonance energy transfer found unequivocal evidences of the presence of the formation of SP-B/SP-C complexes in surfactant membranes (Jimenez Cabre 2009).

In a recent study that compared functional properties of systems prepared by reconstituting defined fractions of native surfactant, some differences were found between the behavior of lipid/protein complexes prepared from the original mixtures and the behavior of complexes reassembled from isolated components (Schurch et al. 2010). It might be possible that proper SP-B/SP-C complexes are only partly re-established once the proteins are mixed after isolation, perhaps because some unknown cofactors were lost, or because the proper conformation of the proteins is altered during the purification process. The present data suggest that it is necessary to be very careful when trying to dissect the potential role and the structure-function relationships of surfactant proteins upon reconstitution of simplified systems that start from fully purified SP-B and SP-C. An imbalance in the appropriate SP-B/SP-C ratio or an inefficient re-assembly of potential multiprotein complexes may end in lipid-protein membranes with structural and functional properties differing much of those exhibited by native surfactant membranes. Besides, the most successful clinical surfactant preparations currently in use for the treatment of respiratory pathologies are derived from extracts of animal-derived surfactants (Blanco and Perez-Gil 2007). These natural formulations probably preserve a fair proportion of the original surfactant protein complexes. Design and production of a new generation of therapeutic surfactants, based on the reconstitution of synthetic or recombinant human versions of surfactant proteins, will require a proper knowledge of the role of protein complexes and the way these complexes can be correctly established.

5. ION PERMEABILITY OF PLANAR LIPID MEMBRANES IN THE PRESENCE OF SP-B AND SP-C

All the experiments included in the present chapter were performed in the Laboratory of Molecular Biophysics (Dep. Physics, Universitat Jaume I, Castellón) assisted and supervised by Antonio Alcaraz and Vicente M. Aguilella, and published in the following article:

"Hydrophobic pulmonary surfactant proteins SP-B and SP-C induce pore formation in planar lipid membranes: evidence for proteolipid pores" Biophysical Journal 2013 Jan 8; 104(1):146-55.

5.1 INTRODUCTION

The ability of hydrophobic surfactant proteins to perturb lipid packing and dynamics of lipid membranes has been well established. On the one hand, the sequence of SP-B is homologous to saposins, a family of membrane-associated proteins that include several recognized cytolysins and membrane-pore forming structures (Olmeda et al. 2013). Amoebapores and NK-lysin, belonging also to the saposin family, induce current fluctuations upon interaction with phospholipid bilayers (Gutsmann et al. 2003). On the other hand, some evidences have been found about the possible dimerization of SP-C in both organic solvents and lipid membranes (Kairys et al. 2004, Luy et al. 2004), which could precede the formation of larger oligomers and the creation of temporary defects or pores in membranes. Besides, in the present Thesis it is shown that both SP-B and SP-C, either together in their physiological mixture or separately, alter the accessibility, structure and permeability of phospholipid membranes (see chapter 4).

Interestingly, the ability of both proteins, SP-B and SP-C, to permeabilize artificial phospholipid bilayers and membranes reconstituted from different clinical surfactant preparations (Chang et al. 1998, Plasencia et al. 2004) has been linked to the existence of some channel-mediated transport (Oelberg and Xu 2000). In the present chapter, a deeper insight into the characterization of these effects was carried out by studying the ion conductance and selectivity of planar lipid membranes (PLM) supplemented with SP-B and/or SP-C, as a function of several factors including lipid composition and membrane potential. Looking for characteristic conductance values and selectivity of the pores, the possible membrane permeabilization mechanism caused by these hydrophobic proteins was investigated: particularly, whether poration proceeds via proteinaceous, channel-like structure, or via protein-promoted lipid pore, lined total or partially by phospholipid polar heads.

5.2 RESULTS

5.2.1 EFFECTS OF THE HYDROPHOBIC PROTEIN FRACTION IN DOPC AND DOPC/DOPG BILAYERS

First of all, planar membranes formed by zwitterionic DOPC or by the negatively charged DOPC/DOPG (85:15, w/w) lipid mixture were formed (see Materials and Methods, section 3.9 for further details). Both types of membranes were found to be very stable and impermeable to ions, at least in the range of applied voltages ($V < 150$ mV) and in the time scale of these experiments. However, when these lipids were supplemented with the total hydrophobic protein fraction (PF) purified from porcine pulmonary surfactant complexes, and lipoprotein bilayers were casted, a high pore-forming activity was found, showing a wide variety of conductance states. Some of the recorded current traces are presented in figure 5.1 for DOPC bilayers, and figure 5.2 for DOPC/DOPG bilayers, both containing PF in a protein/lipid ratio of 0.01% by weight, approximately $1/10^5$ in molar ratio. All bilayers were casted in saline buffer 5 mM HEPES 100 mM KCl, pH 5.5.

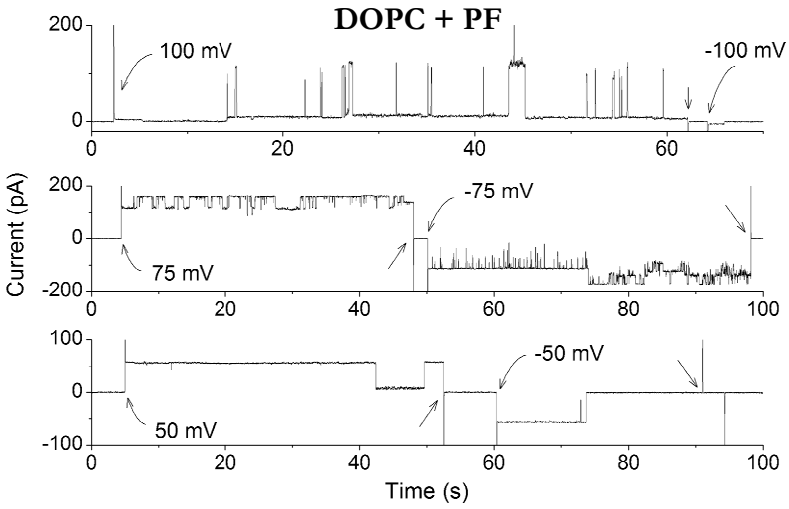

Fig. 5.1: Representative current versus time traces recorded for different applied voltages in DOPC bilayers supplemented with the hydrophobic protein fraction of native surfactant at a protein/lipid ratio of 0.01% by weight. Each trace corresponds to a different casted bilayer, and voltage application is indicated with red arrows. Traces were subsequently filtered using a Bessel (8-pole) filter with a 50Hz -3dB cut-off frequency.

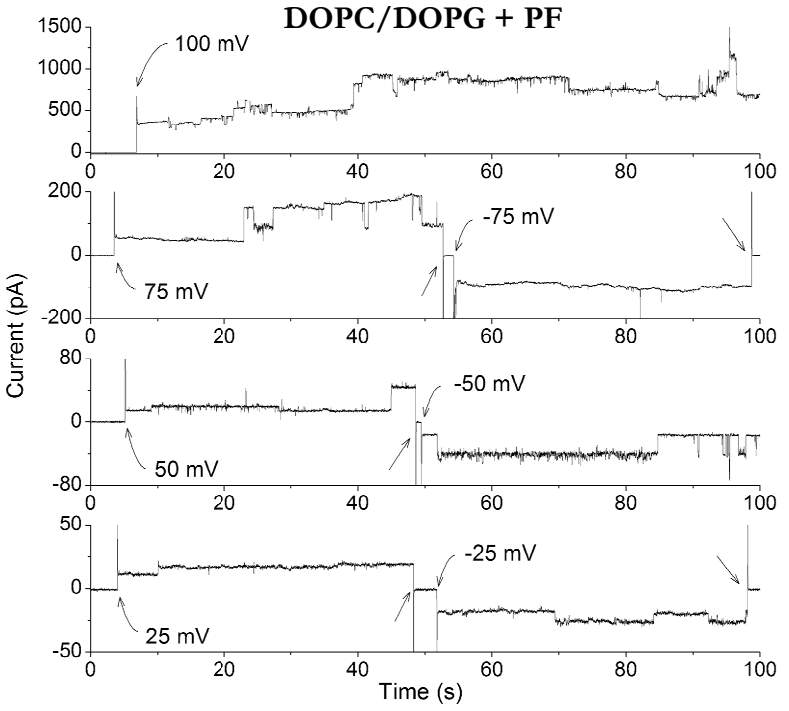

Fig. 5.2: Representative current versus time traces recorded for different applied voltages in DOPC/DOPG (85:15, w/w) bilayers supplemented with the hydrophobic protein fraction of native surfactant at a protein/lipid ratio of 0.01% by weight. Each trace corresponds to a different casted bilayer, and voltage application is indicated with red arrows. Traces were subsequently filtered using a Bessel (8-pole) filter with a 50Hz -3dB cut-off frequency.

The current versus time recordings did not show well-defined and highly reproducible unitary conductances, which are common characteristic of protein channels. Quite the opposite, current values and lifetimes of these states were very heterogeneous, even for the same applied voltage. Such variability allows several explanations: the coexistence of diverse channels in the bilayer, including different number of protein monomers forming the pores and/or different protein conformations; the existence of one single type of channel with a variety of sub-states, or the combination of both.

Conductance values (G) were then calculated from all the average current values registered (I), which were divided by the corresponding applied voltages. In order to find any characteristic, unitary value of conductance, histograms representing all the conductance levels obtained from the traces are shown in figure 5.3, panel A. Regardless of lipid composition, a large dispersion in the measured conductances was observed. Under such conditions, no unitary or characteristic single-channel conductance could be found. Small pores with conductances up to 100 pS were the most common, but almost a continuous distribution of values was obtained, ranging from tens of pS to several nS. The largest G values measured here, in the order of nS, could correspond either to multiple insertions of small pores or to individual wide pores, since the measurements were not done in single-channel conditions and an undefined number of proteins were present in each bilayer. Therefore, in order to discriminate between single and multiple channel conductances, a visual examination of all the records, like those shown in figures 5.1 and 5.2, was used to find the stepwise changes in each trace, identifying all the sudden changes in I (ΔI) that were registered and dividing ΔI by the corresponding applied voltage to obtain the stepwise conductance values, ΔG. Normalized histograms including all the stepwise transitions registered are shown in figure 5.3, panel B.

ΔG histograms are almost identical to those showing the distributions of absolute G values, indicating that the largest values of ΔG are repeatedly obtained from single stepwise transitions. The fact that these large steps presented long lifetimes without any small flickering pointed out to the existence of wide independent structures rather than to the simultaneous opening of the most abundant small structures; for example, see the bottom trace in figure 5.1, where a conductance level of 1 nS opened upon voltage application and spontaneously closed after several seconds without flickering. Apparently, the lipid composition does not have a dramatic impact on the histograms shown in figure 5.3. In both zwitterionic and anionic lipid membranes, a continuous distribution of ΔG can be observed between tens of pS and several nS. However, a close inspection of the histograms reveals a subtle feature: the most frequent values of the stepwise changes in conductance are 93 pS in neutral DOPC and 55 pS in negatively charged DOPC/DOPG membranes.

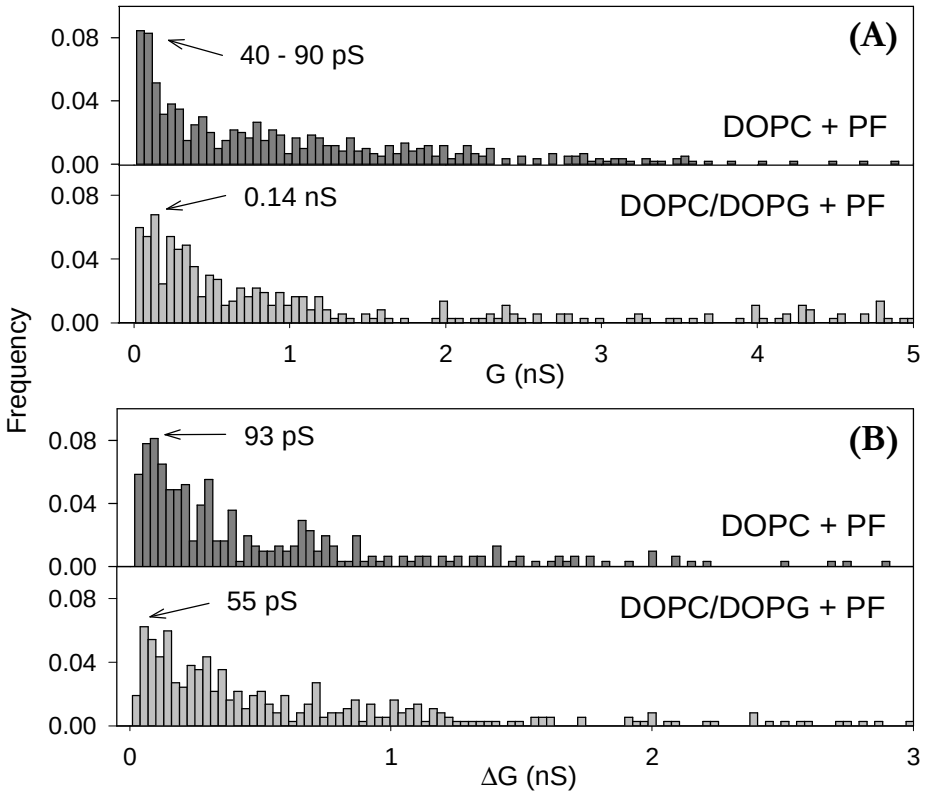

Fig. 5.3: Normalized histograms representing all conductance levels G (panel A) and conductance increments ΔG (panel B) recorded during the experiments with the hydrophobic protein fraction of native surfactant inserted in DOPC (dark grey) or DOPC/DOPG 85:15 bilayers (light grey) at a protein/lipid ratio of 0.01% by weight. Around 30 different bilayers were casted for each sample, obtaining from them around 400 G- and 200 ΔG-values in each case. Most frequent G and ΔG values are indicated.

Looking for additional insights about pore structure, the effect of applied voltage on channel conductance G was also analyzed, as is shown in figure 5.4. The obtained G values were classified as measured either at low (5-50 mV) or high voltages (75-100 mV). Note that only absolute values of voltage were considered since no significant differences were observed between applying positive or negative voltages, in terms of different G or ΔG distributions. In the case of DOPC membranes, high applied voltages increased significantly the probability of finding narrow pores, despite of the fact that the position of the maximum frequency remained almost unchanged (0.04-0.1 nS). This suggests that wide pores may undergo a structural change or "closure" induced by voltage that does not affect the structure of the narrower ones. In contrast, the effect of voltage in DOPC/DOPG membranes is right the opposite: the distribution of relative frequencies is not altered by voltage, although the position of the maximum is slightly shifted. The most frequent conductances are higher for low voltages (around 0.3 nS) than for high voltages (45 pS).

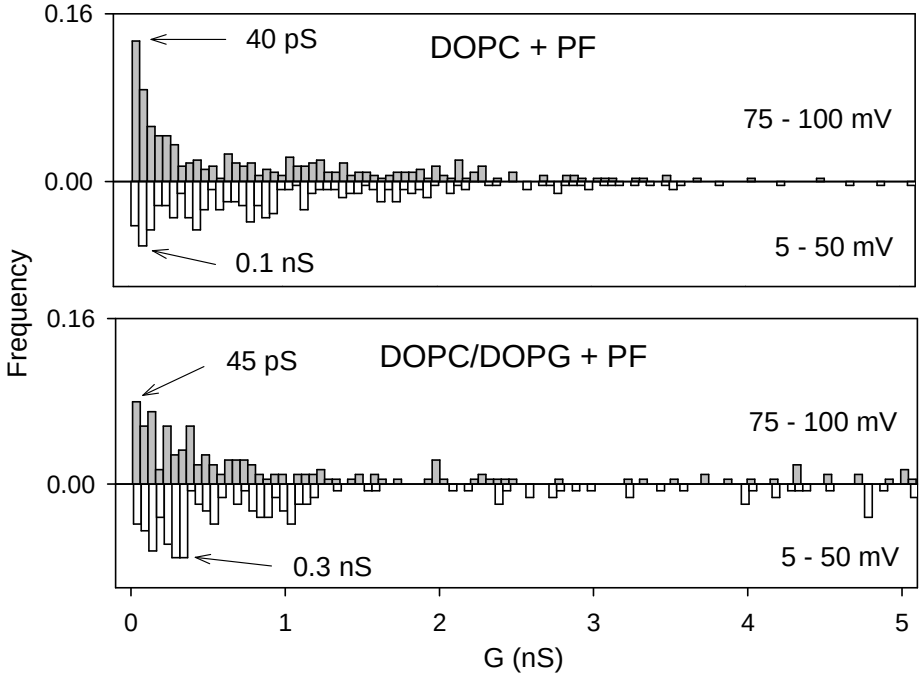

Fig. 5.4: Normalized histograms represent the recorded G values classified by the applied voltage: high voltages (75-100 mV, grey bars) and low voltages (5-50 mV, white inverted bars), in absolute value. Most frequent G values are indicated.

Hitherto, some evidences could suggest that the lipid composition determines not only the amplitude histograms of conductance but also their voltage dependence, which could be explained as a direct incorporation of the phospholipid into the pore structure. Thus, the lipid charge should be critical for the channel selectivity. To explore this possibility, selectivity experiments for both DOPC and DOPC/DOPG bilayers containing PF (0.01% by weight with respect to phospholipids) were carried out. In the presence of a salt concentration gradient between both sides of the bilayer and no applied voltage, there is a net flux of ions and hence an electric current appears. By measuring the applied voltage that is needed to zero the electric current (the so-called reversal potential, E_{rev}), it is possible to investigate the preferential passage of either positive or negative ions (see section 3.9.3 for further details). The results are shown in figure 5.5.

In a zwitterionic phospholipid bilayer such as that formed by DOPC, the pores were found to be selective to anions (upper part of panel A, figure 5.5). This fact is consistent with the positive net charge of both SP-B and SP-C, and, consequently, of the whole membrane surface. It is interesting to stress that no significant differences were observed between adding the proteins to the *cis* or to the *trans* side of the experimental cell while keeping the same KCl concentration ratios, which indicates that there is no charge asymmetry with respect to the membrane plane. Probably, a change of protein orientation could be induced by the application of a potential difference between both sides of the bilayer that would yield to this symmetric conformation of protein charges through the bilayer.

Interestingly, the incorporation of only 15% DOPG by total weight of phospholipids into DOPC bilayers causes a dramatic impact. Regardless of the electrolyte concentration ratio, all the measured reversal potentials were negative (see panel A in figure 5.5), indicating a cationic selectivity. A similar selectivity inversion has also been observed in DPhPC (zwitterionic) and DPhPC/DPhPS 50:50 (negatively charged) bilayers: reversal potential values were measured for a KCl concentration gradient of 6 (50 mM *trans* side, 300 mM *cis* side), obtaining E_{rev} = 26.97 ± 2.95 mV for DPhPC (7 bilayers) and E_{rev} = – 20.70 ± 9.51 mV for DPhPC/DPhPS (5 bilayers), showing again a total inversion of the ion selectivity between neutral and negatively charged membranes. This observation indicates that it is the charge of the lipid polar head which originates this phenomenon.

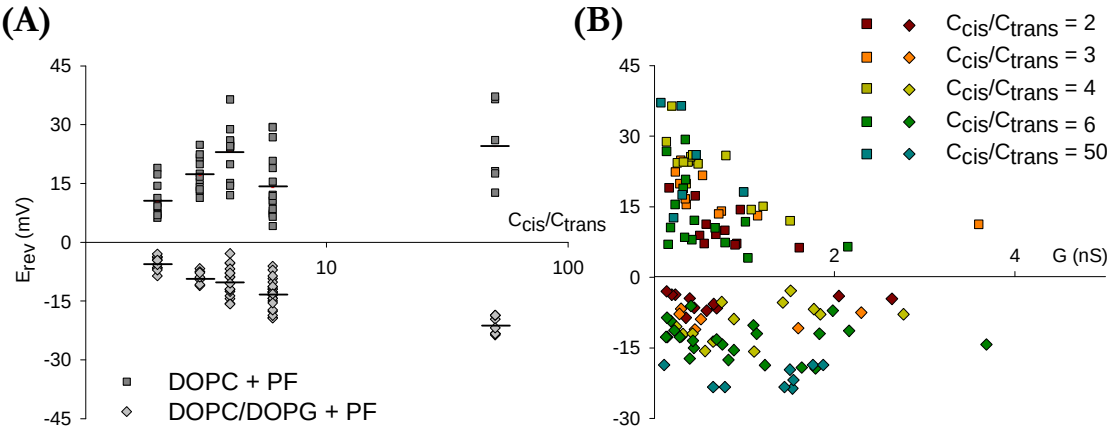

Fig. 5.5: (A) Reversal potential versus KCl concentration gradient (50 mM *trans* side; 100, 150, 200, 300 and 2500 mM *cis* side) for DOPC (dark grey squares) and DOPC/DOPG 85:15 bilayers (light grey diamonds) containing the hydrophobic protein fraction at 0.01% w/w. Logarithmic scale has been used for the x axis. All measured E_{rev} values were plotted, and the black line represents their mean values for each concentration gradient. (B) Reversal potential values represented versus their respective conductances for DOPC (squares) and DOPC/DOPG 85:15 bilayers (diamonds) containing 0.01% PF (w/w) in the presence of the different KCl concentration gradients tested.

The qualitative interpretation of these results can be complemented using the Goldman-Hodgkin-Katz (GHK) equation to calculate the permeability ratio between cations and anions, $P = P_+/P_-$ (Hille 2001), in this case, between K^+ and Cl^-. Considering a constant electric field going through the pore and a steady ionic flow, and also considering that the electrolyte ionic species have equal valence, z, the following expression can be obtained:

$$\frac{P_+}{P_-} = \frac{1 - r \cdot e^{\left(-\frac{zF}{RT}E_{rev}\right)}}{e^{\left(-\frac{zF}{RT}E_{rev}\right)} - r} \qquad (5.1)$$

Where F is the Faraday constant; R the ideal gas constant; T the temperature and $r = C_{cis}/C_{trans}$ the concentration gradient. Using the mean reversal potential values for this calculation, pores in DOPC bilayers were around 2.0-5.5 times more selective for Cl^- than for K^+, while in DOPC/DOPG bilayers, pores were approximately 2-2.5 times more selective for K^+ than for Cl^-. Therefore, the pores created by the physiological mixture of SP-B and SP-C appear to be more selective in zwitterionic than in negatively charged bilayers, probably because negative charges of PG counteract or neutralize the electrostatic interactions between Cl^- ions and positive charges of the polar residues of the proteins.

It is also worth to mention that the measured values of the reversal potential in figure 5.5-A display a considerable dispersion that is clearly beyond the experimental error. Such scattered pattern is consistent with the existence of multiple independent pore structures as suggested by the data. Note that the reversal potential of a collection of identical channels is independent of the actual number of them and should yield the same selectivity as a single unit (Hille 2001). Therefore, if the variety of high conductance states found in current traces and shown in figure 5.3 were actually originated by clusters of small structures, dispersion of reversal potential measurements would be within the experimental error.

Going further in the correlation between reversal potential (~ selectivity) and pore conductance (~ size), the pore conductance was calculated for each selectivity experiment, considering the full current-voltage (I-V) curve (note that when the I-V plot is linear, the slope gives the conductance and the intercept with V axis corresponds to the reversal potential). The correlation between E_{rev} and G can be seen in panel B, figure 5.5. Although the results are clearly scattered, a general trend could be observed especially in the case of DOPC containing PF (squares): higher conductances correspond to lower reversal potentials, which means lower selectivity. This sounds reasonable, since narrow channels display a low conductance and a high discrimination because of the tight interaction between the permeating ions and the charges in the pore wall, whereas wider pores provide an easier and faster pathway at the price of losing selectivity (Aguilella et al. 2011). However, the scenario is likely to be much more complex: in different experiments, pores with a similar conductance but very different reversal potential were detected.

5.2.2 INDEPENDENT ACTION OF PROTEINS SP-B AND SP-C IN DOPC AND DOPC/DOPG BILAYERS

The pore formation observed for physiological SP-B/SP-C mixture could be related to the sole action of one of the proteins or, alternatively, both of them could be necessary. Thus, more experiments were performed in PLM made of DOPC/DOPG (85:15), containing this time low amounts of either SP-B or SP-C (0.005% protein to lipid by weight, around $5 \cdot 10^{-6}$ for SP-B and 10^{-5} for SP-C in molar ratio), isolated from pulmonary tissue. Some representative recorded traces are shown in figures 5.6 and 5.7, respectively. All measurements were done in 5 mM HEPES 100 mM KCl solution, pH 5.5.

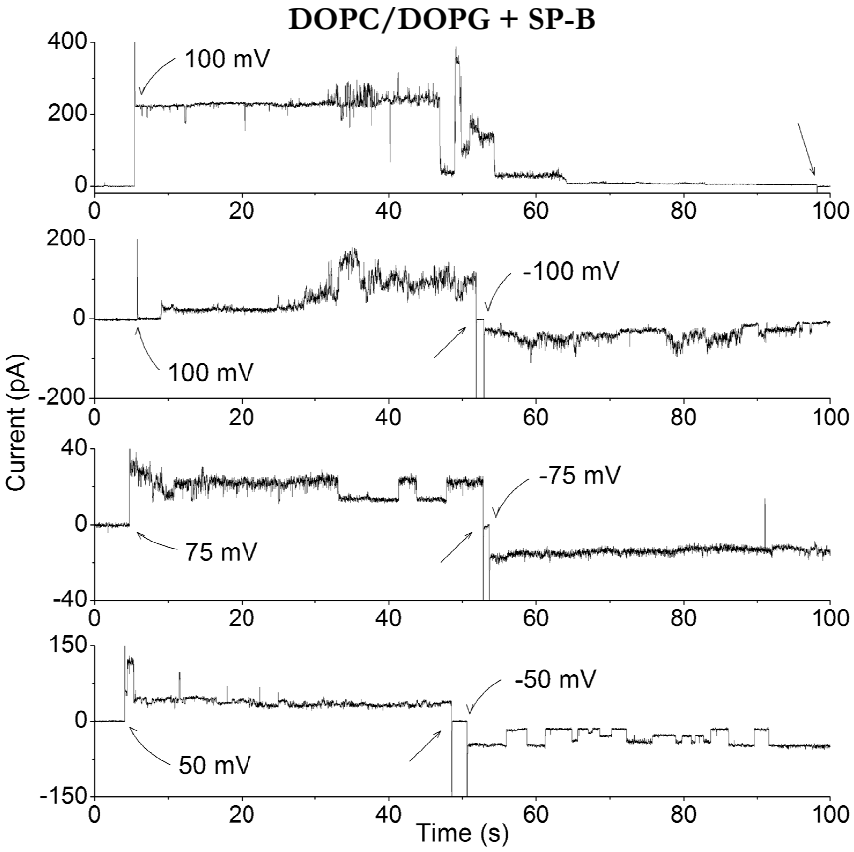

Fig. 5.6: Representative current versus time traces recorded for different applied voltages in DOPC/DOPG (85:15, w/w) bilayers supplemented with isolated SP-B at a protein/lipid ratio of 0.005% by weight. Each trace corresponds to a different casted bilayer, and voltage application is indicated with arrows. Traces were subsequently filtered using a Bessel (8-pole) filter with a 50Hz -3dB cut-off frequency.

Interestingly, each one of the two proteins is able to induce pore formation, and both of them display a huge variety of conductance levels and current flickering. As in the case of the SP-B/SP-C mixture, PF, a visual examination of the recorded traces showed large stepwise conductances for both proteins. This suggests that high conductance states are most probably due to independent wide pores rather than to the concerted action of a cluster of small channels. For example, in the case of SP-B, in the top current trace of figure 5.6 we can observe a "closure" of around 2 nS and a subsequent "opening" of around 3 nS. In figure 5.7, an example for SP-C, a conductance level of around 0.3 nS appeared when applying 75 mV (second trace from top), and later on, two consecutive "opening" and "closing" events occur with stepwise conductances of 0.2 and 0.7 nS respectively. It is noteworthy that progressive opening events in planar bilayers containing SP-B sometimes ended up in membrane rupture, while in the presence of SP-C the conductance levels were more stable in time or openings were always followed by pore closures. Not only well-defined transitions between conductance levels have been observed, but also noisy, irregular traces in which sudden "bursts" of electric activity

appeared, consisting of multiple spikes between different states. For instance, the two first traces shown in figure 5.6 are quite representative of these bursts of conductance transitions: in the time frames between 30 and 45 s for the first trace, and 25 and 45 s for the second trace, this irregular behavior is dominating, in contrast to more ordered, well-defined transitions like those observed in the fourth trace for negative applied voltage. These bursts appeared much more frequently for high potential differences (75-100 mV) and seemed to be more usual in the presence of SP-B, but they were also found in SP-C-containing bilayers.

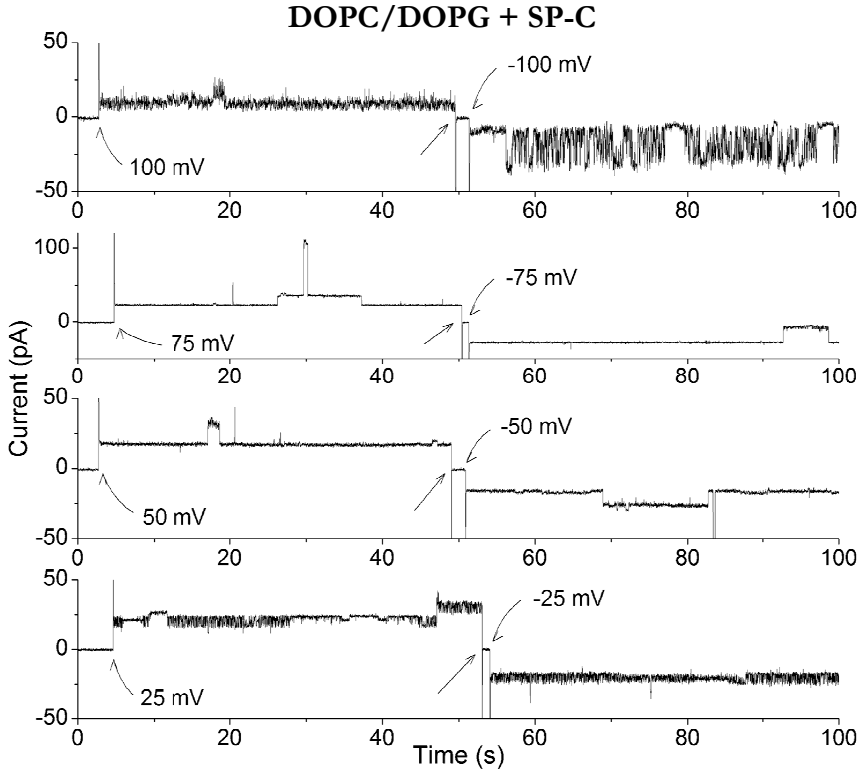

Fig. 5.7: Representative current versus time traces recorded for different applied voltages in DOPC/DOPG (85:15, w/w) bilayers supplemented with isolated SP-C at a protein/lipid ratio of 0.005% by weight. Each trace corresponds to a different casted bilayer, and voltage application is indicated with arrows. Traces were subsequently filtered using a Bessel (8-pole) filter with a 50Hz -3dB cut-off frequency.

Again, G and ΔG values were calculated from average I and ΔI measurements divided by the correspondent applied voltage. The conductance distributions for each individual protein, shown in figure 5.8, resemble qualitatively the results found for the complete protein fraction in figure 5.3. At first sight, panel A in figure 5.8 seems to indicate a slight difference between the two proteins: SP-B-containing DOPC/DOPG bilayers showed a wide range of conductances, being the most commonly recorded around 35 pS. In contrast, the most frequent conductance found for SP-C was approximately 0.3 nS. However, a more careful analysis considering the stepwise conductance (ΔG) distributions (see panel B in figure 5.8) rules out this possibility and yields similar conductance levels for

both proteins. The most frequent recordings in figure 5.8-B were found to be 0.21 nS for SP-B and 0.16 nS for SP-C in DOPC/DOPG bilayers. This means that the most frequent stepwise conductance ΔG is larger for each protein individually than for the native mixture of both proteins (around 0.05 nS in figure 5.3-B).

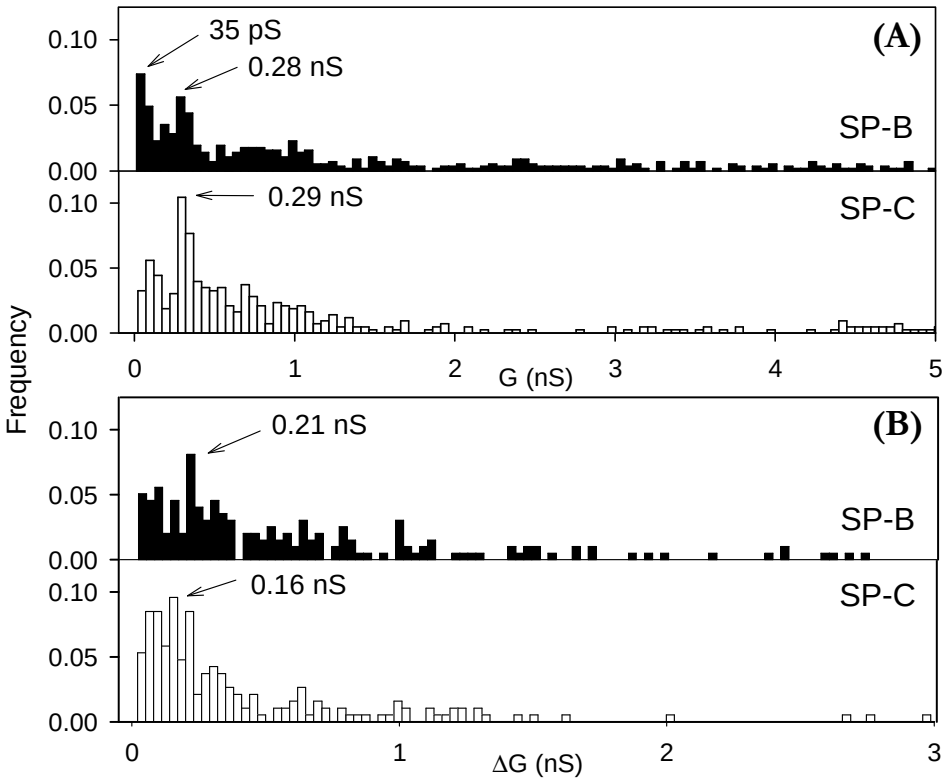

Fig. 5.8: Normalized histograms representing all conductance levels G (A) and conductance increments ΔG (B) detected during the experiments with DOPC/DOPG 85:15 bilayers containing SP-B (black bars) or SP-C (white bars) at a protein/lipid ratio of 0.005% by weight. Around 20 different bilayers were casted for each sample, obtaining from them around 500 G and 200 ΔG values in each case. Most frequent G and ΔG values are indicated.

We also analyzed the effect of the applied potential in the independent SP-B and SP-C conductances measured in DOPC/DOPG bilayers, as shown in figure 5.9. In the case of SP-B, the conductance distribution seems to be independent of applied voltage: there are no significant differences between low (5-50 mV) and high voltages (75-100 mV). In contrast, the normalized histograms for SP-C display a different scenario: the most common conductances at low applied voltages (three peaks at around 80 pS, 0.3 nS and 0.7 nS can be distinguished) become much less frequent at higher potentials, yielding a broader and less clear peak distribution.

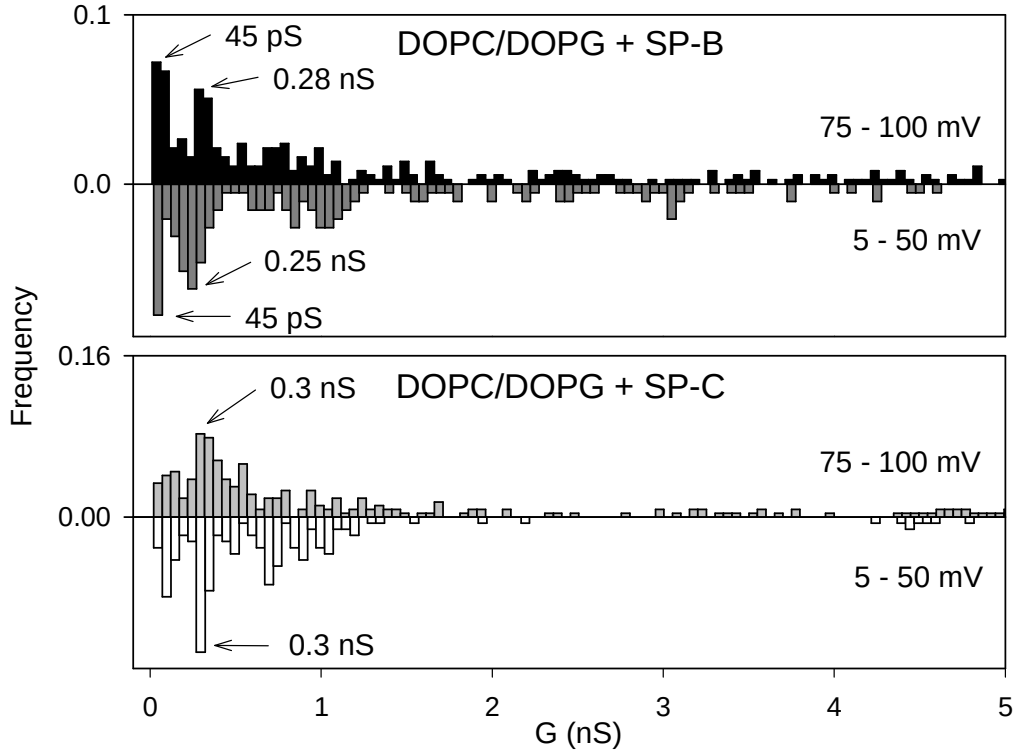

Fig. 5.9: Normalized histograms representing the recorded G values classified by the applied voltage that was applied in each measurement: high voltages (75-100 mV, darker bars) and low voltages (5-50 mV, lighter inverted bars), in absolute value. Most frequent G values are indicated.

Reversal potential experiments in panels A and C from figure 5.10 showed that both SP-B and SP-C form cation selective pores in DOPC/DOPG bilayers, with a preference for K^+ over Cl^-. The relationship between pore conductance and reversal potential is shown for SP-B and SP-C in panels B and D, respectively. The points are considerably scattered, so a possible correlation between pore size and selectivity is not as evident as in the native mixture of SP-B and SP-C shown in figure 5.5-B.

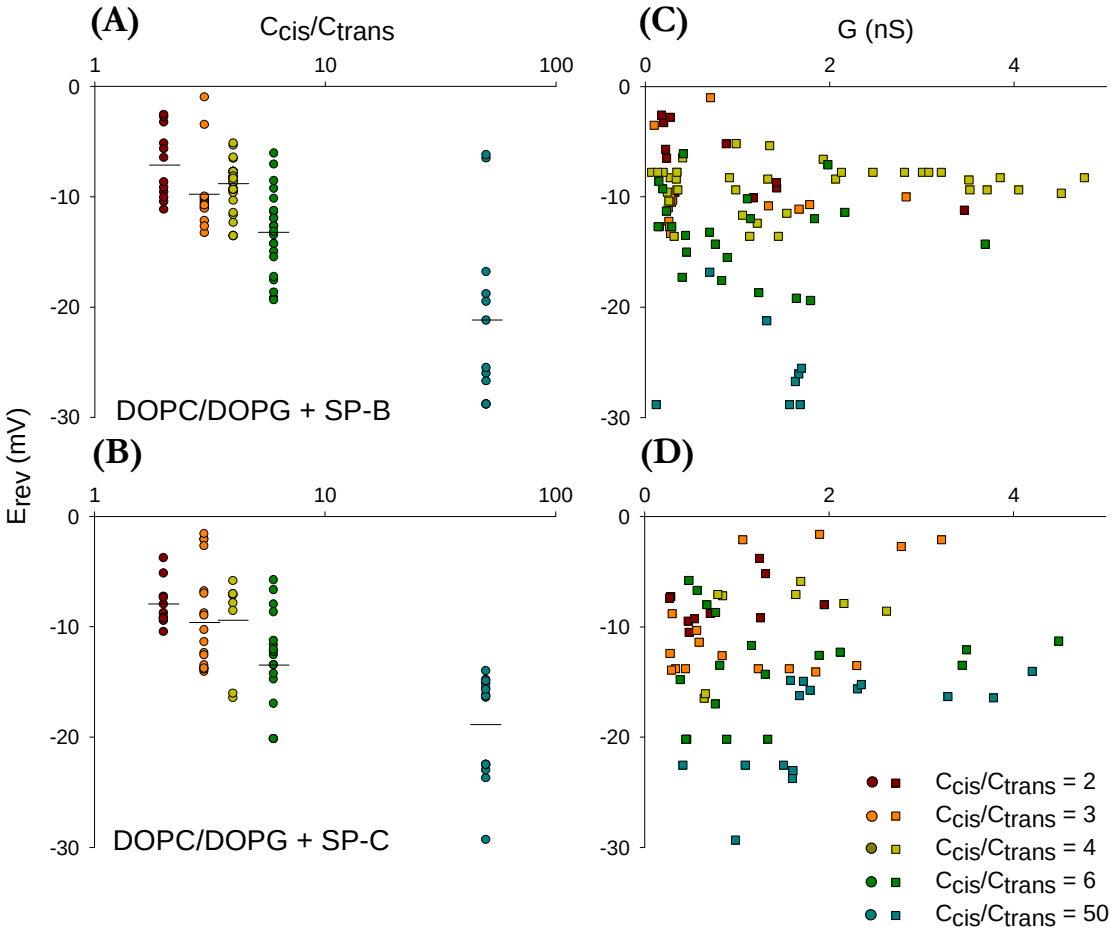

Fig. 5.10: To the left, reversal potential values versus KCl concentration gradient (50 mM *trans* side; 100, 150, 200, 300 and 2500 mM *cis* side) for DOPC/DOPG 85:15 bilayers supplemented with SP-B (A) or SP-C (B) at a protein/lipid ratio of 0.005% by weight. Logarithmic scale has been used for the x axis. All the measured values were plotted, and the black line represents their mean value for each concentration gradient. To the right, reversal potential versus conductance for all the experiments performed with SP-B- (C) or SP-C- (D) containing DOPC/DOPG 85:15 bilayers in the presence of the different KCl concentration gradients tested.

The corresponding permeability ratios P_+/P_- obtained from equation (5.1) were in the range 1.9-2.6 for SP-B and 2.0-2.8 for SP-C. The fact that the selectivity of SP-B and SP-C pores is so similar despite the difference in the net charge of the proteins (+7 versus +2) suggests that the selectivity is mostly regulated by the lipid charge. Indeed, when selectivity experiments were done in zwitterionic DOPC bilayers, pores formed by SP-B always showed a preference for anions over cations, in agreement with the net charge of the protein (+7), as can be observed in figure 5.11-A, while SP-C did not show a well defined selectivity, specially for high KCl concentration gradient: although average values would correspond to non-selective pores, the recorded E_{rev} values were either positive or negative, as is shown in figure 5.11-B. This observation could come from the fact that the net charge of the protein is still positive but considerably less important (+2) so that the experimental error is comparable to the absolute value of the reversal potential.

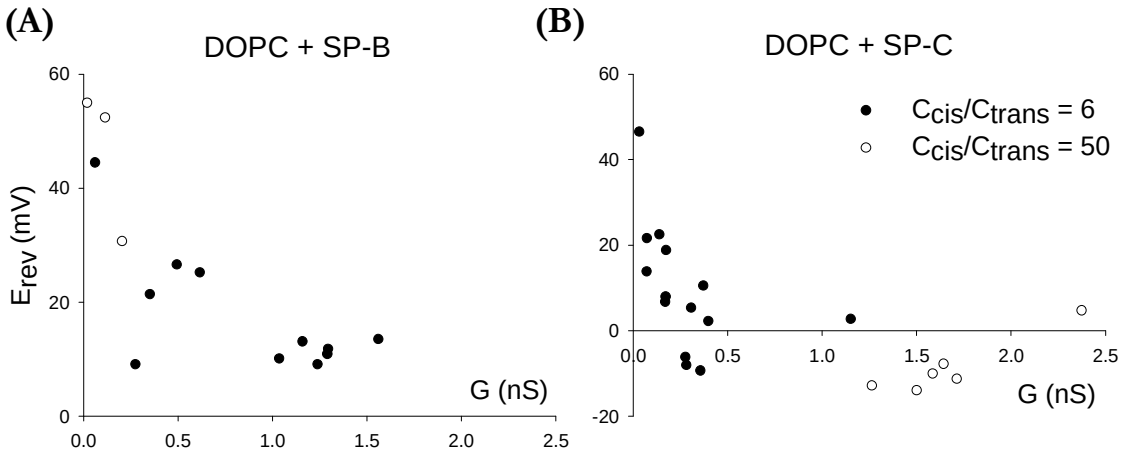

Fig. 5.11: Reversal potential values versus conductance for DOPC bilayers containing SP-B (A) or SP-C (B) at a protein/lipid ratio of 0.005% by weight, tested for two different KCl concentration gradients (50 mM *trans* side; 300 and 2500 mM *cis* side).

5.3 DISCUSSION

The ability of hydrophobic surfactant proteins to alter phospholipid membrane permeability to polar solutes was reported in the chapter 4 of this Thesis. This activity has been usually linked to the properties of these proteins to perturb lipid packing in membranes (Chang et al. 1998, Hawgood et al. 1998, Johansson 1998, Ryan et al. 2005, Perez-Gil 2008), required to facilitate the transfer of surface active species between surfactant membranes and the air-liquid interface. In the present chapter, it is demonstrated that SP-B and SP-C, both together and also individually, create an enormous diversity of defects or pores in phospholipid membranes, with no characteristic size or conformation under the experimental conditions tested here. Indeed, we have found a high variety of conductance states (from pS to nS) that are dependent both on the lipid composition and the applied potential. It was also shown that the type of host lipid crucially determines the ionic selectivity of the observed pores. These results suggest that SP-B and SP-C create pores not as well defined as typical proteinaceous ionic channels, but promote the local breakdown of the membrane bilayer structure creating pores with a surface formed partially or totally by polar lipid groups. SP-B belongs to the saposin-like family of proteins, which includes several members with detergent-like activity and true pore-forming toxins (Olmeda et al. 2013). The present study reveals that the ability of SP-B to alter the permeability barrier of surfactant membranes could be not just the consequence of transient detergent-like local perturbations but of the assembly of long-living protein-lipid poring structures. A previous study had already proposed that a clinical surfactant preparation, with poorly defined lipid and protein composition, could contain ionic pores (Oelberg and Xu 2000), although the unitary single channel conductances of around 50 pS detected in those experiments were far from the large dispersion of small and wide pores found in the present work.

Each one of the two proteins, SP-B and SP-C, seems able to produce a wide range of different conductances. A similar behavior has been observed in the pores formed by certain antibiotic peptides, such as colicin, which present two different conformations that are reflected in the recordings as two kinds of sub-states, a "closed" state with low conductance and relatively large lifetime and an "open" state with high conductance and very short lifetimes. Experimental conductances of these closed and open sub-states are around 50 pS and 0.3-0.4 nS, respectively, for colicin E1 in DPhPC bilayers (Sobko et al. 2004). Colicin-like conductance transitions have been observed for both PF and SP-C alone (see for instance the first trace shown in figure 5.1 and the second one in figure 5.7), suggesting that they could correspond to SP-C action. Here, these particular sub-states would have conductances of ~0.3 nS and ~1 nS, but in general there is no such a sharp distinction between sub-states (see figures 5.3 and 5.8), maybe because the possible conformations that these proteins adopted upon pore formation were more diverse. This may include the presence of different possible oligomerization states (Wustneck et al. 2003). The fact that, for the most frequent stepwise conductance, each protein yields individually larger values (0.21 and 0.16 nS for SP-B and SP-C, respectively; see figure 5.8-B) than those found for the native mixture of both proteins (55 pS; see figure 5.3-B) allows to hypothesize that in the whole protein fraction, SP-B might complex with SP-C to form a combined channel oligomer with average smaller aperture. Furthermore, by ocular inspection of the current traces, a rough classification of all the recorded conductance states has been performed based on their approximate lifetimes: the whole protein fraction showed the most stable behavior, both in DOPC and DOPC/DOPG, where around 30% of the states remained open for the complete recording (~100 s) and 40% had long lifetimes, in the range of seconds. Around 10% of the conductance levels lived for shorter lifetimes, less than seconds. In contrast, isolated SP-B and SP-C showed a significant increase of the shortest events, representing around 20% of the total number, while the stable and long-lived states were found to be only around 20 and 5%, respectively. All proteolipid bilayers presented a significant fraction of noisy current fluctuations (around 15-20%), such as the bursts of electric activity previously mentioned, whose frequency was even higher in the presence of isolated SP-B (approximately 25%). These findings point out again to significant differences between the individual and combined action of surfactant proteins SP-B and SP-C, where their mutual interactions could modulate the permeability of surfactant membranes and their ability to control transmembrane movement of charged species. This idea is fully consistent with the results shown and discussed in chapter 4, regarding the possible pore sizes and calcein equilibration times of proteins SP-B, SP-C and their physiological mixture.

Several evidences in the current study support the concept that phospholipids take part of the surfactant protein-promoted permeabilizating structures. Although we have found that the whole surfactant protein fraction PF introduces a continuous distribution of ΔG between tens of pS and several nS in both zwitterionic and anionic lipid membranes, the most frequent values of the stepwise changes in conductance are larger in neutral DOPC (90 pS) than in negatively charged DOPC/DOPG (55 pS), as was shown in figure 5.3-B. In principle, the negatively charged lipid headgroups in the vicinity of the channel would be expected to accumulate positive ions in excess of their bulk concentration,

increasing then the pore conductance. Indeed, this is the observed effect in model protein channels like gramicidin A, alamethicin or the bacterial porin OmpF (Rostovtseva et al. 1998, Aguilella and Bezrukov 2001, Alcaraz et al. 2009). However, no such clear trend has been observed in proteolipidic pores. Malev et al. reported that negatively charged lipids decreased the conductance of the syringomycin E channel at low electrolyte concentration and they had no clear effect in concentrated solutions (Malev et al. 2002). They suggested that the screening of the positive charges of the peptide and the lipid negative charges worked in opposite direction, partially compensating each other. This could be also the case here: the negative charges of DOPG would balance or even overcompensate the effect of positive charges of both SP-B and SP-C proteins.

The fact that the ionic selectivity of PF is inverted in the presence of negatively-charged phospholipids compared with zwitterionic membranes also argues in favor of a proteolipid channel structure. Surfactant proteins might therefore promote or stabilize the opening of lipid-coated holes in phospholipid membranes, in the line of the so-called toroidal pores induced by other membrane-active peptides (Sengupta et al. 2008, Mihajlovic and Lazaridis 2010). Still, it remains to be demonstrated whether the lipid molecules do actually line the protein-promoted membrane pores. It is also conceivable that the change in lipid selectivity promoted by acidic phospholipids could be alternatively due to a completely different organization of protein oligomers into the membrane. However, the high hydrophobicity of these proteins and their ability to facilitate rapid diffusion of lipids within surfactant membrane complexes, as it was shown in the chapter 4 of the present work, suggest that the lipids are actually lining the pores, at least partially. Different protein oligomers, either combining or not different proteins, could result in a range of different conductances such as those revealed by our experiments. The variety of conductive states could also represent a highly dynamic behavior, in which association/dissociation processes, involving or not homo- or hetero-oligomerization of the proteins, could lead to fluctuations in membrane permeability. It has been reported that surfactant proteins SP-B and SP-C exhibit some affinity for negatively-charged phospholipid species (Perez-Gil et al. 1995, Cabre et al. 2012), with some controversy with respect to the actual specificity towards PG (Seifert et al. 2007, Perez-Gil 2008), an essential phospholipid in surfactant activity. Affinity for anionic lipids is modulated by the ionic strength (Perez-Gil et al. 1995, Cabre et al. 2012). It is therefore possible that the different ionic media used to analyze ion selectivity promote changes in lipid-protein interactions and in the oligomerization levels and conformational states of the proteins, all contributing to the complex picture observed in terms of multiple coexisting conductance situations. Which conductive states are the most relevant under physiological conditions remains to be determined.

In principle, these results cannot be easily extrapolated to the biological context. It is evident that the complex lipid composition in native surfactant membranes was not taken into consideration, and experiments have not been done at the physiological temperature either. However, it is meaningful that these two small lipoproteins, isolated from its natural environment, could be able to create such a significant change in a simple model membrane like the one studied here. PLM made from the full lipid fraction of surfactant were tried to be casted as part of these experiments, but those membranes had a highly fluctuating character, with complex basal conductance states even in the absence of

proteins, and were extremely unstable. This indicates that surfactant membranes with full compositional complexity could still be highly permeable and definitely much more dynamic than the simplified models tested here.

The results presented here open further interesting questions about the proteins themselves, which merit further research. For instance, it is intriguing how SP-C, with its extremely hydrophobic transmembrane helix, could affect the bilayer integrity in order to open aqueous pores. A potentially important role may be played by the polar N-terminal segment of the protein, a region with the intrinsic potential to interact with and perturb phospholipid membranes (Plasencia et al. 2004, Plasencia et al. 2008). SP-B has been involved in modulating the mechanical properties of pulmonary surfactant membranes and films (Schurch et al. 2010, Bernardino de la Serna et al. 2013). A question of interest is how much the alteration of membrane geometry that leads to SP-B-promoted membrane permeabilization sustains the effect of the protein to stabilize multilayered films against mechanical perturbations. Finally, the SP-B and SP-C membrane poration activities reported here are highly indicative of the existence of high-order oligomerized states for the two proteins in membranes, something that has been previously proposed (Wustneck et al. 2003, Olmeda et al. 2013) but whose correlation with the role of the proteins in surfactant is still not properly understood.

6. MECHANICAL PROPERTIES AND STRUCTURAL STABILITY OF PHOSPHOLIPID VESICLES CONTAINING SP-B AND SP-C

All the experiments included in the present chapter were performed in collaboration with Prof. Evan Evans (Duke University, US) and the following members of his research group: Wieslawa Rawicz, Andrew Leung (University of British Columbia, Vancouver, Canada) and Igor Kuznetsov (Duke University, US). The experimental set-up was assembled in the facilities of the Electron Microscopy Centre of Complutense University.

6.1 INTRODUCTION

In general terms, biological membranes present a strong preference for a lamellar configuration, showing a negligible solubility of their amphiphilic molecules in aqueous media; thus, phospholipid vesicles can be in principle considered as closed systems with stable composition. Because of the thin structure of the double layer (around 4-5 nm thick), the measurement of the mechanical properties of membranes is hindered by bilayer fragility and diffraction-limited detectability by optical methods. Micron-sized pipettes are a popular tool for cell micromanipulation and patch-clamp experiments, but they have also been widely employed in direct measurements of the mechanical parameters of phospholipid membranes such as area expansivity, shear or bending moduli (Evans and Skalak 1980, Evans and Needham 1987, Needham and Zhelev 1999). This micromechanical technique has been optimized in order to apply precise linear tension ramps to lipid vesicles with diameters around 20 μm and to obtain their geometric changes with sub-millisecond and sup-pixel resolutions (Heinrich and Rawicz 2005).

In the present chapter, the micropipette aspiration technique was used to determine the impact of hydrophobic surfactant proteins SP-B and SP-C on model membranes in terms of area elasticity and dynamic strength under increasing tension ramps. POPC giant vesicles (GV) were prepared by following the slow hydration method (see section 3.3.4.2 for further details), and their mechanical properties were compared to POPC vesicles containing sub-physiological amounts of hydrophobic proteins SP-B and SP-C: $1/10^6$ and $1/10^5$ protein-to-lipid ratios, respectively, whereas the physiological amount is in the order of 10^{-3}. These low protein densities were chosen in order to avoid crowding or non-specific aggregation effects and to obtain information about the effect of individual proteins. Besides, vesicles containing the physiological amount of SP-B and SP-C are practically undetectable: as it has been demonstrated in previous sections, physiological amounts of both proteins create aqueous pores that disrupt membrane integrity, and membranes become permeable to glucose and sucrose. Thus, it causes that the refraction index gradient between the vesicle and its surrounding medium immediately disappears (see figure 6.1).

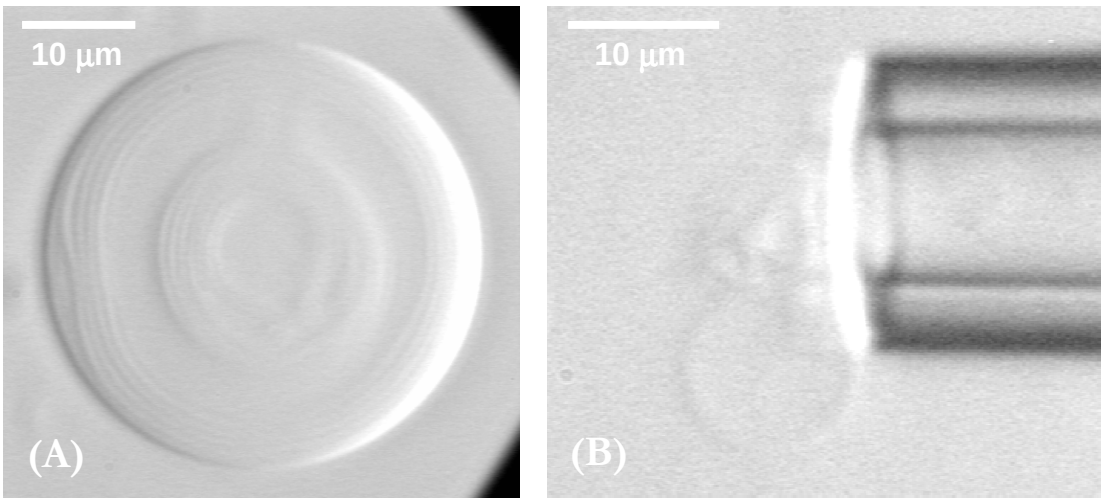

Fig. 6.1: Microscopy images of POPC giant vesicle containing SP-B at $1/10^6$ lipid/protein ratio (A) and at the physiological ratio, $1/10^3$ (B).

6.1.1 BILAYER ELASTICITY

For thin, elastic materials, such as phospholipid membranes, the possible deformations can be represented by simple shape changes of local surface elements (see figure 6.2): (*i*) area dilation or condensation, $\alpha = \Delta A/A_0$; (*ii*) in-plane extension or surface shear at constant surface density, $\lambda = L/L_0$; and (*iii*) bending or curvature change at constant rectangular shape, $\Delta C = \Delta(1/R)$. These independent deformations are caused by forces which specific actions on membrane elements are indicated in figure 6.2: tension σ, proportional to the fractional area dilation or condensation; surface shear τ, proportional to in-plane extension or shear strain; and bending moments M, proportional to changes in membrane curvatures (Evans and Needham 1987).

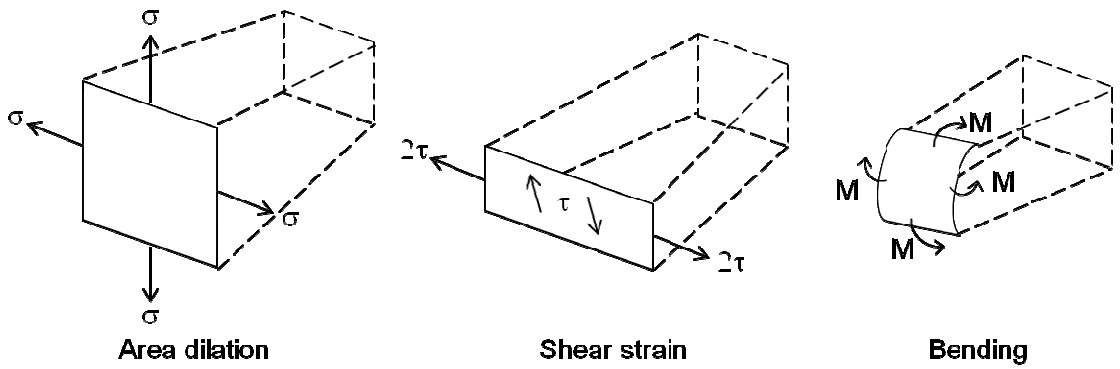

Fig. 6.2: Modes of deformation and force-moment resultants in thin, elastic materials.

The first deformation can be applied both to solid and liquid materials, while the second one is exclusive to solid structures; POPC membranes present liquid-like behavior at temperatures above -2ºC (its T_m), so in general its shear modulus is zero. Finally, the third deformation represents the curvature elasticity of the bilayer. The bending modulus of fluid phospholipid membranes can be determined by different approaches, such as micropipette aspiration (Rawicz et al. 2000), by measuring the entropy-driven tension that appears when thermal bending undulations are smoothed under pipette pressurization. However, these measurements were not in the scope of the present work.

The present study is focused on the area dilation of POPC bilayers under increasing mechanical tensions, in the presence or absence of hydrophobic proteins SP-B or SP-C. Once corrected for thermal fluctuations, the area dilation moduli α_{kc} were obtained by using the so-called **polymer brush model** (Rawicz et al. 2000), proposed in order to explain a nearly constant expansivity modulus of lipids with a 2-fold difference in chain length and a large variation in chain saturation, following the classic theory of Flory for polymers (Flory and Volkenstein 1969). In this model, each monolayer is considered as a collection of extended, structureless polymer chains, and the surface pressure in the fluid bilayer is dominated by confinement of chain entropy, illustrated in figure 6.3, neglecting van der Waals attraction between chains and specific headgroup interactions.

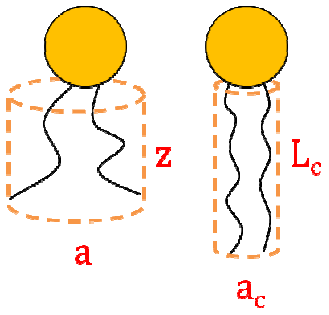

$$x = \frac{z}{L_c} = \frac{a_c}{a}$$

Fig. 6.3: Chain entropy restriction for tight packing at a constant volume, where extension ratio x can be defined either by the ratio of average chain length z to the *all-trans* length L_c or by the ratio of the smallest cross sectional area a_c to the average molecular area (Rawicz et al. 2000).

The elastic energy for chain extension is given by a simple spring model, $\mu_{ce} = Kx^2$, where x is the chain extension and K is determined by temperature and the effective number of degrees of freedom in the chain. Combining this with chain packing requirements explained in figure 6.3 (see (Rawicz et al. 2000) for further details), an anharmonic relationship between surface pressure and area per lipid molecule is subsequently worked out, given by the following expression:

$$\sigma = 2\Pi_0 \left[1 - \frac{1}{\left(1 + \alpha_{k_c}\right)^3} \right] \quad (6.1)$$

Where Π_0 is the monolayer surface pressure in the absence of mechanical tension. From thermodynamic minimization of the free energy with respect to lipid surface density, Π_0 is given by the interfacial energy density for exposing hydrocarbons to water, γ_{hcw}: $\Pi_0 = \gamma_{hcw}$ (Evans and Skalak 1980). Following the polymer brush model, the inverse cube dependence of surface pressure on area per acyl chain and the assumption that surface pressure only depends on chain extension, the elastic modulus K_A is given by monolayer surface pressure as follows:

$$K_A = \left(\frac{\partial \sigma}{\partial \alpha_{k_c}} \right)_{\sigma=0} = 6\Pi_0 \quad (6.2)$$

Consequently, the model predicts that surface pressure and elastic modulus are governed by the interfacial energy density, which is affected by the chemical properties of the acyl chains, such as unsaturation degree, discarding polar interactions at the headgroup level. The anharmonicity of the model is especially noticeable in hyper-stretched vesicles, aspirated at sufficiently fast tension ramps (above 5 mN/m/s, approximately), being able to reach surface tensions higher than 10 mN/m before vesicle rupture thanks to the optimized and automatic set-up that has been used for the present studies. By this way, it is possible to examine both lipid area elasticity and rupture process over a 2-fold greater tension range than in other studies with high accuracy, revealing this anharmonic character of lipid chain interaction.

6.1.2 MEMBRANE RUPTURE

In the experiments performed to determine the elasticity of phospholipid membranes as described in the previous section, giant vesicles were aspirated with different pressure ramps, subjecting them to increasing tensions, which finally lead to the rupture of the vesicle. Therefore, using the same data than for bilayer elasticity, this technique allows studying the phenomenon of membrane rupture under tension, analyzing lysis tensions and vesicle lifetimes for a given membrane composition.

The rupture process can be considered as a kinetic transition between two states, intact vesicle and ruptured vesicle, and modelled as a Bernoulli distribution. Bernoulli distributions describe stochastic discrete-time processes in which each event can have only two different outcomes, "failure" or "success", which are mutually exclusive. If the probability of failure (membrane rupture) is P, the probability of success (membrane survival) is $Q=1-P$. Probabilities are independent, yielding to a memoryless process in which past events provide no information about future outcomes: the probability distribution of future states only depends on the present state and not on the past sequence of events (Durrett 2010). As a special case of binomial distribution, the Poisson distribution is considered to be a good approximation in the case that the number of events is sufficiently high and the probability of occurrence is sufficiently low, so the expected number of events is of intermediate magnitude and can be measured. In fact, it is considered a reasonable approximation of the binomial distribution when the number of events is bigger than 20 and their individual probability is smaller than 0.05 (Croarkin and Tobias 2012). In the present work, Poisson formalism and basic concepts will be employed in order to analyze the stochastic process of rupture of a given vesicle population and to obtain kinetic and thermodynamic information about the process. The main difficulty of this approach is the fact that the probability of failure is not constant in time, since the external stress raises linearly with time during the experiment, thus increasing the rupture probability. Nevertheless, it is possible to cope with this difficulty and directly assay the kinetic rates of rupture from the experimental data. The process of vesicle failure can be modelled as a Bernoulli trial in which each vesicle that breaks gives information about the probability of no failure. Thus, the rupture probability will be determined by the inverse of the exact number of vesicles $N(t)$ that are still intact at each instant of time, and conversely, the probability of no failure is given by Bernoulli distribution property $P+Q \equiv P_f+P_{nf}=1$, obtaining both time-dependent probabilities as it follows:

$$P_f = \frac{1}{N(t)} \quad ; \quad P_{nf} = 1 - \frac{1}{N(t)}$$

Therefore, vesicle rupture is not a simple Bernoulli or Poisson process with a constant probability of occurrence, but the probability of failure will depend on tension and, therefore, on time. In the particular case that the present study is focused in, due to the exponential nature of Poisson distribution, the probability of no failure at a given time window is expressed by:

$$P_{nf} \sim exp\left(-k_{rup} \cdot \Delta t_{nf}\right) \Rightarrow k_{rup} = -lnP_{nf}/\Delta t_{nf} \qquad (6.3)$$

Where k_{rup} is the kinetic rate for failure, also tension- and thus time-dependent, which characterizes the rupture phenomenon under tension and will be obtained in order to extract information about the kinetics and thermodynamics of the process.

At a mesoscopic scale, fluid lipid membranes can be considered as continuous two-dimensional liquids where collective motions of the individual molecules are crucial for dynamic properties. In these particular assays, the application of persistent mechanical stresses on lipid bilayers induces collective lipid motions that eventually lead to membrane rupture by the creation of an unstable, nanometric hole (Deryagin and Gutop 1962, Evans and Smith 2011). It is obvious that the opening of a hydrophilic pore in a lipid bilayer requires a previous rupture of symmetry in the arrangement of amphipathic molecules, from a perpendicular orientation with respect to the membrane plane to a parallel one, as it has been suggested by some experimental evidences (Melikov et al. 2001, Evans et al. 2003) and supported by molecular simulations (Tolpekina et al. 2004, Wohlert et al. 2006). The process of hole nucleation in unstressed membranes is extremely rare, due to the high energies that must be involved, which could be around 15-20K_BT over the collective free energy of the intact bilayer (Tolpekina et al. 2004). Since the energy barrier is extremely high, hole creation under tension must be a thermally activated transition whose kinetic rates can be related to activation energies by employing Arrhenius phenomenology: $-ln(k_{hole}) \approx E_b/K_BT$. For instance, a barrier energy for bilayer rupture of around 20K_BT would imply failure frequencies in the order of $k_{hole} \sim e^{-20} \sim 10^{-9}$ per second, which means that membrane failure in the absence of external stress is a very improbable event.

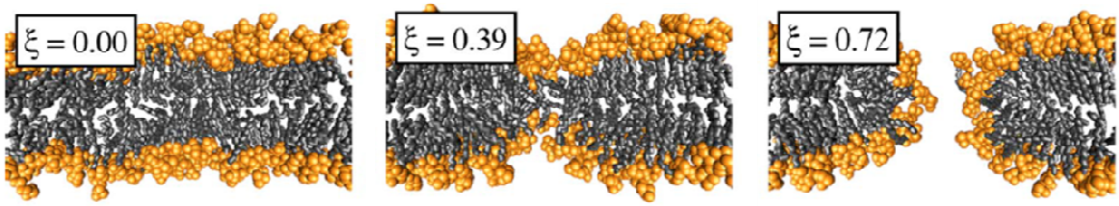

Fig. 6.4: Molecular dynamics simulation of the creation of a transmembrane pore by applying a geometrical constraint to the bilayer. As the reaction coordinate ξ grows, lipids start to rearrange and the membrane surfaces tend to curve inwards, forming a pre-pore state, and eventually an actual hydrophilic pore opens up. Taken from (Wohlert et al. 2006).

In order to explain the process of membrane rupture under external stress, the continuum cavitational model developed in the 1970's is widely accepted (Litster 1975, Taupin et al. 1975), which was based on the early concepts developed by Deryagin and Gutop (Deryagin and Gutop 1962). According to it, membrane rupture under tension is governed by a cavitational energy barrier that appears as a consequence of two opposite contributions in the free energy cost of opening and maintaining a transmembrane pore: first, the cost of having an edge of a certain length opened and exposed to the surrounding medium, which is given by the line tension or edge energy ε and grows linearly with hole radius r; and second, the gain of reducing the membrane area by applying a certain tension

σ, i.e., the mechanical work of tension. It leads to the following mathematical expression when considering circular transmembrane holes in a 2D incompressible fluid:

$$E(r) = 2\pi r\varepsilon - \pi r^2\sigma \quad (6.4)$$

From the maximization of this function, a cavitational energy barrier can be predicted: $E_\beta = \pi\varepsilon^2/\sigma$ positioned at a critical hole radius: $r_\beta = \varepsilon/\sigma$. Therefore, line tension ε dominates at small radii, while it is overcompensated by the mechanical tension σ applied to the membrane at larger radii. The energy landscape corresponding to the Deryagin-Gutop cavitational model is represented in figure 6.5-A, showing the cavitational barrier that is required to be overcome in order to achieve membrane rupture. Thus, this energy barrier is reduced by increasing tensions and the rupture process is therefore enhanced. Depending on the height of the barrier, thermal fluctuations can create defects on lipid bilayers that could be either transient and eventually resealed or could continue to grow and cause membrane rupture.

Furthermore, this model can be modified by including the nucleation of an initial symmetry break, whose energy landscape would have the shape illustrated in figure 6.5-B. Hypothetically, this symmetry break could be followed by a metastable state (*) located between the precursor barrier (δ) and the cavitation barrier (β), although its possible existence and features are still under debate (Tolpekina et al. 2004, Wohlert et al. 2006).

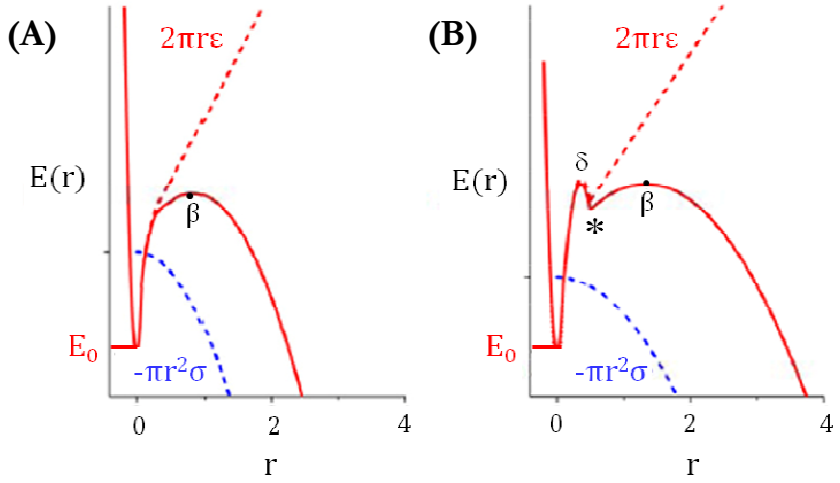

Fig. 6.5: Hypothetical energy landscapes of membrane rupture as a function of hole radius. (A) Cavitation model, where mechanical work of tension $-\pi R^2\sigma$ offsets the hole energy $2\pi R\varepsilon$, yielding a cavitational barrier $E_\beta = \pi\varepsilon^2/\sigma$ which decreases inversely with applied tension. (B) Energy landscape for cavity formation including a precursor barrier E_δ for creation of a symmetry break in the membrane, characterized by the metastable state E_*. For large tensions, the cavitation barrier E_β sunsets below the precursor barrier E_δ. Taken from (Evans and Smith 2011).

Following these ideas, the rupture phenomenon would be the product of two different stochastic processes: first, the creation of a symmetry break or defect in the

bilayer organization, and second, the irreversible rupture of one of these symmetry breaks. Each one of these processes would have different kinetic and thermodynamical properties due to their different nature. Thus, the starting hypothesis of the present study is that membrane rupture occurs due to the appearance of one single catastrophic symmetry break, once the precursor barrier has been overcome. The effect and implications of the possible existence of the cavitational barrier will be evaluated. This theoretical background will be employed in order to analyze the experimental results obtained for POPC membranes subjected to different tension ramps. Furthermore, the impact of hydrophobic proteins SP-B and SP-C in the thermally activated process of hole nucleation under tension will be also studied. To this point, lipid or lipoprotein vesicles were subjected to controlled, uniform and well-defined tension ramps until rupture, and lysis tensions were obtained with high accuracy, as it was described in section 3.10.4, thanks to the automated, high resolution micropipette aspiration set-up employed here.

6.2 RESULTS

6.2.1 POPC GIANT VESICLE ELASTICITY AND EFFECT OF HYDROPHOBIC PROTEINS SP-B AND SP-C

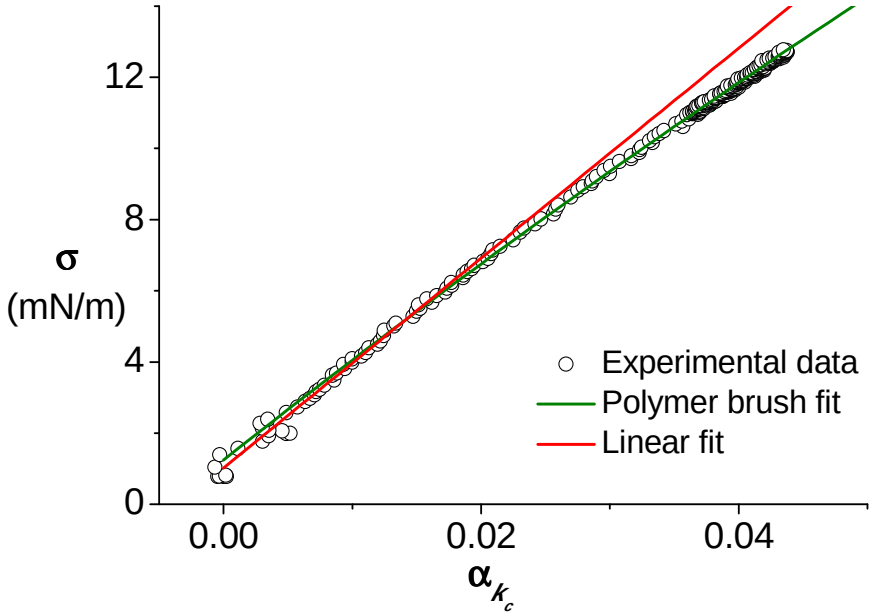

Fig. 6.6: Example of one POPC vesicle area expansion test measured for an increasing tension ramp of 5 mN/m/s. Collected data is represented by white circles and fitted by two different ways: using the polymer brush model (equation (6.1), green line, where $K_A = 6\Pi_0$); and using a linear fit ($\sigma = K_A \cdot \alpha_{kc}$, red line). Notice how, at large tensions, membranes undergo a hyperstretching in comparison with the linear behavior. Area expansion moduli obtained from each fitting were the following: K_A(polymer brush) = 293.16 mN/m; K_A(linear) = 263.47 mN/m.

In order to determine POPC bilayer elasticity and the possible effect of hydrophobic surfactant proteins SP-B and SP-C on this mechanical property, lipid or lipoprotein vesicles containing different protein densities ($1/10^6$ or $1/10^5$ protein-to-lipid ratio) were subjected to steady tension ramps ($\Delta\sigma/\Delta t$ = constant R_σ) of approximately 5 mN/m/s until rupture. After correcting for thermal fluctuations (see equation (3.10) in section 3.10.4) and considering constant volume during the experiment, the area expansivity modulus K_A was calculated for each vesicle by fitting the non-linear polymer brush model to the data for area dilation versus applied tension, as it was given by the expression (6.1). One selected POPC experiment is shown in figure 6.6; it is worth mentioning the evident deviation of area expansion versus tension from linearity and the accuracy of the polymer brush fit.

Dozens of pure lipid and lipoprotein vesicles were tested in order to obtain statistically relevant measurements, and the results are shown in table 6.1 and figure 6.7. All experiments were performed at 18 ± 1ºC.

Sample	N	$\langle K_A \rangle$ (mN/m)	SD (mN/m)
POPC	81	288.36	21.61
POPC + SP-B $1/10^6$ mol	97	306.37	17.64
POPC + SP-B $1/10^5$ mol	67	306.86	14.50
POPC + SP-C $1/10^6$ mol	85	303.09	16.28
POPC + SP-C $1/10^5$ mol	70	303.47	13.09

Table 6.1: Mean values and standard deviations of the elastic moduli obtained from the non-linear fitting given by equation (6.1) for giant unilamellar vesicles made of pure POPC or POPC containing low amounts of SP-B or SP-C ($1/10^6$ or $1/10^5$ protein/lipid ratio). N tests were performed for each membrane composition.

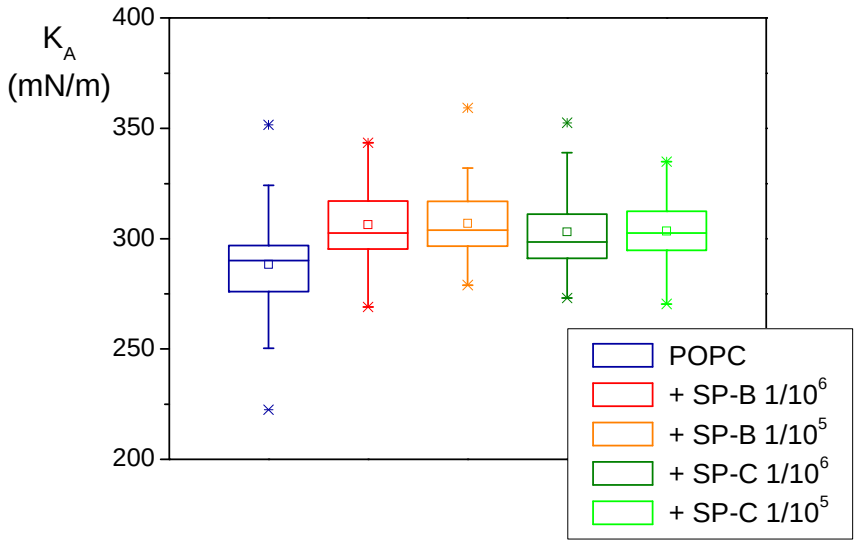

Fig. 6.7: Box representation for the area expansivity moduli estimated for GUVs of different compositions. White square indicates the mean value; horizontal line inside the box indicates the median; the box is determined by the 25th and 75th percentiles and the whiskers by the 5th and 95th percentiles, while asterisks correspond to maximum and minimum values.

In terms of bilayer elasticity, the addition of these low amounts of surfactant proteins SP-B and SP-C seems to have very little effect on POPC bilayers, although a slight increase in the elastic modulus was obtained when the membranes contain either SP-B or SP-C. This observation suggests that both proteins may be slightly increasing the resistance of POPC bilayers to area stretch. However, no concentration dependence was found, at least between the two protein densities tested, $1/10^6$ and $1/10^5$ protein-to-lipid ratio, which are respectively 10^3 and 10^2 times lower than the physiological amount of these proteins in native surfactant membranes.

6.2.2 RUPTURE OF POPC MEMBRANES UNDER TENSION

As it was explained in the introduction of the present chapter, when phospholipid membranes are subjected to persistent tensions, the creation of membrane defects is a stochastic, thermally activated process in which an unstable nanometric hole appears at some time and yields membrane rupture. Aspiration tests of POPC giant vesicles were performed at two different tension ramps, 5 and 29 mN/m/s. Vesicle lifetimes were calculated from equation (3.11), where the tension at the moment of rupture σ_{lysis} is multiplied by the average tension rate R_σ during the individual experiment. Alternatively, lifetimes can be calculated using the mean value $\langle R_\sigma \rangle$ of all the tension rates of the different tests, so that the deviations in vesicle lifetimes due to small differences between the tension ramps applied to different vesicles are smoothed. Then, the vesicle lifetimes t_i for a particular mean tension rate $\langle R_\sigma \rangle$ were arranged in ascending order, and each one was assigned with its corresponding value $N(t_i)$, from N_{total} (total number of tested vesicles) at the shortest lifetime to $N = 1$ at the longest time; this indexed array $N(t)$ represents the vesicle survival in that individual test (i.e., $S(t)$ in equation (6.3)), indicating how many vesicles were still intact at a certain time. In figure 6.8, **survival graphs** of POPC vesicles subjected to increasing tension rates of $\langle R_\sigma \rangle$ = 5.21 or $\langle R_\sigma \rangle$ = 29.06 mN/m/s are shown. One advantage of this specific representation is that double- or multi-layer vesicles that could pass the first visual inspection are clearly distinguished thanks to their larger lifetimes, since they are more resistant to stretch than unilamellar ones, and create a clear deviation branch at the end of the ordered array (see grey circles connected with grey dash lines in the different graphs of figure 6.8). Subsequently, when they are very clear, these outliers were discarded in order to get an actual unilamellar vesicle population, N_{ves}.

The process of vesicle failure can be understood as a binomial process in which there is a finite number of attempts (the number of tested vesicles) that can have different outcomes at every instant of time, as was explained in section 6.1.2. In particular, the possible outcomes are only two: survival or rupture, which corresponds to a Bernoulli-like process. Interestingly, the experimental observation of the absence of failure events during the first instants (around 0.6 s for the lowest tension rate and 0.2 s for the fastest) gives information about the random nature of the rupture process, being the probability of failure of one out of N_{total} vesicles $P = 1/N_{total} \sim 0.01$. Then, the probability of no failure

turns out to be around $1\text{-}P = 0.99$, which can be interpreted as the probability of recovery from a symmetry break in almost non-stressed bilayers.

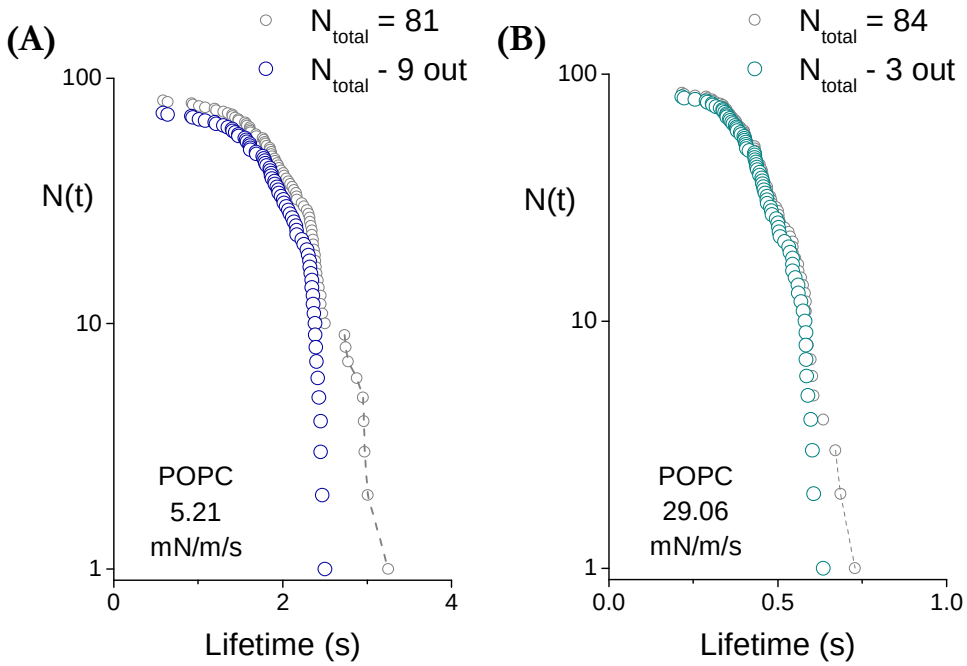

Fig. 6.8: Survival graphs of POPC vesicles tested at common tension ramps of around 5 (A) or 29 mN/m/s (B) both in logarithmic scale. Grey circles correspond to all vesicle lifetimes, (N_{total}) and colored circles to those corresponding only to unilamellar vesicles (N_{ves}), after outlier subtraction (grey circles connected with grey dashed lines).

Nevertheless, the probability of no failure changes significantly as a function of time, due to the increasing levels of external stress. Thus, logarithmic representations of the probability of no failure for sets of POPC vesicles aspirated at 5 or 29 mN/m/s are shown as a function of time in panels C and D of figure 6.9. These probabilities were given by $P_{nf} = 1 - 1/N(t)$. Signs have been changed in order to obtain positive values, since natural logarithms of numbers between 0 and 1 are negative. Histograms representing the number of failure events or ruptured vesicles ($-\Delta N_k$) at given time intervals Δt are represented for both sets of aspiration tests in figure 6.9, panels A and B. Gaussian fits were performed from these histograms, and the centers of the peaks can be identified to the most frequent vesicle lifetime in each case, which can be translated into the tension value at which most vesicles have undergone rupture by multiplying it by the tension rate. This tension can be considered as the **bilayer cohesive strength** under a certain tension ramp, denoted as σ^*. For the two cases tested here, cohesive strengths turned out to be $\sigma^* \sim 10.7$ mN/m for vesicles aspirated at 5 mN/m/s, while it was $\sigma^* \sim 13.1$ mN/m for a faster loading rate, 29.06 mN/m/s.

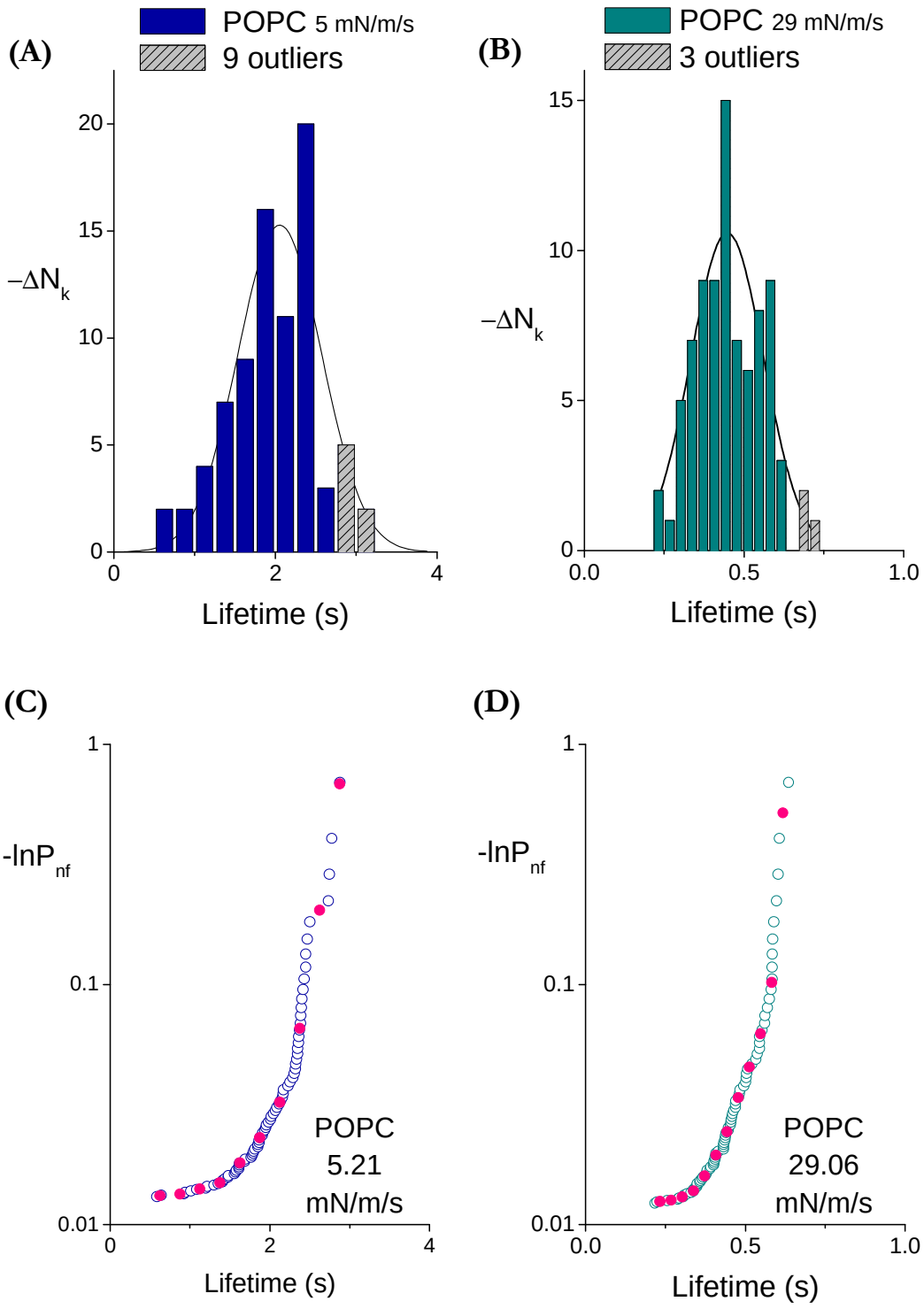

Fig. 6.9: Histograms of rupture probability of POPC vesicles tested at tension ramps of 5 (A) or 29 (B) mN/m/s, representing the number of failure events $-\Delta N_k$ per time increment Δt (0.25 and 0.035 s, respectively). Possible multilayer structures are marked with grey bars. Gaussian fits of the data are shown in each histogram. Logarithmic arrays of probabilities of no failure are shown for tension rates 5 (C) and 29 (D), superposing the values $-lnP_{nf}(t_k)$ found by interpolation at sampling times t_k (solid pink circles).

In order to get further information in terms of the kinetics of vesicle rupture, kinetic rates of vesicle failure k_{rup} were calculated at given times, specifically at the bin centers of the histograms of rupture probability, by employing the expression (6.3). The logarithm of the no-failure probability at those sampling times were found by linear interpolation, identified with pink circles in figures 6.9-C and D. Then, these values need to be divided by the expectation of a time window including no failure events, Δt_{nf}, which were inferred from the histograms of rupture probability shown in figures 6.9-A and B by dividing the bin width by the number of failure events occurred within that bin. Thus, k_{rup} were obtained from the following expression:

$$k_{rup}(t_k) = -lnP_{nf}(t_k) \cdot \frac{-\Delta N_k}{\Delta t} \quad (6.5)$$

These coarse-grained rates obtained from POPC vesicle tests span several orders of magnitude, and therefore results for both tension ramps were plotted in logarithmic scale as a function of vesicle lifetime and of applied tension, as shown in figure 6.10. It is noteworthy how the kinetic rates for hole formation and subsequent membrane rupture are remarkably different between both tension ramps when plotted as a function of vesicle lifetime (see figure 6.10-A), indicating the crucial role of tension rate on time scales.

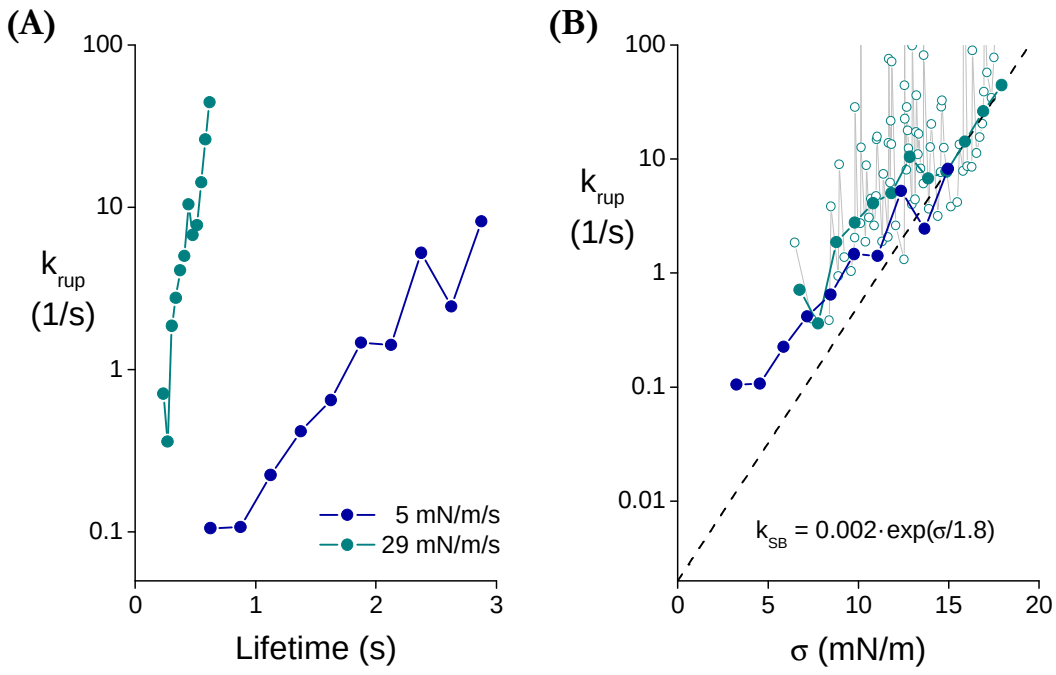

Fig. 6.10: Kinetic rates of membrane failure obtained from the aspiration tests with POPC vesicles at two different tension rates, 5 (blue circles) or 29 mN/m/s (dark cyan circles), plotted as a function of vesicle lifetime (A) and applied tension at the moment of rupture (B). In panel B, instantaneous frequencies corresponding to the aspiration test at 29 mN/m/s are shown (open circles), highlighting the random nature of vesicle rupture process, and the exponential function that best fits the high-tension frequencies is represented (dashed line).

On the other hand, when converting kinetic rates into functions of applied tension, as can be observed in graph B, this difference almost disappears and both tension rates show a similar tendency in the logarithmic plot, represented by filled circles. Kinetic rates for faster tension ramps tend to move upwards to higher lysis tensions, reaching tensions around 20 mN/m, while by applying slower rates, like 5 mN/m/s, it is possible to explore the rupture at lower tensions, below 4 mN/m. Besides, these results show that hole creation is favored by fastest tension rates: failure frequencies were always higher for 29 than for 5 mN/m/s considering the same value of applied tension. Nevertheless, both rates appear to share a common exponential tendency, especially the last points: they can be fitted by a single exponential equation, which would explain the failure frequencies of POPC membranes for tensions higher than a certain value ($\sigma_{\otimes}$ ~ 13.5 for 5 mN/m/s and $\sigma_{\otimes}$ ~ 15 mN/m for 29 mN/m/s), which will be termed as the crossover tension. The best fit for those high-tension points was found to be given by the exponential expression $f(\sigma) = 0.002 \cdot exp(\sigma/1.8)$, which is represented in figure 6.10-B.

In order to highlight the stochastic nature of the rupture phenomenon under tension, "instantaneous" kinetic rates have been obtained by calculating the inverse numbers of the dwell times measured between events, and are represented with open circles in figure 6.10-B only for the fastest aspiration ramp, 29 mN/m/s, for the sake of clarity. The randomness of the process is evidenced by the large levels of noise, corresponding to 10-fold or even higher variations between consecutive dwell times. Besides, noise comes from the limited number of experiments in each test, n ~ 100 in these particular cases, while a larger number of trials would be need in order to achieve a more regular distribution of dwell times. Thus, failure frequencies k_{rup}, represented with filled circles in figure 6.10-B, can be seen as averaged instantaneous frequencies over a given time window, which allows smoothing the random noise.

This exponential tendency observed at high rupture tensions is totally consistent with a failure process dominated by symmetry break creation (Evans et al. 2003, Evans and Smith 2011), and can be understood as the behavior of the system in the hypothetical case that the occurrence of one single catastrophic defect in lipid organization leads to membrane rupture. Thus, the exponential function $f(\sigma) = 0.002 \cdot exp(\sigma/1.8)$ will be considered as the frequency of symmetry break creation (k_{SB}) from now onwards. The pre-exponential factor could be interpreted as the zero-tension frequency for symmetry breaking: k_{SB}^0 = 0.002 s^{-1}, while the Arrhenius factor $exp(\sigma/\sigma_{SB})$ describes the mechanical susceptibility of kinetics to high tensions, set by the thermal tension scale σ_{SB} = 1.8 mN/m, which is related to defect size by the following expression (Evans and Smith 2011):

$$a_{SB} = \frac{K_B T}{\sigma_{SB}} = \frac{4.08\ pN \cdot nm}{1.8\ pN/nm} \approx 2.3 nm^2$$

As it can be noticed in figure 6.10-B, failure frequencies at intermediate tensions were always higher than the values given by k_{SB}, which perfectly describes the rupture process for tensions above the crossover point $\sigma_{\otimes}$. Thus, it is possible to identify two different regimes in the failure frequency plots, each of them showing a distinct kinetic behavior

revealed as substantial differences in failure frequencies. Nevertheless, they appeared to lie parallel in this specific representation, meaning that their failure frequencies could be described by using the same exponential function and only changing the pre-factor k_{SB}^{0}.

The kinetic rate of symmetry break formation can be therefore employed as a reference to study the rupture rates in the first kinetic regime. The ratios between experimental frequencies k_{rup} and defect creation rates k_{SB}, termed as N_{SB}, were calculated at sampling tensions obtained from histogram bin centers t_k: $\sigma_k = \langle R_\sigma \rangle \cdot t_k$, by employing the following expression:

$$N_{SB}(\sigma_k) = \frac{k_{rup}(\sigma_k)}{\langle k_{SB} \rangle (\sigma_k)} \quad ; \quad \text{where } \langle k_{SB} \rangle (\sigma_k) = \frac{1}{\Delta\sigma} \int_{\sigma_k + \Delta\sigma/2}^{\sigma_k + \Delta\sigma/2} k_{SB}(\sigma) \cdot d\sigma \qquad (6.6)$$

Thus, kinetic rates for symmetry break creation were the average values of k_{SB} within the tension intervals $\Delta\sigma = \langle R_\sigma \rangle \cdot \Delta t$ that contain the sampling tensions σ_k, and were calculated by integrating the exponential function $k_{SB}(\sigma)$ between the upper and lower limits of the tension intervals and dividing by the total tension increment. Then, the ratios between k_{rup} and these $\langle k_{SB} \rangle$ were calculated for each set of experiments and are represented as a function of tension in figure 6.11.

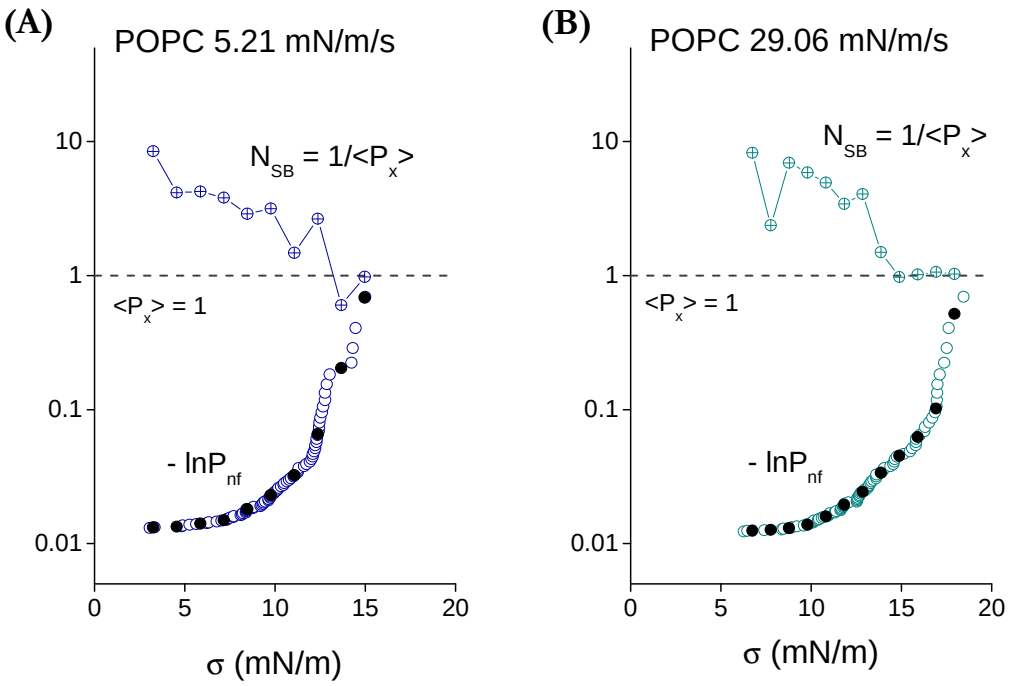

Fig. 6.11: Logarithmic representations showing the tension dependence of no-failure probability in aspiration tests of POPC vesicles at 5 (A) or 29 mN/m/s (B), used to calculate the frequencies of membrane failure k_{rup} and the frequencies of symmetry break creation k_{SB} at sampling tensions σ_k (black circles). Ratios between both frequencies are shown with crossed circles, which tend to be equal to 1 at high rupture tensions.

The dependence on mechanical tension of frequency ratios N_{SB} highlight again the possible existence of two different kinetic regimes, more clearly observed in the case of the fastest tension ramp, probably because higher aspiration rates allows exploring higher rupture tensions, above 15 mN/m, which appears to be the crossover tension between both regimes in pure POPC. Ratios N_{SB} give information about the effective difference in failure frequencies between both regimes: in POPC vesicles aspirated at 5 mN/m/s, rupture occurs around 3 times faster below $\sigma_{\otimes}$ than above that point, while at 29 mN/m/s vesicles rupture even faster, at around 5 times with respect to the high-tension regime.

Going down to the mesoscopic scale, each one of the tested vesicles would present a certain number of possible sites for membrane rupture, homogeneously distributed all over its surface. The total rupture probability must remain constant and equal to 1 according to Poisson criteria, which means that the product of the total number of events (bilayer defects) and their individual and identical probabilities of occurrence must be: $N_{SB} \cdot \langle P_x \rangle = 1$. This idea is reflected in figure 6.11, where the horizontal dashed line represents the limit case $N_{SB} = 1$, true at tension values higher than the crossover point $\sigma_{\otimes}$ where it has been hypothesized that failure is due to the creation of one single symmetry break in bilayers. Thus, for tensions lower than $\sigma_{\otimes}$, the proportionality factor N_{SB} could be interpreted as the effective number of symmetry break sites needed to lead to membrane rupture.

Furthermore, it is possible to employ Arrhenius formalism in order to correlate this frequency variations into differences in barrier energies for membrane rupture: in thermal units, energy differences are directly related to logarithmic changes between kinetic rates, i.e.: $k_{rup}/k_{SB} = exp(-\Delta E/K_B T)$ (Evans and Smith 2011). Thus, an e-fold change in failure frequencies, approximately the one observed between low and high tensions for POPC aspirated at 5 mN/m/s, would correspond to an energy difference of $1 K_B T$, while at 29 mN/m/s the energy difference could be twice this value, around $2 K_B T$.

6.2.3 EFFECT OF PROTEINS SP-B AND SP-C ON MEMBRANE RUPTURE

Once the model phospholipid system, the POPC bilayers, has been characterized, the impact of hydrophobic surfactant proteins SP-B and SP-C on membrane rupture under tension was investigated. Very low, subphysiological amounts of SP-B or SP-C were incorporated in POPC lipid stocks and giant vesicles were prepared. In total, four different lipid-protein samples were tested at a common tension ramp of 5 mN/m/s, the same vesicles analyzed in terms of bilayer elasticity: POPC giant vesicles containing $1/10^6$ of SP-B; $1/10^6$ of SP-C; $1/10^5$ of SP-B, or $1/10^5$ of SP-C (all in molar ratio). Panels A and B in figures 6.12 and 6.13 show the lifetime ordered arrays for the four sets of aspiration tests of POPC giant vesicles containing SP-B or SP-C, representing the number of vesicles that are still intact at a given instant of time.

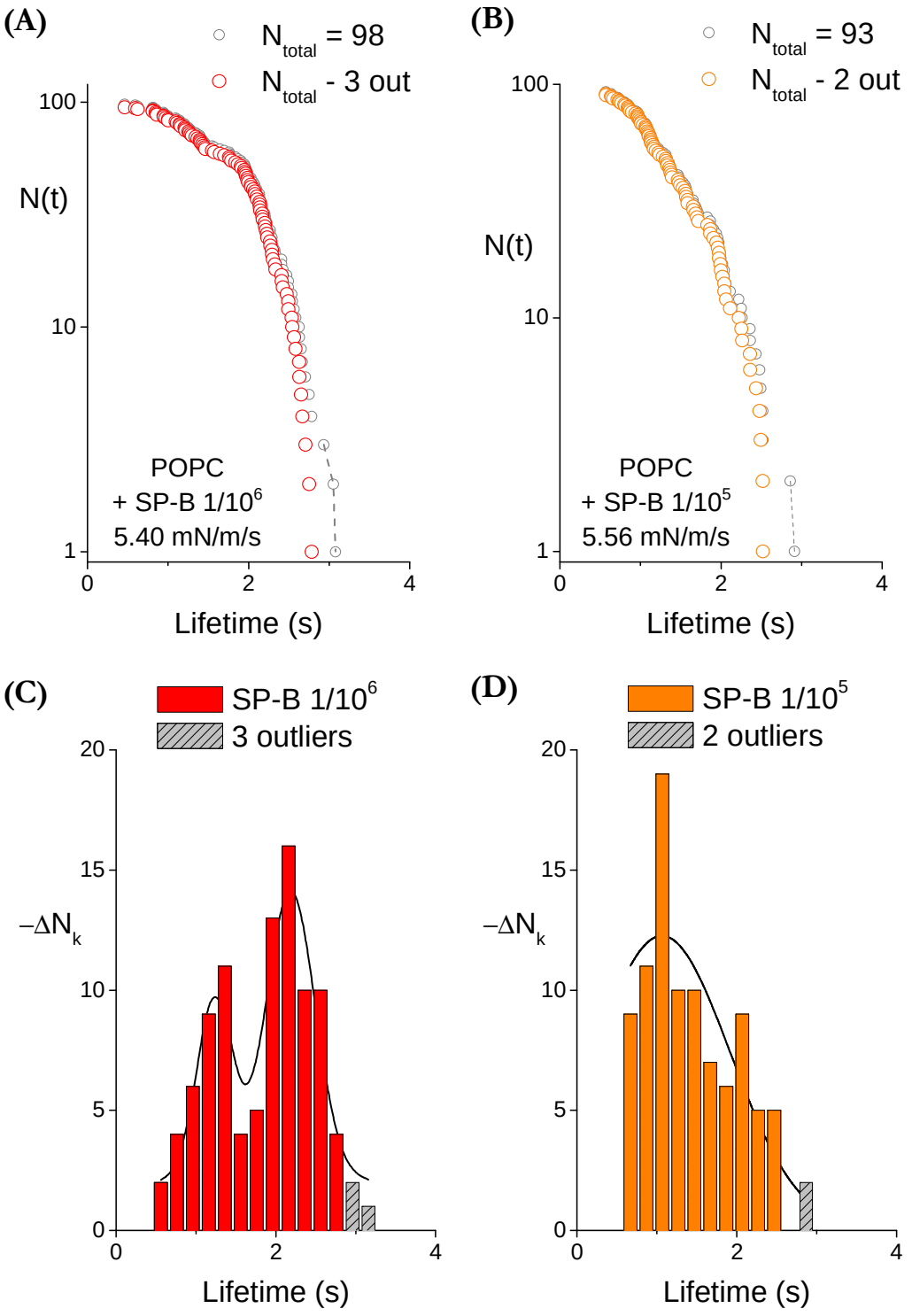

Fig. 6.12: Survival graphs of POPC vesicles containing SP-B at two different protein concentrations, $1/10^6$ (A) or $1/10^5$ (B), tested at common tension ramps of 5 mN/m/s, showing indexed ascending arrays of vesicle lifetimes. Rupture histograms of POPC vesicles containing SP-B at $1/10^6$ (C) or $1/10^5$ (D), representing the number of failure events ΔN_k per time increment Δt (0.2 s). Possible multilayer structures are marked with grey dash lines in (A) and (B) and grey bars in (C) and (D). Gaussian fits of the data are shown in each histogram.

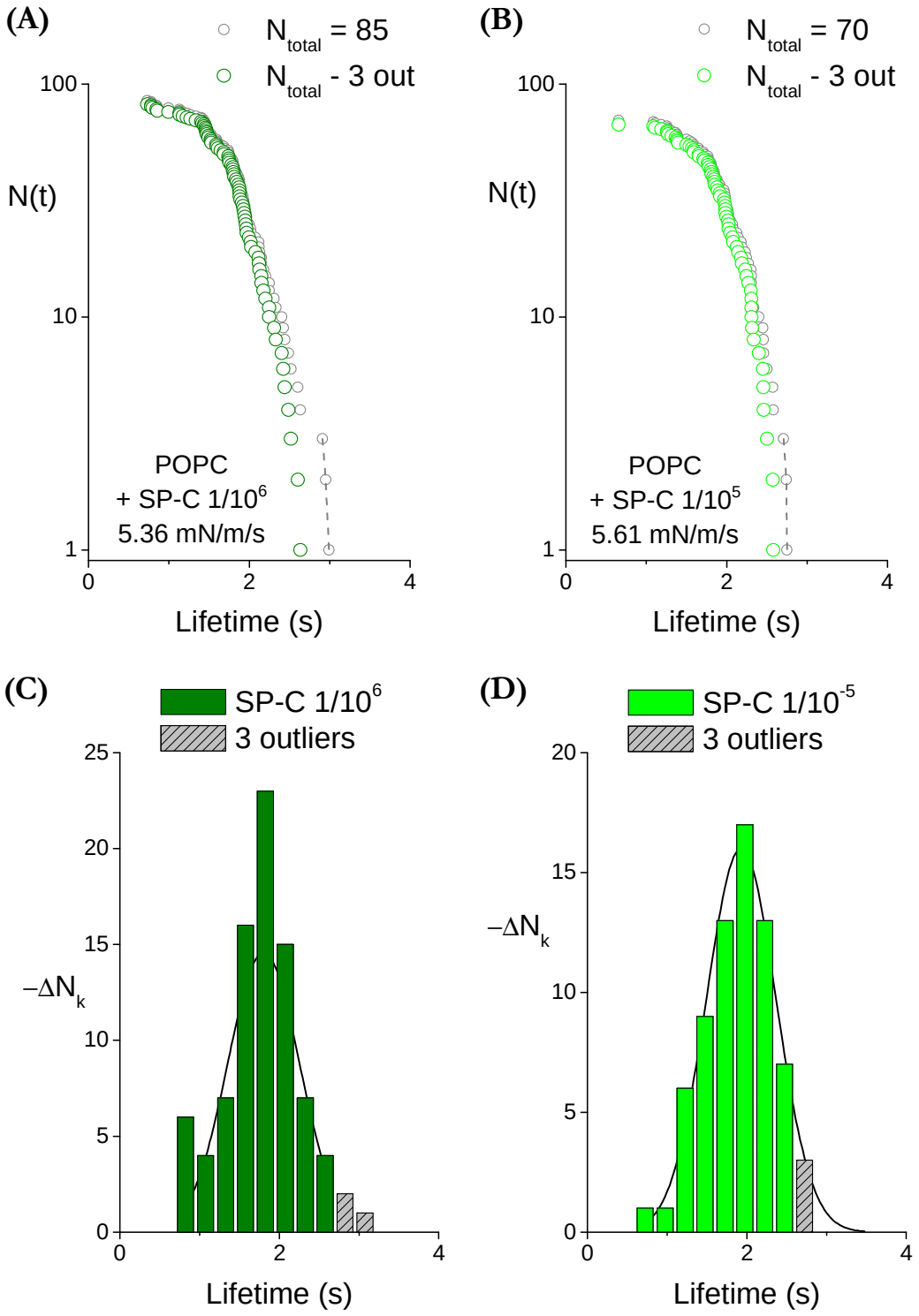

Fig. 6.13: Survival graphs of POPC vesicles containing SP-C at two different protein concentrations, $1/10^6$ (A) or $1/10^5$ (B), tested at common tension ramps of 5 mN/m/s, showing indexed ascending arrays of vesicle lifetimes. Rupture histograms of POPC vesicles containing SP-C at $1/10^6$ (C) or $1/10^5$ (D), representing the number of failure events ΔN_k per time increment Δt (0.25 s in both cases). Possible multilayer structures are marked with grey dash lines in (A) and (B) and grey bars in (C) and (D). Gaussian fits of the data are shown in each histogram.

In the case of SP-B at a molar ratio $1/10^6$ (see graph C in figure 6.12), gaussian fits from probability densities of rupture presented a main peak centered at 2.2 s and a secondary, less frequent peak at 1.2 s; interestingly, when increasing the protein concentration one order of magnitude, the peak centered at around 1 s became the most frequent. These lifetimes yielded two vesicle populations with cohesive strengths $\sigma^* \sim 6$ and 12 mN/m for SP-B at $1/10^6$ and a predominant population of $\sigma^* \sim 6$ mN/m for SP-B at $1/10^5$. This result could suggest a slight bilayer weakening for increasing SP-B concentrations. On the other hand, isolated SP-C appeared to have little effect on POPC bilayers in terms of the probability density of rupture, as can be observed in figure 6.13-C and D: one single gaussian-like distribution was present in the histograms for both $1/10^6$ and $1/10^5$ SP-C molar ratios, whose most frequent lifetimes were 1.8 and 1.9 s, respectively. These lifetimes corresponded to cohesive strengths of $\sigma^* \sim 9.7$ mN/m for SP-C $1/10^6$ and 10.7 mN/m for SP-C $1/10^5$, very similar to that calculated for protein-free POPC vesicles (around 10.7 mN/m).

From the information obtained from the probability distributions and from the logarithmic plots containing the time-dependent probability of no-failure for each set of experiments, coarse-grained kinetic rates of membrane failure k_{rup} were obtained for sampling lysis tension, by using the expression (6.5), and represented in figure 6.14. Besides, non-averaged, instantaneous kinetic rates of rupture were calculated from the dwell times between individual events in each set of experiments, demonstrating again the intrinsic stochastic nature of the rupture process, similarly to protein-free vesicles. As it can be noticed, averaged failure frequencies nicely lied in all cases on the observed tendency for pure POPC vesicles at high tensions, although the pre-factor appeared to be slightly higher. This tendency of the high-tension failure rates is especially evident in the case of SP-B supplemented at $1/10^6$ protein-to-lipid ratio, as it can be noticed in figure 6.14-A, and the behavior of all the tested sets of protein-containing POPC vesicles can be described by the same exponential function $k_{SB} = 0.003 \cdot exp(\sigma/1.8)$, which would then characterize the expected frequencies of rupture due to the creation of one single symmetry break in protein-containing bilayers. Thus, the pre-exponential factor or zero-tension frequency for symmetry break creation, $k_{SB}^0 = 0.003$ s^{-1}, may be influenced by the presence of SP-B and SP-C since it resulted slightly higher than in protein-free vesicles, where $k_{SB}^0 = 0.002$ s^{-1}. On the other hand, the thermal tension scale appeared to be the same for both protein-free and protein-containing bilayers, $\sigma_{SB} = 1.8$ mN/m, and therefore symmetry break sizes were apparently not affected by the presence of proteins.

Similarly to pure POPC vesicles, at tensions lower than the crossover points $\sigma_{\otimes}$, failure frequencies were always higher than k_{SB} and presented a very similar behavior in the case of SP-C-containing vesicles. However, the presence of SP-B impacted on failure frequencies below $\sigma_{\otimes}$ dramatically, increasing them and also displacing $\sigma_{\otimes}$ to lower values. The kinetic rates of symmetry break formation were then employed as a reference to study the rupture rates in this low-tension regime, by calculating the ratios N_{SB} between experimental frequencies k_{rup} and defect creation rates k_{SB} with expression (6.6), as was done for protein-free vesicles. Results are shown in figure 6.15.

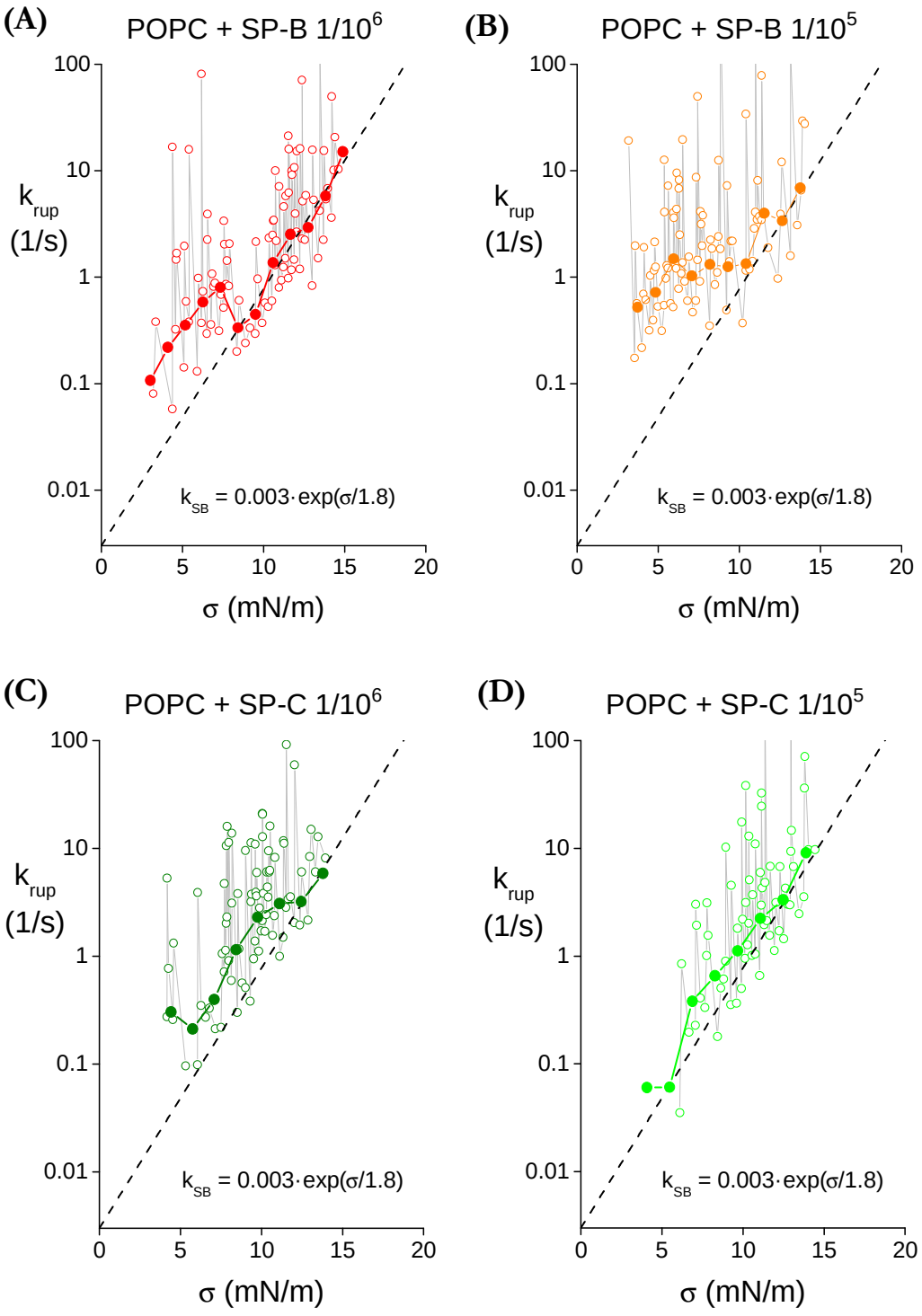

Fig. 6.14: Kinetic rates of membrane failure as a function of rupture tension, obtained from the aspiration tests with POPC vesicles containing SP-B (panels A and B) or SP-C (panels C and D) at two different concentrations, 10^{-6} or 10^{-5} in molar ratio with respect to lipids, represented with filled circles. The exponential function that best fits the high-tension kinetic rates for all tests is represented, considered as the rate of symmetry break creation k_{SB} (dashed line). Instantaneous frequencies calculated for each set of experiments are also shown (open circles), highlighting the random nature of vesicle rupture process.

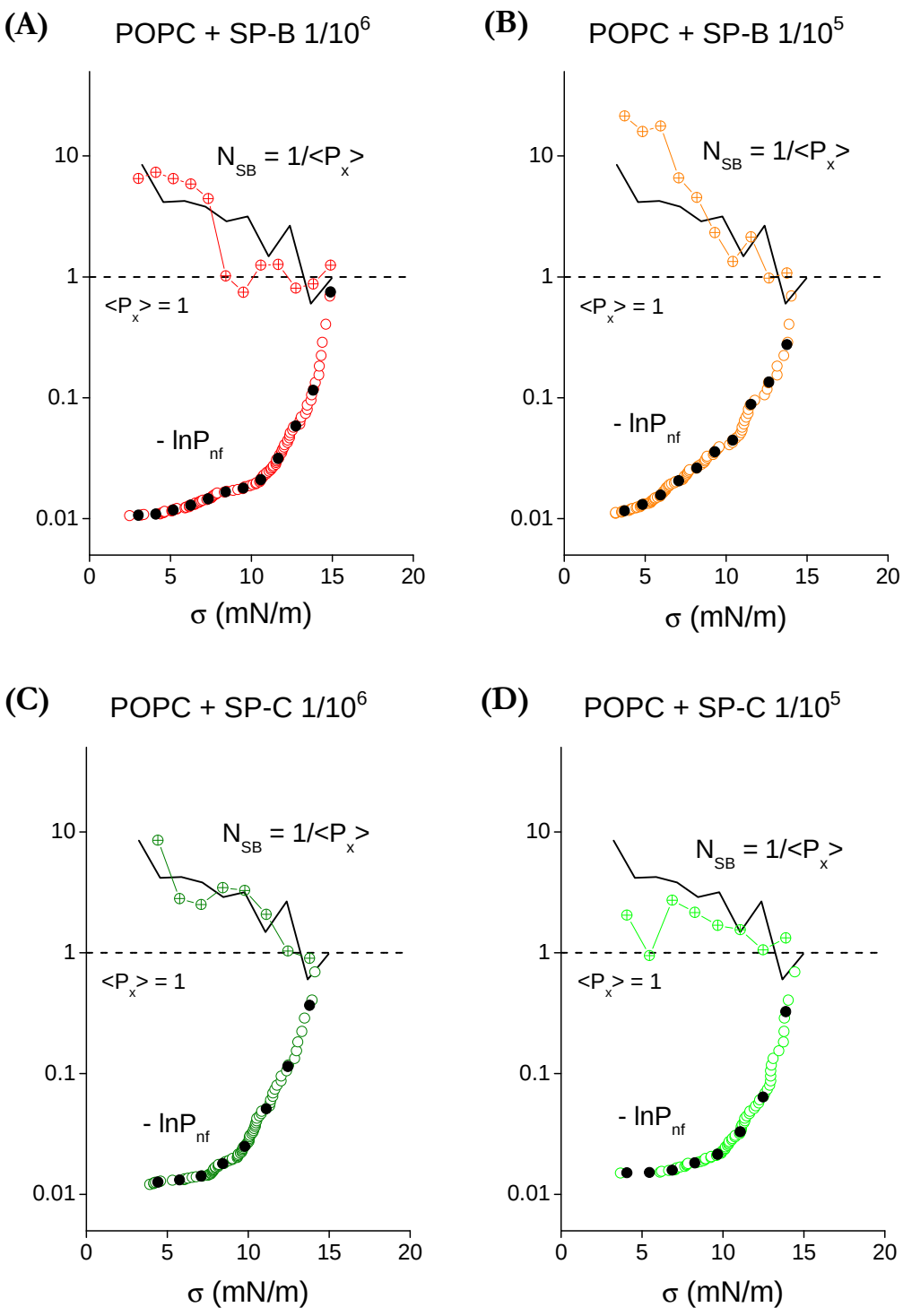

Fig. 6.15: Logarithmic representations showing the tension dependence of no-failure probability in aspiration tests of POPC vesicles containing SP-B (panels A and B) or SP-C (panels C and D) at two different concentrations, 10^{-6} or 10^{-5} in molar ratio with respect to lipids (open circles), which were used to calculate the frequencies of membrane failure k_{rup} and the frequencies of one symmetry break creation k_{SB} at sampling tensions σ_k (black circles). Ratios N_{SB} between both frequencies are shown with crossed circles, which tend to be equal to 1 at high rupture tensions. For the sake of comparison, the frequency ratios N_{SB} for pure POPC vesicles aspirated at the same tension rate are represented with a black solid line.

It is noteworthy that, at intermediate tensions, SP-B-containing vesicles ruptured much faster than the high-tension region, and significantly faster than protein-free bilayers. Supplemented at a molar concentration of $1/10^6$, this protein increased the failure frequencies at intermediate tensions (between 2 and $\sigma_{\otimes}$ = 8.5 mN/m) 5-fold with respect to k_{SB}, while one more order of magnitude of SP-B concentration increased it around 18 times for the lowest rupture tensions, suggesting an exponential dependence of failure frequencies on SP-B molar concentration. This variations in failure frequencies would correspond to energy differences of around 1.6 and $3K_BT$ respectively, significantly higher to the difference found for pure POPC bilayers, of approximately $1K_BT$.

In order to summarize the obtained results, experimental values of tension-free failure frequencies k_{SB}^0 and thermal tension scale σ_{SB} for defect-driven rupture, symmetry break sizes a_{SB} and crossover tensions between high- and intermediate-tension kinetic regimes $\sigma_{\otimes}$ are listed in table 6.2 for all the tested vesicle compositions, aspirated with common tension ramps of 5 mN/m/s.

Sample	k_{SB}^0 (1/s)	σ_{SB} (mN/m)	a_{SB} (nm^2)	$\sigma_{\otimes}$ (mN/m)
POPC	0.002	1.8	2.3	15
SP-B 1/10^6	0.003	1.8	2.3	8.5
SP-B 1/10^5	0.003	1.8	2.3	10
SP-C 1/10^6	0.003	1.8	2.3	12.5
SP-C 1/10^5	0.003	1.8	2.3	12.5

Table 6.2: Experimental values of the following parameters in the different sets of samples: tension-free failure frequencies (k_{SB}^0), tension scale (σ_{SB}) and defect size at the symmetry break region (a_{SB}); and crossover points between the high- and intermediate-tension regimes ($\sigma_{\otimes}$).

6.3 DISCUSSION

In the present chapter, the mechanical behavior and strength of fluid phospholipid membranes were investigated by using the widely spread technique of micropipette aspiration, having here the advantages of an automatic, high-resolution setup that offers a sub-pixel image resolution and a sub-millisecond time resolution, which allows determining geometrical changes in vesicle area or volume with high precision, to apply uniform tension ramps with well-defined loading rates between 0 and 100 mN/m/s and to accurately obtain the tension values at the moment of rupture. This optimized technique has been used in previous works for micromechanical studies of membranes made of a wide variety of phospholipids and lipid mixtures (Rawicz et al. 2000, Rawicz et al. 2008) and even lipid vesicles supplemented with membrane peptides (Tung et al. 1999).

The bilayer elasticity of pure POPC (C16:0/C18:1 PC) membranes obtained from these measurements (288 ± 22 mN/m in the absence of proteins) is fully consistent with previous results with similar phospholipid membranes. By using micropipette aspiration as well, the elastic modulus of DOPC (C18:1/C18:1 PC) giant vesicles was determined to be

around 300 mN/m, and in the case of SOPC (C18:0/C18:1 PC), a phospholipid that is molecularly similar to POPC except in acyl chain length, and containing one single unsaturation, K_A was measured to be around 290 mN/m (Rawicz et al. 2008). The 4-7% variations from the mean value are likely reflecting deviations from the idealized model due to the behavior of the lipid acyl chains, headgroup interactions or other hydrophobic or interfacial interactions such as protein-lipid or protein-protein interactions, together with systematic errors of the experimental approach. This elastic modulus yields a value for bilayer surface pressure at zero tension Π_0 = 48 mN/m, consistent again with previous results of both bilayers and monolayers made of unsaturated phospholipids (Smaby et al. 1997).

Four different samples were tested in the presence of hydrophobic surfactant proteins SP-B and SP-C in comparison with pure POPC GUV, specifically, POPC containing $1/10^6$ (mol/mol) SP-B; $1/10^6$ SP-C; $1/10^5$ SP-B; and $1/10^5$ SP-C. These two protein densities, $1/10^6$ and $1/10^5$, are respectively 10^3 and 10^2 times lower than the physiological protein concentration, around 1% by weight with respect to phospholipids, as it has been estimated in native surfactant membranes (Johansson and Curstedt 1997). The interest of the present study was not analyzing the effect of these proteins in the physiological conditions, but to isolate the individual and specific contributions of SP-B and SP-C to mechanical properties and structural stability of model membranes, trying to avoid possible crowding or non-specific aggregation or clustering of protein monomers. Moreover, as it was demonstrated in previous chapters of the present work (see sections 4 and 5), physiological concentrations of SP-B and SP-C create changes in the permeability of model membranes to ions and soluble molecules such as calcein. On the one hand, this effect implies important technical drawbacks, since creating a gradient of glucose-sucrose refraction index between the inner and outer vesicle media was impossible, hindering considerably the visualization of GUVs and the automatic tracking of vesicle edges. On the other hand, and from a conceptual point of view, the fact that there were pre-formed protein-mediated holes in POPC membranes was obviously incompatible with the study of the process of hole nucleation under applied tension. These are the main reasons why very low protein densities were selected to perform the experiments described in the present chapter.

The elasticity of POPC bilayers was demonstrated not to change significantly upon addition of hydrophobic proteins SP-B and SP-C: only a slight rigidification, around 6-7%, was observed when $1/10^6$ or $1/10^5$ protein-to-lipids were added, either for SP-B or SP-C. This is consistent with certain experimental evidences obtained by measuring the lateral diffusion of fluorescent probes in natural surfactant extracts, which pointed out to a possible rigidification of the bilayer in the presence of hydrophobic proteins (Schram and Hall 2004). Within the theoretical framework that has been used in the present study, the so-called polymer brush model, which determines that elastic modulus is governed by the interfacial energy density for exposing hydrocarbon chains to water and discards polar or headgroup interactions (Rawicz et al. 2000), no significant changes in POPC bilayer elasticity were estimated for the case of SP-B, a polypeptide with relatively shallow interaction with membranes whose interaction with acyl chains would be weak. However,

SP-C is known to adopt a transmembrane orientation, parallel to the hydrocarbon chains, and therefore with a more profound expected impact on phospholipid lateral mobility, which should in principle reflect an acyl chain confinement that has not been observed here. Nevertheless, it is important to remark that the protein concentrations tested are 100- and 1000-fold below the physiological amount, and could be not enough to originate measurable effects, while crucial changes in bilayer elasticity could still be possible for higher protein concentrations. The problem is that the increase in both SP-B and SP-C concentrations could create a new scenario, where protein aggregation or oligomerization could also introduce significant effects in bilayer mechanical properties.

From the results on cohesive strength of POPC bilayers in the presence of low protein densities, different effects were suggested for isolated SP-B and SP-C. On one hand, SP-B seemed to create two different vesicle populations with distinct cohesive strength, one of which was significantly weaker than pure POPC bilayers and became even more fragile and more frequent for higher SP-B concentration, while SP-C did not show any significant effect. These results highlight the different nature of membrane elasticity and strength, although both are membrane features in response to mechanical tension. Area expansivity modulus K_A and bilayer cohesive strength σ^* were demonstrated to be not related (Rawicz et al. 2008): on the one hand, bilayer elasticity mainly depends on hydrophobic interactions between the phospholipid acyl chains and their entropic confinement. Hydrocarbon exposure to water involves a very high energy penalty: $\gamma_{hcw} \equiv \Pi_0$ (Evans and Skalak 1980), which was found to be 48 mN/m for POPC. In comparison, experimental lysis tensions for POPC giant unilamellar vesicles, between 3 and 20 mN/m, are much lower. Moreover, line tensions of hydrophobic pores are expected to be around 48 pN/nm · 4 nm ~ 200 pN, considering a bilayer thickness of 4 nm, around one order of magnitude higher than the line tensions found in previous works, ε ~ 10 pN for POPC (Zhelev and Needham 1993, Evans et al. 2003). Besides, it has been reported that the edge energy emerging from opening a membrane hole crucially depends on acyl chain unsaturation or cholesterol content, in such a way that bending stiffness, line tension and rupture tensions increase together (Evans and Rawicz 1990, Rawicz et al. 2000). All these evidences indicate that rupture must be driven by other process than hydrophobic pores, probably involving lipid rearrangements in order to create a first symmetry break or precursor state, as suggested by experimental evidences and molecular simulations (Melikov et al. 2001, Evans et al. 2003, Tolpekina et al. 2004, Wohlert et al. 2006). This concept of a single symmetry break causing bilayer breakdown has been used as a basis for the kinetic analysis of vesicle rupture described in sections 6.2.2 and 6.2.3.

Together with these studies on bilayer elasticity, a detailed analysis of the stochastic process of membrane rupture under tension by hole nucleation has been performed. When giant unilamellar vesicles (diameter ~ 20 μm) are aspirated by applying increasing tension values, bilayer breakdown would occur by the appearance of a catastrophic defect on lipid organization, following the concepts developed by Deryagin and Gutop (Deryagin and Gutop 1962). Regarding the membrane rupture assays performed with pure POPC bilayers at two different tension rates, it was shown that faster loading rates shift the failure frequencies to higher tension values, indicating that the rate at which the tension is applied

directly affects vesicle cohesive strength, and is directly related to the well-known connection between strength and time: the faster a tension ramp, the higher the rupture tension values supported by fluid membranes (Evans et al. 2003, Evans and Smith 2011). Based on Poisson formalism, failure frequencies have been obtained for lipid and proteolipid vesicles as a function of time and rupture tension, and values for the kinetic rate of rupture in non-stressed bilayers due to the creation of one single symmetry break have been estimated: 0.002 s^{-1} in pure POPC and 0.003 s^{-1} in SP-B- and SP-C-containing vesicles. For increasing mechanical tension, rupture frequencies are further enhanced by following the exponential tendency given by the Arrhenius-like factor $exp(\sigma/1.8)$, pointing out again to the impact of mechanical tension on the energy barriers involved in membrane rupture. Nevertheless, there is a relatively large discrepancy between experimental k_{rup} and expected values of failure frequencies due to the creation of one single symmetry break given by k_{SB}, specifically at tensions below the so-called crossover points $\sigma_{\otimes}$. As it was explained in section 6.1.2., the free energy of the system is given by expression (6.4), as it follows from the Deryagin-Gutop cavitational model (Deryagin and Gutop 1962), so it is possible that the existence of a cavitation barrier is therefore affecting the effective kinetic rates of bilayer failure below a given threshold of tension given by $\sigma_{\otimes}$, while for higher tensions the cavitation barrier becomes too low and the system is dominated by the energy barrier involved in symmetry break creation.

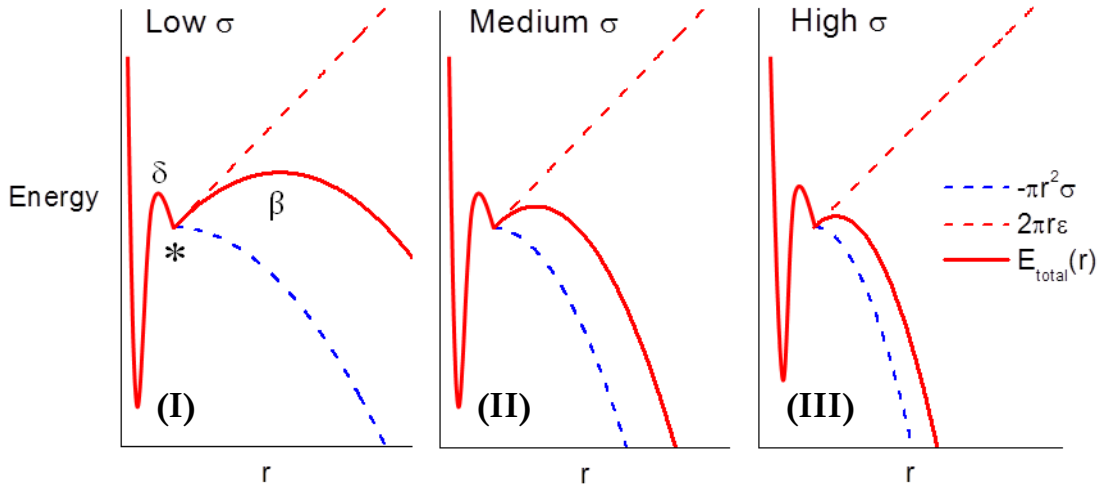

Fig. 6.16: Hypothetical energy landscapes of membrane rupture as a function of hole radius, proposed to explain the experimental results. The cavitational barrier E_β decreases inversely with applied tension, while the precursor barrier E_δ for creation of a symmetry break in the membrane remains constant, yielding that the cavitation barrier E_β sunsets below the precursor barrier E_δ for high tensions (region III). The metastable state E_* creates a weak confinement between both barriers only for intermediate tensions, thus increasing the failure frequency (region II).

Therefore, from the kinetics of membrane failure under increasing mechanical stress of both protein-free and SP-B- or SP-C-containing vesicles, it is possible to hypothesize the existence of three distinct kinetic regions as a function of mechanical tension. These

experimental observations can be connected to energy landscape transformations due to external stress, and the following model is proposed in order to explain them, which is graphically depicted in figure 6.16:

(I) Line tension-dominated regime: At very low tensions, below 2-4 mN/m in general terms, no vesicle ruptures were registered, suggesting extremely low failure frequencies, as expected from a relatively high cavitational barrier (β), dominated by line tension, following the Deryagin-Gutop cavitational model described by equation (6.4). In general, possible sites of hole nucleation do not have enough thermal energy to cross the energy barrier and yield rupture.

(II) Metastable confinement region: At intermediate tensions, approximately between 2-4 mN/m and the crossover values $\sigma_{\otimes}$ ~ 10-15 mN/m (see table 6.2 for experimental values), rupture events start to appear. This crossover point is easily detected at fast aspiration rates, since higher levels of rupture tension are reached, and could depend on protein content at a certain extent. Failure frequencies in this region are higher than for the high-tension regime, which will be later described. This suggests the existence of a different energy state that would facilitate bilayer breakdown for intermediate tensions, which could correspond to the already proposed intermediate state (*), created by metastable confinement between precursor (δ) and cavitation (β) barriers. This metastable state would be hidden except for these intermediate values of tension, when the height of both barriers is comparable and a weak confinement of states is possible at this higher-energy level, which is closer to membrane rupture. From the present results it is possible to speculate about the depth of this hypothetical state, which could be around $1 K_B T$, the energy difference between intermediate- and high-tension regimes estimated from the logarithmic variation of failure frequencies between both regions. The rupture processes occurring in this region are related to the opening of actual holes, as a consequence of the balance between edge energy and external stress that governs hole nucleation, whose critical size for membrane rupture is given by: $r_{\beta} = \varepsilon / \sigma$, as can be easily derived from equation (6.4). Considering typical values of line tension for POPC bilayers (around 10 pN), hole radii could vary between 2.5 nm for a rupture tension of 4 mN/m and 0.7 nm for 15 mN/m.

(III) Defect-limited regime: At high mechanical tensions, larger than crossover values $\sigma_{\otimes}$, the cavitational barrier "sunsets" below the precursor barrier, thus disappearing the metastable confinement between the precursor (δ) and the cavitation barrier (β). Only one energy barrier, E_{δ}, dominates the system at high tensions, confining the possible nucleation sites in the ground state until they are able to overcome the precursor barrier and directly create rupture. In this region, failure frequencies in all tested samples showed the same exponential tendency, a tendency that is predicted by the molecular-scale theory that characterizes an stochastic, thermally activated process of molecular diffusion across an energy barrier (Kramers 1940, Evans and Smith 2011). This region appears to be common for all tested bilayer compositions, being probably the symmetry break creation dominated by the lipids, and from the exponential dependence of kinetic rates on tension, $exp(\sigma/\sigma_{SB})$, the thermal tension scale ($\sigma_{SB} = 1.8$ mN/m) and the defect size a_{SB} (around 2.3 nm^2) were estimated for all tested bilayer compositions. Considering holes with circular

geometry, this area would correspond to a radius of 0.85 nm, which is larger than the cross-sectional radius of a phospholipid molecule, around 0.62 nm^2 for POPC at 20ºC (Nagle et al. 1996) so it must involve the rearrangement of several molecules. Besides, a spontaneous failure frequency caused by defect creation can be estimated from the exponential fit: 0.002 s^{-1} in pure POPC and 0.003 s^{-1} in SP-B- and SP-C-containing vesicles.

The crossover point between kinetic regimes II and III is clearly one of the most important features of the rupture process, since it is determined by the tension value at which the cavitation barrier vanishes. Small values of crossover tension are related to low cavitation barriers and, therefore, it is possible to estimate a scale for the energy landscapes represented in figure 6.16 by finding the ratio between $\sigma_{\otimes}$ and the thermal tension scale for the precursor barrier, σ_{SB}: $E \sim \sigma_{\otimes} / \sigma_{SB}$. Thus, the significant decrease of the crossover tension in the presence of SP-B with respect to protein-free POPC bilayers can be translated into differences in energy scales: it is around 15/1.8 ~ 8.3 K_BT for POPC and 9/1.8 ~ 5 K_BT for SP-B-containing POPC vesicles. In the case that SP-B causes a reduction in the cavitation barrier, it would be most likely due to a reduction in line tension of POPC bilayers.

Besides this possible effect on the cavitation barrier and therefore on the formation of open holes in lipid bilayers, SP-B could have some effects on the stability of the proposed metastable state, since failure frequencies in the kinetic regime II were profoundly affected by its presence: failure frequencies at this region were increased 5 times in the presence of 10^{-6} proteins per lipid molecule with respect to the high-tension regime, while one order of magnitude higher, 10^{-5} in molar ratio, increased them around 18 times, suggesting an exponential dependence on SP-B molar concentration. SP-B is clearly facilitating the process of membrane rupture from this metastable state, but without changing the nucleation of precursor defects. This effect could be due to the already proposed effect on lowering the cavitation barrier, related to a reduction in the edge energy for maintaining a hole open, but there is an alternative explanation that does not involve changes in the energy landscape, but variations on the number of possible nucleation sites, related to the calculation of the ratio N_{SB} between frequencies at intermediate and high tensions that was shown in section 6.2.3. Failure frequencies and total energies would scale with the number of possible sites for symmetry break, which would increase exponentially with SP-B concentration, consistent with the observed effects of SP-B in POPC membranes. At higher tensions, nevertheless, the protein does not seem to affect rupture kinetics, being the creation of pre-pore defects probably dominated only by the lipid. SP-C, on the contrary, was not found to deeply impact on this process, at least at the low concentrations tested here (10^2 and 10^3 times lower than the physiological amount) and the kinetic and thermodynamical analysis produced similar results to pure POPC bilayers, in terms of rupture frequencies and energy barriers.

The results for SP-B could be connected with the well-known ability of this protein to promote membrane binding, destabilization, and ultimately lipid mixing and fusion (Shiffer et al. 1988, Oosterlaken-Dijksterhuis et al. 1992, Poulain et al. 1992, Ryan et al. 2005), both between bilayers or between bilayers and interfacial films. Besides, several

computer simulations have found that SP-B could drive the formation of a lipid bridge between leaflets, prior to hemifusion and total fusion, by reducing the energy barrier for stalk formation (Baoukina and Tieleman 2010), and could attach bilayers to monolayers by the same kind of lipid bridge and mediate lipid transfer between them (Baoukina and Tieleman 2011). This lipid structure probably represents the rate-limiting step in surfactant adsorption to an air-water interface (Serrano and Perez-Gil 2006, Rugonyi et al. 2008). In the light of the present results, these activities could be due to the creation of symmetry breaks in lipid arrangement, decreasing the energy barriers for local geometry transformations in membranes such as stalks or lipid bridges between bilayers or between bilayers and monolayers, but also for other kind of phenomena like leakage and pore formation. Therefore, these subtle abilities of SP-B to decrease energy barriers for membrane transformations and to stabilize the metastable state for defect creation, the precursor of membrane rupture, maybe by increasing the number of possible sites for symmetry break or by reducing the line tension of the pure lipid bilayer, appear to be closely related to the protein activities in the context of pulmonary surfactant function.

7. GENERAL DISCUSSION

Hydrophobic surfactant proteins SP-B and SP-C were first isolated and described in the mid- and late-1970s (Gil and Reiss 1973, King et al. 1973, Phizackerley et al. 1979), and their functional role in enhancing the surface activity of protein-depleted surfactant lipid fractions or synthetic phospholipids, reproducing the surface activity of natural pulmonary surfactant, have been widely investigated from the early 1980s onward (Johansson and Curstedt 1997, Serrano and Perez-Gil 2006).

Diverse functions are currently associated to each of these hydrophobic proteins: on the one hand, SP-B is indispensable for breathing, being its lack incompatible with life (Clark et al. 1995). SP-B is known to be strictly required for lamellar body and tubular myelin assembly and for complete processing of SP-C mature form (Suzuki et al. 1989, Clark et al. 1995, Foster et al. 2003). It also enhances surfactant lipid adsorption to the air-water interface, which then achieves much lower surface tensions than those produced by protein-depleted lipid mixtures (Rodriguez-Capote et al. 2001). SP-B also provides a high stability to surface-active films subjected to dynamic cyclic conditions (Schurch et al. 2010). All these effects are commonly attributed to SP-B membrane-remodeling abilities, such as lytic and fusogenic properties upon interaction with phospholipid membranes *in vitro* (Chang et al. 1998, Ryan et al. 2005). Nevertheless, the reconstitution method has been proven to be crucial to define the mode and extent of interaction of SP-B with membranes: the studies reporting membrane lytic and fusogenic properties of SP-B were performed by injecting the protein into phospholipid vesicle aqueous suspensions, giving rise to a relatively more superficial interaction. In contrast, the mixture of lipids and proteins prior to vesicle reconstitution is thought to create a much deeper interaction between protein and bilayers (Cruz et al. 1997). Fusogenic or lytic properties of SP-B had been never reported in suspensions reconstituted from lipid/protein mixtures, and the present Thesis has shown that SP-B also presents a strong tendency to promote vesicle aggregation and membrane-membrane contacts when it is surrounded by lipids from the very first moment of the reconstitution of lipid/protein bilayers, together with clear pore-forming abilities. The results obtained by electrophysiological measurements of ion conductance and selectivity suggest that SP-B may be creating proteolipid pores in simple phospholipid bilayers such as DOPC or DOPC/DOPG mixtures. This possibility does not come into conflict with the most likely superficial orientation of the protein in membranes (Baatz et al. 1991, Morrow et al. 1993, Cabre et al. 2012), since the creation of the so-called toroidal pores involves lipid rearrangement from perpendicular to parallel orientation with respect to the membrane plane, but not necessarily protein reorientation with respect to the lipid polar heads (Bertelsen et al. 2012).

SP-B pore-forming ability could be supported by its amino acid sequence, which is homologous to that of the saposin-like family, a group of proteins that includes several membrane-permeabilizing polypeptides such as NK-lysin, granulysin or amoebapores (Bruhn 2005). Taking into account this homology, a unified model for the different saposin-like protein actions over membranes has been recently proposed, hypothesizing that the molecular mechanism behind SP-B/membrane interaction could depend on conformational changes, oligomerization and different levels of penetration of the protein into phospholipid membranes (Olmeda et al. 2013). According to this model, the creation

of proteolipid pores, which has been proposed in the present work as a basis for the mechanism of membrane permeabilization by SP-B, could be achieved through protein-promoted bilayer perturbation at the level of phospholipid headgroups or even a deeper penetration, yielding changes in bilayer geometry that could be associated with the hypothetical formation of SP-B oligomers. Regarding the geometrical effects of the protein on lipid structure, a phase transition from a lamellar configuration to a direct hexagonal phase (H_I, a curved geometry in which the hydrophilic face of a phospholipid leaflet is convex, which is arbitrarily considered as a positive curvature) is required to occur locally at the nucleation site in order to form an open pore. The possible existence of different oligomeric states of SP-B beyond dimerization has been reported in several studies, found to be closely related to the animal source, the purification method or the protein-to-lipid ratio in the reconstituted complexes. Trimers of SP-B have been described in sheep and bovine lungs and even larger oligomers have been also described at increasing protein concentrations or upon exposure to certain solvents (Hawgood et al. 1998, Wustneck et al. 2003). The existence of SP-B oligomeric states has been also suggested from different experimental evidences, such as the observation of SP-B two-dimensional aggregates in compressed surfactant monolayers (Cruz et al. 2004), the creation of irreversible clusters of SP-B at the liposome surface after SP-B addition to the aqueous medium, prior to leakage and membrane fusion (Chang et al. 1998), or the requirement for the presence of SP-B in both membrane sides in order to promote multilayer deposits (Cabre et al. 2009). Besides, in the present work, a significant protein clustering has been observed by fluorescence immuno-labeling of phospholipid giant vesicles, which was found to be particularly enhanced at certain membrane locations, such as contact sites between vesicles. The potential oligomerization of SP-B could be required for the creation of highly curved membrane regions and, thus, for inducing toroidal pore formation, since the electrostatic repulsion of SP-B positive charges could create changes on local curvature, in a similar way than that proposed for NK-lysin (Gutsmann et al. 2003). Besides, this effect of SP-B to induce positively-curved regions may be closely related to the results of some recent investigations about the possible directionality of the formation of surface-associated reservoirs with respect to the interface. It seems that compression of surfactant films induces their folding towards the air side, challenging the commonly accepted orientation of these multilayers, considered to fold towards the aqueous phase (Sachan and Galla 2013).

It is noteworthy that those geometrical constraints defining the formation of positively-curved states (toroidal pores, air-oriented multilayers) are in principle opposite to those transformations involved in the interfacial adsorption process, in which negatively curved stalks between bilayer and monolayer must be created in order to facilitate lipid transfer (Possmayer et al. 1984). Some evidences point out to the induction of inverse hexagonal phases (H_{II}) by hydrophobic surfactant proteins in phosphatidylethanolamine leaflets, negatively-curved structures qualitatively similar to the proposed stalk-intermediate for adsorption (Chavarha et al. 2010, Chavarha et al. 2013). Nevertheless, the two types of geometries apparently promoted by SP-B in phospholipid structures seem contradictory; a possible explanation for these diverse effects of SP-B on membranes could lie in the conformational flexibility of the protein, which may present two or more distinct

organizations based on different configurations of the saposin fold, as it has been demonstrated in saposins A, B and C (Olmeda et al. 2013). The saposin fold is the common structural feature of all saposin-like proteins, consisting of the disulphide bonding of the four or five α-helices in two leaves, one containing the N- and C-terminal helices, the other including the central helices. In saposins A and C, it has been shown that these two leaves can adopt two different conformations: an open state, consisting of a V-shape whose concave face houses the hydrophobic residues (Hawkins et al. 2005, Rossmann et al. 2008, Popovic et al. 2012), and a close state, in which the hydrophobic surface of the leaves are buried by adopting a globular configuration (de Alba et al. 2003, Ahn et al. 2006). Saposin B also presents two conformations that differ in the kink of the third α-helix at Tyr54, which are crucial for its functional activity of lipid extraction for enzymatic hydrolysis (Ahn et al. 2003). This tyrosine is highly conserved in the saposin-like family, including SP-B. Thus, a hypothetical conformational flexibility of SP-B could involve this possible kink at Tyr54 together with different packing degrees of the saposin fold, yielding a large diversity of possible combinations between monomers to form dimers or even higher order oligomers. This conformational flexibility can be also closely related to the wide variety of conductance states, from pS to nS, that have been found in the present work when studying the electrophysiological features of planar phospholipid membranes containing low amounts of SP-B. One can speculate about a very dynamic process of binding and unbinding of SP-B dimers, whose monomers could adopt several structural conformations (open or close saposin fold, different kinks at Tyr54…). All these configurations could interact with phospholipids at different extents, and may impose different curvatures to the membrane that could induce locally either a positive or a negative curvature change as a basis of all the different structural effects that have been related to the interaction of SP-B with membranes: leakage by creation of toroidal pores, adsorption and fusion intermediates and lipid transfer, both air- and water-oriented multilayers, et cetera.

As a clue for this speculation, the present work proposes that SP-B could be stabilizing the precursor state for membrane rupture under tension, considered as a symmetry break of the phospholipid organization in the bilayer, and thus reducing the activation energies needed for this transition from a lamellar state (intact bilayer) to a direct hexagonal phase (lipid pore). Here, the transition from lamellar to hexagonal phase is favored by applied tension, but symmetry breaks are fluctuations on phospholipid arrangement that theoretically can either narrow or thicken the bilayer, being the initiators of opposite curvature transformations (see figure 7.1). Therefore, it allows speculating that SP-B could act as a catalyst between states of different geometry, both positively- and negatively-curved regions, consistent to its diversity of structural effects on phospholipid and surfactant membranes. SP-B orientation is represented symmetrically with respect to the bilayer plane in the toroidal pore representation since no charge asymmetry was detected by the electrophysiological assays in planar lipid membranes. Note that these schemes in figure 7.1 are side views of SP-B/phospholipid membranes, and the possible lateral interactions between SP-B monomers in order to form dimers or higher order oligomers are not shown. It is possible to speculate about SP-B-based ring-like structures around the edges of toroidal pores or stabilizing fusion/adsorption intermediate stalks.

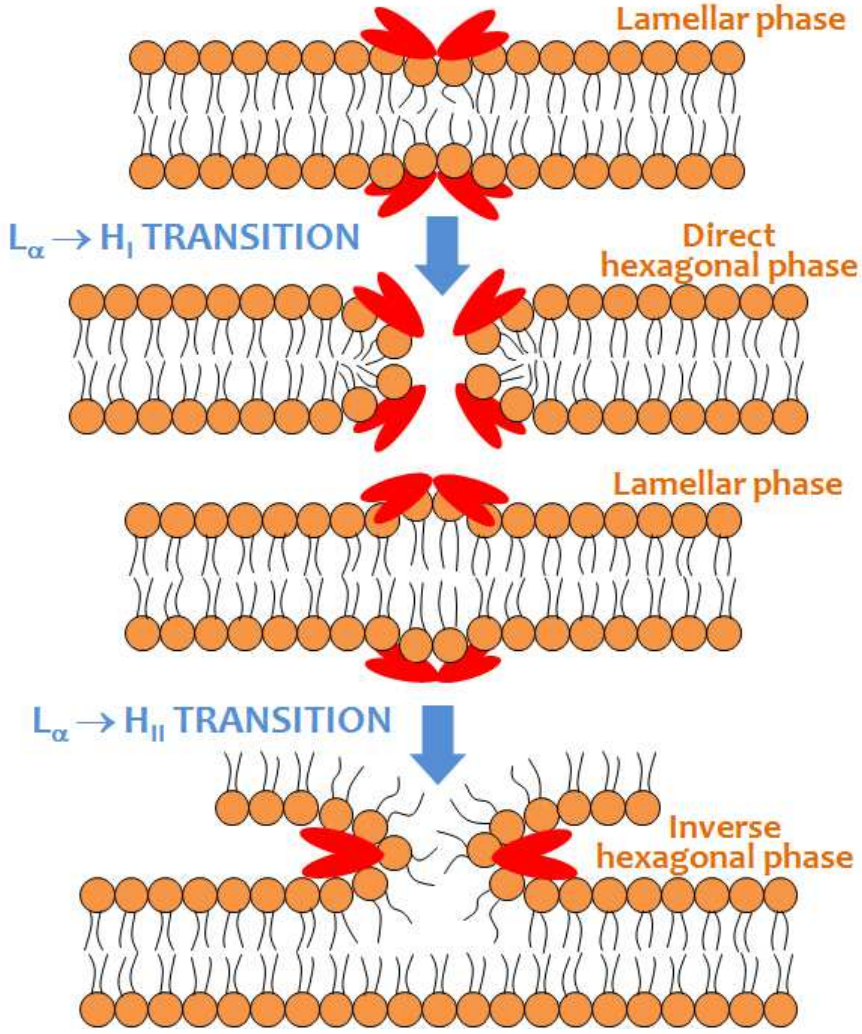

Fig. 7.1: Schematic representation of symmetry breaks in lipid bilayer reorganization and structural transitions from lamellar (L_α) to opposite hexagonal phases: (A) direct hexagonal phase H_I, involved in toroidal pore formation or air-oriented multilayers; and (B) inverse hexagonal phase H_{II}, related to lipid stalks for processes as membrane fusion or interfacial adsorption. Possible orientations of a simplified model of SP-B monomers (red heart-like figures) and dimers are depicted in each of the lipid geometries, based on hypothetical SP-B conformational flexibility.

Nevertheless, this is a rather simplistic model that does not consider other possibilities for SP-B orientation, which could have charge symmetry but no structural symmetry, or different degrees of oligomerization and protein-protein interactions such as lateral contacts between proteins within the same bilayer (intra-membrane interactions) or frontal contacts between opposing membranes (inter-membrane interactions). Further investigation on the molecular features of SP-B-phospholipid and SP-B/SP-B interactions is needed in order to improve the model and refine the specific mechanisms of action of this protein in lipid membranes.

Regarding the other hydrophobic surfactant protein, SP-C, its absence is associated to chronic respiratory diseases, although SP-C-deficient animals are able to breath and survive after birth (Glasser et al. 2001, Glasser et al. 2003, Lawson et al. 2005). It has been demonstrated that SP-C facilitates interfacial adsorption of lipids (Ross et al. 2002) and could be essential to maintain the association of multilayer lipid reservoirs with the interface at the end of exhalation, when compression reaches the highest levels (Baumgart et al. 2010). Its N-terminal segment appears to possess a highly dynamic character and has been shown to interact with membranes even in the absence of palmitoylation, perturbing phospholipid packing in both bilayers and monolayers (Plasencia et al. 2004, Plasencia et al. 2005), which is consistent with the observed instability of SP-C-containing POPC giant vesicles under the microscope, including large shape fluctuations that yielded to membrane budding and even to vesicle fission. This could be closely related to SP-C ability to promote lipid adsorption from bilayers into the interfacial film.

In the present Thesis, a new SP-C effect on phospholipid membranes that was unknown to date has been proposed: its ability to create pores in bilayers, as it has been demonstrated by electrophysiology measurements on ion selectivity of DOPC and DOPC/DOPG planar membranes containing small amounts of the protein. SP-C-promoted pores could also support the permeabilization of giant vesicles towards soluble molecules such as FM1-43, calcein and relatively large dextrans. According to their effects on GUV permeability, SP-C appears to create larger defects on membranes than SP-B. As a matter of fact, both proteins seem to create larger pores individually than those formed by their native mixture, as confirmed both by fluorescence microscopy of GUV permeability and by ion conductance measurements in planar lipid membranes. Although specific SP-B/SP-C interactions have been discarded in the past (Wang et al. 1996, Plasencia et al. 2001), recent studies have proposed that a mutual interaction might exist, which could modulate the surface activity of both hydrophobic proteins (Almlen et al. 2008, Jimenez Cabre 2009, Schurch et al. 2010). The results shown in the present work also support a combined action of the two proteins: *i*) structural effects on membranes as observed by electron microscopy and fluorescence microscopy; *ii*) distribution of pore sizes in dextran-permeability assays; and *iii*) ion conductances and pore lifetimes in planar lipid membranes, all showed subtle or significant differences when comparing the individual action of each of the proteins with their combined action, which cannot be considered as a mere addition of their individual effects.

Thus, the extent of membrane perturbation induced by SP-C may be greater than expected, being able both to facilitate lipid transfer between membranes and to form aqueous pores in membranes. The structure of SP-C as a single transmembrane helical segment could induce to think that transmembrane pores could be created by oligomerization of a few helices. However, it is difficult to envision how such a hydrophobic amino acid sequence could create pores coated by a polar surface. Alternatively, pore-forming abilities of SP-C are consistent with a mechanism of pore formation based on the nucleation of toroidal pores, in which both the polar residues of the N-terminal protein segment and the phospholipid polar heads could participate in creating the pore walls. The N-terminal segment could then have a major role in this

process due to its membrane-perturbing abilities. On the other hand, the high variety of conductance states registered by the electrophysiological measurements in planar lipid membranes containing SP-C is very similar to those found for SP-B, in spite of the fact that the conformational plasticity of SP-C would be in principle low: it mainly consists of a rigid transmembrane helix and, although its N-terminal is unstructured and seems highly dynamic, the double palmitoylation appears to anchor and fix it to the membrane (Bi et al. 2002, Plasencia et al. 2008). Another possible explanation for SP-C pore-forming abilities and its wide range of pore sizes could be the existence of a variety of protein oligomers, which may create large and profound perturbations inside the bilayer core, yielding membrane permeabilization. Several experimental evidences for this hypothetical SP-C oligomerization have been reported, besides a non-specific, complex oligomerization related to an α-helix to β-amyloid-like structural transition, probably involved in pulmonary alveolar proteinosis (Szyperski et al. 1998). The existence of a possible dimeric form has been proposed by some experimental evidences (Baatz et al. 1992, Luy et al. 2004), which may be created by hydrogen bonding between the C-terminal carboxyl groups or by the 7-residue C-terminal segment, strictly conserved, since it shows an Ala-X-X-X-Gly motif very similar to the dimerization region of glycophorin A (Kairys et al. 2004). The resulting V-shape dimers could impose some curvature to the phospholipid membrane (Epand and Epand 2000), which could promote the creation of evaginations, tethers and membrane budding, processes that have been observed in the present work to be enhanced in the presence of SP-C. Furthermore, higher order oligomers have been proposed by molecular dynamics simulations, describing protein-protein interactions that could yield even heptameric aggregates (Ramirez et al. 2006).

The accumulation of SP-C observed in the present work by fluorescence microscopy on the surface of immuno-labeled SP-C-containing giant vesicles may point out to the existence of protein clusters at the tested, close to physiological, concentrations. This effect could be strongly concentration-dependent, according to the results also shown in the present work regarding the degree of membrane accessibility of the fluorescent dye FM1-43 as studied by fluorescence spectroscopy: both SP-B and SP-C promoted the entrance of the probe to the inner membranes of POPC multilamellar vesicles, although showing different kinetics and concentration dependence. SP-B promoted a faster and more efficient incorporation of the dye to phospholipid membranes, achieving the maximum accessibility even for the lowest concentration tested; on the other hand, SP-C facilitated FM1-43 entrance in a more progressive fashion and the maximum membrane accessibility corresponded to its physiological ratio, while subphysiological concentrations only promoted a partial incorporation of the probe. This observed concentration dependence of SP-C perturbation in phospholipid membranes may be the reason why no clear evidences have been found for a possible change on bilayer elasticity and stability under tension of POPC giant vesicles containing subphysiological concentrations of SP-C. However, similar low SP-C concentrations were tested in DOPC/DOPG planar lipid membranes and were demonstrated to originate ion-conducting pores with a defined selectivity for anions and a wide range of conductance values, which can be naïvely considered as a large diversity of pore sizes. Maybe the presence of 15% of anionic phospholipids in the bilayer could promote clustering of the positively-charged SP-C and thus enhance membrane

perturbation and facilitate pore formation. Besides, the voltage sensitivity of these SP-C pores cannot be discarded, and the effects of an electrical potential difference on these proteolipid bilayers could be very different to those created by an external stress such as a tangential field of mechanical tension like those created in the micropipette aspiration tests. Based on the dimeric form proposed by Kairys et al. (Kairys et al. 2004), which would show a V-shape that could induce a certain spontaneous curvature to the membrane, a very simple model for the interaction of SP-C with bilayers and its orientation in both planar and direct hexagonal geometries, i.e., bilayers and toroidal pores, is presented in figure 7.2. First, the aggregation or clustering of SP-C monomers, which would be concentration-dependent and could be also promoted by the presence of anionic phospholipids, could yield to dimerization or even oligomerization of the protein. Then, dimer V-shape might induce the formation of positively-curved regions such as toroidal pore edges, specially upon application of an electric potential difference, when SP-C may be forced to adopt a different orientation and even to undergo a translocation by the electric field acting on its positive charges.

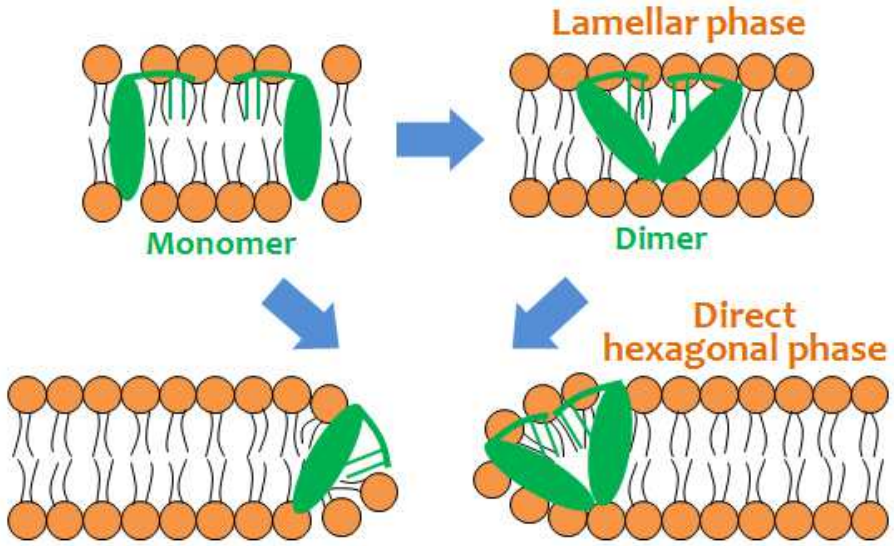

Fig. 7.2: Simplified model of SP-C monomers and their possible dimerization, representing their possible orientations within lamellar and H_I phases, such as toroidal pore edges. The model for SP-C dimer is based on (Weaver and Conkright 2001).

As it was mentioned before, a possible mutual interaction between SP-B and SP-C cannot be discarded, so these simple models for SP-B and SP-C interaction with bilayers in order to promote different geometry transformations could correspond only to their isolated action on membranes. It is even more difficult to model and represent their combined presence in phospholipid membranes since it could involve in principle multiple combinations of monomers, homo- and heterodimers to form higher order oligomers, due to the lack of specific information about possible sites and modes of interaction between SP-B and SP-C molecules.

Interestingly, a correlation between micromechanical studies of protein-containing giant vesicles by pipette pressurization and the electrophysiological measurements of proteins reconstituted in planar lipid membranes can be noticed: pore formation processes were analyzed in the present work under two different external stresses, i.e. mechanical tension and electric potential difference, respectively. The effects of membrane proteins SP-B and SP-C on phospholipid bilayers were then evaluated in each case. It has been shown that very low amounts of hydrophobic proteins SP-B and SP-C, together or individually, were able to create pores in phospholipid bilayers under applied voltage, and it has been also proposed that SP-B could have a profound impact on the thermally-activated, kinetic process of hole nucleation under tension. The existence of a precursor state previous to rupture in stretched phospholipid bilayers has been suggested here, seen as a symmetry break in the molecular organization, necessary for the opening and expansion of lipid-lined aqueous pores, and the presence of SP-B in these bilayers seems to stabilize symmetry breaks or to create more nucleation sites. This could be directly connected to the frequent appearance of instantaneous spikes on most of the conductance traces recorded for SP-B and/or SP-C reconstituted in DOPC or DOPC/DOPG bilayers, indicative of fast transitions between different conductance levels that have been previously interpreted as sudden opening and closing of metastable pores in pure lipid membranes subjected to relatively high voltages (150 mV and beyond) (Melikov et al. 2001). Besides, the recording of bursts of electrical activity in the presence of SP-B and/or SP-C could be an additional evidence for the existence of a non-conductive pre-pore state, since the occurrence of these short-lived states is far to be considered as random: these multiple spikes inside a single burst could correspond to transitions between two different states, a conductive pore and a non-conductive precursor that would have a higher probability of forming open pores than the non-excited membrane (Melikov et al. 2001). It is noticeable that these common patterns in the conductance traces were previously found in pure phospholipid bilayers subjected to very high voltages, needed to induce these excitations, while, in the light of the present results, the presence of SP-B and/or SP-C clearly enhanced the electrical activity of lipid bilayers even under relatively low voltages, between 5 and 100 mV.

In order to unify the experimental results obtained by micropipette aspiration of giant vesicles and electrophysiology experiments on planar lipid membranes, the following model of SP-B/SP-C interaction with phospholipid membranes is proposed: upon application of an electric potential difference, similarly to the application of mechanical tension, the bilayer organization is locally and transiently disrupted by the creation of a certain pre-pore state, which would be facilitated and/or stabilized by SP-B, and may undergo a transition to an open state facilitated by the presence of SP-B and/or SP-C, which can be either sealed again or yield membrane rupture. It is noteworthy that progressive opening events in planar bilayers containing SP-B frequently ended up in membrane rupture, especially when they were subjected to relatively high voltages (75-100 mV), while in the presence of SP-C the conductance levels were more stable in time and openings were always followed by pore closing, pointing out to a more profound effect of SP-B in membrane rupture that is fully consistent to the vesicle rupture analysis performed by micropipette aspiration.

An important question refers to the physiological meaning of the intrinsically permeable character of surfactant membranes. It is possible that the permeability to ions and polar solutes imparted to membranes by surfactant proteins could be merely a consequence of the molecular architecture of the machinery that ensures a rapid and efficient flow of surface active lipid species along the membranous assemblies, from the surfactant-producing cells to the interface. However, it is also possible that an efficient and unrestricted movement of polar molecules through the membrane network developed by surfactant at the thin water layer lining the alveoli is also important for alveolar homeostasis. It has been recently proposed that surfactant membranes might form a bi-continuous phase at the respiratory surface, evolutionarily optimized to allow the diffusion of both hydrophobic surface active species and soluble molecules through the alveolar hypophase (Perez-Gil 2008). A fully interconnected network of membranes could be important to facilitate a rapid diffusion of lipids towards the interface, where they must form the surface active film that reduces surface tension and stabilizes the lung. Besides, the continuity of all the aqueous compartments could be equally important to ensure proper equilibrium of water and ions and to facilitate free diffusion of soluble components like collectins, defensins and other molecules, involved in innate defense and sterility of the alveolar surface (Perez-Gil and Weaver 2010). Furthermore, recent studies have suggested a potential role of both SP-B and SP-C in innate host defense and pathogen removal (Blanco and Perez-Gil 2007, Garcia-Verdugo et al. 2009), which could be closely related to their membrane-permeabilizing effects. Surface active proteins and peptides, such as those currently under scrutiny as potential additive in artificial surfactants (Mingarro et al. 2008), could be active enough to ensure interfacial transfer of lipids and formation of surfactant films but still be inefficient to form a fully functional bi-continuous membrane network, and could also lack potential host defense abilities. The elucidation of the molecular architecture and the specific actions of surfactant protein complexes is therefore crucial for improving the possibilities to develop new enhanced surfactant-based therapies.

8. CONCLUSIONS

The work presented in this doctoral Thesis reveals further details on the investigation of pulmonary surfactant proteins SP-B and SP-C and contributes to the study of their physical effects on lipid membranes, providing new evidences that could help to unravel the possible mechanisms of action of both proteins in their physiological context.

1. The presence of hydrophobic proteins SP-B and SP-C in native surfactant complexes and membranes reconstituted from its native lipid species facilitated the entrance of polar membrane-impermeable dyes such as FM1-43 into membrane complexes, apparently with different kinetics and concentration dependences: SP-B was extremely efficient in facilitating FM1-43 permeability, even for subphysiological protein densities (0.1-0.5% w/w), while SP-C showed a more gradual effect both in time and concentration dependence.

2. Subtle differences were observed between native surfactant complexes and membranes reconstituted from its organic extract or its whole lipid fraction in terms of fluidity/lipid mobility, as analyzed by ESR: the regions sensed by the spin probe 14-PCSL, close to the middle plane of the bilayer, showed slightly lower mobilities in NS than in OE or LF membranes for the whole temperature range, from 22 to 60ºC, likely due to the native structure and complexity. Besides, an effect of hydrophobic proteins SP-B and SP-C on lipid mobility was detected, since their presence increased lipid packing but only at temperatures lower than 37ºC, the melting point of surfactant lipids. No evidences for clear thermotropic transitions were found in either of the materials.

3. The degree of complexity of different surfactant membrane assemblies differed, as visualized by transmission electron microscopy, with the most complex structures being those observed in NS, followed by membranes reconstituted from its OE and LF, in this order. These differences in complexity and multilamerallity among materials can be related to the differences in fluidity/lipid mobility, but did not correlate to different degrees of membrane accessibility, since the most complex were highly permeable to the amphipathic dye FM1-43 due to the presence of SP-B and SP-C. Furthermore, SP-B showed a dramatic effect on membrane ultrastructure, creating large inter-bilayer contacts on POPC vesicles that had been subjected to extrusion, apparently reproducing the native complexity of surfactant.

4. POPC giant vesicles containing either SP-B or SP-C or their physiological mixture were highly permeable to FM1-43 and to the water-soluble dye calcein, suggesting the presence of aqueous pores in phospholipid membranes created by physiological amounts of SP-B and SP-C, whose sizes appeared to be heterogeneous. A threshold in molecular permeability was found for membranes containing the whole hydrophobic protein fraction or isolated SP-B: only dextrans with hydrodynamic radii shorter than 1.5 and 4 nm, respectively, were able to permeate. In contrast, SP-C induced membrane permeability towards all tested dextrans, in a higher or lower proportion depending on their molecular size.

5. The localization of hydrophobic proteins SP-B and SP-C on model POPC membranes was achieved by immunofluorescence of giant lipid-protein vesicles, which allowed the detection of intensely fluorescent spots spread across the vesicle surface,

especially at regions such as intermembrane contacts, vesicle protuberances or tethers, which could suggest a certain degree of protein clustering associated with membrane activity.

6. Electrophysiology measurements on planar lipid membranes demonstrated that SP-B and SP-C, either together or separately, are able to induce membrane poration even at very low, subphysiological concentrations, upon application of an electric potential difference. Pores created in DOPC or DOPC/DOPG bilayers by the whole hydrophobic protein fraction of surfactant or by isolated SP-B or SP-C showed a wide variety of conductance states, from pS to nS, being difficult to identify characteristic single-channel conductances, although the most frequent conductance values were significantly higher for isolated SP-B and SP-C than for their physiological mixture. Besides, pore conductances presented some voltage sensitivity, especially those created in the presence of SP-C.

7. Studies on planar lipid bilayers containing the physiological mixture of SP-B/SP-C in the presence of different KCl concentration gradients and no applied voltage demonstrated that lipid composition strongly influenced the pore selectivity for anions or cations. A total inversion of the selectivity was found between neutral zwitterionic and negatively charged membranes, which is consistent with the formation of toroidal or proteolipid pores, with the hydrophilic parts of both the proteins and the phospholipids coating the pore walls.

8. Micromechanical studies on SP-B- or SP-C-containing bilayers by micropipette aspiration of giant unilamellar vesicles showed that subphysiological amounts of either SP-B or SP-C have very little effect on POPC bilayer elasticity, although a slight rigidification was observed. Kinetic and thermodynamical analysis of the process of vesicle rupture under increasing mechanical stress highlighted the possible existence of a precursor state for bilayer breakdown that has been proposed to be a symmetry break of the molecular organization prior to the creation of a hydrophilic pore in pure POPC bilayers. Besides, SP-B was demonstrated to impact dramatically on the failure frequencies of aspirated POPC vesicles by enhancing the creation of these pre-pore states or by reducing the line tension at pore edges, while SP-C showed no significant effects in this process.

9. REFERENCES

Aguilella, V. M. and S. M. Bezrukov (2001). "Alamethicin channel conductance modified by lipid charge." Eur Biophys J **30**(4): 233-241.

Aguilella, V. M., M. Queralt-Martin, M. Aguilella-Arzo and A. Alcaraz (2011). "Insights on the permeability of wide protein channels: measurement and interpretation of ion selectivity." Integr Biol (Camb) **3**(3): 159-172.

Ahn, V. E., K. F. Faull, J. P. Whitelegge, A. L. Fluharty and G. G. Prive (2003). "Crystal structure of saposin B reveals a dimeric shell for lipid binding." Proc Natl Acad Sci U S A **100**(1): 38-43.

Ahn, V. E., P. Leyko, J. R. Alattia, L. Chen and G. G. Prive (2006). "Crystal structures of saposins A and C." Protein Sci **15**(8): 1849-1857.

Akiyama, J., A. Hoffman, C. Brown, L. Allen, J. Edmondson, F. Poulain and S. Hawgood (2002). "Tissue distribution of surfactant proteins A and D in the mouse." J Histochem Cytochem **50**(7): 993-996.

Alcaraz, A., E. M. Nestorovich, M. L. Lopez, E. Garcia-Gimenez, S. M. Bezrukov and V. M. Aguilella (2009). "Diffusion, exclusion, and specific binding in a large channel: a study of OmpF selectivity inversion." Biophys J **96**(1): 56-66.

Almlen, A., G. Stichtenoth, B. Linderholm, M. Haegerstrand-Bjorkman, B. Robertson, J. Johansson and T. Curstedt (2008). "Surfactant proteins B and C are both necessary for alveolar stability at end expiration in premature rabbits with respiratory distress syndrome." J Appl Physiol **104**(4): 1101-1108.

Andersson, M., T. Curstedt, H. Jornvall and J. Johansson (1995). "An amphipathic helical motif common to tumourolytic polypeptide NK-lysin and pulmonary surfactant polypeptide SP-B." FEBS Lett **362**(3): 328-332.

Angelova, M. I. and D. S. Dimitrov (1986). "Liposome electroformation." Faraday Discussions of the Chemical Society **81**(0): 303-311.

Anzueto, A., A. Jubran, J. A. Ohar, C. A. Piquette, S. I. Rennard, G. Colice, E. N. Pattishall, J. Barrett, M. Engle, K. A. Perret and B. K. Rubin (1997). "Effects of aerosolized surfactant in patients with stable chronic bronchitis: a prospective randomized controlled trial." JAMA **278**(17): 1426-1431.

Ariki, S., C. Nishitani and Y. Kuroki (2012). "Diverse functions of pulmonary collectins in host defense of the lung." J Biomed Biotechnol **2012**: 532071.

Baatz, J. E., B. Elledge and J. A. Whitsett (1990). "Surfactant protein SP-B induces ordering at the surface of model membrane bilayers." Biochemistry **29**(28): 6714-6720.

Baatz, J. E., V. Sarin, D. R. Absolom, C. Baxter and J. A. Whitsett (1991). "Effects of surfactant-associated protein SP-B synthetic analogs on the structure and surface activity of model membrane bilayers." Chem Phys Lipids **60**(2): 163-178.

Baatz, J. E., K. L. Smyth, J. A. Whitsett, C. Baxter and D. R. Absolom (1992). "Structure and functions of a dimeric form of surfactant protein SP-C: a Fourier transform infrared and surfactometry study." Chem Phys Lipids **63**(1-2): 91-104.

Bachofen, H., U. Gerber, P. Gehr, M. Amrein and S. Schurch (2005). "Structures of pulmonary surfactant films adsorbed to an air-liquid interface in vitro." Biochim Biophys Acta **1720**(1-2): 59-72.

Bagatolli, L. A. (2006). "To see or not to see: lateral organization of biological membranes and fluorescence microscopy." Biochim Biophys Acta **1758**(10): 1541-1556.

Bagatolli, L. A., J. H. Ipsen, A. C. Simonsen and O. G. Mouritsen (2010). "An outlook on organization of lipids in membranes: searching for a realistic connection with the organization of biological membranes." Prog Lipid Res **49**(4): 378-389.

Ban, N., Y. Matsumura, H. Sakai, Y. Takanezawa, M. Sasaki, H. Arai and N. Inagaki (2007). "ABCA3 as a lipid transporter in pulmonary surfactant biogenesis." J Biol Chem **282**(13): 9628-9634.

Baoukina, S. and D. P. Tieleman (2010). "Direct simulation of protein-mediated vesicle fusion: lung surfactant protein B." Biophys J **99**(7): 2134-2142.

Baoukina, S. and D. P. Tieleman (2011). "Lung surfactant protein SP-B promotes formation of bilayer reservoirs from monolayer and lipid transfer between the interface and subphase." Biophys J **100**(7): 1678-1687.

Baumgart, F., O. L. Ospina, I. Mingarro, I. Rodriguez-Crespo and J. Perez-Gil (2010). "Palmitoylation of pulmonary surfactant protein SP-C is critical for its functional cooperation with SP-B to sustain compression/expansion dynamics in cholesterol-containing surfactant films." Biophys J **99**(10): 3234-3243.

Beers, M. F. (1996). "Inhibition of cellular processing of surfactant protein C by drugs affecting intracellular pH gradients." J Biol Chem **271**(24): 14361-14370.

Bernardino de la Serna, J., G. Oradd, L. A. Bagatolli, A. C. Simonsen, D. Marsh, G. Lindblom and J. Perez-Gil (2009). "Segregated phases in pulmonary surfactant membranes do not show coexistence of lipid populations with differentiated dynamic properties." Biophys J **97**(5): 1381-1389.

Bernardino de la Serna, J., J. Perez-Gil, A. C. Simonsen and L. A. Bagatolli (2004). "Cholesterol rules: direct observation of the coexistence of two fluid phases in native pulmonary surfactant membranes at physiological temperatures." J Biol Chem **279**(39): 40715-40722.

Bernardino de la Serna, J., R. Vargas, V. Picardi, A. Cruz, R. Arranz, J. M. Valpuesta, L. Mateu and J. Perez-Gil (2013). "Segregated ordered lipid phases and protein-promoted membrane cohesivity are required for pulmonary surfactant films to stabilize and protect the respiratory surface." Faraday Discussions **161**(0): 535-548.

Bertelsen, K., J. Dorosz, S. K. Hansen, N. C. Nielsen and T. Vosegaard (2012). "Mechanisms of peptide-induced pore formation in lipid bilayers investigated by oriented 31P solid-state NMR spectroscopy." PLoS One **7**(10): e47745.

Betz, W. J., F. Mao and C. B. Smith (1996). "Imaging exocytosis and endocytosis." Curr Opin Neurobiol **6**(3): 365-371.

Bezrukov, S. M. and I. Vodyanoy (1993). "Probing alamethicin channels with water-soluble polymers. Effect on conductance of channel states." Biophys J **64**(1): 16-25.

Bi, X., C. R. Flach, J. Perez-Gil, I. Plasencia, D. Andreu, E. Oliveira and R. Mendelsohn (2002). "Secondary structure and lipid interactions of the N-terminal segment of pulmonary surfactant SP-C in Langmuir films: IR reflection-absorption spectroscopy and surface pressure studies." Biochemistry **41**(26): 8385-8395.

Blanco, O. and J. Perez-Gil (2007). "Biochemical and pharmacological differences between preparations of exogenous natural surfactant used to treat Respiratory Distress Syndrome: role of the different components in an efficient pulmonary surfactant." Eur J Pharmacol **568**(1-3): 1-15.

Bligh, E. G. and W. J. Dyer (1959). "A rapid method of total lipid extraction and purification." Can J Biochem Physiol **37**(8): 911-917.

Bockris, J. O. M. and A. K. N. Reddy (1970). Ionics. Modern electrochemistry. New York, Plenum Press. **2**.

Bradford, M. M. (1976). "A rapid and sensitive method for the quantitation of microgram quantities of protein utilizing the principle of protein-dye binding." Anal Biochem **72**: 248-254.

Bruhn, H. (2005). "A short guided tour through functional and structural features of saposin-like proteins." Biochem J **389**(Pt 2): 249-257.

Cabre, E. J., L. M. Loura, A. Fedorov, J. Perez-Gil and M. Prieto (2012). "Topology and lipid selectivity of pulmonary surfactant protein SP-B in membranes: Answers from fluorescence." Biochim Biophys Acta **1818**(7): 1717-1725.

Cabre, E. J., J. Malmstrom, D. Sutherland, J. Perez-Gil and D. E. Otzen (2009). "Surfactant protein SP-B strongly modifies surface collapse of phospholipid vesicles: insights from a quartz crystal microbalance with dissipation." Biophys J **97**(3): 768-776.

Cantor, R. S. (1997). "The lateral pressure profile in membranes: a physical mechanism of general anesthesia." Biochemistry **36**(9): 2339-2344.

Casals, C. (2001). "Role of surfactant protein A (SP-A)/lipid interactions for SP-A functions in the lung." Pediatr Pathol Mol Med **20**(4): 249-268.

Casals, C., L. Herrera, E. Miguel, P. Garcia-Barreno and A. M. Municio (1989). "Comparison between intra- and extracellular surfactant in respiratory distress induced by oleic acid." Biochim Biophys Acta **1003**(2): 201-203.

Casals, C., E. Miguel and J. Perez-Gil (1993). "Tryptophan fluorescence study on the interaction of pulmonary surfactant protein A with phospholipid vesicles." Biochem J **296 (Pt 3)**: 585-593.

Clark, J. C., S. E. Wert, C. J. Bachurski, M. T. Stahlman, B. R. Stripp, T. E. Weaver and J. A. Whitsett (1995). "Targeted disruption of the surfactant protein B gene disrupts surfactant homeostasis, causing respiratory failure in newborn mice." Proc Natl Acad Sci U S A **92**(17): 7794-7798.

Clements, J. A. (1977). "Functions of the alveolar lining." Am Rev Respir Dis **115**(6 Pt 2): 67-71.

Creuwels, L. A., E. H. Boer, R. A. Demel, L. M. van Golde and H. P. Haagsman (1995). "Neutralization of the positive charges of surfactant protein C. Effects on structure and function." J Biol Chem **270**(27): 16225-16229.

Croarkin, C. and P. E. Tobias (2012). P. NIST/SEMATECH e-Handbook of Statistical Methods. C. Croarkin and P. Tobias.

Cruz, A., C. Casals, K. M. Keough and J. Perez-Gil (1997). "Different modes of interaction of pulmonary surfactant protein SP-B in phosphatidylcholine bilayers." Biochem J **327 (Pt 1)**: 133-138.

Cruz, A., C. Casals, I. Plasencia, D. Marsh and J. Perez-Gil (1998). "Depth profiles of pulmonary surfactant protein B in phosphatidylcholine bilayers, studied by fluorescence and electron spin resonance spectroscopy." Biochemistry **37**(26): 9488-9496.

Cruz, A., L. Vazquez, M. Velez and J. Perez-Gil (2004). "Effect of pulmonary surfactant protein SP-B on the micro- and nanostructure of phospholipid films." Biophys J **86**(1 Pt 1): 308-320.

Cruz, A., L. A. Worthman, A. G. Serrano, C. Casals, K. M. Keough and J. Perez-Gil (2000). "Microstructure and dynamic surface properties of surfactant protein SP-B/dipalmitoylphosphatidylcholine interfacial films spread from lipid-protein bilayers." Eur Biophys J **29**(3): 204-213.

Curstedt, T., H. Jornvall, B. Robertson, T. Bergman and P. Berggren (1987). "Two hydrophobic low-molecular-mass protein fractions of pulmonary surfactant. Characterization and biophysical activity." Eur J Biochem **168**(2): 255-262.

Chang, R., S. Nir and F. R. Poulain (1998). "Analysis of binding and membrane destabilization of phospholipid membranes by surfactant apoprotein B." Biochim Biophys Acta **1371**(2): 254-264.

Chavarha, M., H. Khoojinian, L. E. Schulwitz, Jr., S. C. Biswas, S. B. Rananavare and S. B. Hall (2010). "Hydrophobic surfactant proteins induce a phosphatidylethanolamine to form cubic phases." Biophys J **98**(8): 1549-1557.

Chavarha, M., R. W. Loney, S. B. Rananavare and S. B. Hall (2013). "An anionic phospholipid enables the hydrophobic surfactant proteins to alter spontaneous curvature." Biophys J **104**(3): 594-603.

Cheong, N., H. Zhang, M. Madesh, M. Zhao, K. Yu, C. Dodia, A. B. Fisher, R. C. Savani and H. Shuman (2007). "ABCA3 is critical for lamellar body biogenesis in vivo." J Biol Chem **282**(33): 23811-23817.

Daniels, C. B. and S. Orgeig (2001). "The comparative biology of pulmonary surfactant: past, present and future." Comp Biochem Physiol A Mol Integr Physiol **129**(1): 9-36.

Daniels, C. B. and S. Orgeig (2003). "Pulmonary surfactant: the key to the evolution of air breathing." News Physiol Sci **18**: 151-157.

de Alba, E., S. Weiler and N. Tjandra (2003). "Solution structure of human saposin C: pH-dependent interaction with phospholipid vesicles." Biochemistry **42**(50): 14729-14740.

Deryagin, B. V. and Y. V. Gutop (1962). "Theory of the breakdown (rupture) of free films." Kolloidn. Zh. **24**: 370-374.

Discher, B. M., K. M. Maloney, W. R. Schief, Jr., D. W. Grainger, V. Vogel and S. B. Hall (1996). "Lateral phase separation in interfacial films of pulmonary surfactant." Biophys J **71**(5): 2583-2590.

Dluhy, R. A., S. Shanmukh, J. B. Leapard, P. Kruger and J. E. Baatz (2003). "Deacylated pulmonary surfactant protein SP-C transforms from alpha-helical to amyloid fibril structure via a pH-dependent mechanism: an infrared structural investigation." Biophys J **85**(4): 2417-2429.

Durrett, R. (2010). Probability : theory and examples. Cambridge ; New York, Cambridge University Press.

Dushianthan, A., M. P. Grocott, A. D. Postle and R. Cusack (2011). "Acute respiratory distress syndrome and acute lung injury." Postgrad Med J **87**(1031): 612-622.

Dutton, J. M., K. Goss, K. R. Khubchandani, C. D. Shah, R. J. Smith and J. M. Snyder (1999). "Surfactant protein A in rabbit sinus and middle ear mucosa." Ann Otol Rhinol Laryngol **108**(10): 915-924.

Epand, R. M. (1998). "Lipid polymorphism and protein-lipid interactions." Biochim Biophys Acta **1376**(3): 353-368.

Epand, R. M. and R. F. Epand (2000). "Modulation of membrane curvature by peptides." Biopolymers **55**(5): 358-363.

Evans, E., V. Heinrich, F. Ludwig and W. Rawicz (2003). "Dynamic tension spectroscopy and strength of biomembranes." Biophys J **85**(4): 2342-2350.

Evans, E. and D. Needham (1987). "Physical properties of surfactant bilayer membranes: thermal transitions, elasticity, rigidity, cohesion and colloidal interactions." The Journal of Physical Chemistry **91**(16): 4219-4228.

Evans, E. and W. Rawicz (1990). "Entropy-driven tension and bending elasticity in condensed-fluid membranes." Phys Rev Lett **64**(17): 2094-2097.

Evans, E. and R. Skalak (1980). Mechanics and thermodynamics of biomembranes. Boca Raton, Fla., CRC Press.

Evans, E. and B. A. Smith (2011). "Kinetics of Hole Nucleation in Biomembrane Rupture." New J Phys **13**.

Fidorra, M., T. Heimburg and L. A. Bagatolli (2009). "Direct visualization of the lateral structure of porcine brain cerebrosides/POPC mixtures in presence and absence of cholesterol." Biophys J **97**(1): 142-154.

Flory, P. J. and M. Volkenstein (1969). "Statistical mechanics of chain molecules." Biopolymers **8**(5): 699-700.

Foster, C. D., P. X. Zhang, L. W. Gonzales and S. H. Guttentag (2003). "In vitro surfactant protein B deficiency inhibits lamellar body formation." Am J Respir Cell Mol Biol **29**(2): 259-266.

Fullagar, W. K., K. A. Aberdeen, D. G. Bucknall, P. A. Kroon and I. R. Gentle (2003). "Conformational changes in SP-B as a function of surface pressure." Biophys J **85**(4): 2624-2632.

Garcia-Verdugo, I., E. Garcia de Paco, Q. Espinassous, A. Gonzalez-Horta, M. Synguelakis, J. Kanellopoulos, L. Rivas, R. Chaby and J. Perez-Gil (2009). "Synthetic peptides representing the N-terminal segment of surfactant protein C modulate LPS-stimulated TNF-alpha production by macrophages." Innate Immun **15**(1): 53-62.

Gil, J. and O. K. Reiss (1973). "Isolation and characterization of lamellar bodies and tubular myelin from rat lung homogenates." J Cell Biol **58**(1): 152-171.

Glasser, S. W., M. S. Burhans, T. R. Korfhagen, C. L. Na, P. D. Sly, G. F. Ross, M. Ikegami and J. A. Whitsett (2001). "Altered stability of pulmonary surfactant in SP-C-deficient mice." Proc Natl Acad Sci U S A **98**(11): 6366-6371.

Glasser, S. W., E. A. Detmer, M. Ikegami, C. L. Na, M. T. Stahlman and J. A. Whitsett (2003). "Pneumonitis and emphysema in sp-C gene targeted mice." J Biol Chem **278**(16): 14291-14298.

Goerke, J. (1998). "Pulmonary surfactant: functions and molecular composition." Biochim Biophys Acta **1408**(2-3): 79-89.

Gomez-Gil, L., J. Perez-Gil and E. Goormaghtigh (2009). "Cholesterol modulates the exposure and orientation of pulmonary surfactant protein SP-C in model surfactant membranes." Biochim Biophys Acta **1788**(9): 1907-1915.

Gomez-Gil, L., D. Schurch, E. Goormaghtigh and J. Perez-Gil (2009). "Pulmonary surfactant protein SP-C counteracts the deleterious effects of cholesterol on the activity of surfactant films under physiologically relevant compression-expansion dynamics." Biophys J **97**(10): 2736-2745.

Greenspan, P., E. P. Mayer and S. D. Fowler (1985). "Nile red: a selective fluorescent stain for intracellular lipid droplets." J Cell Biol **100**(3): 965-973.

Griffith, O. H., D. W. Cornell and H. M. McConnell (1965). "Nitrogen Hyperfine Tensor and g Tensor of Nitroxide Radicals." The Journal of Chemical Physics **43**(8): 2909-2910.

Gunther, A., R. Schmidt, A. Feustel, U. Meier, C. Pucker, M. Ermert and W. Seeger (1999). "Surfactant subtype conversion is related to loss of surfactant apoprotein B and surface activity in large surfactant aggregates. Experimental and clinical studies." Am J Respir Crit Care Med **159**(1): 244-251.

Gunther, A., R. Schmidt, F. Nix, M. Yabut-Perez, C. Guth, S. Rosseau, C. Siebert, F. Grimminger, H. Morr, H. G. Velcovsky and W. Seeger (1999). "Surfactant abnormalities in idiopathic pulmonary fibrosis, hypersensitivity pneumonitis and sarcoidosis." Eur Respir J **14**(3): 565-573.

Gutsmann, T., B. Riekens, H. Bruhn, A. Wiese, U. Seydel and M. Leippe (2003). "Interaction of amoebapores and NK-lysin with symmetric phospholipid and asymmetric lipopolysaccharide/phospholipid bilayers." Biochemistry **42**(32): 9804-9812.

Haller, T., P. Dietl, H. Stockner, M. Frick, N. Mair, I. Tinhofer, A. Ritsch, G. Enhorning and G. Putz (2004). "Tracing surfactant transformation from cellular release to insertion into an air-liquid interface." Am J Physiol Lung Cell Mol Physiol **286**(5): L1009-1015.

Haller, T., J. Ortmayr, F. Friedrich, H. Volkl and P. Dietl (1998). "Dynamics of surfactant release in alveolar type II cells." Proc Natl Acad Sci U S A **95**(4): 1579-1584.

Hawco, M. W., P. J. Davis and K. M. Keough (1981). "Lipid fluidity in lung surfactant: monolayers of saturated and unsaturated lecithins." J Appl Physiol **51**(2): 509-515.

Hawgood, S., M. Derrick and F. Poulain (1998). "Structure and properties of surfactant protein B." Biochim Biophys Acta **1408**(2-3): 150-160.

Hawkins, C. A., E. de Alba and N. Tjandra (2005). "Solution structure of human saposin C in a detergent environment." J Mol Biol **346**(5): 1381-1392.

Heinrich, V. and W. Rawicz (2005). "Automated, high-resolution micropipet aspiration reveals new insight into the physical properties of fluid membranes." Langmuir **21**(5): 1962-1971.

Helfrich, W. (1973). "Elastic properties of lipid bilayers: theory and possible experiments." Z Naturforsch C **28**(11): 693-703.

Heukeshoven, J. and R. Dernick (1988). "Improved silver staining procedure for fast staining in PhastSystem Development Unit. I. Staining of sodium dodecyl sulfate gels." Electrophoresis **9**(1): 28-32.

Hille, B. (2001). Ion channels of excitable membranes. Sunderland, Mass., Sinauer.

Ikegami, M., S. Grant, T. Korfhagen, R. K. Scheule and J. A. Whitsett (2009). "Surfactant protein-D regulates the postnatal maturation of pulmonary surfactant lipid pool sizes." J Appl Physiol **106**(5): 1545-1552.

Ikegami, M., C. L. Na, T. R. Korfhagen and J. A. Whitsett (2005). "Surfactant protein D influences surfactant ultrastructure and uptake by alveolar type II cells." Am J Physiol Lung Cell Mol Physiol **288**(3): L552-561.

Ikegami, M., N. Takabatake and T. E. Weaver (2002). "Intersubunit disulfide bridge is not required for the protective role of SP-B against lung inflammation." J Appl Physiol **93**(2): 505-511.

Jimenez Cabre, E. (2009). "Determinants and effects of surfactant protein SP-B integration in lipidic membranes", Universidad Complutense de Madrid.

Johansson, J. (1998). "Structure and properties of surfactant protein C." Biochim Biophys Acta **1408**(2-3): 161-172.

Johansson, J. and T. Curstedt (1997). "Molecular structures and interactions of pulmonary surfactant components." Eur J Biochem **244**(3): 675-693.

Johansson, J., T. Szyperski, T. Curstedt and K. Wuthrich (1994). "The NMR structure of the pulmonary surfactant-associated polypeptide SP-C in an apolar solvent contains a valyl-rich alpha-helix." Biochemistry **33**(19): 6015-6023.

Kairys, V., M. K. Gilson and B. Luy (2004). "Structural model for an AxxxG-mediated dimer of surfactant-associated protein C." Eur J Biochem **271**(11): 2086-2092.

Keating, E., Y. Y. Zuo, S. M. Tadayyon, N. O. Petersen, F. Possmayer and R. A. Veldhuizen (2012). "A modified squeeze-out mechanism for generating high surface pressures with pulmonary surfactant." Biochim Biophys Acta **1818**(5): 1225-1234.

King, R. J., D. J. Klass, E. G. Gikas and J. A. Clements (1973). "Isolation of apoproteins from canine surface active material." Am J Physiol **224**(4): 788-795.

Kramer, A., A. Wintergalen, M. Sieber, H. J. Galla, M. Amrein and R. Guckenberger (2000). "Distribution of the surfactant-associated protein C within a lung surfactant model film investigated by near-field optical microscopy." Biophys J **78**(1): 458-465.

Kramers, H. A. (1940). "Brownian motion in a field of force and the diffusion model of chemical reactions." Physica **7**(4): 284-304.

Krol, S., M. Ross, M. Sieber, S. Kunneke, H. J. Galla and A. Janshoff (2000). "Formation of three-dimensional protein-lipid aggregates in monolayer films induced by surfactant protein B." Biophys J **79**(2): 904-918.

Kropski, J. A., W. E. Lawson, L. R. Young and T. S. Blackwell (2013). "Genetic studies provide clues on the pathogenesis of idiopathic pulmonary fibrosis." Dis Model Mech **6**(1): 9-17.

Kwok, R. and E. Evans (1981). "Thermoelasticity of large lecithin bilayer vesicles." Biophys J **35**(3): 637-652.

Lawson, P. R. and K. B. Reid (2000). "The roles of surfactant proteins A and D in innate immunity." Immunol Rev **173**: 66-78.

Lawson, W. E., V. V. Polosukhin, G. T. Stathopoulos, O. Zoia, W. Han, K. B. Lane, B. Li, E. F. Donnelly, G. E. Holburn, K. G. Lewis, R. D. Collins, W. M. Hull, S. W. Glasser, J. A. Whitsett and T. S. Blackwell (2005). "Increased and prolonged pulmonary fibrosis in surfactant protein C-deficient mice following intratracheal bleomycin." Am J Pathol **167**(5): 1267-1277.

Leippe, M., H. Bruhn, O. Hecht and J. Grotzinger (2005). "Ancient weapons: the three-dimensional structure of amoebapore A." Trends Parasitol **21**(1): 5-7.

Lindahl, E. and O. Edholm (2000). "Mesoscopic undulations and thickness fluctuations in lipid bilayers from molecular dynamics simulations." Biophys J **79**(1): 426-433.

Litster, J. D. (1975). "Stability of lipid bilayers and red blood cell membranes." Physics Letters A **53**(3): 193-194.

Lopez-Rodriguez, E., M. Echaide, A. Cruz, H. W. Taeusch and J. Perez-Gil (2011). "Meconium impairs pulmonary surfactant by a combined action of cholesterol and bile acids." Biophys J **100**(3): 646-655.

Lopez-Rodriguez, E., O. L. Ospina, M. Echaide, H. W. Taeusch and J. Perez-Gil (2012). "Exposure to polymers reverses inhibition of pulmonary surfactant by serum, meconium, or cholesterol in the captive bubble surfactometer." Biophys J **103**(7): 1451-1459.

Lowry, O. H., N. J. Rosebrough, A. L. Farr and R. J. Randall (1951). "Protein measurement with the Folin phenol reagent." J Biol Chem **193**(1): 265-275.

Lukovic, D., A. Cruz, A. Gonzalez-Horta, A. Almlen, T. Curstedt, I. Mingarro and J. Perez-Gil (2012). "Interfacial behavior of recombinant forms of human pulmonary surfactant protein SP-C." Langmuir **28**(20): 7811-7825.

Luy, B., A. Diener, R. P. Hummel, E. Sturm, W. R. Ulrich and C. Griesinger (2004). "Structure and potential C-terminal dimerization of a recombinant mutant of surfactant-associated protein C in chloroform/methanol." Eur J Biochem **271**(11): 2076-2085.

Malev, V. V., L. V. Schagina, P. A. Gurnev, J. Y. Takemoto, E. M. Nestorovich and S. M. Bezrukov (2002). "Syringomycin E channel: a lipidic pore stabilized by lipopeptide?" Biophys J **82**(4): 1985-1994.

Marsh, D. (1981). Electron spin resonance: spin labels. Membrane Spectroscopy. E. Grell. Berlin, Springer-Verlag. **31:** 51-142.

Marsh, D. (1996). "Lateral pressure in membranes." Biochim Biophys Acta **1286**(3): 183-223.

Marsh, D. (2012). "Thermodynamics of phospholipid self-assembly." Biophys J **102**(5): 1079-1087.

Mathai, J. C., S. Tristram-Nagle, J. F. Nagle and M. L. Zeidel (2008). "Structural determinants of water permeability through the lipid membrane." J Gen Physiol **131**(1): 69-76.

Mathivet, L., S. Cribier and P. F. Devaux (1996). "Shape change and physical properties of giant phospholipid vesicles prepared in the presence of an AC electric field." Biophys J **70**(3): 1112-1121.

Melikov, K. C., V. A. Frolov, A. Shcherbakov, A. V. Samsonov, Y. A. Chizmadzhev and L. V. Chernomordik (2001). "Voltage-induced nonconductive pre-pores and metastable single pores in unmodified planar lipid bilayer." Biophys J **80**(4): 1829-1836.

Melton, K. R., L. L. Nesslein, M. Ikegami, J. W. Tichelaar, J. C. Clark, J. A. Whitsett and T. E. Weaver (2003). "SP-B deficiency causes respiratory failure in adult mice." Am J Physiol Lung Cell Mol Physiol **285**(3): L543-549.

Meyer, K. C. and J. J. Zimmerman (2002). "Inflammation and surfactant." Paediatr Respir Rev **3**(4): 308-314.

Mihajlovic, M. and T. Lazaridis (2010). "Antimicrobial peptides in toroidal and cylindrical pores." Biochim Biophys Acta **1798**(8): 1485-1493.

Mingarro, I., D. Lukovic, M. Vilar and J. Perez-Gil (2008). "Synthetic pulmonary surfactant preparations: new developments and future trends." Curr Med Chem **15**(4): 393-403.

Mitchell, D. C. and B. J. Litman (1998). "Effect of cholesterol on molecular order and dynamics in highly polyunsaturated phospholipid bilayers." Biophys J **75**(2): 896-908.

Miteva, M., M. Andersson, A. Karshikoff and G. Otting (1999). "Molecular electroporation: a unifying concept for the description of membrane pore formation by antibacterial peptides, exemplified with NK-lysin." FEBS Lett **462**(1-2): 155-158.

Montal, M. and P. Mueller (1972). "Formation of bimolecular membranes from lipid monolayers and a study of their electrical properties." Proc Natl Acad Sci U S A **69**(12): 3561-3566.

Morrow, M. R., N. Abu-Libdeh, J. Stewart and K. M. Keough (2003). "Interaction of pulmonary surfactant protein SP-A with DPPC/egg-PG bilayers." Biophys J **85**(4): 2397-2405.

Morrow, M. R., J. Perez-Gil, G. Simatos, C. Boland, J. Stewart, D. Absolom, V. Sarin and K. M. Keough (1993). "Pulmonary surfactant-associated protein SP-B has little effect on acyl chains in dipalmitoylphosphatidylcholine dispersions." Biochemistry **32**(16): 4397-4402.

Mouritsen, O. G. and K. Jorgensen (1994). "Dynamical order and disorder in lipid bilayers." Chem Phys Lipids **73**(1-2): 3-25.

Mouritsen, O. G. and M. J. Zuckermann (1985). "Softening of lipid bilayers." Eur Biophys J **12**(2): 75-86.

Mueller, P., D. O. Rudin, H. T. Tien and W. C. Wescott (1962). "Reconstitution of cell membrane structure in vitro and its transformation into an excitable system." Nature **194**: 979-980.

Nag, K., C. Boland, N. Rich and K. M. Keough (1991). "Epifluorescence microscopic observation of monolayers of dipalmitoylphosphatidylcholine: dependence of domain size on compression rates." Biochim Biophys Acta **1068**(2): 157-160.

Nag, K., J. G. Munro, S. A. Hearn, J. Rasmusson, N. O. Petersen and F. Possmayer (1999). "Correlated atomic force and transmission electron microscopy of nanotubular structures in pulmonary surfactant." J Struct Biol **126**(1): 1-15.

Nag, K., J. Perez-Gil, A. Cruz and K. M. Keough (1996). "Fluorescently labeled pulmonary surfactant protein C in spread phospholipid monolayers." Biophys J **71**(1): 246-256.

Nag, K., S. G. Taneva, J. Perez-Gil, A. Cruz and K. M. Keough (1997). "Combinations of fluorescently labeled pulmonary surfactant proteins SP-B and SP-C in phospholipid films." Biophys J **72**(6): 2638-2650.

Nagle, J. F., R. Zhang, S. Tristram-Nagle, W. Sun, H. I. Petrache and R. M. Suter (1996). "X-ray structure determination of fully hydrated L alpha phase dipalmitoylphosphatidylcholine bilayers." Biophys J **70**(3): 1419-1431.

Needham, D., T. J. McIntosh and E. Evans (1988). "Thermomechanical and transition properties of dimyristoylphosphatidylcholine/cholesterol bilayers." Biochemistry **27**(13): 4668-4673.

Needham, D. and D. Zhelev (1999). Use of micropipet manipulation techniques to measure the properties of giant lipid vesicles. Giant vesicles. Perspectives in supramolecular chemistry. P. L. a. W. Luisi, P. New York, John Wiley & Sons Ltd**:** 103-148.

Nesslein, L. L., K. R. Melton, M. Ikegami, C. L. Na, S. E. Wert, W. R. Rice, J. A. Whitsett and T. E. Weaver (2005). "Partial SP-B deficiency perturbs lung function and causes air space abnormalities." Am J Physiol Lung Cell Mol Physiol **288**(6): L1154-1161.

Nogee, L. M., D. E. de Mello, L. P. Dehner and H. R. Colten (1993). "Brief report: deficiency of pulmonary surfactant protein B in congenital alveolar proteinosis." N Engl J Med **328**(6): 406-410.

Nogee, L. M., G. Garnier, H. C. Dietz, L. Singer, A. M. Murphy, D. E. deMello and H. R. Colten (1994). "A mutation in the surfactant protein B gene responsible for fatal neonatal respiratory disease in multiple kindreds." J Clin Invest **93**(4): 1860-1863.

Nogee, L. M., S. E. Wert, S. A. Proffit, W. M. Hull and J. A. Whitsett (2000). "Allelic heterogeneity in hereditary surfactant protein B (SP-B) deficiency." Am J Respir Crit Care Med **161**(3 Pt 1): 973-981.

Ochs, M., J. R. Nyengaard, A. Jung, L. Knudsen, M. Voigt, T. Wahlers, J. Richter and H. J. Gundersen (2004). "The number of alveoli in the human lung." Am J Respir Crit Care Med **169**(1): 120-124.

Oelberg, D. G. and F. Xu (2000). "Pulmonary surfactant proteins insert cation-permeable channels in planar bilayers." Mol Genet Metab **70**(4): 295-300.

Olbrich, K., W. Rawicz, D. Needham and E. Evans (2000). "Water permeability and mechanical strength of polyunsaturated lipid bilayers." Biophys J **79**(1): 321-327.

Olmeda, B., B. Garcia-Alvarez and J. Perez-Gil (2013). "Structure-function correlations of pulmonary surfactant protein SP-B and the saposin-like family of proteins." Eur Biophys J **42**(2-3): 209-222.

Oosterlaken-Dijksterhuis, M. A., H. P. Haagsman, L. M. van Golde and R. A. Demel (1991). "Characterization of lipid insertion into monomolecular layers mediated by lung surfactant proteins SP-B and SP-C." Biochemistry **30**(45): 10965-10971.

Oosterlaken-Dijksterhuis, M. A., M. van Eijk, L. M. van Golde and H. P. Haagsman (1992). "Lipid mixing is mediated by the hydrophobic surfactant protein SP-B but not by SP-C." Biochim Biophys Acta **1110**(1): 45-50.

Orgeig, S., P. S. Hiemstra, E. J. Veldhuizen, C. Casals, H. W. Clark, A. Haczku, L. Knudsen and F. Possmayer (2010). "Recent advances in alveolar biology: evolution and function of alveolar proteins." Respir Physiol Neurobiol **173 Suppl**: S43-54.

Palaniyar, N., M. Ikegami, T. Korfhagen, J. Whitsett and F. X. McCormack (2001). "Domains of surfactant protein A that affect protein oligomerization, lipid structure and surface tension." Comp Biochem Physiol A Mol Integr Physiol **129**(1): 109-127.

Patthy, L. (1991). "Homology of the precursor of pulmonary surfactant-associated protein SP-B with prosaposin and sulfated glycoprotein 1." J Biol Chem **266**(10): 6035-6037.

Perez-Gil, J. (2002). "Molecular interactions in pulmonary surfactant films." Biol Neonate **81 Suppl 1**: 6-15.

Perez-Gil, J. (2008). "Structure of pulmonary surfactant membranes and films: the role of proteins and lipid-protein interactions." Biochim Biophys Acta **1778**(7-8): 1676-1695.

Perez-Gil, J., C. Casals and D. Marsh (1995). "Interactions of hydrophobic lung surfactant proteins SP-B and SP-C with dipalmitoylphosphatidylcholine and dipalmitoylphosphatidylglycerol bilayers studied by electron spin resonance spectroscopy." Biochemistry **34**(12): 3964-3971.

Perez-Gil, J., A. Cruz and C. Casals (1993). "Solubility of hydrophobic surfactant proteins in organic solvent/water mixtures. Structural studies on SP-B and SP-C in aqueous organic solvents and lipids." Biochim Biophys Acta **1168**(3): 261-270.

Perez-Gil, J. and K. M. Keough (1998). "Interfacial properties of surfactant proteins." Biochim Biophys Acta **1408**(2-3): 203-217.

Perez-Gil, J., K. Nag, S. Taneva and K. M. Keough (1992). "Pulmonary surfactant protein SP-C causes packing rearrangements of dipalmitoylphosphatidylcholine in spread monolayers." Biophys J **63**(1): 197-204.

Perez-Gil, J., J. Tucker, G. Simatos and K. M. Keough (1992). "Interfacial adsorption of simple lipid mixtures combined with hydrophobic surfactant protein from pig lung." Biochem Cell Biol **70**(5): 332-338.

Perez-Gil, J. and T. E. Weaver (2010). "Pulmonary surfactant pathophysiology: current models and open questions." Physiology (Bethesda) **25**(3): 132-141.

Perry, S. F. (1989). Structure and function of the reptilian respiratory system. Comparative Pulmonary Physiology. Current Concepts. S. C. Wood. New York, Marcel Dekker**:** 193-236.

Phizackerley, P. J., M. H. Town and G. E. Newman (1979). "Hydrophobic proteins of lamellated osmiophilic bodies isolated from pig lung." Biochem J **183**(3): 731-736.

Plasencia, I., F. Baumgart, D. Andreu, D. Marsh and J. Perez-Gil (2008). "Effect of acylation on the interaction of the N-Terminal segment of pulmonary surfactant protein SP-C with phospholipid membranes." Biochim Biophys Acta **1778**(5): 1274-1282.

Plasencia, I., A. Cruz, C. Casals and J. Perez-Gil (2001). "Superficial disposition of the N-terminal region of the surfactant protein SP-C and the absence of specific SP-B-SP-C interactions in phospholipid bilayers." Biochem J **359**(Pt 3): 651-659.

Plasencia, I., K. M. Keough and J. Perez-Gil (2005). "Interaction of the N-terminal segment of pulmonary surfactant protein SP-C with interfacial phospholipid films." Biochim Biophys Acta **1713**(2): 118-128.

Plasencia, I., L. Rivas, K. M. Keough, D. Marsh and J. Perez-Gil (2004). "The N-terminal segment of pulmonary surfactant lipopeptide SP-C has intrinsic propensity to interact with and perturb phospholipid bilayers." Biochem J **377**(Pt 1): 183-193.

Popovic, K., J. Holyoake, R. Pomes and G. G. Prive (2012). "Structure of saposin A lipoprotein discs." Proc Natl Acad Sci U S A **109**(8): 2908-2912.

Possmayer, F., S. H. Yu, J. M. Weber and P. G. Harding (1984). "Pulmonary surfactant." Can J Biochem Cell Biol **62**(11): 1121-1133.

Poulain, F. R., L. Allen, M. C. Williams, R. L. Hamilton and S. Hawgood (1992). "Effects of surfactant apolipoproteins on liposome structure: implications for tubular myelin formation." Am J Physiol **262**(6 Pt 1): L730-739.

Poulain, F. R., S. Nir and S. Hawgood (1996). "Kinetics of phospholipid membrane fusion induced by surfactant apoproteins A and B." Biochim Biophys Acta **1278**(2): 169-175.

Ramirez, E., A. Santana, A. Cruz, I. Plasencia and G. E. Lopez (2006). "Molecular dynamics of surfactant protein C: from single molecule to heptameric aggregates." Biophys J **90**(8): 2698-2705.

Ravasio, A., B. Olmeda, C. Bertocchi, T. Haller and J. Perez-Gil (2010). "Lamellar bodies form solid three-dimensional films at the respiratory air-liquid interface." J Biol Chem **285**(36): 28174-28182.

Rawicz, W., K. C. Olbrich, T. McIntosh, D. Needham and E. Evans (2000). "Effect of chain length and unsaturation on elasticity of lipid bilayers." Biophys J **79**(1): 328-339.

Rawicz, W., B. A. Smith, T. J. McIntosh, S. A. Simon and E. Evans (2008). "Elasticity, strength, and water permeability of bilayers that contain raft microdomain-forming lipids." Biophys J **94**(12): 4725-4736.

Robinson, R. A. and R. H. Stokes (1957). "Solutions of Electrolytes and Diffusion in Liquids." Annual Review of Physical Chemistry **8**(1): 37-54.

Rodriguez-Capote, K., K. Nag, S. Schurch and F. Possmayer (2001). "Surfactant protein interactions with neutral and acidic phospholipid films." Am J Physiol Lung Cell Mol Physiol **281**(1): L231-242.

Rooney, S. A., S. L. Young and C. R. Mendelson (1994). "Molecular and cellular processing of lung surfactant." FASEB J **8**(12): 957-967.

Ross, M., S. Krol, A. Janshoff and H. J. Galla (2002). "Kinetics of phospholipid insertion into monolayers containing the lung surfactant proteins SP-B or SP-C." Eur Biophys J **31**(1): 52-61.

Rossmann, M., R. Schultz-Heienbrok, J. Behlke, N. Remmel, C. Alings, K. Sandhoff, W. Saenger and T. Maier (2008). "Crystal structures of human saposins C andD: implications for lipid recognition and membrane interactions." Structure **16**(5): 809-817.

Rostovtseva, T. K., V. M. Aguilella, I. Vodyanoy, S. M. Bezrukov and V. A. Parsegian (1998). "Membrane surface-charge titration probed by gramicidin A channel conductance." Biophys J **75**(4): 1783-1792.

Rouser, G., A. N. Siakotos and S. Fleischer (1966). "Quantitative analysis of phospholipids by thin-layer chromatography and phosphorus analysis of spots." Lipids **1**(1): 85-86.

Ruano, M. L., E. Miguel, J. Perez-Gil and C. Casals (1996). "Comparison of lipid aggregation and self-aggregation activities of pulmonary surfactant-associated protein A." Biochem J **313 (Pt 2)**: 683-689.

Rugonyi, S., S. C. Biswas and S. B. Hall (2008). "The biophysical function of pulmonary surfactant." Respir Physiol Neurobiol **163**(1-3): 244-255.

Rushing, S. and L. R. Ment (2004). "Preterm birth: a cost benefit analysis." Semin Perinatol **28**(6): 444-450.

Ryan, M. A., X. Qi, A. G. Serrano, M. Ikegami, J. Perez-Gil, J. Johansson and T. E. Weaver (2005). "Mapping and analysis of the lytic and fusogenic domains of surfactant protein B." Biochemistry **44**(3): 861-872.

Sachan, A. K. and H. J. Galla (2013). "Bidirectional surface analysis of monomolecular membrane harboring nanoscale reversible collapse structures." Nano Lett **13**(3): 961-966.

Saenz, A., O. Canadas, L. A. Bagatolli, F. Sanchez-Barbero, M. E. Johnson and C. Casals (2007). "Effect of surfactant protein A on the physical properties and surface activity of KL4-surfactant." Biophys J **92**(2): 482-492.

Schneider, C. A., W. S. Rasband and K. W. Eliceiri (2012). "NIH Image to ImageJ: 25 years of image analysis." Nat Methods **9**(7): 671-675.

Schram, V. and S. B. Hall (2004). "SP-B and SP-C alter diffusion in bilayers of pulmonary surfactant." Biophys J **86**(6): 3734-3743.

Schurch, D., O. L. Ospina, A. Cruz and J. Perez-Gil (2010). "Combined and independent action of proteins SP-B and SP-C in the surface behavior and mechanical stability of pulmonary surfactant films." Biophys J **99**(10): 3290-3299.

Schurch, S., R. Qanbar, H. Bachofen and F. Possmayer (1995). "The surface-associated surfactant reservoir in the alveolar lining." Biol Neonate **67 Suppl 1**: 61-76.

Seifert, M., D. Breitenstein, U. Klenz, M. C. Meyer and H. J. Galla (2007). "Solubility versus electrostatics: what determines lipid/protein interaction in lung surfactant." Biophys J **93**(4): 1192-1203.

Sengupta, D., H. Leontiadou, A. E. Mark and S. J. Marrink (2008). "Toroidal pores formed by antimicrobial peptides show significant disorder." Biochim Biophys Acta **1778**(10): 2308-2317.

Serrano, A. G., E. J. Cabre and J. Perez-Gil (2007). "Identification of a segment in the precursor of pulmonary surfactant protein SP-B, potentially involved in pH-dependent membrane assembly of the protein." Biochim Biophys Acta **1768**(5): 1059-1069.

Serrano, A. G. and J. Perez-Gil (2006). "Protein-lipid interactions and surface activity in the pulmonary surfactant system." Chem Phys Lipids **141**(1-2): 105-118.

Shiffer, K., S. Hawgood, N. Duzgunes and J. Goerke (1988). "Interactions of the low molecular weight group of surfactant-associated proteins (SP 5-18) with pulmonary surfactant lipids." Biochemistry **27**(8): 2689-2695.

Shiffer, K., S. Hawgood, H. P. Haagsman, B. Benson, J. A. Clements and J. Goerke (1993). "Lung surfactant proteins, SP-B and SP-C, alter the thermodynamic properties of phospholipid membranes: a differential calorimetry study." Biochemistry **32**(2): 590-597.

Shulenin, S., L. M. Nogee, T. Annilo, S. E. Wert, J. A. Whitsett and M. Dean (2004). "ABCA3 gene mutations in newborns with fatal surfactant deficiency." N Engl J Med **350**(13): 1296-1303.

Smaby, J. M., M. M. Momsen, H. L. Brockman and R. E. Brown (1997). "Phosphatidylcholine acyl unsaturation modulates the decrease in interfacial elasticity induced by cholesterol." Biophys J **73**(3): 1492-1505.

Smith, E. C., J. M. Crane, T. G. Laderas and S. B. Hall (2003). "Metastability of a supercompressed fluid monolayer." Biophys J **85**(5): 3048-3057.

Sobko, A. A., E. A. Kotova, Y. N. Antonenko, S. D. Zakharov and W. A. Cramer (2004). "Effect of lipids with different spontaneous curvature on the channel activity of colicin E1: evidence in favor of a toroidal pore." FEBS Lett **576**(1-2): 205-210.

Stachowiak, J. C., E. M. Schmid, C. J. Ryan, H. S. Ann, D. Y. Sasaki, M. B. Sherman, P. L. Geissler, D. A. Fletcher and C. C. Hayden (2012). "Membrane bending by protein-protein crowding." Nat Cell Biol **14**(9): 944-949.

Stahlman, M. T., M. P. Gray, M. W. Falconieri, J. A. Whitsett and T. E. Weaver (2000). "Lamellar body formation in normal and surfactant protein B-deficient fetal mice." Lab Invest **80**(3): 395-403.

Suzuki, Y., Y. Fujita and K. Kogishi (1989). "Reconstitution of tubular myelin from synthetic lipids and proteins associated with pig pulmonary surfactant." Am Rev Respir Dis **140**(1): 75-81.

Swamy, M. J., U. Wurz and D. Marsh (1995). "Phase polymorphism, molecular interactions, and miscibility of binary mixtures of dimyristoyl-N-biotinylphosphatidylethanolamine with dimyristoylphosphatidylcholine." Biochemistry **34**(22): 7295-7302.

Szyperski, T., G. Vandenbussche, T. Curstedt, J. M. Ruysschaert, K. Wuthrich and J. Johansson (1998). "Pulmonary surfactant-associated polypeptide C in a mixed organic solvent transforms from a monomeric alpha-helical state into insoluble beta-sheet aggregates." Protein Sci **7**(12): 2533-2540.

Taeusch, H. W., J. Bernardino de la Serna, J. Perez-Gil, C. Alonso and J. A. Zasadzinski (2005). "Inactivation of pulmonary surfactant due to serum-inhibited adsorption and reversal by hydrophilic polymers: experimental." Biophys J **89**(3): 1769-1779.

Taupin, C., M. Dvolaitzky and C. Sauterey (1975). "Osmotic pressure induced pores in phospholipid vesicles." Biochemistry **14**(21): 4771-4775.

Tilcock, C. P. (1986). "Lipid polymorphism." Chem Phys Lipids **40**(2-4): 109-125.

Tolpekina, T. V., W. K. den Otter and W. J. Briels (2004). "Nucleation free energy of pore formation in an amphiphilic bilayer studied by molecular dynamics simulations." The Journal of Chemical Physics **121**(23): 12060-12066.

Tung, L., G. C. Troiano, V. Sharma, R. M. Raphael and K. J. Stebe (1999). "Changes in electroporation thresholds of lipid membranes by surfactants and peptides." Ann N Y Acad Sci **888**: 249-265.

van den Brink-van der Laan, E., J. A. Killian and B. de Kruijff (2004). "Nonbilayer lipids affect peripheral and integral membrane proteins via changes in the lateral pressure profile." Biochim Biophys Acta **1666**(1-2): 275-288.

Vandenbussche, G., A. Clercx, M. Clercx, T. Curstedt, J. Johansson, H. Jornvall and J. M. Ruysschaert (1992). "Secondary structure and orientation of the surfactant protein SP-B in a lipid environment. A Fourier transform infrared spectroscopy study." Biochemistry **31**(38): 9169-9176.

Vandenbussche, G., A. Clercx, T. Curstedt, J. Johansson, H. Jornvall and J. M. Ruysschaert (1992). "Structure and orientation of the surfactant-associated protein C in a lipid bilayer." Eur J Biochem **203**(1-2): 201-209.

Veatch, S. L. (2007). Electro-Formation and Fluorescence Microscopy of Giant Vesicles With Coexisting Liquid Phases. Lipid Rafts. **398:** 59-72.

Veatch, S. L. and S. L. Keller (2003). "Separation of liquid phases in giant vesicles of ternary mixtures of phospholipids and cholesterol." Biophys J **85**(5): 3074-3083.

Veatch, S. L., I. V. Polozov, K. Gawrisch and S. L. Keller (2004). "Liquid domains in vesicles investigated by NMR and fluorescence microscopy." Biophys J **86**(5): 2910-2922.

Veldhuizen, E. J. and H. P. Haagsman (2000). "Role of pulmonary surfactant components in surface film formation and dynamics." Biochim Biophys Acta **1467**(2): 255-270.

Walde, P. (2010). "Building artificial cells and protocell models: experimental approaches with lipid vesicles." Bioessays **32**(4): 296-303.

Wang, L., P. Cai, H. J. Galla, H. He, C. R. Flach and R. Mendelsohn (2005). "Monolayer-multilayer transitions in a lung surfactant model: IR reflection-absorption spectroscopy and atomic force microscopy." Eur Biophys J **34**(3): 243-254.

Wang, Z., O. Gurel, J. E. Baatz and R. H. Notter (1996). "Differential activity and lack of synergy of lung surfactant proteins SP-B and SP-C in interactions with phospholipids." J Lipid Res **37**(8): 1749-1760.

Watkins, J. C. (1968). "The surface properties of pure phospholipids in relation to those of lung extracts." Biochim Biophys Acta **152**(2): 293-306.

Weaver, T. E. (1998). "Synthesis, processing and secretion of surfactant proteins B and C." Biochim Biophys Acta **1408**(2-3): 173-179.

Weaver, T. E. and D. C. Beck (1999). "Use of knockout mice to study surfactant protein structure and function." Biol Neonate **76 Suppl 1**: 15-18.

Weaver, T. E. and J. J. Conkright (2001). "Function of surfactant proteins B and C." Annu Rev Physiol **63**: 555-578.

Weaver, T. E., C. L. Na and M. Stahlman (2002). "Biogenesis of lamellar bodies, lysosome-related organelles involved in storage and secretion of pulmonary surfactant." Semin Cell Dev Biol **13**(4): 263-270.

Weaver, T. E. and J. A. Whitsett (1991). "Function and regulation of expression of pulmonary surfactant-associated proteins." Biochem J **273(Pt 2)**: 249-264.

Wert, S. E., J. A. Whitsett and L. M. Nogee (2009). "Genetic disorders of surfactant dysfunction." Pediatr Dev Pathol **12**(4): 253-274.

Wertz, J. E. and J. R. Bolton (1986). Electron spin resonance : elementary theory and practical applications. New York etc., Chapman and Hall.

West, J. B. (2008). Respiratory physiology : the essentials. Philadelphia, Wolters Kluwer Health/Lippincott Williams & Wilkins.

Williams, M. C. (1977). "Conversion of lamellar body membranes into tubular myelin in alveoli of fetal rat lungs." J Cell Biol **72**(2): 260-277.

Wohlert, J., W. K. den Otter, O. Edholm and W. J. Briels (2006). "Free energy of a trans-membrane pore calculated from atomistic molecular dynamics simulations." J Chem Phys **124**(15): 154905.

Worthman, L. A., K. Nag, N. Rich, M. L. Ruano, C. Casals, J. Perez-Gil and K. M. Keough (2000). "Pulmonary surfactant protein A interacts with gel-like regions in monolayers of pulmonary surfactant lipid extract." Biophys J **79**(5): 2657-2666.

Wright, J. R. (2003). "Pulmonary surfactant: a front line of lung host defense." J Clin Invest **111**(10): 1453-1455.

Wright, J. R. and J. A. Clements (1987). "Metabolism and turnover of lung surfactant." Am Rev Respir Dis **136**(2): 426-444.

Wu, H., A. Kuzmenko, S. Wan, L. Schaffer, A. Weiss, J. H. Fisher, K. S. Kim and F. X. McCormack (2003). "Surfactant proteins A and D inhibit the growth of Gram-negative bacteria by increasing membrane permeability." J Clin Invest **111**(10): 1589-1602.

Wustneck, N., R. Wustneck, J. Perez-Gil and U. Pison (2003). "Effects of oligomerization and secondary structure on the surface behavior of pulmonary surfactant proteins SP-B and SP-C." Biophys J **84**(3): 1940-1949.

Wustneck, R., J. Perez-Gil, N. Wustneck, A. Cruz, V. B. Fainerman and U. Pison (2005). "Interfacial properties of pulmonary surfactant layers." Adv Colloid Interface Sci **117**(1-3): 33-58.

Yang, L., J. Johansson, R. Ridsdale, H. Willander, M. Fitzen, H. T. Akinbi and T. E. Weaver (2010). "Surfactant protein B propeptide contains a saposin-like protein domain with antimicrobial activity at low pH." J Immunol **184**(2): 975-983.

Zaltash, S., W. J. Griffiths, D. Beck, C. X. Duan, T. E. Weaver and J. Johansson (2001). "Membrane activity of (Cys48Ser) lung surfactant protein B increases with dimerisation." Biol Chem **382**(6): 933-939.

Zaltash, S., M. Palmblad, T. Curstedt, J. Johansson and B. Persson (2000). "Pulmonary surfactant protein B: a structural model and a functional analogue." Biochim Biophys Acta **1466**(1-2): 179-186.

Zhelev, D. V. and D. Needham (1993). "Tension-stabilized pores in giant vesicles: determination of pore size and pore line tension." Biochim Biophys Acta **1147**(1): 89-104.

Zhou, Y. and R. M. Raphael (2007). "Solution pH alters mechanical and electrical properties of phosphatidylcholine membranes: relation between interfacial electrostatics, intramembrane potential, and bending elasticity." Biophys J **92**(7): 2451-2462.

10. APPENDIX: PUBLICATIONS

BJ www.biochemj.org

BJ Structure

Biochem. J. (2011) **438**, 555–564 (Printed in Great Britain) doi:10.1042/BJ20110681

A combined action of pulmonary surfactant proteins SP-B and SP-C modulates permeability and dynamics of phospholipid membranes

Elisa PARRA*, Lara H. MOLEIRO†, Ivan LÓPEZ-MONTERO†, Antonio CRUZ*, Francisco MONROY† and Jesús PÉREZ-GIL*[1]

*Dept. Bioquímica, Fac. Biología, Universidad Complutense, Ciudad Universitaria s/n, 28040 Madrid, Spain, and †Dept. Química Fisica, Fac. CC. Quimicas, Universidad Complutense, Ciudad Universitaria s/n, 28040 Madrid, Spain

Proteins SP-B and SP-C are essential to promote formation of surface-active films at the respiratory interface, but their mechanism of action is still under investigation. In the present study we have analysed the effect of the proteins on the accessibility of native, quasi-native and model surfactant membranes to incorporation of the fluorescent probes Nile Red (permeable) and FM 1-43 (impermeable) into membranes. We have also analysed the effect of single or combined proteins on membrane permeation using the soluble fluorescent dye calcein. The fluorescence of FM 1-43 was always higher in membranes containing SP-B and/or SP-C than in protein-depleted membranes, in contrast with Nile Red which was very similar in all of the materials tested. SP-B and SP-C promoted probe partition with markedly different kinetics. On the other hand, physiological proportions of SP-B and SP-C caused giant oligolamellar vesicles to incorporate FM 1-43 from the external medium into apparently most of the membranes instantaneously. In contrast, oligolamellar pure lipid vesicles appeared to be mainly labelled in the outermost membrane layer. Pure lipidic vesicles were impermeable to calcein, whereas it permeated through membranes containing SP-B and/or SP-C. Vesicles containing only SP-B were stable, but prone to vesicle–vesicle interactions, whereas those containing only SP-C were extremely dynamic, undergoing frequent fluctuations and ruptures. Differential structural effects of proteins on vesicles were confirmed by electron microscopy. These results suggest that SP-B and SP-C have different contributions to inter- and intra-membrane lipid dynamics, and that their combined action could provide unique effects to modulate structure and dynamics of pulmonary surfactant membranes and films.

Key words: lipid–protein interaction, lung surfactant, membrane permeability, membrane perturbation, membrane pore, membrane protein.

INTRODUCTION

Pulmonary surfactant, a membrane-based lipid–protein complex, is strictly required for breathing in pulmonated organisms. The presence of a surfactant layer at the respiratory surface is simultaneously responsible for biophysical-stabilizing activities [1] and innate defence mechanisms [2]. The lack, deficiency or inactivation of the surfactant system is associated with severe respiratory disorders such as NRDS (neonatal respiratory distress syndrome) in preterm babies [3], or the pulmonary dysfunction associated with ARDS (acute respiratory distress syndrome) in cases of lung injury [4].

In general terms, the composition of surfactant consists of approximately 90 % lipids and 8–10 % specific surfactant proteins, including two families: SP-A and SP-D, hydrophilic in nature, and SP-B and SP-C, both hydrophobic and membrane-associated [5]. The phospholipid fraction in surfactant is essentially responsible for its ability to dramatically reduce the surface tension at the air–liquid interface of alveolar spaces. Approximately 80 % of surfactant by mass is composed of PC (phosphatidylcholine), approximately half of which is DPPC (dipalmitoylphosphatidylcholine) [6]. The acidic phospholipids phosphatidylglycerol and phosphatidylinositol represent 8–15 % of the total surfactant phospholipid pool. Cholesterol is the main neutral lipid in surfactant, accounting for up to 8–10 % by mass. The presence of proteins, specifically SP-B and SP-C, is absolutely necessary for interfacial adsorption, film stability and re-spreading activities of surfactant along the successive compression–expansion breathing cycles [7]. SP-B is thought to be the most important protein for respiratory physiology, as its lack or deficiency is associated with lethal respiratory failure [8]. It has been shown previously that SP-B induces aggregation, fusion and lysis of phospholipid vesicles [9], and these activities have been associated with a putative role of SP-B to promote lipid transfer and membrane restructuring processes required to form the alveolar surface active films [10]. The role of SP-C in surfactant is not as crucial [11], but SP-C has been involved in membrane–membrane and membrane–interface contacts [12,13]. The combined action of both hydrophobic proteins is considered to be responsible for the proper organization of functional membrane arrays in surfactant complexes.

The pulmonary surfactant system constitutes an excellent example of dynamic membrane polymorphism and how it controls some biological functions through specific lipid–lipid and lipid–protein interactions. Surfactant is assembled by alveolar type II pneumocytes in the form of tightly packed membranes stored in specialized organelles called LBs (lamellar bodies) [14]. Once secreted, surfactant develops a membrane-based network that covers the whole alveolar surface very rapidly and efficiently. From surfactant assembly until its adsorption into the interface, several restructuring processes take place: membrane packing and unpacking in LBs, rearrangement of LB membranes into TM (tubular myelin), reorganization of surfactant membranes to form layers close to the air–water interface, and transfer of surface-active lipid species from these complexes into the interface, and vice versa, during expansion–compression respiratory cycles

Abbreviations used: GV, giant vesicle; LB, lamellar body; LUV, large unilamellar vesicle; MLV, multilamellar membrane suspension; POPC, 1-palmitoyl-2-oleoyl phosphatidylcholine; SUV, small unilamellar vesicle.

[1] To whom correspondence should be addressed (email jpg@bbm1.ucm.es).

(for a review see [7]). Surfactant proteins have a major role in facilitating all of these processes, but the elucidation of their precise molecular mechanism is a challenging task.

Different studies have suggested that pulmonary surfactant structures are composed of particularly dynamic membranes [15], and it is not clear whether those membranes are actually isolating different membrane or aqueous compartments. In the present study, we have analysed the permeability and accessibility of native surfactant complexes and membranes reconstituted from different surfactant fractions to the incorporation of the membrane-sensitive fluorescent probes Nile Red and FM 1-43, able and unable respectively to permeate across phospholipid membranes. In particular, we have evaluated the dependence of the accessibility of membranes and the environment sensed by the probes on the lipid and protein composition. Samples characterized in the present study include complexes of native surfactant purified from porcine lungs and membranes reconstituted from whole-surfactant organic extract or from partial fractions obtained by size-exclusion chromatography, which were compared with model lipid membranes. The effect of SP-B and SP-C on the permeability of model membranes has been also analysed by fluorescence microscopy, through the reconstitution of POPC (1-palmitoyl-2-oleoyl phosphatidylcholine) GVs (giant vesicles) in the absence or presence of the hydrophobic protein fraction of surfactant, or purified SP-B or SP-C.

EXPERIMENTAL

Materials

Native pulmonary surfactant materials were obtained from bronchoalveolar lavage of porcine lungs as described previously [16]. Organic extraction of purified surfactant and chromatographic separation in Sephadex LH-20 (Pharmacia) allowed acquisition of the hydrophobic protein fraction and the lipid surfactant fractions [15,17]. A subsequent chromatographic step in LH-60 yielded purification of SP-B and SP-C separately [17]. In general terms, we obtained a proportion of approximately 0.8 % SP-B and 1.1 % SP-C with respect to phospholipid mass in the surfactant organic extract. The total phospholipid concentration in the different samples was determined by phosphorus analysis upon phospholipid mineralization [18]. Proteins and lipids were stored as chloroform/methanol (2:1, v/v) solutions at $-20\,^{\circ}C$. Protein solutions were routinely checked for purity by SDS/PAGE and quantified by amino acid analysis. POPC was purchased from Avanti Polar Lipids. The fluorescent dyes Nile Red and FM 1-43 were from Molecular Probes, and calcein was from Sigma–Aldrich. Chloroform and methanol solvents, HPLC grade, were from Scharlau.

Vesicle preparation

Stock suspensions of native pulmonary surfactant were in 5 mM Tris buffer (pH 7), containing 150 mM NaCl. MLVs (multilamellar membrane suspensions) of surfactant organic extract, the different surfactant lipid fractions or POPC supplemented or not with proteins SP-B and/or SP-C were prepared as follows. The appropriate amounts of proteins and lipids in chloroform/methanol (2:1) were mixed and the samples were then evaporated to dryness under nitrogen and for 2 h in a vacuum chamber to form a thin film, which was later resuspended at 45 °C (for native materials) or 37 °C (for POPC samples) in the desired final volume of 5 mM Tris buffer (pH 7), containing 150 mM NaCl. LUVs (large unilamellar vesicles) were prepared using a Mini-Extruder (Avanti Polar Lipids) with 10 mm diameter drain discs and 0.1 μm diameter Nuclepore Track-Etched membranes (Whatman), passing the MLV suspension 11 times through the filters at 50 °C, in the case of native or quasi-native material, or 37 °C for POPC samples with or without proteins. SUVs (small unilamellar vesicles) were obtained by sonication (UP200, Hierlscher) of MLV suspensions (0.6 cycles, 65 % amplitude; four cycles of 2 min each). LUV and SUV suspensions were used immediately.

Fluorescence spectroscopy with Nile Red and FM 1-43

The fluorescent probes Nile Red or FM 1-43 were incorporated into the membrane suspensions at a final concentration of 3 and 2 μM respectively, and incubated at room temperature ($25 \pm 1\,^{\circ}C$) protected from light for 30 min. To follow the incorporation kinetics of FM 1-43, the fluorescence emission was measured immediately after incorporation of the probe into the suspensions. Fluorescence emission spectra were registered in a JASCO FP 6200 spectrofluorimeter thermostatically controlled at 37 °C, using 5 nm excitation and 10 nm emission slit widths. Nile Red fluorescence was monitored upon excitation at 548 nm and recording emission from 550 to 700 nm, whereas samples labelled by FM 1-43 were measured upon excitation at 479 nm and recording emission from 500 to 650 nm.

Electron microscopy

Droplets of a unilamellar suspension of POPC (1 mg/ml) with or without protein (full hydrophobic protein fraction, 1 % SP-B or 1 % SP-C by mass), prepared by extrusion, were placed on carbon-coated grids (Electron Microscopy Sciences) for 4 min, stained with uranyl acetate for 40 s and observed under a JEOL JEM-1010 transmission electron microscope.

GV preparation

GVs made up of POPC or POPC supplemented with 1 % (w/w) of SP-B, SP-C or both were prepared following a slightly modified electroformation protocol [19]. Briefly, 10 μl of 1 mg/ml lipid or lipid–protein solution in chloroform were spread in an ITO (indium tin oxide)-coated glass slide (Sigma–Aldrich). The fabrication chamber is composed of two conductor glass slides separated by a Teflon spacer of 1 mm. After organic solvent evaporation, the film was re-hydrated with a sucrose solution (300 mM). The chamber was then connected to an AC power supply (8 Hz and 1.1 V) for 3 h. Then, the frequency was decreased to 4 Hz for 30 min. The vesicles obtained had a spherical shape and a large proportion of oligolamellar vesicles were found. A volume of 25 μl of the solution containing GVs was transferred from the fabrication chamber to the observation chamber containing 75 μl of glucose solution (310 mM).

Visualization of permeability of GVs to calcein and FM 1-43

In order to test the membrane permeability of GVs with different compositions, GVs were transferred to a glucose (310 mM) solution containing 0.05 mM FM 1-43. In some experiments, the liposomes were incubated first in glucose containing 1 mM of the bulk fluorescent marker calcein (Sigma–Aldrich, 494 nm excitation, 517 nm emission) and then diluted in glucose/FM 1-43. Calcein and FM 1-43 fluorescence was then monitored under a fluorescence microscope (Nikon Eclipse TE2000 using a 100 W mercury lamp, and FITC and Texas Red filter sets), and recorded with a cooled CCD (charge-coupled device) camera (Nikon DS-1QM, 14 fps, 1 megapixel). All GV suspensions were

observed freshly made, preferably on the same day of preparation, although no significant changes were observed in permeability or morphology of the vesicles observed up to 48 h after lipid hydration and vesicle preparation.

Reproducibility

When possible, Figures represent means ± S.E.M. for at least three different experiments, with at least two and often three entirely different surfactant and protein batches. In other cases, such as in GV images, illustrative experiments are shown after repeating at least three experiments that exhibited consistent behaviour.

RESULTS

To assess the effect of the presence of hydrophobic surfactant proteins SP-B and/or SP-C on the permeability of phospholipid membranes, we have taken advantage of the fluorescence emission of two extrinsic probes. Nile Red is a phenoxazone dye that fluoresces intensely in organic solvents and membrane environments, but is completely quenched in aqueous medium [20]. The emission properties of this probe depend strongly on the relative hydrophobicity of the surrounding environment. Phospholipid bilayers are highly permeable to Nile Red, so in principle it should label every single membrane in the samples. On the other hand, FM 1-43 is a styryl dye which is water-soluble and also exhibits a high affinity for lipid environments, although it does not translocate through membranes; consequently, it only labels the external leaflet of lipid vesicles. In addition, this probe only emits fluorescence once incorporated into membranes, as water molecules strongly quench its fluorescence emission [21].

Figure 1 compares the emission fluorescence intensity of Nile Red and FM 1-43 as a function of their incorporation into increasing concentrations of different lipid and lipid–protein suspensions, including native pulmonary surfactant complexes (NS) and multilamellar vesicles reconstituted from the whole surfactant organic extract (OE), the protein-free lipid fraction of surfactant (LF), surfactant lipid fraction depleted of cholesterol (LFΔChol), or the lipid fraction depleted of cholesterol but supplemented with the hydrophobic protein fraction of surfactant (LFΔChol + PF). For comparison, the fluorescence of the probes in increasing equivalent concentrations of multilamellar vesicles of POPC has also been determined. The effect of the presence of the different membrane materials on the fluorescence of the two probes was completely different. The fluorescence emission of Nile Red showed similar dependence on lipid concentration, within the experimental error, for the different materials tested up to concentrations of approximately 200 μg/ml (left-hand panel in Figure 1), indicating that all of these materials exhibit similar accessibility to this membrane-permeable probe. For higher lipid amounts, some differences in the emission intensity of Nile Red become relevant, probably as a consequence of local differences in the polarity of the environment sensed by the probe. The probe shows higher emission in materials containing cholesterol and other neutral lipids (NS, OE and LF) than in membranes prepared from fractions depleted of cholesterol and, especially, in pure POPC membranes. This is probably a consequence of the well-known effect of cholesterol to seal membranes and reduce their level of hydration [22,23]. The environment sensed by Nile Red in cholesterol-containing surfactant membranes would then be more dehydrated, and therefore more hydrophobic, than that in cholesterol-free bilayers, leading to a higher intensity of

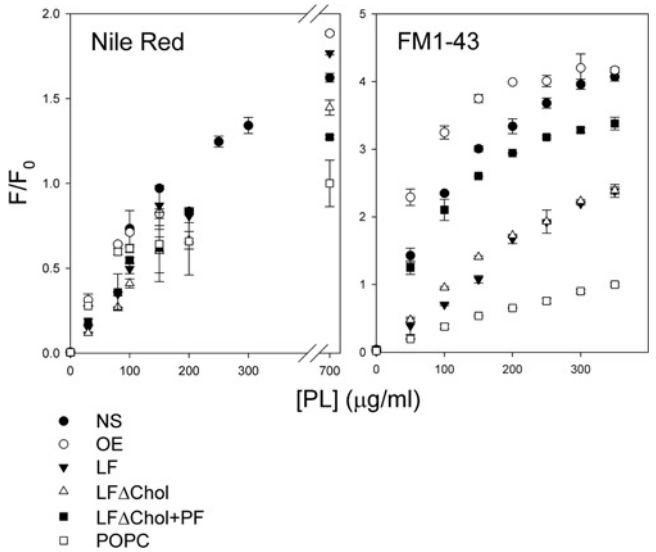

Figure 1 Dependence of Nile Red and FM 1-43 (1 μg/ml) fluorescence emission on phospholipid concentration in different materials

All values have been normalized, F_0 being the maximum emission of each probe corresponding to the highest phospholipid (PL) concentration tested: 700 μg/ml in the case of Nile Red and 350 μg/ml for FM 1-43. LF, protein-free lipid fraction; LFΔChol, LF depleted of cholesterol; LFΔChol + PF, LFΔChol supplemented with the hydrophobic protein fraction of surfactant; NS, native pulmonary surfactant; OE, organic extract.

fluorescence emission. There are no apparent effects of the protein content on the fluorescence of this probe.

In contrast with Nile Red, the fluorescence emission of FM 1-43 is remarkably different in the different membranes studied (right-hand panel of Figure 1). The probe showed approximately 2-fold higher fluorescence in protein-containing membranes, i.e. those from native surfactant, its organic extract or its lipid fraction depleted of cholesterol but supplemented with SP-B and SP-C, than in those made of protein-free surfactant lipids. The fluorescence of the probe in surfactant lipid membranes was also substantially higher than measured in POPC bilayers. The presence of proteins SP-B and SP-C therefore seems important to provide lipid membranes with full accessibility to membrane-impermeable probes such as FM 1-43. Interestingly, Nile Red fluorescence increases rather linearly with phospholipid concentration, whereas FM 1-43 fluorescence seems somehow to plateau, which could reflect differences in partitioning of the two probes between different surfactant lipid phases [15,24], and therefore different levels of probe accumulation.

The differences in accessibility to FM 1-43 of the different membrane suspensions are probably manifested due to their multilamellar character. The outermost impermeable membranes would impede exposure of inner membranes to the probe. In Figure 2 we have compared probe accessibility of native surfactant membranes, membranes reconstituted from the whole-surfactant organic extract and model POPC bilayers, when preparing suspensions with different lamellarity. As would be expected, FM 1-43 produced higher fluorescence emission in unilamellar (LUV or SUV) vesicles than in multilamellar suspensions of POPC (right-hand panel of Figure 2), as a consequence of the larger surface of membranes exposed to the externally added probe. In contrast, there were no apparent differences in the fluorescence emission of the probe partitioning in unilamellar or multilamellar suspensions of either native surfactant or its organic extract. Again this result points to a

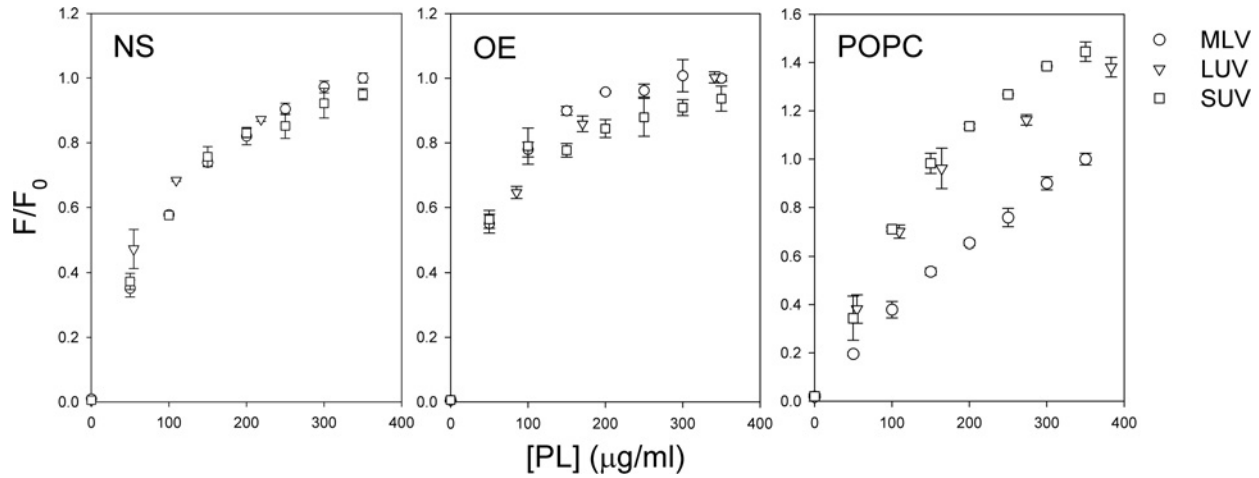

Figure 2 Comparison between unilamellar and multilamellar systems for native pulmonary surfactant, organic extract and POPC

The reference value F_0 is specific for each material, corresponding to the emission of FM 1-43 in the multilamellar sample with the highest lipid concentration tested.

potential role of surfactant proteins in facilitating accessibility of the membrane-impermeable probe across different membranes.

To test whether the mere presence of SP-B and/or SP-C would be enough to facilitate partition of FM 1-43 across membranes, we have tested the effect of introducing surfactant proteins on the differences in probe accessibility when comparing unilamellar and multilamellar suspensions of simple POPC vesicles. Figure 3 compares the fluorescence of FM 1-43 added to increasing concentrations of unilamellar or multilamellar suspensions of pure POPC in the absence or in the presence of hydrophobic surfactant proteins. Also, we have compared POPC membranes supplemented with the whole protein fraction of surfactant (SP-B + SP-C at an equivalent lipid-to-protein ratio to that obtained in the LH-20 chromatography) with membranes containing only 1 % of purified SP-B or SP-C. Figure 3 (left-hand panel) shows that the fluorescence emission of FM 1-43 is 4-fold higher in all protein-containing POPC MLVs than in pure phospholipid membranes, with small but consistent differences between the different protein-containing samples. The order of accessibility of membranes to the probe was always with respect to the protein content SP-B > SP-B + SP-C > SP-C. In contrast, the differences between protein-containing and protein-free POPC membranes with respect to the fluorescence of FM 1-43 were much reduced in unilamellar POPC suspensions (right-hand panel of Figure 3).

To gain further insight into the differences between the effect of SP-B and SP-C on facilitating accessibility to FM 1-43 across multilamellar membrane arrays, we have compared in Figure 4 the kinetics of incorporation of the probe to different amounts of POPC multilamellar suspensions containing 0.25, 1.0 or 2.0 % (protein-to-lipid, by mass) of either purified SP-B or SP-C. Physiological proportions of these proteins are thought to be approximately 1 % in native surfactant, but we wanted to test much lower subphysiological proportions to maximize kinetic differences. The kinetics of incorporation of FM 1-43 into the POPC membranes was significantly different when comparing the effect of SP-B and SP-C. In all of the SP-B-containing membranes tested, the fluorescence emission intensity of the probe reached the maximum in less than 30 s after the addition of the dye, whereas, in SP-C-containing samples, the emission increased gradually for the first 30 min, especially in the samples containing the lowest proportion of protein. Figure 5 compares the full dependence of maximal emission of FM 1-43 into POPC

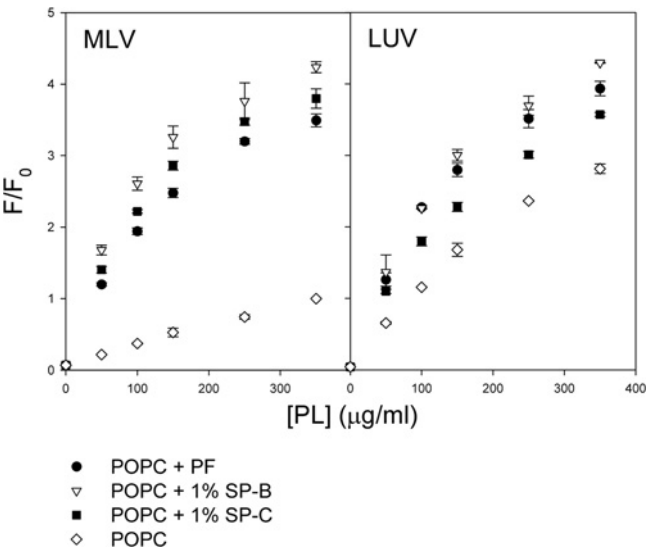

Figure 3 Comparison between unilamellar and multilamellar systems for model membranes of POPC and membranes of POPC supplemented with the hydrophobic protein fraction, 1 % (w/w) SP-B and 1 % (w/w) SP-C

The reference value F_0 corresponds to the emission of FM 1-43 in the pure POPC MLVs with the highest lipid concentration tested.

MLVs compared with the protein density in the membranes for both SP-B and SP-C. Below a 0.5 % protein-to-lipid ratio (w/w), SP-B always produced higher fluorescence, and hence better partition of the probe across membranes, than SP-C. The lower proportion of SP-B tested, a 0.1 % protein-to-lipid ratio (w/w), already produced maximal incorporation of FM 1-43 into POPC membranes, suggesting that SP-B is extremely efficient in facilitating permeability of this membrane-impermeable probe across bilayers.

The different behaviours of SP-B and SP-C with respect to the kinetics of incorporation of FM 1-43 across membranes suggests that intrinsic differences must exist between the mode and extent of perturbation by the two proteins of the structure and the permeability barrier of membranes. To gain further insight into the effect of the two proteins on the structure of the model membranes used in the present study, we have examined, by

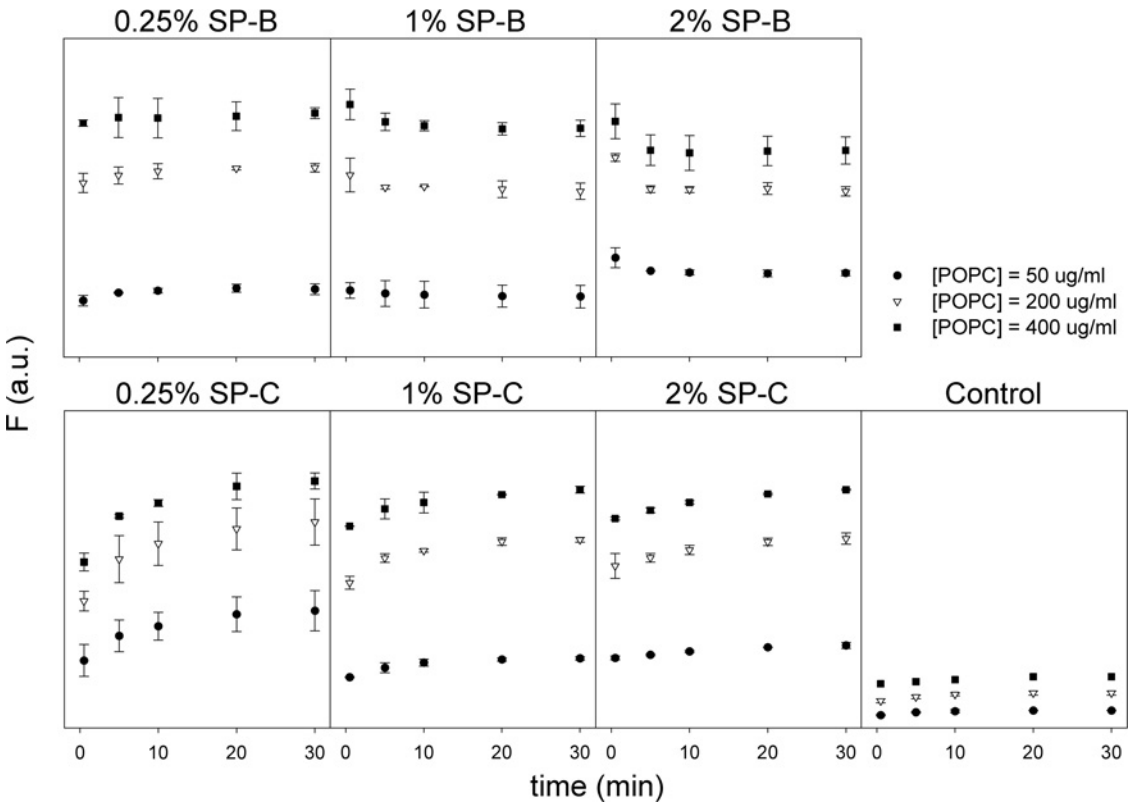

Figure 4 Kinetic studies of the incorporation of FM 1-43 into multilamellar vesicles of POPC supplemented with different percentages (by weight of phospholipids) of SP-B and SP-C

Results correspond to three different phospholipid concentrations: 50 (●), 200 (▽) and 400 μg/ml (■). Results are shown in comparison with the control sample, MLV of pure POPC.

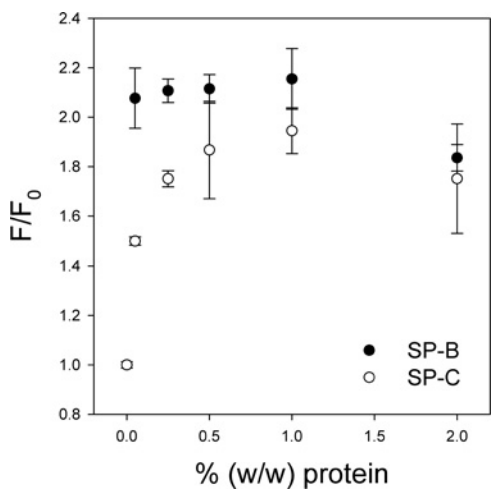

Figure 5 Fluorescence emission of the probe FM 1-43 in POPC multilamellar vesicles (200 μg/ml) as a function of protein density in membranes

electron microscopy, the ultrastructure of POPC LUVs prepared in the absence or in the presence of the whole hydrophobic surfactant protein fraction or 1 % (by mass) of purified SP-B or SP-C. Figure 6 shows representative images obtained by negative staining and transmission electron microscopy of these lipid and lipid–protein samples. Pure POPC suspensions contained a relatively homogeneous population of vesicles with homogeneous size, and presumably unilamellar character (Figure 6A), as well as the suspension of POPC supplemented with the mixture of SP-B and SP-C (Figure 6B). The POPC/SP-B suspension presented a high complexity, since it was totally made up of large, apparently multilamellar, membrane complexes with a diameter in the micrometre scale, despite the fact that they were originally extruded through 100 nm pores. The vesicles prepared with POPC plus 1 % SP-C showed a higher level of aggregation than pure POPC vesicles, but it still consisted of unilamellar and oligolamellar vesicles with a more or less spherical shape.

In order to achieve a direct visualization of the effect of surfactant proteins on the membrane labelling by FM 1-43, in a more homogeneous and controlled membrane structural context, a series of fluorescence microscopy experiments have been carried out in which we have monitored the ability of the probe to label the different membranes in oligolamellar GVs of POPC in the absence or presence of hydrophobic surfactant proteins. The large size of GVs prepared by electroformation allows their visualization under an optical microscope and the simultaneous examination of fluorescent probe partition and membrane macroscopic morphology. Figure 7 compares the morphology and FM 1-43 labelling of pure POPC oligolamellar GVs and GVs formed from POPC supplemented with the hydrophobic surfactant protein fraction (PF) obtained after LH-20 chromatography, at proportions mimicking lipid/protein ratios in surfactant organic extract. Two representative GVs of each sample are shown, exhibiting a clear oligolamellar structure under the optical microscope operated under phase contrast. Upon incubation with FM 1-43, pure POPC oligolamellar GVs were labelled only in the outermost layer (Figures 7B and 7D). In contrast, exposure to the probe produced almost instantaneous labelling of every membrane in POPC/PF vesicles (Figures 7F

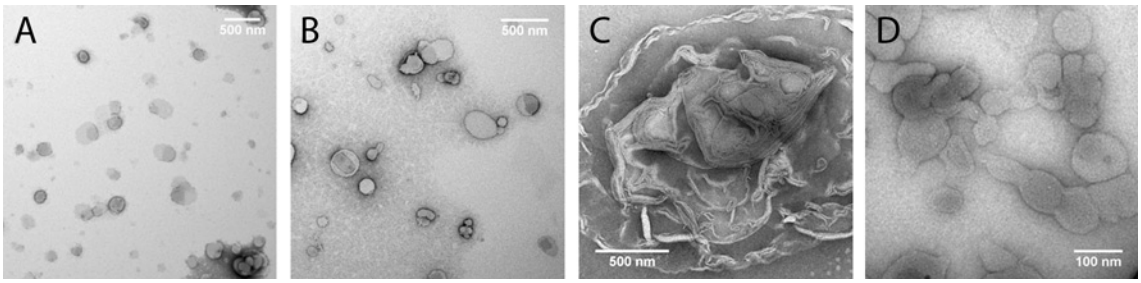

Figure 6 Electron microscopy images of vesicle suspensions prepared by extrusion, which correspond to different lipid–protein compositions

(**A**) POPC, (**B**) POPC supplemented with the hydrophobic protein fraction of pulmonary surfactant, (**C**) POPC with 1 % SP-B and (**D**) POPC with 1 % SP-C, by weight of phospholipids. Samples were prepared by negative staining.

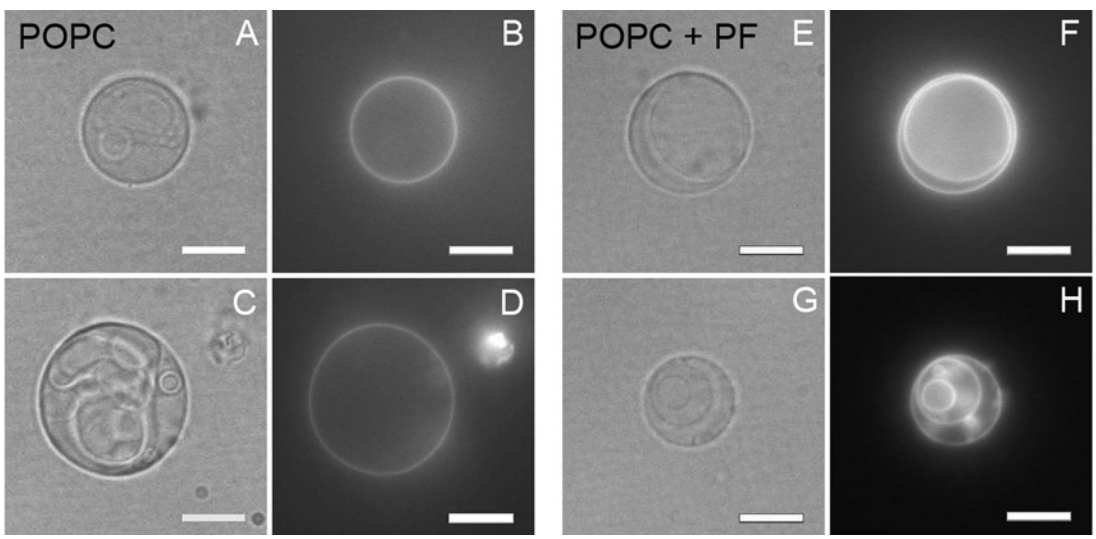

Figure 7 Giant oligolamellar vesicles of POPC (A–D) and POPC supplemented with the hydrophobic protein fraction of pulmonary surfactant (E–H)

(**A**, **C**, **E** and **G**) Transmission images. (**B**, **D**, **F** and **H**) Fluorescent images. All of the giant vesicles are labelled with FM 1-43. Scale bars correspond to 10 μm.

and 7H). Similar experiments were carried out with GVs made up of POPC supplemented with 1 % (by mass) of either purified SP-B or SP-C. Surprisingly, the morphology of these giant liposomes containing only one of the surfactant proteins was substantially different to that of liposomes containing no protein or the full hydrophobic protein fraction. No clear oligolamellar GVs could be seen that were made up of the POPC/SP-B mixture. As illustrated in Figure 8, suspensions of POPC/SP-B vesicles were entirely composed of apparently unilamellar giant liposomes, with different sizes and a strong trend towards aggregation (Figures 8A–8D), which were fully labelled by FM 1-43. Suspensions of POPC/SP-C vesicles contained a large number of oligolamellar liposomes, but most of them became very unstable when observed under the microscope, showing a high tendency to distortion, rupture and reorganization. Figure 9 shows sequential frames taken from a video recording, illustrating the rupture of two giant oligolamellar vesicles: at first, the shape of both vesicles looked very irregular and their membranes started fluctuating; then some membrane regions protruded and formed evaginations, which finally released smaller vesicles to the medium before again becoming spherical and stable. The complete recording is available at http://bbm1.ucm.es/biomil/video/Video_Parra_BJ_2011.avi. We never saw such dynamic behaviour in pure lipidic vesicles or in liposomes containing SP-B.

To further analyse the effect of surfactant proteins on the permeability of membranes to polar molecules, we tested the ability of the fluorescent dye calcein to permeate through POPC liposomes in the absence or presence of the proteins. Figure 10 illustrates how pure POPC GVs can be incubated for several hours in a calcein solution without internalization of the dye. Vesicles appeared as dark spheres when observed under the blue light used to excite calcein (Figure 10B). In contrast, incubation of vesicles of POPC supplemented with the hydrophobic surfactant protein fraction with calcein led to the entrance of the dye. Figure 10(E) illustrates how calcein entered into protein-containing POPC vesicles, showing even higher fluorescence than the liposome external medium. This indicates that equilibration of the calcein concentration across the membrane takes some time once the concentration of the dye in the solution has been diluted down. Calcein could also permeate through POPC liposomes containing only SP-B or SP-C, but with an apparently different pattern to that observed in liposomes containing the two proteins together. In the presence of either of the hydrophobic surfactant proteins, no difference in fluorescence emission could be seen between the different compartments (Figures 10H and 10K), indicating that calcein fluorescence equilibrated rapidly between the internal and external liposome compartments. Interestingly, images of calcein fluorescence in liposomes containing SP-B showed large segments of the membrane that were much darker than the

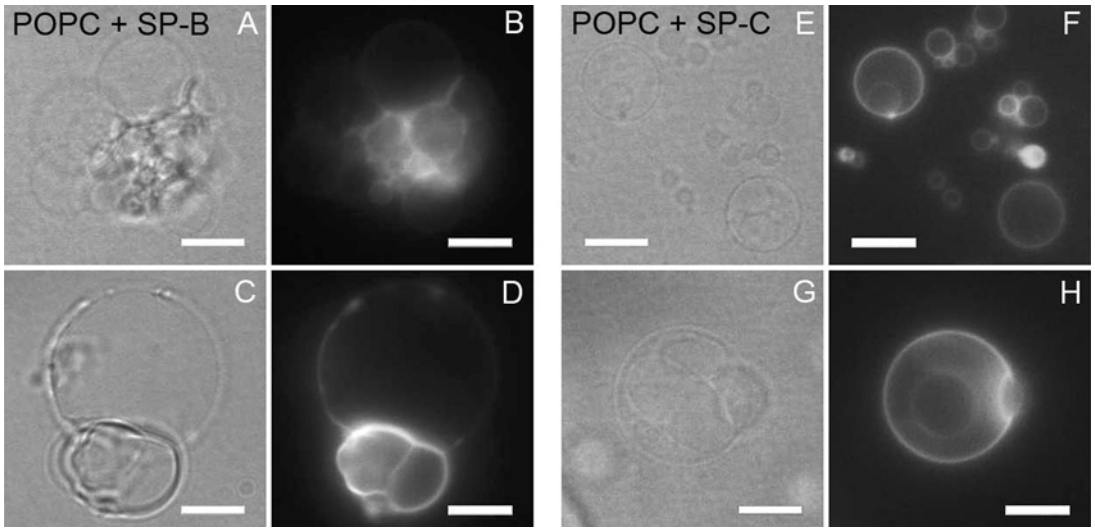

Figure 8 Giant oligolamellar vesicles of POPC supplemented with 1% (w/w) SP-B (A–D) and 1% (w/w) SP-C (E–H)

(**A**, **C**, **E** and **G**) Transmission images. (**B**, **D**, **F** and **H**) Fluorescent images. Giant vesicles are labelled with FM 1-43. Scale bars correspond to 10 μm.

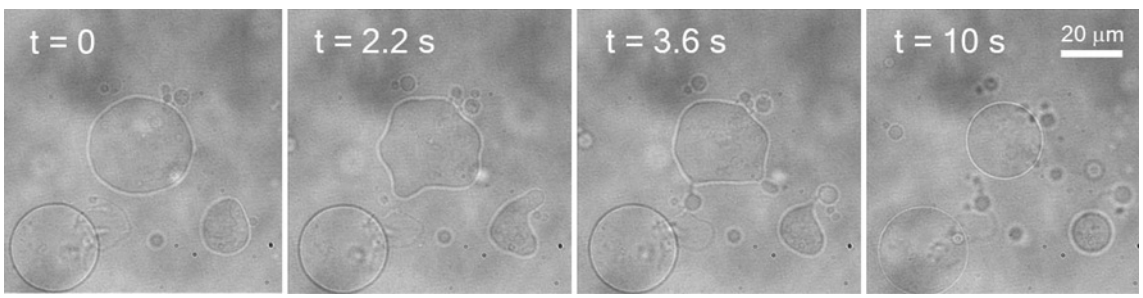

Figure 9 Image sequence extracted from a video recording

Giant vesicles of POPC supplemented with 1% (w/w) SP-C became very unstable and dynamic when observed under the microscope, even exocytotic-like processes were seen. The complete recording is available at http://bbm1.ucm.es/biomil/video/Video_Parra_BJ_2011.avi. Scale bar corresponds to 20 μm.

aqueous calcein solution, as if calcein would be highly excluded from perimembranal regions.

DISCUSSION

The ability of proteins SP-B and SP-C to introduce significant perturbations of structure and dynamics in surfactant phospholipid membranes has been largely documented. These perturbations have been mainly interpreted in the context of the role of the proteins to promote the structural transformations associated with pulmonary surfactant biogenesis, secretion and adsorption into the air–liquid interface. However, the intrinsic properties imparted by the particular lipid and protein composition to native-like pulmonary surfactant membranes have not been completely described. Little is known, for instance, with respect to the symmetric or asymmetric character of these membranes as they are assembled, or their permeability to polar solutes. We have tested the accessibility of membranes with different native-like or model lipid and protein composition to the membrane-fluorescent probe FM 1-43. This probe has been extensively used as a marker for lamellar body exocytosis, in order to obtain a direct visualization of pulmonary surfactant secretion in alveolar type II cells [25]. FM 1-43 stains intensely the whole lamellar body content immediately after the opening of the exocytotic fusion pore. This suggests the existence of a direct topological connection between all of the lamellar body membranes and/or the interlamellar compartments. Our starting hypothesis was that the assemblies in which hydrophobic proteins SP-B and SP-C participate are involved in the free diffusion of probes like FM 1-43 across surfactant membranes once surfactant is released from type II pneumocytes.

The present results confirm that the hydrophobic proteins SP-B and SP-C are responsible for making phospholipid membranes highly permeable to polar molecules, as had been largely suspected. The ability of these proteins to alter the permeability barrier of phospholipid membranes had been reported, but mainly as a consequence of their interaction with membranes upon injection as concentrated solutions in organic solvents [26–28]. In the present study, we demonstrate that (i) native surfactant membranes are indeed intrinsically permeable, (ii) proteins SP-B and SP-C are responsible for the permeability properties of surfactant structures, and (iii) hydrophobic surfactant proteins are by themselves able to make a simple phospholipid membrane highly permeable to both membrane and soluble probes. This could be consistent with the assembly in the membranes of some sort of proteinaceous or proteolipid pores, because the mere introduction of the hydrophobic surfactant proteins into a single lipid model membrane is enough to permeabilize it. Permeabilization of membranes by surfactant proteins produces

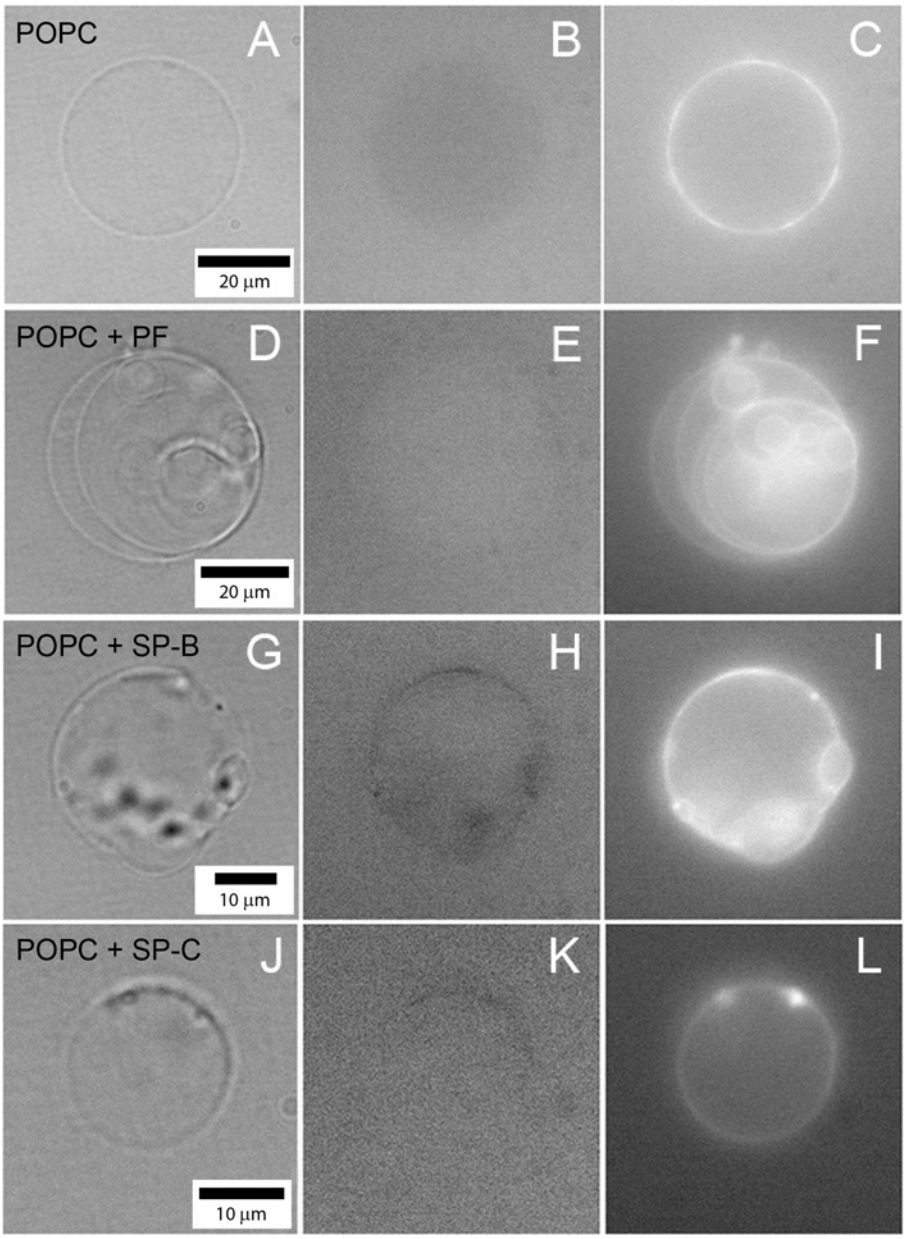

Figure 10 Giant vesicles of POPC (A–C), POPC supplemented with the hydrophobic protein fraction of pulmonary surfactant (D–F), with 1% (w/w) SP-B (G–I) and 1% (w/w) SP-C (J–L)

(**A**, **D**, **G** and **J**) Transmission images. (**B**, **E**, **H** and **K**) Fluorescent images obtained with an FITC filter set. (**C**, **F**, **I** and **L**) Fluorescent images obtained with a Texas Red filter set. Giant vesicles were incubated in a calcein solution for several hours, and then diluted in a glucose solution and finally labelled with FM 1-43 prior to the observation. See the Experimental section for more detail.

as a consequence a rapid equilibration of molecules, which are intrinsically impermeable through pure lipid membranes, among the different compartments. We cannot discard the idea that membrane-permeabilizing protein assemblies are also not promoting membrane–membrane contacts that would facilitate even further the rapid movement of polar and non-polar molecules through the different membranes and compartments. The effect of the proteins to facilitate lipid dynamics in large multilamellar arrays has been widely reported [15,29]. The results of the present study introduce the effects on membrane permeability as an additional factor on surfactant dynamics.

Several studies have already suggested a potential effect of surfactant proteins on membrane permeability. SP-B has been reported to promote association and fusion of phospholipid membranes [26,30]. This SP-B-promoted fusion of lipid vesicles was described as 'leaky', meaning that the protein-promoted merging of membrane compartments was always associated with leakage of at least part of the vesicle contents into the outer spaces. Our results suggest that leakage could not only occur at the fusion sites, but that membrane fusion and the subsequent transfer of the protein into the different lipid structures could end in the complete permeabilization of all of the membranes. This permeabilization could also be behind the reported ability of hydrophobic surfactant proteins to permeabilize membranes to ions [31], a property that could not be explained and has not been characterized any further. Also, we and others had noticed the problems in encapsulating polar solutes into membrane vesicles made from pulmonary surfactant, a relevant technology in the context of

drug-delivering strategies, but that may be more difficult to achieve than anticipated in the light of the present results. The difference in the kinetics of membrane probe equilibration is consistent with SP-B and SP-C promoting membrane permeability by different mechanisms. The almost instantaneous permeation of probes through phospholipid membranes containing minimal amounts of SP-B could be indicative of the protein forming true pores. The sequence of SP-B is homologous with saposins, a family of membrane-associated proteins that includes several recognized cytolysins and membrane-pore-forming structures [32–34]. We propose that pore-like oligomeric SP-B assemblies could be at the same time responsible for establishing membrane–membrane contacts and for facilitating rapid transfer of lipids and polar molecules between the contacted membrane compartments. In contrast, the kinetics of probe permeation by SP-C is much slower than that promoted by SP-B, and much more dependent on a high enough proportion of protein into the membranes. We propose that, in contrast with SP-B, membrane permeabilization by SP-C could be rather dependent on the deep perturbation of the membrane core by the protein. These profound perturbations could also be the cause of the extraordinarily dynamic behaviour imparted by SP-C into the membrane morphology, as we have observed in the GV fluctuations. The ability of SP-C to introduce a dynamic contribution into phospholipid membranes has already been outlined, in which the N-terminal, relatively polar, segment of the protein seems to participate significantly [35,36].

The results of the present study strongly suggest that the combination of SP-B and SP-C impart special properties to membranes, which are clearly distinct from the effects of each individual protein by itself. Surfactant membranes are the most stable in the simultaneous presence of both SP-B and SP-C, whereas the individual proteins seem to have apparently opposite destabilizing effects. SP-B alone promotes transformation of single vesicles into large, complex, presumably multilamellar, membrane structures. This ability of the protein to promote association and eventually fusion of membranes, with the important participation of protein–protein interactions, has in fact been widely documented [9,10,26,30,37]. SP-C, on the other hand, seems to strongly destabilize bilayers, promoting their disintegration and dispersion. This activity could be behind the ability of the protein to promote insertion of phospholipids into the interface [38,39]. However, the incorporation of SP-B–SP-C complexes, with the precise protein stoichiometry obtained from the natural surfactant mixtures, apparently maintains the morphology of the lipid–protein membranes, at least in the context of the models studied in the present paper, suggesting that SP-B and SP-C might modulate each other. An obvious possibility is that the two proteins participate in common macromolecular protein complexes in the context of surfactant membranes. The differences in permeability induced upon introduction of single or combined proteins into giant liposomes are very illustrative. In the presence of SP-B–SP-C complexes, lipid membranes are permeable to calcein, which can permeate through pores of presumably limited size, considering that dilution of external calcein does not produce a concomitant immediate dilution of calcein from the internal liposome compartments. Equilibration of inner and outer calcein concentrations is much faster in GVs containing either SP-B or SP-C, suggesting that the permeation structures assembled by a single protein permit a much more rapid flow of the probe. Although previous results certainly suggest that a concerted action of the two proteins facilitates breathing dynamics *in vivo* [40], we and others were unable to find evidence for specific SP-B–SP-C interactions [35]. In a recent study in which we have compared functional properties of systems prepared by reconstituting defined fractions of native surfactant, we have found that some differences exist between the behaviour of lipid–protein complexes prepared from the original mixtures and the behaviour of complexes reunited from isolated components [41]. It is possible that proper SP-B–SP-C complexes are poorly re-established once the proteins are re-mixed, perhaps because some unknown cofactors were lost, or because the proper conformation of the proteins is altered during the purification process. The results of the present study suggest that much care has to be taken to dissect the potential role and the structure–function relationships of surfactant proteins upon reconstitution of simplified systems that start from fully purified SP-B and SP-C. An imbalance in the appropriate SP-B/SP-C ratio or an inefficient re-assembly of potential multiprotein complexes may end in lipid–protein membranes with structural and functional properties differing greatly from those exhibited by native surfactant membranes. The most successful clinical surfactant preparations currently in use for the treatment of respiratory pathologies are derived from extracts of animal-derived surfactants [42]. These natural formulations probably preserve a fair proportion of the original surfactant protein complexes. Design and production of a new generation of therapeutic surfactants, based on the reconstitution of synthetic or recombinant human versions of surfactant proteins, will require a proper knowledge of the role of protein complexes and the way these complexes can be correctly established.

An important question is what the physiological meaning of the intrinsic permeable character of surfactant membranes is. It is possible that the permeability to polar solutes imparted to membranes by the surfactant protein complexes is only a consequence of the architecture of the machinery that ensures a rapid and efficient flow of surface-active lipid species along the membranous assemblies, all the way up to the interface. However, it is also possible that an efficient and unrestricted movement of polar molecules through the membrane structures developed by surfactant at the thin water layer lining the alveoli is also important for alveolar homoeostasis. It has been proposed that surfactant might form a sort of 'bi-continuous' membrane-based phase at the respiratory surface [7,43]. A fully interconnected network of membranes could be important to facilitate a rapid diffusion of lipids towards the interface, where they must form the surface-active film that reduces surface tension and stabilizes the lung. However, the continuity of all of the aqueous compartments could be equally important to ensure proper equilibrium of water and ions, and to facilitate free diffusion of soluble components such as many of those in charge of maintaining the sterility of the alveolar surface. Surface-active proteins and peptides, such as those currently under scrutiny as potential additives in artificial surfactants [44], could be active enough to ensure interfacial transfer of lipids and formation of surfactant films, but still be inefficient to form a fully functional bi-continuous membrane network. The elucidation of the molecular architecture and the determinants of potential surfactant protein complexes is therefore a must to improve the possibilities to develop new enhanced surfactant-based therapies.

AUTHOR CONTRIBUTION

The present study was conceived by Jesús Pérez-Gil, Antonio Cruz and Elisa Parra. Elisa Parra carried out most of the individual experiments, assisted by Lara Moleiro and Ivan López-Montero in the GV studies, which were also supervised by Francisco Monroy. Antonio Cruz helped particularly with the electron microscopy experiments and supervised all of the spectroscopic measurements. All of the authors were involved in the interpretation and discussion of the results, and the paper was written by Elisa Parra, Antonio Cruz and Jesús Pérez-Gil.

FUNDING

This work was supported by the Spanish Ministry of Science [grant numbers BIO2009-09694, FIS2009-14650-C02-01, CONSOLIDER-INGENIO 2010 CSD2007-00010]; the Community of Madrid [grant number S2009MAT-1507]; and Universidad Complutense.

REFERENCES

1 Serrano, A. G. and Perez-Gil, J. (2006) Protein-lipid interactions and surface activity in the pulmonary surfactant system. Chem. Phys. Lipids **141**, 105–118
2 Wright, J. R. (2005) Immunoregulatory functions of surfactant proteins. Nat. Rev. Immunol. **5**, 58–68
3 Seeger, W., Gunther, A., Walmrath, H. D., Grimminger, F. and Lasch, H. G. (1993) Alveolar surfactant and adult respiratory distress syndrome. Pathogenetic role and therapeutic prospects. Clin. Invest. **71**, 177–190
4 Hallman, M., Glumoff, V. and Ramet, M. (2001) Surfactant in respiratory distress syndrome and lung injury. Comp. Biochem. Physiol. A Mol. Integr. Physiol. **129**, 287–294
5 Goerke, J. (1998) Pulmonary surfactant: functions and molecular composition. Biochim. Biophys. Acta **1408**, 79–89
6 Veldhuizen, R., Nag, K., Orgeig, S. and Possmayer, F. (1998) The role of lipids in pulmonary surfactant. Biochim. Biophys. Acta **1408**, 90–108
7 Perez-Gil, J. (2008) Structure of pulmonary surfactant membranes and films: the role of proteins and lipid-protein interactions. Biochim. Biophys. Acta **1778**, 1676–1695
8 Melton, K. R., Nesslein, L. L., Ikegami, M., Tichelaar, J. W., Clark, J. C., Whitsett, J. A. and Weaver, T. E. (2003) SP-B deficiency causes respiratory failure in adult mice. Am. J. Physiol. Lung Cell. Mol. Physiol. **285**, L543–L549
9 Ryan, M. A., Qi, X., Serrano, A. G., Ikegami, M., Perez-Gil, J., Johansson, J. and Weaver, T. E. (2005) Mapping and analysis of the lytic and fusogenic domains of surfactant protein B. Biochemistry **44**, 861–872
10 Cruz, A., Worthman, L. A., Serrano, A. G., Casals, C., Keough, K. M. and Perez-Gil, J. (2000) Microstructure and dynamic surface properties of surfactant protein SP-B/dipalmitoylphosphatidylcholine interfacial films spread from lipid-protein bilayers. Eur. Biophys. J. **29**, 204–213
11 Glasser, S. W., Burhans, M. S., Korfhagen, T. R., Na, C. L., Sly, P. D., Ross, G. F., Ikegami, M. and Whitsett, J. A. (2001) Altered stability of pulmonary surfactant in SP-C-deficient mice. Proc. Natl. Acad. Sci. U.S.A. **98**, 6366–6371
12 Creuwels, L. A., Boer, E. H., Demel, R. A., van Golde, L. M. and Haagsman, H. P. (1995) Neutralization of the positive charges of surfactant protein C. Effects on structure and function. J. Biol. Chem. **270**, 16225–16229
13 Ross, M., Krol, S., Janshoff, A. and Galla, H. J. (2002) Kinetics of phospholipid insertion into monolayers containing the lung surfactant proteins SP-B or SP-C. Eur. Biophys. J. **31**, 52–61
14 Weaver, T. E., Na, C. L. and Stahlman, M. (2002) Biogenesis of lamellar bodies, lysosome-related organelles involved in storage and secretion of pulmonary surfactant. Semin. Cell Dev. Biol. **13**, 263–270
15 Bernardino de la Serna, J., Oradd, G., Bagatolli, L. A., Simonsen, A. C., Marsh, D., Lindblom, G. and Perez-Gil, J. (2009) Segregated phases in pulmonary surfactant membranes do not show coexistence of lipid populations with differentiated dynamic properties. Biophys. J. **97**, 1381–1389
16 Taeusch, H. W., de la Serna, J. B., Perez-Gil, J., Alonso, C. and Zasadzinski, J. A. (2005) Inactivation of pulmonary surfactant due to serum-inhibited adsorption and reversal by hydrophilic polymers: experimental. Biophys. J. **89**, 1769–1779
17 Perez-Gil, J., Cruz, A. and Casals, C. (1993) Solubility of hydrophobic surfactant proteins in organic solvent/water mixtures. Structural studies on SP-B and SP-C in aqueous organic solvents and lipids. Biochim. Biophys. Acta **1168**, 261–270
18 Rouser, G., Siakotos, A. N. and Fleischer, S. (1966) Quantitative analysis of phospholipids by thin-layer chromatography and phosphorus analysis of spots. Lipids **1**, 85–86
19 Mathivet, L., Cribier, S. and Devaux, P. F. (1996) Shape change and physical properties of giant phospholipid vesicles prepared in the presence of an AC electric field. Biophys. J. **70**, 1112–1121
20 Greenspan, P., Mayer, E. P. and Fowler, S. D. (1985) Nile red: a selective fluorescent stain for intracellular lipid droplets. J. Cell Biol. **100**, 965–973
21 Betz, W. J., Mao, F. and Smith, C. B. (1996) Imaging exocytosis and endocytosis. Curr. Opin. Neurobiol. **6**, 365–371
22 Arrais, D. and Martins, J. (2007) Bilayer polarity and its thermal dependency in the I_0 and I_d phases of binary phosphatidylcholine/cholesterol mixtures. Biochim. Biophys. Acta **1768**, 2914–2922
23 Theunissen, J. J., Jackson, R. L., Kempen, H. J. and Demel, R. A. (1986) Membrane properties of oxysterols. Interfacial orientation, influence on membrane permeability and redistribution between membranes. Biochim. Biophys. Acta **860**, 66–74
24 Bernardino de la Serna, J., Perez-Gil, J., Simonsen, A. C. and Bagatolli, L. A. (2004) Cholesterol rules: direct observation of the coexistence of two fluid phases in native pulmonary surfactant membranes at physiological temperatures. J. Biol. Chem. **279**, 40715–40722
25 Haller, T., Ortmayr, J., Friedrich, F., Volkl, H. and Dietl, P. (1998) Dynamics of surfactant release in alveolar type II cells. Proc. Natl. Acad. Sci. U.S.A. **95**, 1579–1584
26 Chang, R., Nir, S. and Poulain, F. R. (1998) Analysis of binding and membrane destabilization of phospholipid membranes by surfactant apoprotein B. Biochim. Biophys. Acta **1371**, 254–264
27 Cruz, A., Casals, C., Keough, K. M. and Perez-Gil, J. (1997) Different modes of interaction of pulmonary surfactant protein SP-B in phosphatidylcholine bilayers. Biochem. J. **327**, 133–138
28 Shiffer, K., Hawgood, S., Duzgunes, N. and Goerke, J. (1988) Interactions of the low molecular weight group of surfactant-associated proteins (SP 5-18) with pulmonary surfactant lipids. Biochemistry **27**, 2689–2695
29 Perez-Gil, J., Casals, C. and Marsh, D. (1995) Interactions of hydrophobic lung surfactant proteins SP-B and SP-C with dipalmitoylphosphatidylcholine and dipalmitoylphosphatidylglycerol bilayers studied by electron spin resonance spectroscopy. Biochemistry **34**, 3964–3971
30 Poulain, F. R., Nir, S. and Hawgood, S. (1996) Kinetics of phospholipid membrane fusion induced by surfactant apoproteins A and B. Biochim. Biophys. Acta **1278**, 169–175
31 Oelberg, D. G. and Xu, F. (2000) Pulmonary surfactant proteins insert cation-permeable channels in planar bilayers. Mol. Genet. Metab. **70**, 295–300
32 Leippe, M., Bruhn, H., Hecht, O. and Grotzinger, J. (2005) Ancient weapons: the three-dimensional structure of amoebapore A. Trends Parasitol. **21**, 5–7
33 Miteva, M., Andersson, M., Karshikoff, A. and Otting, G. (1999) Molecular electroporation: a unifying concept for the description of membrane pore formation by antibacterial peptides, exemplified with NK-lysin. FEBS Lett. **462**, 155–158
34 Patthy, L. (1991) Homology of the precursor of pulmonary surfactant-associated protein SP-B with prosaposin and sulfated glycoprotein 1. J. Biol. Chem. **266**, 6035–6037
35 Plasencia, I., Cruz, A., Casals, C. and Perez-Gil, J. (2001) Superficial disposition of the N-terminal region of the surfactant protein SP-C and the absence of specific SP-B–SP-C interactions in phospholipid bilayers. Biochem. J. **359**, 651–659
36 Plasencia, I., Rivas, L., Keough, K. M., Marsh, D. and Perez-Gil, J. (2004) The N-terminal segment of pulmonary surfactant lipopeptide SP-C has intrinsic propensity to interact with and perturb phospholipid bilayers. Biochem. J. **377**, 183–193
37 Poulain, F. R., Allen, L., Williams, M. C., Hamilton, R. L. and Hawgood, S. (1992) Effects of surfactant apolipoproteins on liposome structure: implications for tubular myelin formation. Am. J. Physiol. **262**, 730–739
38 Oosterlaken-Dijksterhuis, M. A., Haagsman, H. P., van Golde, L. M. and Demel, R. A. (1991) Characterization of lipid insertion into monomolecular layers mediated by lung surfactant proteins SP-B and SP-C. Biochemistry **30**, 10965–10971
39 Perez-Gil, J., Tucker, J., Simatos, G. and Keough, K. M. (1992) Interfacial adsorption of simple lipid mixtures combined with hydrophobic surfactant protein from pig lung. Biochem. Cell Biol. **70**, 332–338
40 Almlen, A., Stichtenoth, G., Linderholm, B., Haegerstrand-Bjorkman, M., Robertson, B., Johansson, J. and Curstedt, T. (2008) Surfactant proteins B and C are both necessary for alveolar stability at end expiration in premature rabbits with respiratory distress syndrome. J. Appl. Physiol. **104**, 1101–1108
41 Schurch, D., Ospina, O. L., Cruz, A. and Perez-Gil, J. (2010) Combined and independent action of proteins SP-B and SP-C in the surface behavior and mechanical stability of pulmonary surfactant films. Biophys. J. **99**, 3290–3299
42 Blanco, O. and Perez-Gil, J. (2007) Biochemical and pharmacological differences between preparations of exogenous natural surfactant used to treat Respiratory Distress Syndrome: role of the different components in an efficient pulmonary surfactant. Eur. J. Pharmacol. **568**, 1–15
43 Perez-Gil, J. and Weaver, T. E. (2010) Pulmonary surfactant pathophysiology: current models and open questions. Physiology (Bethesda) **25**, 132–141
44 Mingarro, I., Lukovic, D., Vilar, M. and Perez-Gil, J. (2008) Synthetic pulmonary surfactant preparations: new developments and future trends. Curr. Med. Chem. **15**, 393–403

Received 18 April 2011/13 June 2011; accepted 16 June 2011
Published as BJ Immediate Publication 16 June 2011, doi:10.1042/BJ20110681

Hydrophobic Pulmonary Surfactant Proteins SP-B and SP-C Induce Pore Formation in Planar Lipid Membranes: Evidence for Proteolipid Pores

Elisa Parra,[†] Antonio Alcaraz,[‡] Antonio Cruz,[†] Vicente M. Aguilella,[‡] and Jesús Pérez-Gil[†*]
[†]Department of Biochemistry and Molecular Biology, Faculty of Biology, Complutense University, Madrid, Spain; and [‡]Department of Physics, Laboratory of Molecular Biophysics, Universitat Jaume I, Castellón, Spain

ABSTRACT Pulmonary surfactant is a complex mixture of lipids and specific surfactant proteins, including the hydrophobic proteins SP-B and SP-C, in charge of stabilizing the respiratory surface of mammalian lungs. The combined action of both proteins is responsible for the proper structure and dynamics of membrane arrays in the pulmonary surfactant network that covers the respiratory surface. In this study, we explore the possibility that proteins SP-B and SP-C induce the permeabilization of phospholipid membranes via pore formation. To this end, electrophysiological measurements have been carried out in planar lipid membranes prepared with different lipid/protein mixtures. Our main result is that channel-like structures are detected in the presence of SP-B, SP-C, or the native mixture of both proteins. Current traces show a high variety of conductance states (from pS to nS) that are dependent both on the lipid composition and the applied potential. We also show that the type of host lipid crucially determines the ionic selectivity of the observed pores: the anionic selectivity observed in zwitterionic membranes is inverted to cationic selectivity in the presence of negatively charged lipids. All those results suggest that SP-B and SP-C proteins promote the formation of proteolipid channels in which lipid molecules are functionally involved. We propose that proteolipidic membrane-permeabilizing structures may have an important role to tune ionic and lipidic flows through the pulmonary surfactant membrane network at the alveolar surfaces.

INTRODUCTION

Pulmonary surfactant is a membrane-based system found in all pulmonated animals, which plays a crucial role to facilitate respiratory mechanics, stabilizing the air-water alveolar interface against the physical forces that induce alveoli to collapse (1). Furthermore, different components in surfactant are also responsible for the first innate response that is required to maintain the lung interface free of pathogens (2). The lack, deficiency, or inactivation of this system is associated with severe respiratory disorders such as the neonatal respiratory distress syndrome in premature babies (3) or the pulmonary dysfunction associated with acute respiratory distress syndrome in cases of lung injury (4).

Surfactant is a complex mixture of lipids and proteins, consisting of around 90% of lipids by mass, mainly phospholipids. An essential part (40–50% of the total mixture) is saturated phosphatidylcholines including dipalmitoylphosphatidylcholine, which is the main component responsible for reducing the interfacial surface tension down to nearly zero (5). There are also unsaturated phosphatidylcholines, anionic phospholipids such as phosphatidylglycerol (PG) and phosphatidylinositol, and an important fraction of neutral lipids, mainly cholesterol, which can account for up to 5–10% of the total lipid amount. The remaining 8–10% of the total mixture is constituted by specific proteins (6), which can be classified into two families: the hydrophilic proteins SP-A and SP-D, primarily related to the innate immune response in the alveolar barrier, and the hydrophobic proteins SP-B and SP-C, essential for the biophysical activity of pulmonary surfactant. Indeed, the presence of these two proteins is absolutely necessary for an efficient interfacial adsorption, film stability, and respreading processes of surfactant along the continuous compression-expansion breathing cycles (1).

SP-B is the only surfactant protein strictly required for breathing. Indeed, the absence of SP-B is associated with a lethal respiratory failure (7). SP-B is a 79-residue polypeptide, found as a 19 kDa homodimer in surfactant membranes (8). It belongs to the saposin-like protein family and consists of five amphipatic α-helices connected by highly apolar loops, exhibiting a positive net charge of $+7e$, which yield a preferential interaction with anionic phospholipids (9,10). In vitro, it has been shown that SP-B induces aggregation, fusion, and lysis of phospholipid vesicles (11), which has been associated with in vivo activities such as lipid transfer between bilayers and monolayers (12) and all the membrane restructuration processes that are required during the metabolic cycle of pulmonary surfactant. SP-B, for instance, is known to be essential for the formation of lamellar bodies, the organelles through which type II pneumocytes assemble, store, and secrete pulmonary surfactant membranes (13). It is also required, together with SP-A, for membrane rearrangement processes converting the onion-like lamellar body particles into net-like structures called tubular myelin that spread along the alveolar aqueous subphase. Unraveled from tubular myelin or independently of it, membranes are reorganized into layers near the interface to facilitate the transfer of surface-active

Submitted July 31, 2012, and accepted for publication November 12, 2012.
*Correspondence: jperezgil@bio.ucm.es
Editor: Ka Yee Lee.

0006-3495/13/01/0146/10 $2.00
http://dx.doi.org/10.1016/j.bpj.2012.11.014

species from the subphase into the interface and vice versa (see review (14)).

The other hydrophobic surfactant protein, SP-C, is the only component of pulmonary surfactant that has been found exclusively in the lung tissue (15). It has been described to be a monomer of 4.5 kDa and 35 residues that forms a single α-helix, 37 Å long, whose central 23 Å segment is highly hydrophobic and spans the thickness of a dipalmitoylphosphatidylcholine bilayer with a transmembrane orientation (16). The SP-C N-terminal tail exhibits a higher hydrophilicity providing to the protein a net charge of $+2e$. Cysteins 5 and 6 in this N-terminal segment are palmitoylated, contributing to maintain a tight association of this segment of the protein with bilayers and interfacial films (17). SP-C is believed to promote and stabilize membrane-membrane and membrane-interface contacts (18,19), facilitating lipid exchange between bilayers or between bilayers and monolayers, with a likely participation of the N-terminal segment, which has been reported to induce perturbations in lipid packing (20). The combined action of both SP-B and SP-C is considered to be responsible for the proper arrangement of functional membrane arrays in surfactant complexes.

The ability of hydrophobic surfactant proteins to perturb lipid packing and dynamics in membranes has been well established. On the one hand, the sequence of SP-B is homologous to saposins, a family of membrane-associated proteins that include several recognized cytolysins and membrane pore-forming structures (21–23). Amoebapores and NK-lysin, belonging also to the saposin family, induce current fluctuations upon interaction with phospholipid bilayers (24). On the other hand, some evidences have been found about the possible dimerization of SP-C in both organic solvents and lipid membranes (25,26), which could precede formation of larger oligomers and the creation of temporary defects or pores in membranes. In a previous work, it was shown that both SP-B and SP-C, either together in their physiological mixture or separately, alter the structure and permeability of phospholipid membranes (27).

Interestingly, the ability of both SP-B and SP-C proteins to permeabilize artificial phospholipid membranes and different clinical surfactant preparations (28,29) has been linked to the existence of some channel-mediated transport (30). In this study, we get deeper insight into the characterization of these effects by studying the permeability of planar lipid membranes (PLM) supplemented with SP-B and/or SP-C, as a function of several factors including lipid composition and membrane potential. We show that SP-B and SP-C, both together and also individually, create pores that are not as well defined as typical proteinaceous ionic channels. Indeed, we find a high variety of conductance states (from pS to nS) that are dependent both on the lipid composition and the applied potential. We also demonstrate that the type of host lipid crucially determines the ionic selectivity of the observed pores. Our results suggest that SP-B and SP-C induce permeabilization changes in membranes via the formation of proteolipidic pores, where the proteins could act as scaffolds to induce formation of lipidic pores, with the lipid polar heads lining totally or partially the pore wall.

MATERIALS AND METHODS

Materials

Native hydrophobic surfactant proteins were obtained from porcine lungs as described previously (31). Organic extraction of purified surfactant and chromatographic separation in Sephadex LH-20 (Pharmacia, Uppsala, Sweden) allowed obtention of the hydrophobic protein fraction (PF) separately from the surfactant lipid fractions (32,33). A subsequent chromatographic step in LH-60 yielded purification of SP-B and SP-C (33). Protein solutions were routinely checked for purity by SDS-PAGE and quantified by amino acid analysis. 1,2-dioleyl-*sn*-glycero-3-phosphocholine (DOPC), 1,2-dioleyl-*sn*-glycero-3-phospho-(1′-rac-glycerol) (DOPG), 1,2-diphytanoyl-*sn*-glycero-3-phosphocholine (DPhPC), and 1,2-diphytanoyl-*sn*-glycero-3-phosphoserine (DPhPS) were purchased from Avanti Polar Lipids (Alabaster, AL). Total phospholipid concentration in the different samples was determined by phosphorus analysis upon phospholipid mineralization. Proteins and lipids were stored as chloroform/methanol 2:1 (v/v) solutions at −20°C.

PLM

The experiments were carried out by using a very low amount (0.01% for PF and 0.005% for isolated SP-B or SP-C, with respect to lipid weight) of hydrophobic surfactant proteins supplemented in phospholipid bilayers. Two monolayers were made from 5 mg/ml pentane solutions of DOPC or DOPC/DOPG (85:15, w/w) mixture onto subphases buffered with 5 mM Hepes pH 6.0 at different KCl concentrations at both sides of the Teflon chambers partitioned by a 15 μm thick Teflon film with 70–100 μm diameter orifices. Planar lipid bilayers were formed by monolayer apposition on the orifices previously treated with a 1% solution of hexadecane in pentane. Proteins (SP-B, SP-C, or the physiological mixture of both, PF) in chloroform/methanol were supplemented to the lipid solutions before monolayer formation only in one of the chamber sides, the *cis* side. Bilayer formation was directly detected and its thickness could be estimated by capacitance measurements. All the experiments were carried out at 25 ± 1°C.

Channel conductance measurements

An electric potential was applied using Ag/AgCl electrodes in 2 M KCl, 1.5% agarose bridges assembled within standard 250 ml pipette tips. Potential is defined as positive when it is higher at the side of the protein addition (the *cis* side), whereas the *trans* side is set to ground. An Axopatch 200B amplifier (Molecular Devices, Sunnyvale, CA) in the voltage-clamp mode was used for measuring the current and applying potential. The membrane chamber and the head stage were isolated from external noise sources with a double metal screen (Amuneal Manufacturing, Philadelphia, PA).

Reversal potential measurements

Lipoprotein bilayers were formed with different salt concentrations at each side. A net ionic current appeared due to the concentration gradient, and it was manually set to zero by adjusting the applied potential. The potential needed to achieve zero current was then corrected by the liquid junction potential calculated from Henderson's equation to obtain the zero current potential or reversal potential (E_{rev}) (34).

RESULTS

Hydrophobic surfactant protein fraction in DOPC and DOPC/DOPG bilayers

Planar membranes formed by zwitterionic DOPC or by the negatively charged DOPC/DOPG (85:15, w/w) lipid mixture are impermeable to ions, at least in the range of applied voltages ($V < 150$ mV) and in the timescale of these experiments. However, when these lipids were supplemented with the total hydrophobic PF purified from porcine pulmonary surfactant complexes, we found a high pore-forming activity showing a wide variety of conductance states. Some of the recorded current traces are presented in Fig. 1 *A* for DOPC plus PF and in Fig. 1 *B* for DOPC/DOPG plus PF bilayers (protein/lipid ratio of 0.01% by weight, ~$1/10^5$ in molar ratio). The current versus time recordings do not show well-defined and highly reproducible unitary conductances characteristic of protein channels. Quite the opposite, current values and lifetimes of these states were very heterogeneous, even for the same applied voltage. Such variability allows several explanations: the coexistence of diverse channels in the bilayer, including a different number of protein monomers forming the pores and/or different protein conformations; the existence of one single kind of channel with a variety of substates, or the combination of both.

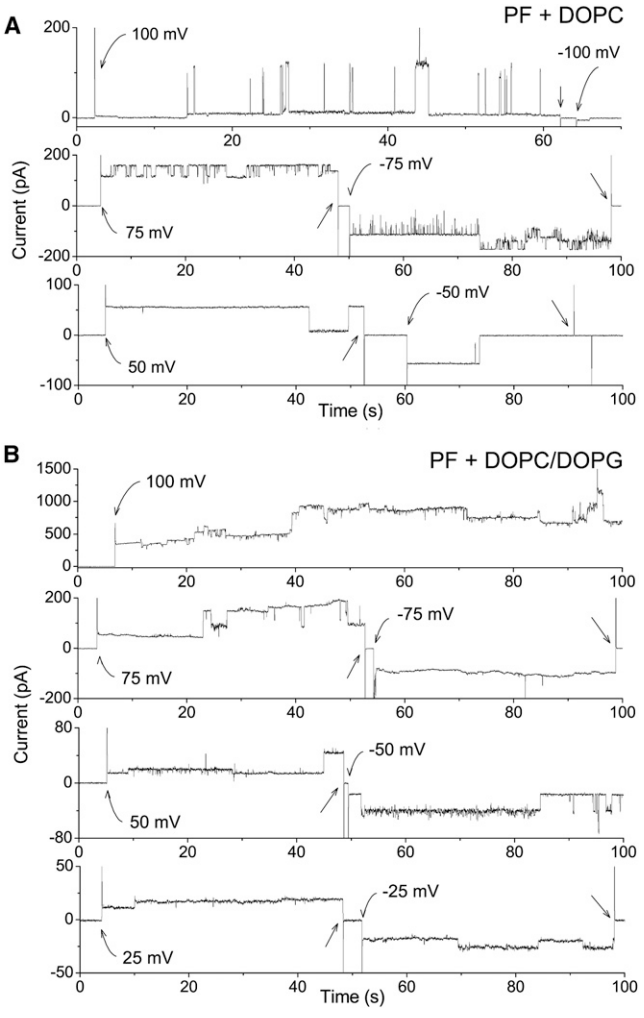

FIGURE 1 Effect of the hydrophobic surfactant protein fraction on the conductivity of zwitterionic and anionic phospholipid membranes. Several representative current versus time traces recorded for different applied voltages in DOPC (*A*) or DOPC/DOPG (85:15, w/w) (*B*); bilayers supplemented with the hydrophobic protein fraction of native surfactant, at a protein/lipid ratio of 0.01% by weight, in 5 mM Hepes 100 mM KCl solution, pH 5.5. Each trace corresponds to a different casted bilayer. Traces were subsequently filtered using a Bessel (8-pole) filter with a 50Hz −3dB cutoff frequency.

Histograms representing the conductance (G) levels of the current traces are shown in Fig. 2 *A*. Regardless of the lipid composition, a large dispersion in the measured conductance is observed. Under such conditions, we did not find a unitary or characteristic single-channel conductance. Small pores with conductance up to 100 pS were the most common, but we also found almost a continuous distribution of values ranging from tens of pS to several nS. We wondered whether the large values of conductance shown here in Fig. 1 correspond to multiple insertions of small pores rather than to individual wide pores. To discriminate between single- and multiple-channel conductances, a visual examination of the records shown in Fig. 1 was used to find the stepwise changes in each trace. Normalized histograms were then calculated from the conductance difference (ΔG) of the stepwise transitions as shown in Fig. 2 *B*. The plots of ΔG are almost identical to those of the absolute value of G, indicating that large values of ΔG are repeatedly obtained from single stepwise transitions. Because these large steps present long lifetimes without any small flickering (see the *bottom trace* in Fig. 1 *A*), it points to the existence of wide independent structures rather than to the simultaneous opening of the most abundant small structures. Apparently, the lipid composition does not have a dramatic impact on the histograms shown in Fig. 2 *A* and Fig. 2 *B*. In both zwitterionic and anionic lipid membranes, a somewhat continuous distribution of ΔG can be observed between tens of pS and several nS. However, a close inspection of the histograms reveals a subtle feature: the most frequent values of the stepwise changes in conductance are 93 pS in neutral DOPC and 55 pS in negatively charged DOPC/DOPG membranes.

Looking for additional insights about the pore structure, we also analyzed the effect of applied voltage on channel conductance G, as shown in Fig. 2 *C*. The obtained conductance values were classified as measured either at low (5–50 mV) or high voltages (75–100 mV). Note that we refer always to absolute values, as we observed no differences between applying positive or negative voltages. In the case of DOPC membranes high applied voltages increase significantly the probability of finding narrow pores, although the position of the maximum probability remains almost unchanged. This suggests that wide pores may

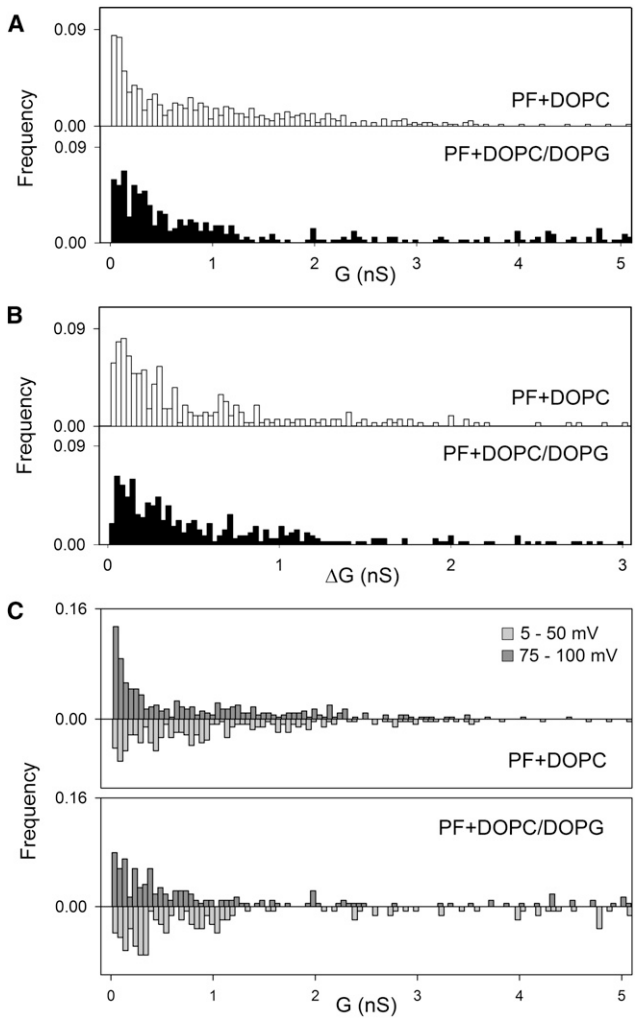

FIGURE 2 Quantitative analysis of the effect of surfactant proteins on the conductivity of zwitterionic and anionic phospholipid membranes. Normalized histograms representing all the conductance levels G (*A*) and conductance increments ΔG (*B*) recorded during the experiments with the hydrophobic protein fraction of native surfactant inserted in DOPC (*white bars*) or DOPC/DOPG (*black bars*) bilayers at a protein/lipid ratio of 0.01% by weight. Values of G and ΔG were calculated from average I and ΔI measurements divided by the correspondent applied voltage. In *C*, normalized histograms represent the recorded G-values classified by the voltage that was applied in each measurement: high voltages (75–100 mV, *dark gray*) and low voltages (5–50 mV in absolute value, *gray inverted bars*). These measurements were done in 5 mM Hepes 100 mM KCl solution, pH 5.5. Around 30 different bilayers were casted for each sample, obtaining from them around 400 G- and 200 ΔG-values in each case.

undergo a structural change or closure induced by voltage that does not affect the structure of the narrower ones. This could be due to squeezing out of solvent at high voltages, an effect already observed in membranes pretreated with hexadecane, as is the case here. In contrast, the effect of voltage in DOPC/DOPG membranes is just the opposite. The distribution of relative frequencies is not altered by voltage, although the position of the maximum is slightly shifted. The most frequent conductances are higher for low voltages (around 0.3 nS) than for high voltages (50 pS).

Hitherto, we have shown how the lipid composition determines not only the amplitude histograms of conductance but also their voltage dependence, suggesting a direct incorporation of lipid into the pore structure. Thus, the lipid charge is likely to be critical for the channel selectivity. To explore this possibility, we carried out selectivity experiments for the entire hydrophobic surfactant protein fraction supplemented to both DOPC and DOPC/DOPG bilayers, as shown in Fig. 3 *A*. In the presence of a salt gradient concentration between both sides of the bilayer and no applied voltage, there is a net flux of ions and hence an electric current appears. By measuring the applied voltage that is needed to zero the electric current (the so-called reversal potential, E_{rev}), it is possible to investigate the preferential passage of either positive or negative ions. In a zwitterionic phospholipid bilayer such as that formed by DOPC, the pores were found to be selective to anions (*upper part* of Fig. 3 *A*). This fact is consistent with the positive net charge of both SP-B and SP-C, and, consequently, of the whole membrane surface. It is interesting to stress that no significant differences were observed between adding the proteins to the *cis* or to the *trans* side of the experimental cell while keeping the same KCl concentration ratios (results not shown), which suggests that there is no charge asymmetry with respect to the membrane plane. Interestingly, the incorporation of only 15% of DOPG by total weight of phospholipids into DOPC bilayers causes a dramatic impact. Regardless of the electrolyte concentration ratio, all the measured reversal potentials were negative (*bottom part* of Fig. 3 *A*), yielding a cationic selectivity. A similar selectivity inversion has also been observed in DPhPC (zwitterionic) and DPhPC/DPhPS (negatively charged) bilayers (results not shown here), indicating that it is the charge of the lipid polar head that originates this phenomenon. The critical importance of the lipid charges was already shown in the work by Oelberg and Xu (30), who used negatively charged membranes and reported cationic selectivity, consistently with the results presented here.

The qualitative interpretation of Fig. 3 *A* can be complemented using the well-known Goldman-Hodgkin-Katz equation to calculate the permeability ratio $P = P_+/P_-$ (35). Thus, the pores in DOPC bilayers are around 2.0–5.5 times more selective for Cl^- than for K^+, whereas in DOPC/DOPG bilayers the pores were between 2 and 2.5 times more selective for K^+ than for Cl^-. Therefore, the pores formed by the physiological mixture of SP-B and SP-C appear to be somehow more selective in zwitterionic than in negatively charged bilayers, probably because negative charges of PG counteract or neutralize the electrostatic interactions between Cl^- ions and positive charges of the polar residues of the proteins.

It is also worth mentioning that the measured values of the reversal potential in Fig. 3 *A* display a considerable

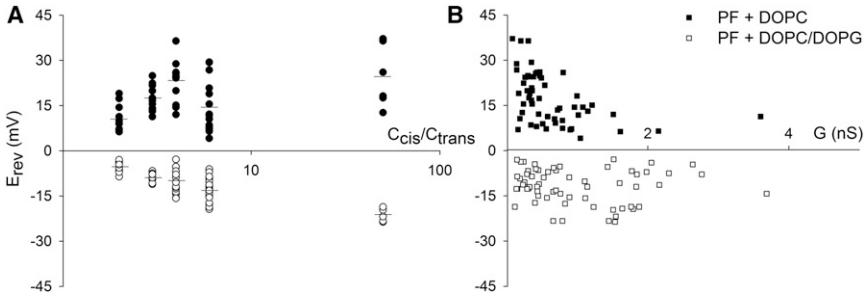

FIGURE 3 Ionic selectivity in zwitterionic and anionic phospholipid membranes containing the hydrophobic surfactant protein fraction. (*A*) Reversal potential versus KCl gradient concentration (50 mM trans side; 100, 150, 200, 300, and 2500 mM *cis* side) for DOPC (*solid circles*) or DOPC/DOPG 85:15 (*open circles*) bilayers supplemented with the hydrophobic protein fraction at a protein/lipid ratio of 0.01% by weight. Logarithmic scale has been used for the *x* axis. All the measured values have been plotted, and the black line represents the average of the measurements for each gradient concentration. (*B*) Reversal potential versus conductance for all the experiments performed with the hydrophobic protein fraction supplementing DOPC (*solid circles*) or DOPC/DOPG 85:15 (*open circles*) bilayers.

dispersion that is clearly beyond the experimental error. Such a scattered pattern is consistent with the existence of multiple independent pore structures as suggested by the data of Fig. 1. Note that the reversal potential of a collection of identical channels is independent of the actual number of them and should yield the same selectivity as a single unit (35). Therefore, if the variety of high conductance states found in Fig. 1 were actually originated by clusters of small structures, dispersion of reversal potential measurements would be within the experimental error.

We aimed to go a step further in the correlation between reversal potential (~selectivity) and pore conductance (~size); therefore, we calculated the conductance of the bilayer in each selectivity experiment, considering the full current-voltage (I-V) curve (note that when the I-V plot is linear, the slope gives the conductance and the intercept with V axis corresponds to the reversal potential). The correlation between E_{rev} and G can be seen in Fig. 3 *B*. Although the results are clearly scattered, a general trend could be observed, especially in the case of PF+DOPC (*solid symbols*): higher conductances correspond to lower reversal potentials, which means lower selectivity. This sounds reasonable, because narrow channels display a low conductance and a high discrimination because of the tight interaction between the permeating ions and the charges in the pore wall, whereas wider pores provide an easier and faster pathway at the price of losing selectivity (36). However, we should be cautious about this, because the scenario is likely to be much more complex: in different experiments we have found structures with a similar conductance but very different reversal potential.

Independent action of SP-B and SP-C in DOPC/DOPG bilayers

Having come this far, we can wonder whether the pore formation observed for the physiological SP-B/SP-C mixture is related to the sole action of one of the proteins or if alternatively, both of them are necessary. Experiments performed in planar lipid bilayers made of the DOPC/DOPG (85:15) mixture containing low amounts of either SP-B or SP-C (0.005% protein to lipid by weight, around $5\cdot10^{-6}$ for SP-B and 10^{-5} for SP-C in molar ratio) are shown in Fig. 4, *A* and *B*, respectively. Interestingly, each protein is able to induce pore formation, and both of them display a huge variety of conductance levels and current flickering. As in the case of the native mixture of SP-B and SP-C, a visual examination of the recorded traces shows large stepwise conductances for both proteins. This suggests that high conductance states are probably due to independent wide pores rather than to the concerted action of a cluster of small channels. Thus, in the top trace of Fig. 4 *A* (SP-B), we can observe a closure of around 2 nS and a subsequent opening of around 3 nS. In Fig. 4 *B* (SP-C) a conductance state of around 0.3 nS appears when applying 75 mV (*second trace from top*), and later on, two consecutive opening and closing events occur with stepwise conductances of 0.2 and 0.7 nS, respectively.

The histograms of conductance for each individual protein, shown in Fig. 5, resemble qualitatively the results found for the complete protein fraction in Fig. 2. At first sight, Fig. 5 *A* seems to indicate a slight difference between the two proteins. SP-B supplemented in DOPC/DOPG bilayers showed a wide range of conductances; being the most commonly recorded around 40 pS. In contrast, the most frequent conductance found for SP-C was around 0.3 nS. However, a more careful analysis considering the stepwise conductance (ΔG) distributions (see Fig. 5 *B*) rules out this possibility and yields similar conductance levels for both proteins. The most frequent recordings in Fig. 5 *B* were found to be 0.21 nS for SP-B and 0.16 nS for SP-C in DOPC/DOPG bilayers. This means that the most frequent stepwise conductance is larger for each protein individually than for the native mixture of both proteins (0.05 nS in Fig. 2 *B*). We also analyzed the effect of the applied potential in the independent SP-B and SP-C conductances measured in DOPC/DOPG bilayers, as shown in Fig. 5 *C*. In the case of SP-B the conductance distribution seems to be independent of applied voltage: there is no significant difference between low (5–50 mV) and high voltages (75–100 mV). In contrast, the normalized histograms for SP-C display a different scenario: the most common conductances at low applied voltages become much less frequent at higher potentials yielding a broader and less clear peak distribution.

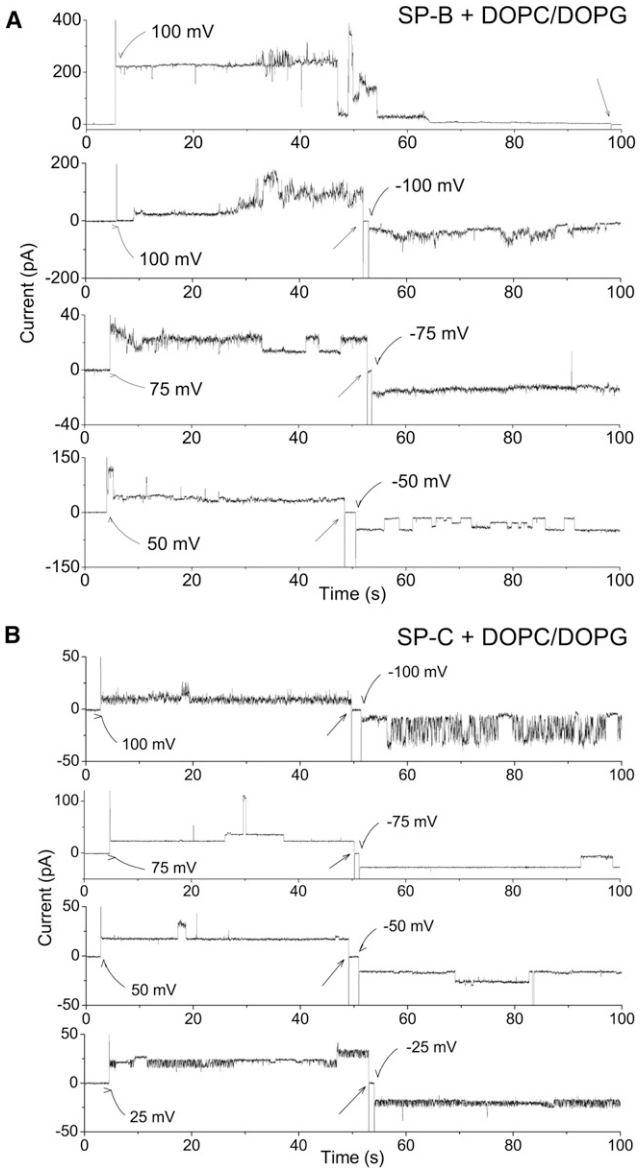

FIGURE 4 Effect of isolated protein SP-B or SP-C on the conductivity of anionic phospholipid membranes. Plotted are several representative current versus time traces recorded for different applied voltages in DOPC/DOPG 85:15 bilayers supplemented with SP-B (*A*) or SP-C (*B*) at a protein/lipid ratio of 0.005% by weight of phospholipids (around $5\cdot10^{-6}$ for SP-B and 10^{-5} for SP-C in molar ratio), in 5 mM Hepes 100 mM KCl solution, pH 5.5. Each trace corresponds to a different casted bilayer. Traces were subsequently filtered using a Bessel (8-pole) filter with a 50Hz −3dB cutoff frequency.

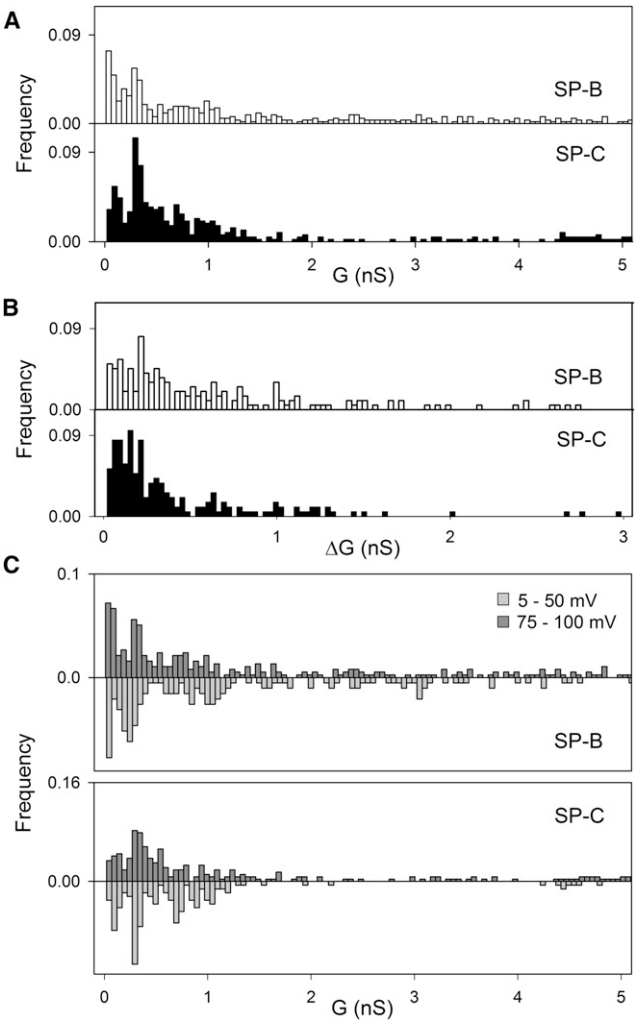

FIGURE 5 Quantitative analysis of the effect of isolated protein SP-B or SP-C on the conductivity of anionic phospholipid membranes. Normalized histograms representing all the conductance levels G (*A*) and conductance increments ΔG (*B*) recorded during the experiments with DOPC/DOPG 85:15 bilayers supplemented with SP-B (*white bars*) or SP-C (*black bars*) at a protein/lipid ratio of 0.005% by weight. Values of G and ΔG were calculated from average I and ΔI measurements divided by the correspondent applied voltage. In *C*, normalized histograms represent the recorded G-values classified by the voltage that was applied in each measurement: high voltages (75–100 mV, *dark gray*) and low voltages (5–50 mV in absolute value, *gray inverted bars*). These measurements were done in 5 mM Hepes 100 mM KCl solution, pH 5.5. Around 20 different bilayers were casted for each sample, obtaining from them around 500 G- and 200 ΔG-values in each case.

Reversal potential experiments in Fig. 6, *A* and *C*, show that both SP-B and SP-C form cation selective pores in DOPC/DOPG bilayers with a preference for K^+ over Cl^-. The corresponding permeability ratios P_+/P_- are in the range 1.9–2.6 for SP-B and 2.0–2.8 for SP-C. Because the selectivity of SP-B and SP-C pores is so similar despite the difference in the net charge of the proteins (+7 versus +2) suggests that the selectivity is mostly regulated by the lipid charge. Indeed, when selectivity experiments were done in zwitterionic DOPC bilayers (experiments not shown), pores formed by SP-B showed a preference for anions over cations, in agreement with the net charge of the protein (+7), whereas SP-C, in contrast, did not show a well-defined selectivity. Although average values would correspond to nonselective pores, we recorded small values of E_{rev} that were either positive or negative. This observation could occur because the net charge of the protein is still positive but considerably less important (+2) so that the

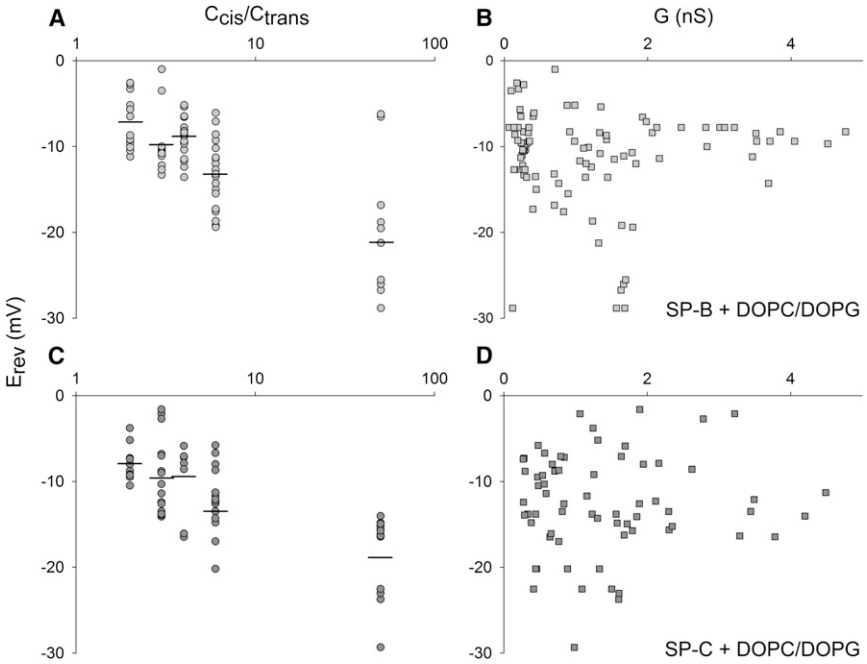

FIGURE 6 Ionic selectivity in anionic phospholipid membranes containing isolated protein SP-B or SP-C. (*A* and *C*) Reversal potential versus KCl gradient concentration (50 mM *trans* side; 100, 150, 200, 300, and 2500 mM *cis* side) for DOPC/DOPG 85:15 bilayers supplemented with SP-B (*A*) or SP-C (*C*) at a protein/lipid ratio of 0.005% by weight. Logarithmic scale has been used for the *x* axis. All the measured values have been plotted, and the black line represents the average of the measurements for each gradient concentration. (*B* and *D*) Reversal potential versus conductance for all the experiments performed with SP-B (*B*) or SP-C (*D*) supplementing DOPC/DOPG 85:15 bilayers.

experimental error is comparable to the absolute value of the reversal potential.

The relationship between pore conductance and reversal potential is shown for SP-B and SP-C in Fig. 6, *B* and *D*, respectively. The points are considerably scattered, therefore a possible correlation between pore size and selectivity is not as evident as in the native mixture of SP-B and SP-C shown in Fig. 3 *B*.

DISCUSSION

Numerous studies have reported the ability of hydrophobic surfactant proteins to alter the permeability of phospholipid membranes to polar solutes (8,11,14,16,27,28). This property has been usually linked to their properties to perturb lipid packing in membranes, required to facilitate the transfer of surface active species between surfactant membranes and the air-liquid interface. However, and beyond large membrane restructuration, it was recently shown that the mere presence of SP-B, SP-C, or both proteins together, make phospholipid membranes intrinsically permeable to polar, even charged, molecules (27). In this study, we have shown that SP-B and SP-C, both together and also individually, create an enormous diversity of defects or pores in phospholipid membranes, with no characteristic size or conformation in the experimental conditions tested here. Indeed, we have found a high variety of conductance states (from pS to nS) that are dependent both on the lipid composition and the applied potential. We have also shown that the type of host lipid crucially determines the ionic selectivity of the observed pores. These results suggest that SP-B and SP-C create pores not as well defined as typical proteinaceous ionic channels, but promote the local breakdown of the membrane bilayer structure creating pores with a surface formed partially or totally by polar lipid groups. SP-B belongs to the saposin-like family of proteins, which includes several members with detergent-like activity and true pore-forming toxins. This study reveals that the ability of SP-B to alter the permeability barrier of surfactant membranes could be not just the consequence of transient detergent-like local perturbations but of the assembly of long-living protein-lipid pore structures. A preliminary study had already proposed that a clinical surfactant preparation, with poorly defined lipid and protein composition, could contain ionic pores (30), although the unitary single-channel conductances of around 50 pS detected in those experiments were far from the large dispersion of small and wide pores found in our experiments with well-defined surfactant proteolipid membranes.

Each of the two proteins, SP-B and SP-C, seem able to produce a wide range of different conductances. A similar behavior has been observed in the pores formed by certain antibiotic peptides, such as colicin, which present two different conformations that are reflected in the recordings as two kinds of substates, a closed state with low conductance and an open state with high conductance (~0.05 nS and ~0.3–0.4 nS, respectively for colicin E1 in DPhPC bilayers) (37). In the case of SP-B and SP-C, there is no such sharp distinction between substates (see Fig. 2), perhaps because the possible conformations that these proteins adopted upon pore formation are more diverse. This may include the presence of different possible oligomerization states (38). The fact that, for the most frequent stepwise conductance, each protein yields individually larger values

than those found for the native mixture of both proteins (*0.05 nS* in Fig. 2 *B*) led us to hypothesize that in the entire protein fraction, SP-B might complex with SP-C to form a combined channel oligomer with average smaller aperture. The combined action of SP-B and SP-C could therefore somehow modulate the permeability of surfactant membranes and their ability to control transmembrane movement of charged species.

Several evidences in the current study support the concept that phospholipids take part of the surfactant protein-promoted permeabilizating structures. Although we have found that the full surfactant protein fraction PF introduces a continuous distribution of ΔG between tens of pS and several nS in both zwitterionic and anionic lipid membranes, the most frequent values of the stepwise changes in conductance are larger in neutral DOPC (93 pS) than in negatively charged DOPC/DOPG (55 pS). In principle, the negatively charged lipid headgroups in the vicinity of the channel would be expected to accumulate positive ions in excess of their bulk concentration, increasing then the pore conductance. Indeed, this is the observed effect in model protein channels like gramicidin A, alamethicin, or the bacterial porin OmpF (39–41). However, no such clear trend has been observed in proteolipidic pores. Malev et al. (42) reported that negatively charged lipids decreased the conductance of the syringomycin E channel at low electrolyte concentration and they had no clear effect in concentrated solutions. They suggested that the screening of the positive charges of the peptide and the lipid negative charges worked in opposite directions, partially compensating each other. We speculate that this could be also the case here. The negative charges of the DOPG lipid could balance or even overcompensate the effect of positive charges of both SP-B and SP-C proteins.

The fact that the ionic selectivity is inverted in the presence of negatively charged phospholipids compared with the behavior of the simultaneous presence of SP-B and SP-C in zwitterionic membranes, also argues in favor of a proteolipidic channel structure. Surfactant proteins might therefore promote or stabilize the opening of lipid-coated holes in phospholipid membranes, in the line of the so-called toroidal pores induced by other membrane-active peptides (43,44). Still, it remains to be demonstrated that the lipid molecules do actually line the protein-promoted membrane pores. It is also conceivable that the change in lipid selectivity promoted by acidic phospholipids could be alternatively due to a completely different organization of protein oligomers into the membrane. However, the high hydrophobicity of these proteins and their reported ability to facilitate rapid diffusion of lipids within surfactant membrane complexes (27), leads us to believe that the lipids must be lining the pores, at least partially. Different protein oligomers, either combining or not different proteins, could result in a range of different conductances such as those revealed by our experiments. The variety of conductive states could also represent a highly dynamic behavior, in which association/dissociation processes, involving or not protein homo- or heterooligomerization, could lead to fluctuations in membrane permeability. It has been reported that surfactant proteins SP-B and SP-C exhibit some affinity for negatively charged phospholipid species (9,10), with some controversy with respect to the actual specificity toward PG (45, 46), an essential phospholipid in surfactant activity. Affinity for anionic lipids is modulated by the ionic strength (9,10). It is therefore possible that the different ionic media used to analyze ion selectivity promote changes in lipid-protein interactions and in the oligomerization levels and conformational states of the proteins, all contributing to the complex picture observed in terms of multiple coexisting conductance situations. The conductive states that are the most relevant under physiological conditions remain to be determined.

We are aware that our results cannot be easily extrapolated to the biological system. It is evident that we are not taking into consideration the complex lipid composition in native surfactant membranes, and experiments have not been done at the physiological temperature. However, it is meaningful that these two small lipoproteins, isolated from its natural environment, could create such a significant change in a simple model membrane such as the one studied here. It had already been observed that the presence of SP-B and/or SP-C also increases dramatically the permeability of membranes made of the full lipid fraction of native surfactant (27). We have tried to prepare PLMs using the full lipid fraction of surfactant, but these membranes had a highly fluctuating character, with complex basal conductance states even in the absence of proteins (not shown), and were extremely unstable. This indicates that surfactant membranes with full compositional complexity could still be highly permeable but much more dynamic than the simplified models tested here.

The results we present here open, in our opinion, further interesting questions about the proteins themselves, which merit further research. For instance, it is intriguing how SP-C, with its extremely hydrophobic transmembrane helix, could affect the bilayer integrity to open aqueous pores. We speculate that a potentially important role may be played by the polar N-terminal segment of the protein, a region with the intrinsic potential to interact with and permeabilize phospholipid membranes (29,47). SP-B has been involved in modulating the mechanical properties of pulmonary surfactant membranes and films (48,49). A question of interest is how much the alteration of membrane geometry that leads to SP-B-promoted membrane permeabilization sustains the effect of the protein to stabilize multilayered films against mechanical perturbations. Finally, the SP-B and SP-C membrane poration activities reported here are highly indicative of the existence of high-order oligomerized states for the two proteins in membranes, something that has been previously proposed (38,50) but whose correlation with

the role of the proteins in surfactant is still not properly understood.

With respect to the biological significance of the existence of pores in surfactant membranes, we speculate that it could be related to the necessity of a continuous aqueous medium in the respiratory subphase to make it completely accessible for all the soluble molecules involved in innate defense (collectins, defensins are all hydrophilic molecules) and other processes in the lung interface (51). A highly permeable character of the membrane network formed by surfactant could be also important for a proper equilibrium of fluid and ions along the whole alveolar subphase. Permeability to polar molecules could be an intrinsic feature of what has been proposed as a potential bicontinuous surfactant membrane phase (14), evolutionarily optimized to permit simultaneously rapid diffusion of hydrophobic surface active species toward the respiratory interface and soluble molecules through the alveolar hypophase.

We acknowledge funding from the Spanish Ministry of Economy and Competitivity (BFU2010-11538-E, BIO2012-30733, FIS2010-19810, CSD2007-0010), Fundació Caixa Castelló-Bancaixa (P1-1A2009-13), Generalitat Valenciana (Prometeo 2012/069), Madrid Regional Government (S2009MAT-1507), and a fellowship from the Spanish Society for Pneumology and Thoracic Surgery (SEPAR 956/2010).

REFERENCES

1. Serrano, A. G., and J. Pérez-Gil. 2006. Protein-lipid interactions and surface activity in the pulmonary surfactant system. *Chem. Phys. Lipids.* 141:105–118.
2. Wright, J. R. 2005. Immunoregulatory functions of surfactant proteins. *Nat. Rev. Immunol.* 5:58–68.
3. Merrill, J. D., and R. A. Ballard. 2003. Pulmonary surfactant for neonatal respiratory disorders. *Curr. Opin. Pediatr.* 15:149–154.
4. Hallman, M., V. Glumoff, and M. Rämet. 2001. Surfactant in respiratory distress syndrome and lung injury. *Comp. Biochem. Physiol. A Mol. Integr. Physiol.* 129:287–294.
5. Veldhuizen, R., K. Nag, …, F. Possmayer. 1998. The role of lipids in pulmonary surfactant. *Biochim. Biophys. Acta.* 1408:90–108.
6. Goerke, J. 1998. Pulmonary surfactant: functions and molecular composition. *Biochim. Biophys. Acta.* 1408:79–89.
7. Melton, K. R., L. L. Nesslein, …, T. E. Weaver. 2003. SP-B deficiency causes respiratory failure in adult mice. *Am. J. Physiol. Lung Cell. Mol. Physiol.* 285:L543–L549.
8. Hawgood, S., M. Derrick, and F. Poulain. 1998. Structure and properties of surfactant protein B. *Biochim. Biophys. Acta.* 1408:150–160.
9. Cabré, E. J., L. M. Loura, …, M. Prieto. 2012. Topology and lipid selectivity of pulmonary surfactant protein SP-B in membranes: answers from fluorescence. *Biochim. Biophys. Acta.* 1818:1717–1725.
10. Pérez-Gil, J., C. Casals, and D. Marsh. 1995. Interactions of hydrophobic lung surfactant proteins SP-B and SP-C with dipalmitoylphosphatidylcholine and dipalmitoylphosphatidylglycerol bilayers studied by electron spin resonance spectroscopy. *Biochemistry.* 34:3964–3971.
11. Ryan, M. A., X. Qi, …, T. E. Weaver. 2005. Mapping and analysis of the lytic and fusogenic domains of surfactant protein B. *Biochemistry.* 44:861–872.
12. Cruz, A., L. A. Worthman, …, J. Pérez-Gil. 2000. Microstructure and dynamic surface properties of surfactant protein SP-B/dipalmitoylphosphatidylcholine interfacial films spread from lipid-protein bilayers. *Eur. Biophys. J.* 29:204–213.
13. Stahlman, M. T., M. P. Gray, …, T. E. Weaver. 2000. Lamellar body formation in normal and surfactant protein B-deficient fetal mice. *Lab. Invest.* 80:395–403.
14. Pérez-Gil, J. 2008. Structure of pulmonary surfactant membranes and films: the role of proteins and lipid-protein interactions. *Biochim. Biophys. Acta.* 1778:1676–1695.
15. Weaver, T. E., and J. A. Whitsett. 1991. Function and regulation of expression of pulmonary surfactant-associated proteins. *Biochem. J.* 273:249–264.
16. Johansson, J. 1998. Structure and properties of surfactant protein C. *Biochim. Biophys. Acta.* 1408:161–172.
17. Plasencia, I., A. Cruz, …, J. Pérez-Gil. 2001. Superficial disposition of the N-terminal region of the surfactant protein SP-C and the absence of specific SP-B-SP-C interactions in phospholipid bilayers. *Biochem. J.* 359:651–659.
18. Creuwels, L. A., E. H. Boer, …, H. P. Haagsman. 1995. Neutralization of the positive charges of surfactant protein C. Effects on structure and function. *J. Biol. Chem.* 270:16225–16229.
19. Ross, M., S. Krol, …, H. J. Galla. 2002. Kinetics of phospholipid insertion into monolayers containing the lung surfactant proteins SP-B or SP-C. *Eur. Biophys. J.* 31:52–61.
20. Pérez-Gil, J., K. Nag, …, K. M. Keough. 1992. Pulmonary surfactant protein SP-C causes packing rearrangements of dipalmitoylphosphatidylcholine in spread monolayers. *Biophys. J.* 63:197–204.
21. Leippe, M., H. Bruhn, …, J. Grötzinger. 2005. Ancient weapons: the three-dimensional structure of amoebapore A. *Trends Parasitol.* 21:5–7.
22. Miteva, M., M. Andersson, …, G. Otting. 1999. Molecular electroporation: a unifying concept for the description of membrane pore formation by antibacterial peptides, exemplified with NK-lysin. *FEBS Lett.* 462:155–158.
23. Patthy, L. 1991. Homology of the precursor of pulmonary surfactant-associated protein SP-B with prosaposin and sulfated glycoprotein 1. *J. Biol. Chem.* 266:6035–6037.
24. Gutsmann, T., B. Riekens, …, M. Leippe. 2003. Interaction of amoebapores and NK-lysin with symmetric phospholipid and asymmetric lipopolysaccharide/phospholipid bilayers. *Biochemistry.* 42:9804–9812.
25. Kairys, V., M. K. Gilson, and B. Luy. 2004. Structural model for an AxxxG-mediated dimer of surfactant-associated protein C. *Eur. J. Biochem.* 271:2086–2092.
26. Luy, B., A. Diener, …, C. Griesinger. 2004. Structure and potential C-terminal dimerization of a recombinant mutant of surfactant-associated protein C in chloroform/methanol. *Eur. J. Biochem.* 271:2076–2085.
27. Parra, E., L. H. Moleiro, …, J. Pérez-Gil. 2011. A combined action of pulmonary surfactant proteins SP-B and SP-C modulates permeability and dynamics of phospholipid membranes. *Biochem. J.* 438:555–564.
28. Chang, R., S. Nir, and F. R. Poulain. 1998. Analysis of binding and membrane destabilization of phospholipid membranes by surfactant apoprotein B. *Biochim. Biophys. Acta.* 1371:254–264.
29. Plasencia, I., L. Rivas, …, J. Pérez-Gil. 2004. The N-terminal segment of pulmonary surfactant lipopeptide SP-C has intrinsic propensity to interact with and perturb phospholipid bilayers. *Biochem. J.* 377: 183–193.
30. Oelberg, D. G., and F. Xu. 2000. Pulmonary surfactant proteins insert cation-permeable channels in planar bilayers. *Mol. Genet. Metab.* 70: 295–300.
31. Taeusch, H. W., J. Bernardino de la Serna, …, J. A. Zasadzinski. 2005. Inactivation of pulmonary surfactant due to serum-inhibited adsorption and reversal by hydrophilic polymers: experimental. *Biophys. J.* 89: 1769–1779.
32. Bernardino de la Serna, J., G. Orädd, …, J. Perez-Gil. 2009. Segregated phases in pulmonary surfactant membranes do not show coexistence of lipid populations with differentiated dynamic properties. *Biophys. J.* 97:1381–1389.

33. Pérez-Gil, J., A. Cruz, and C. Casals. 1993. Solubility of hydrophobic surfactant proteins in organic solvent/water mixtures. Structural studies on SP-B and SP-C in aqueous organic solvents and lipids. *Biochim. Biophys. Acta.* 1168:261–270.

34. Alcaraz, A., E. M. Nestorovich, …, V. M. Aguilella. 2009. Diffusion, exclusion, and specific binding in a large channel: a study of OmpF selectivity inversion. *Biophys. J.* 96:56–66.

35. Hille, B. 2001. Ion Channels of Excitable Membranes. Sinauer, Sunderland, MA.

36. Aguilella, V. M., M. Queralt-Martín, …, A. Alcaraz. 2011. Insights on the permeability of wide protein channels: measurement and interpretation of ion selectivity. *Integr. Biol. (Camb).* 3:159–172.

37. Sobko, A. A., E. A. Kotova, …, W. A. Cramer. 2004. Effect of lipids with different spontaneous curvature on the channel activity of colicin E1: evidence in favor of a toroidal pore. *FEBS Lett.* 576:205–210.

38. Wüstneck, N., R. Wüstneck, …, U. Pison. 2003. Effects of oligomerization and secondary structure on the surface behavior of pulmonary surfactant proteins SP-B and SP-C. *Biophys. J.* 84:1940–1949.

39. Aguilella, V. M., and S. M. Bezrukov. 2001. Alamethicin channel conductance modified by lipid charge. *Eur. Biophys. J.* 30:233–241.

40. Alcaraz, A., E. M. Nestorovich, …, S. M. Bezrukov. 2004. Salting out the ionic selectivity of a wide channel: the asymmetry of OmpF. *Biophys. J.* 87:943–957.

41. Rostovtseva, T. K., V. M. Aguilella, …, V. A. Parsegian. 1998. Membrane surface-charge titration probed by gramicidin A channel conductance. *Biophys. J.* 75:1783–1792.

42. Malev, V. V., L. V. Schagina, …, S. M. Bezrukov. 2002. Syringomycin E channel: a lipidic pore stabilized by lipopeptide? *Biophys. J.* 82: 1985–1994.

43. Mihajlovic, M., and T. Lazaridis. 2010. Antimicrobial peptides in toroidal and cylindrical pores. *Biochim. Biophys. Acta.* 1798:1485–1493.

44. Sengupta, D., H. Leontiadou, …, S. J. Marrink. 2008. Toroidal pores formed by antimicrobial peptides show significant disorder. *Biochim. Biophys. Acta.* 1778:2308–2317.

45. Pérez-Gil, J. 2008. Properly interpreting lipid-protein specificities in pulmonary surfactant. *Biophys. J.* 94:1542–1543, discussion 1544.

46. Seifert, M., D. Breitenstein, …, H. J. Galla. 2007. Solubility versus electrostatics: what determines lipid/protein interaction in lung surfactant. *Biophys. J.* 93:1192–1203.

47. Plasencia, I., F. Baumgart, …, J. Pérez-Gil. 2008. Effect of acylation on the interaction of the N-Terminal segment of pulmonary surfactant protein SP-C with phospholipid membranes. *Biochim. Biophys. Acta.* 1778:1274–1282.

48. Bernardino de la Serna, J., R. Vargas, …, J. Perez-Gil. 2012. Segregated ordered lipid phases and protein-promoted membrane cohesivity are required for pulmonary surfactant films to stabilize and protect the respiratory surface. *Faraday Discuss.* 10.1039/c2fd20096a In press.

49. Schürch, D., O. L. Ospina, …, J. Pérez-Gil. 2010. Combined and independent action of proteins SP-B and SP-C in the surface behavior and mechanical stability of pulmonary surfactant films. *Biophys. J.* 99: 3290–3299.

50. Olmeda, B., B. García-Álvarez, and J. Pérez-Gil. 2012. Structure-function correlations of pulmonary surfactant protein SP-B and the saposin-like family of proteins. *Eur. Biophys. J.*

51. Perez-Gil, J., and T. E. Weaver. 2010. Pulmonary surfactant pathophysiology: current models and open questions. *Physiology (Bethesda).* 25:132–141.